UNIVERSITY OF
BIRMINGHAM

University of Birmingham Research Archive

e-theses repository

This unpublished thesis/dissertation is copyright of the author and/or third parties. The intellectual property rights of the author or third parties in respect of this work are as defined by The Copyright Designs and Patents Act 1988 or as modified by any successor legislation.

Any use made of information contained in this thesis/dissertation must be in accordance with that legislation and must be properly acknowledged. Further distribution or reproduction in any format is prohibited without the permission of the copyright holder.

3rd of 3 files

Chapters 4-5, Appendices and References

IMPROVED SOL BASED CERAMIC MOULDS FOR USE IN INVESTMENT CASTING

by
SAMANTHA JONES

A thesis submitted to the
Faculty of Engineering
of the
University of Birmingham
for the degree of
DOCTOR OF PHILOSOPHY

School of Metallurgy and Materials
University of Birmingham
Edgbaston
Birmingham
B152TT
England
May 1993

CHAPTER FOUR

4.1: Basic Mould Structure

4.1.1: Introduction

The results of an investigation into the basic structure of silica based ceramic moulds prepared at Deritend Precision Castings will be presented in the next section. The underlying principle throughout the research was to locate possible causes for high temperature distortion of large investment castings. Metal casting into a ceramic mould is a very severe procedure. A series of mechanical and thermal stresses are induced which the mould must accomodate without undue deformation or failure.

The structural integrity and resistance to surface interaction of an investment casting mould directly determine the quality of the finished metal casting. These factors are dependant upon the ability of the ceramic shell to retain its original dimensions without reaction or undue deformation during a prolonged high temperature cycle. Moulds, although identical in composition and structure, are subjected to a range of load and temperature regimes due to the relative size of the components produced. The same basic system is therefore required to withstand very different environments to produce a sound casting.

If the mould were made of a fully dense single refractory the ability to withstand this casting environment could easily be measured, quantified or even predicted. However, since the ceramic shell comprises of a range of refractory materials and is manufactured by a process which produces an inherently porous structure, the thermal and mechanical response is very difficult to measure or predict. A detailed microstructural examination was therefore undertaken to determine the overall structure and distribution of phases. This will allow failure mechanisms to be identified, leading to a clearer understanding of the basic mould weaknesses. This information should make it possible to predict casting responses and reduce the incidence of mould failure.

4.1.2: The Mould System

The mould system under investigation consists of a water based primary coat with granular zirconium silicate stucco, followed by a series of alcohol based secondary coats with prehydrolysed ethyl silicate solution as binder and alumino-silicate stucco in a range of particle sizes. The primary and secondary coat formulations are detailed in Appendices 7 and 8. The mould section is built up by dipping of a wax pattern into the appropriate slurry followed by the application of the stucco with increasing grain size as the shell thickness increases.

Details of the slurry/stucco regime can be found in Appendix 9. The primary coat is gelled by air-drying but secondary coats are gelled in an ammoniating atmosphere before being air-dried. Although ethyl-silicate binders can be gelled in air the process is slow, and the addition of a gellation catalyst increases the rate of mould production.

4.1.3: Structure of The Mould

The investigation began with a microstructural examination of a section through the mould wall using scanning electron microscopy. The wide range of refractory particle sizes within the mould made it difficult to study the entire section at a single magnification. At low magnifications the larger particles, such as the stucco, were visible but the structure of the filler phase was difficult to distinguish. At higher magnifications the situation was reversed. In order to study both stucco and filler structures relevant to each other it was necessary to build up a montage from individual high magnification micrographs. The micrographs were matched together to gain an overall view of the mould structure at a high magnification (Figure 80). To aid identification of the separate phases a schematic structure was generated (Figure 81).

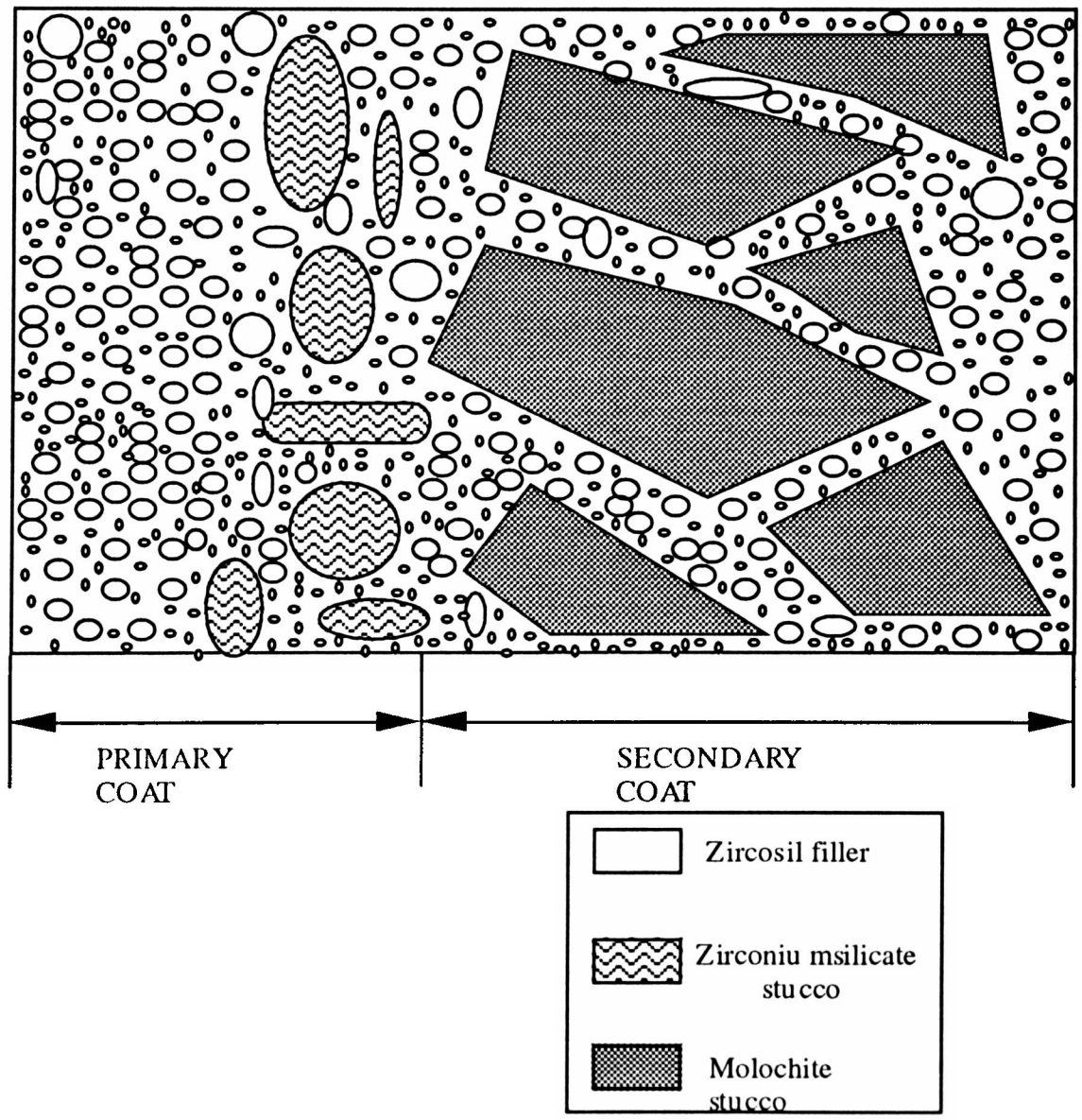


Figure 81: Schematic illustration of the structure of an air-cast mould

Primary Coat

Secondary Coat



Figure 80: Montage of a fired air-cast mould. Magnification : x 1,500

The mould appears to consist of a series of non-uniform refractory phases held together in a inconsistent and unpredictable network. Several possible structural weaknesses can be identified, most notably the non-uniform filler particle distribution. The filler appears to have a wide range of particle sizes and morphology, with most being highly angular. These particles do not have the ability to close pack, which results in a distribution of pore sizes within the bulk of the mould structure. Indeed the section contains several large holes greater than 620 μm in length (Figure 82). This type of structure can lead to heat flow problems due to the fact that conduction through the still air contained within the pores is lower than through the ceramic constituents. As such, heat transfer through the mould section will be irregular and 'hot-spots' may be produced in some areas. Loss of mechanical strength due to the presence of what are essentially defects within the structure is also possible.

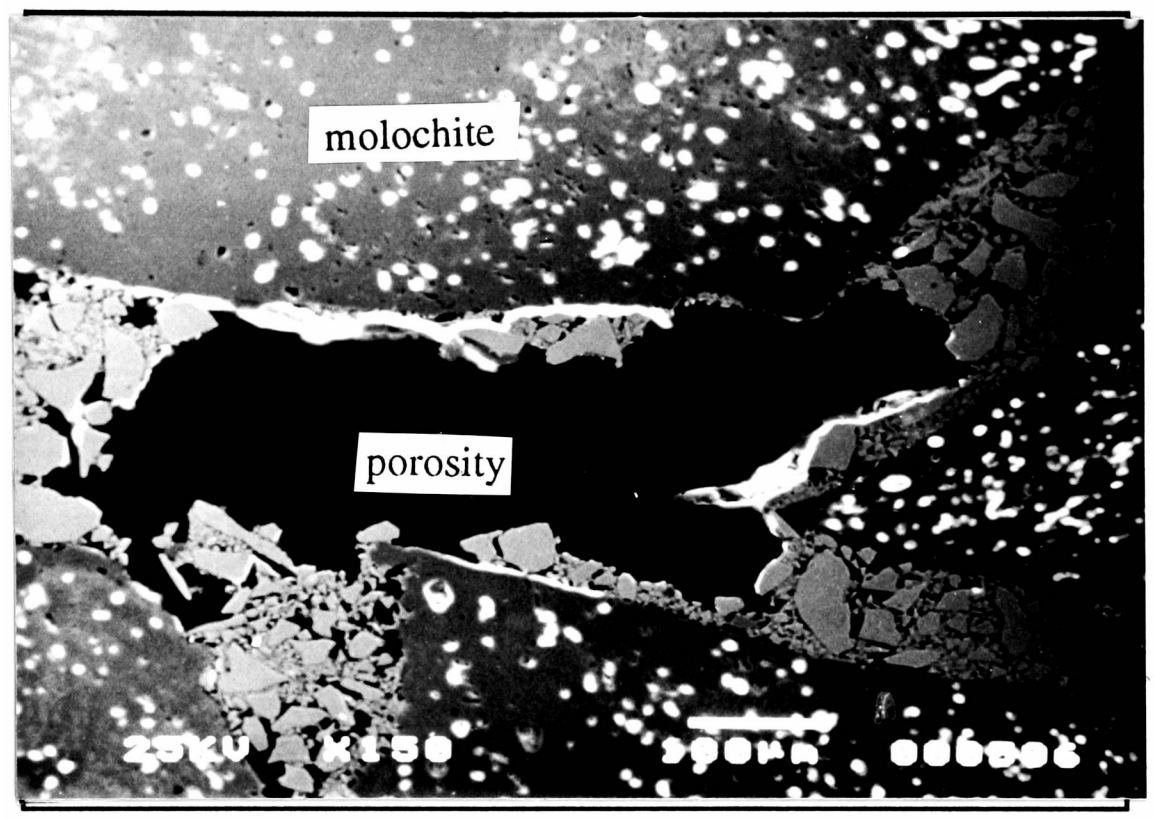


Figure 82: Porosity within the secondary coats of an air-cast mould mag = x 150

The montage also serves to illustrate the large amount of open porosity within the primary coat of the mould. This could directly contribute to a poor casting surface and metal-mould interaction. Porosity provides a direct pathway for liquid metal which, through capillary action, may be drawn into the mould structure in much the same way as a sponge draws up water. Metal penetrating the primary coat may melt and interact preferentially with the silica binder as the melting temperature is lower than the other refractory constituents. This would produce a rough casting surface containing a high percentage of silica. The interaction could also weaken the binder network to such an extent that small sections of the primary coat could be broken away. These would then be incorporated into the metal surface and become primary coat inclusions which require removal prior to casting and may even lead to quality control failure.

The silica bonding phase was not evident at the magnification used for the montage. However, as many of the theories concerning the cause of casting bulge (Section 2.7.1) consider the role of the binder to be critical, further investigation into the distribution of this phase was undertaken. Higher magnification SEM revealed that the distribution of the silica binder falls into two categories. There are regions where the silica has agglomerated to form a mass between the larger ceramic particles (Figures 83 and 84). The remainder surrounds the finer filler particles in small, thin regions (Figures 85 and 86).

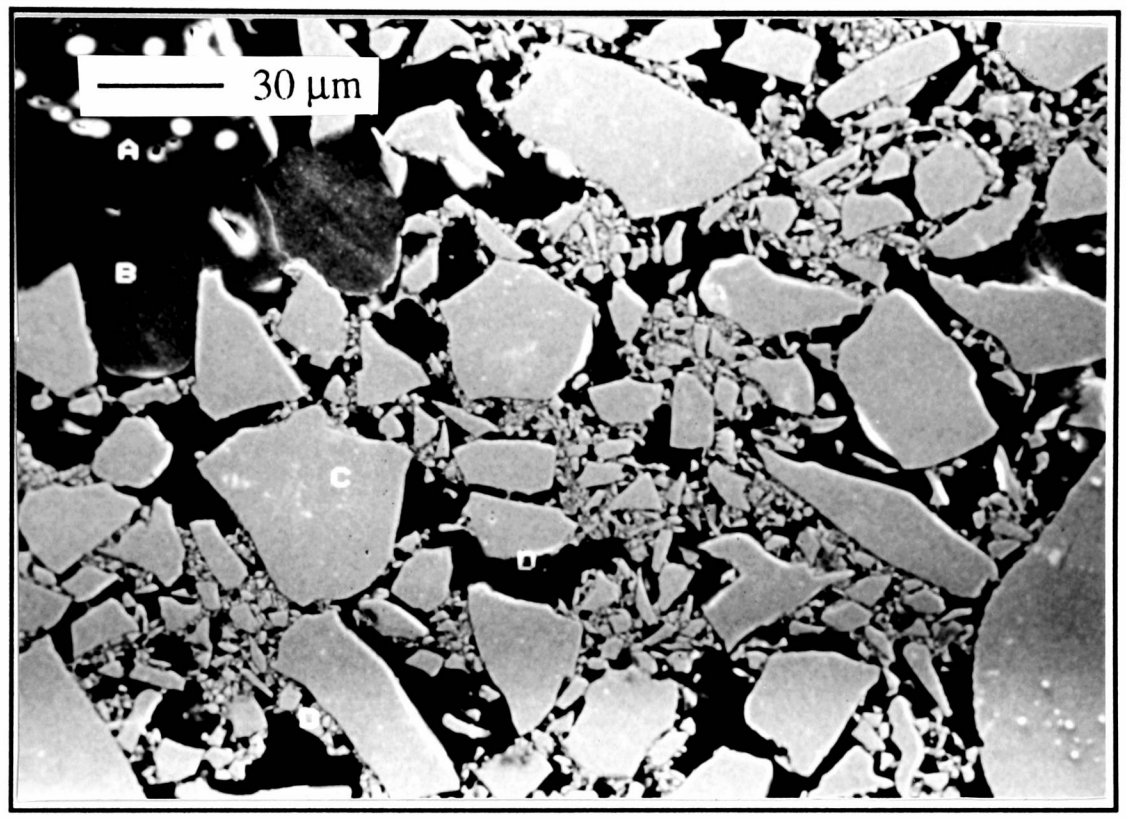


Figure 83: Agglomerated silica binder in an air-cast mould. Magnification x410

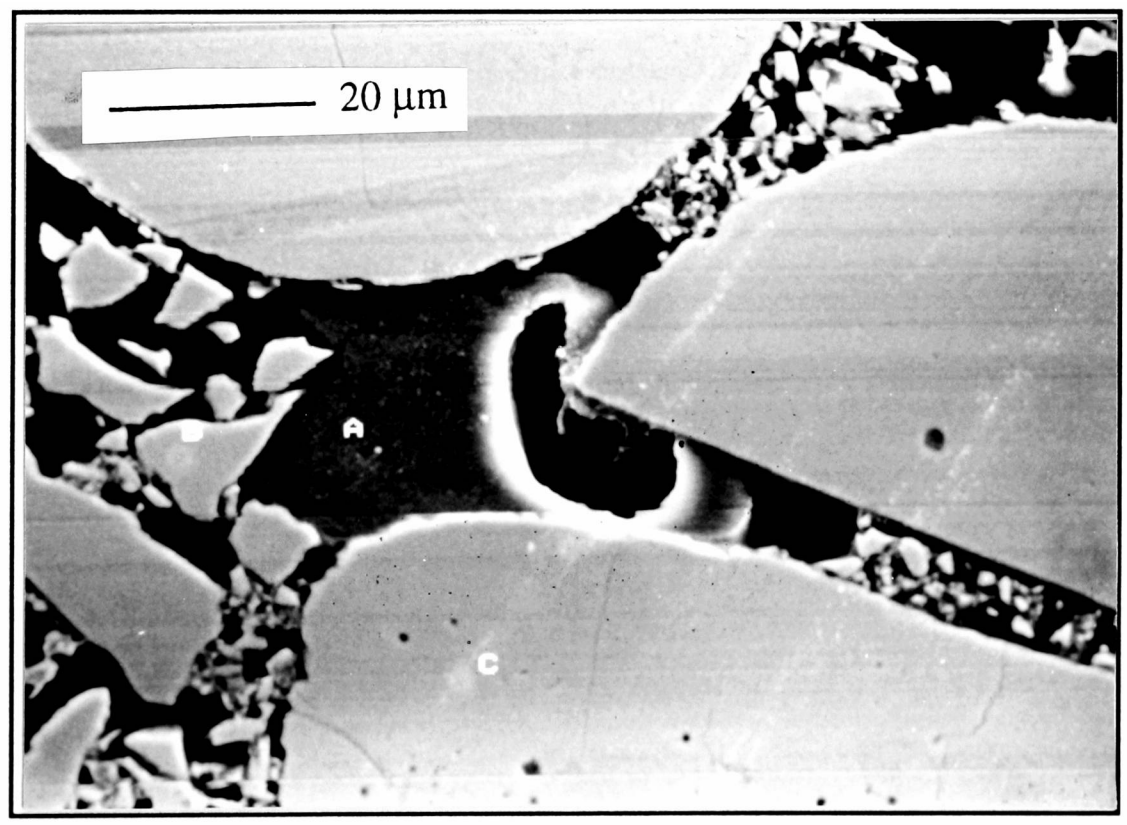


Figure 84: Agglomerated silica binder in an air-cast mould. Magnification x 1,030

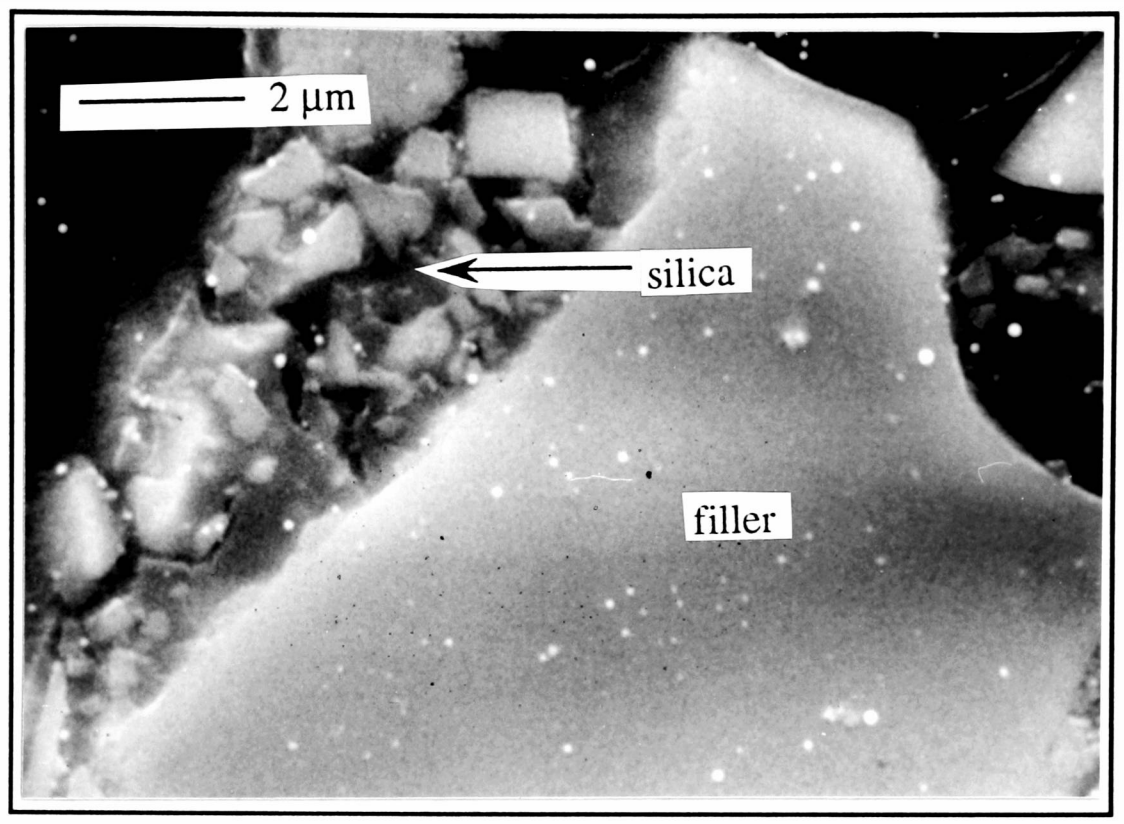


Figure 85: Thin areas of silica around finer filler particles. Magnification x 7,800

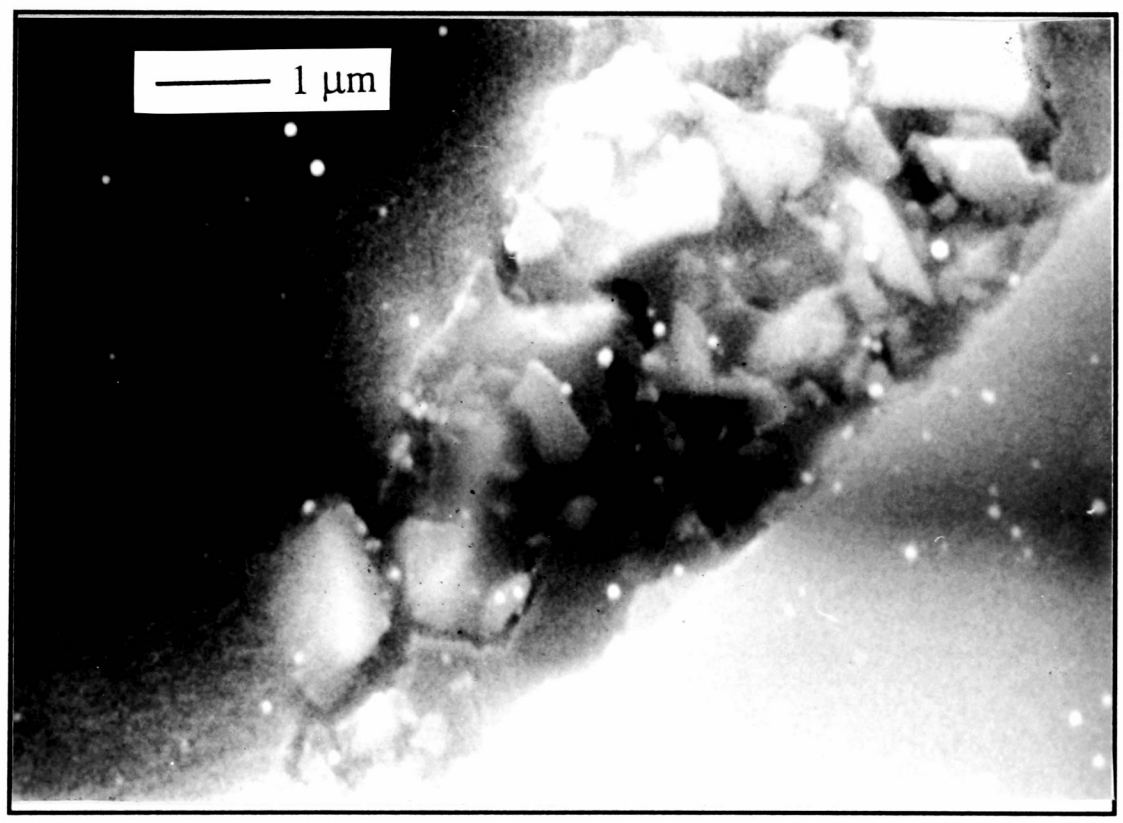


Figure 86: Higher magnification micrograph of thin areas of silica around finer filler particles Magnification x 11,400

Regions of fine filler particles surrounded by silica binder form the main network contact between the refractory particles. Contact between the larger ceramic particles is achieved through small 'bridges' of binder and filler. Since the regions of agglomerated silica are few, it can be concluded that the thin areas of silica will form the main load bearing points within the mould structure. As such, the overall structural response of the mould will be governed by the response of the binder. Therefore the key to producing an improved mould system lies within a greater understanding of the structure, thermal response and mechanical properties of the binder system.

4.1.4: Phase Structure and Composition of the Silica Binder

The phase structure of the binder is an important consideration, since silica can exist in an amorphous structure, or as any one of a number of distinct polymorphic crystalline forms (Section 2.3). The various phases of silica exhibit a range of thermal and physical properties which could affect the structural integrity of the mould during casting.

Crystallinity can be detected using X-ray diffraction and patterns obtained from samples of unfired and fired moulds can be seen in Figures 87 and 88. Both patterns are identical with peaks identifiable as mullite (a constituent of the Molochite stucco) and zirconium silicate (the filler material). Neither pattern shows any evidence of crystalline silica. It could be assumed that the binder must therefore be amorphous but, since the lower detection limit for X-ray diffraction is only 5%, there is a possibility that crystalline silica is present but in relatively small amounts.

This conclusion is verified by the diffraction pattern obtained from a sample of Syton X30, mixed with a small amount of Zircosil refractory, fired to 1,000°C as for the moulds themselves (Figure 89). In this case the relative percentage of silica is much higher and the pattern shows the presence of alpha cristobalite. As such, it cannot be assumed that the silica binder within a mould is present in its amorphous state, and the exact phase structure will have to be determined by analysis of binder samples fired seperately under identical thermal conditions.

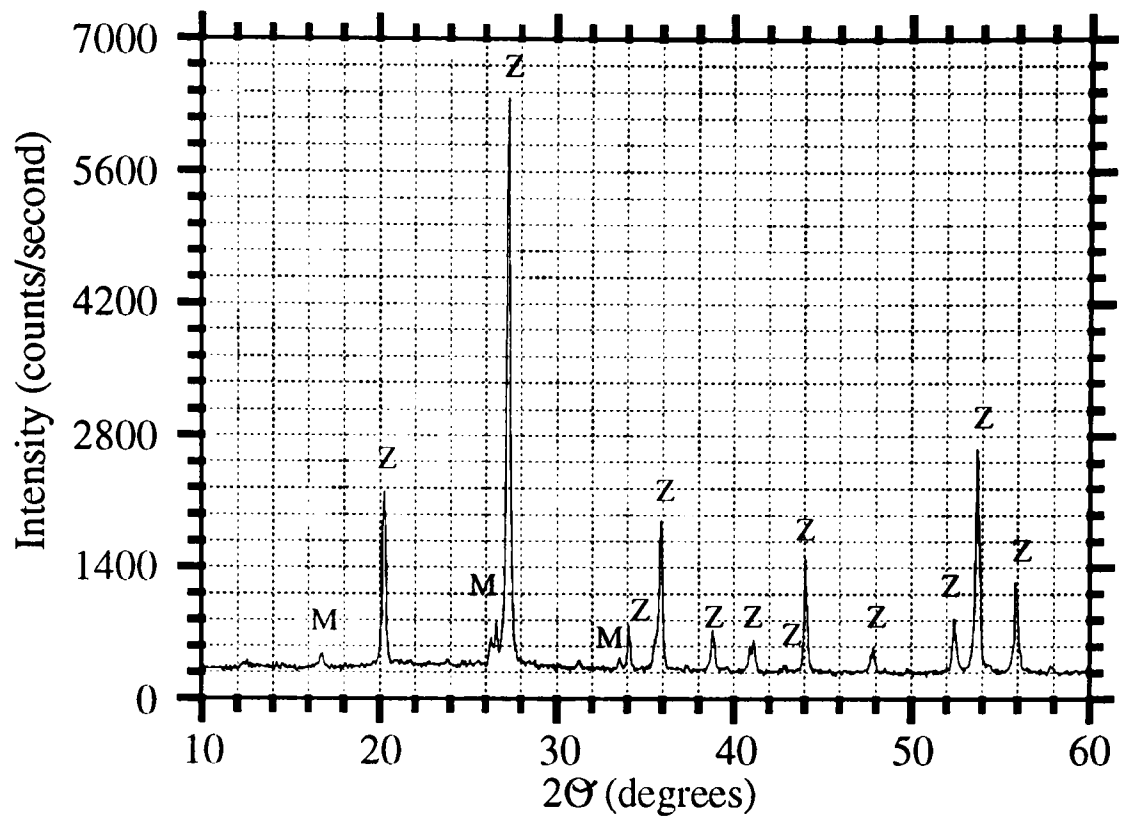


Figure 87: X-ray diffraction pattern of an unfired investment casting mould
M = mullite Z = zirconium silicate

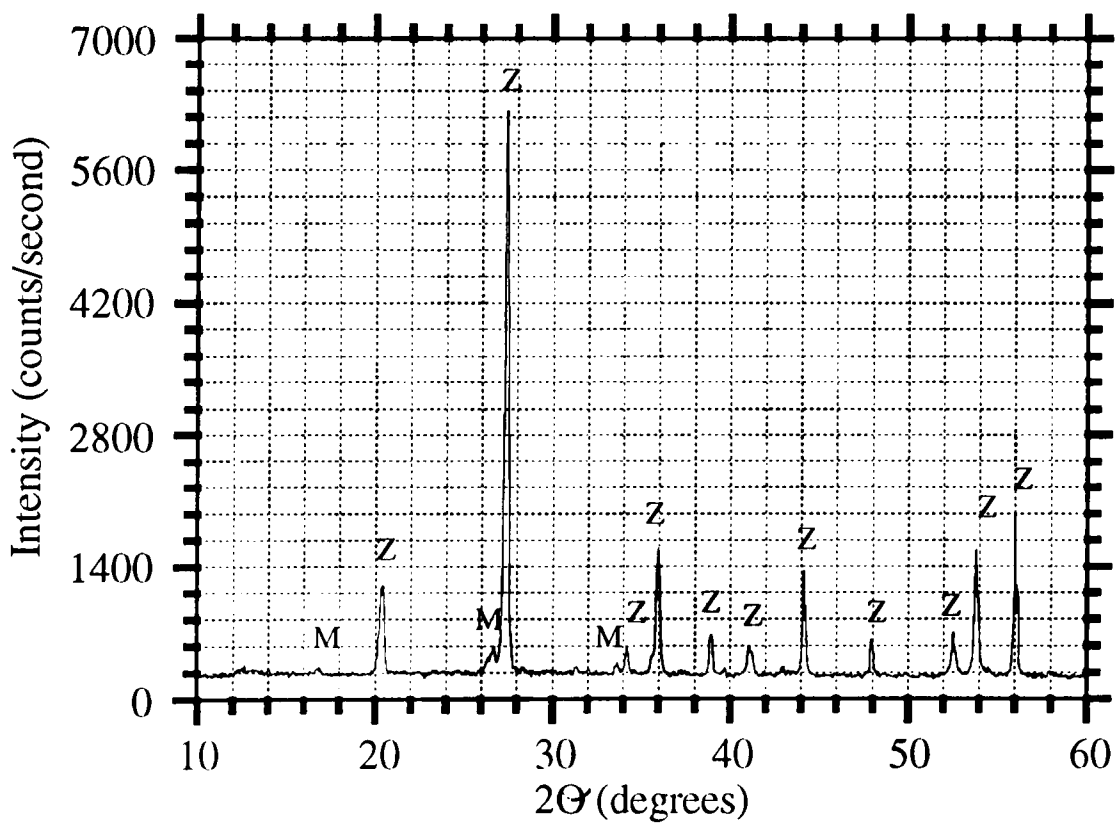


Figure 88: X-ray diffraction pattern of a fired investment casting mould
M = mullite Z = zirconium silicate

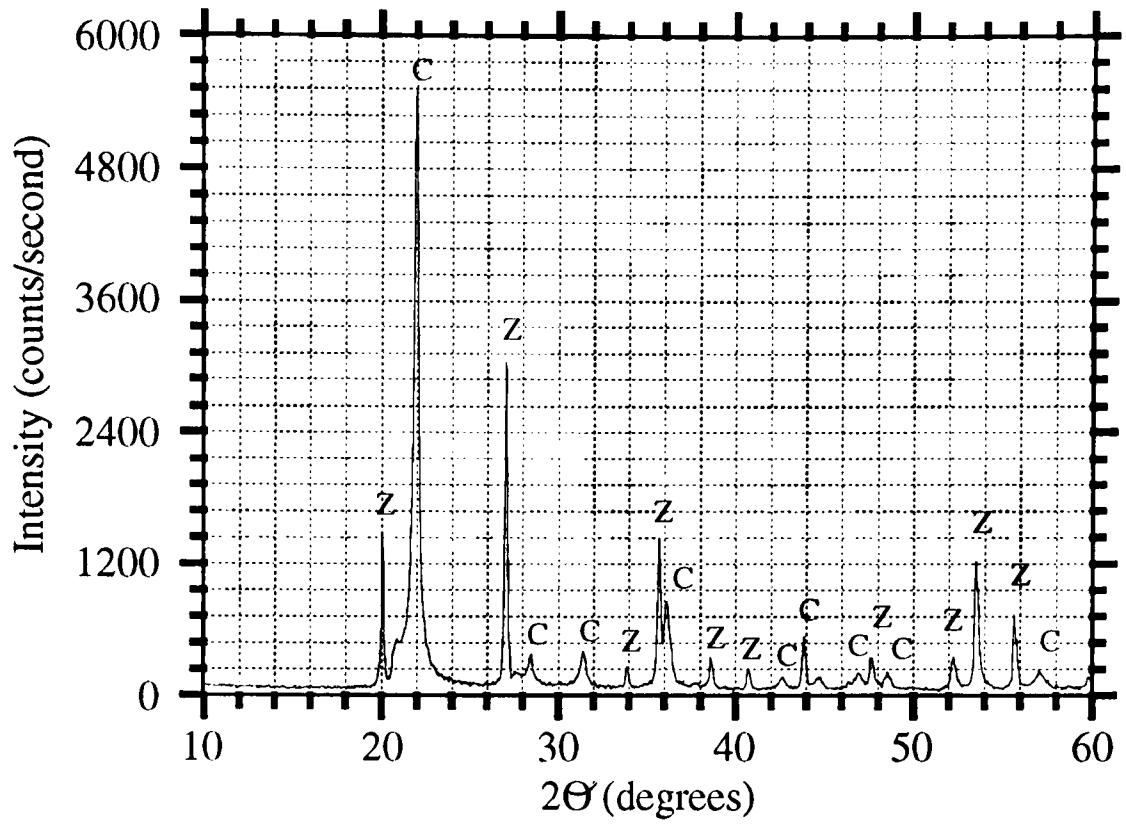
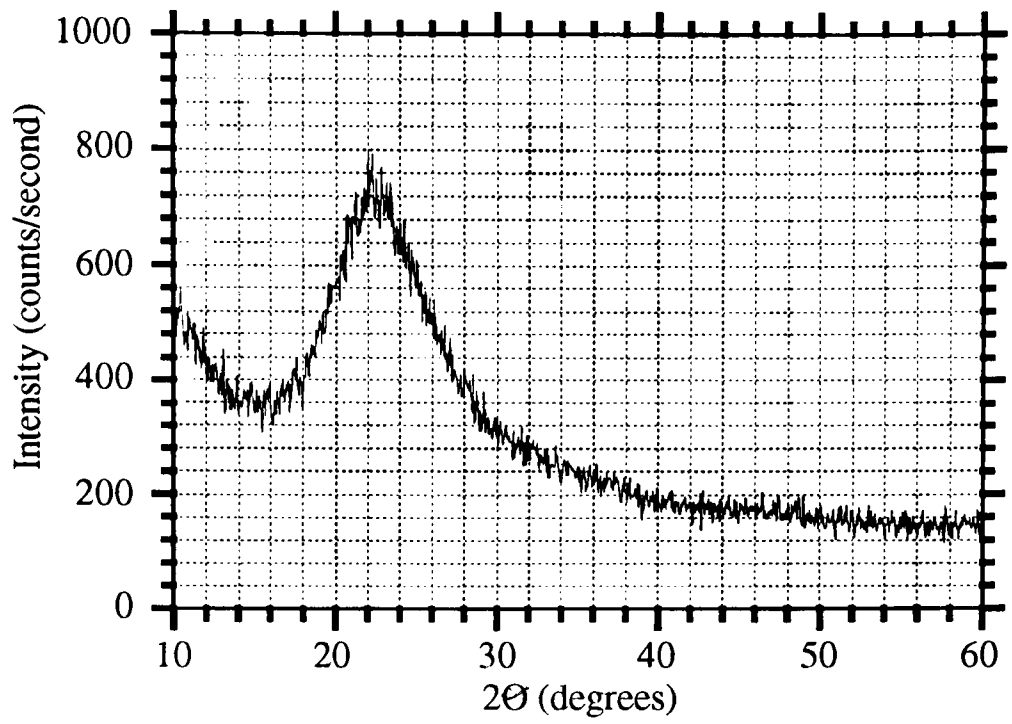
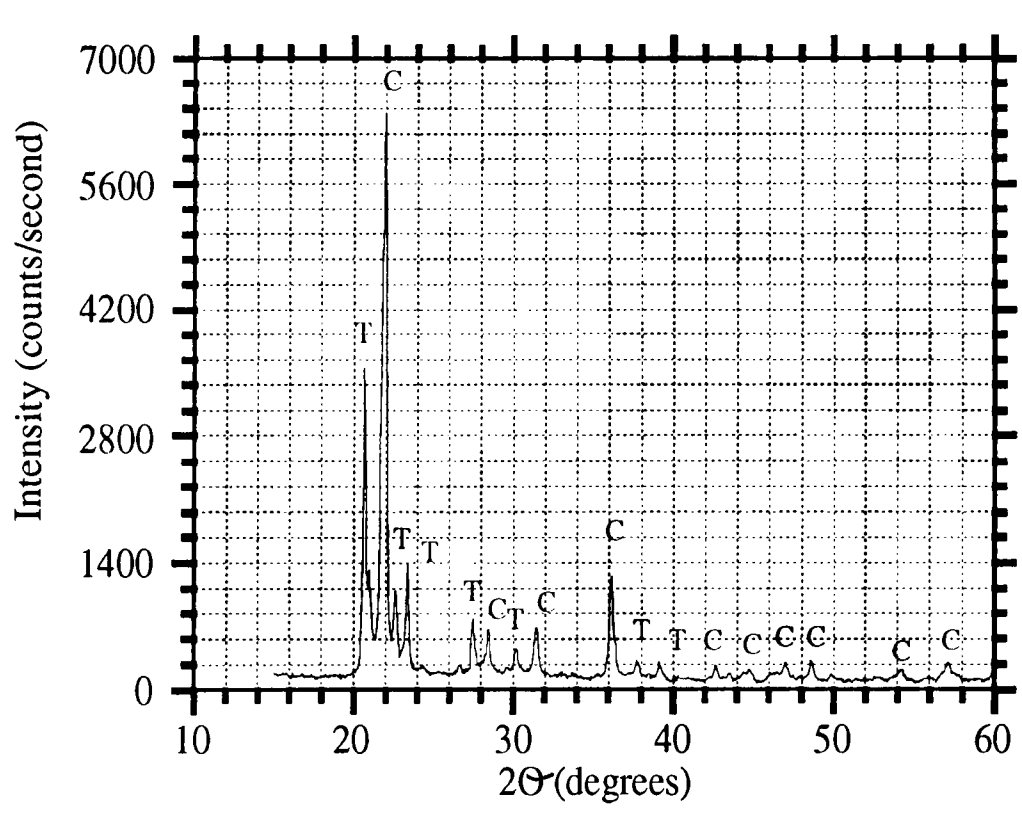


Figure 89: X-ray diffraction pattern for 40ml Syton X30 mixed with 5g Zircosil and fired at 1,000°C for 60 minutes.
C = α cristobalite Z = zirconium silicate

To establish the phase state of the silica within the mould, binder samples were individually gelled, dried, fired and then subjected to X-ray analysis. Gelled Syton X30 is amorphous, displaying the characteristic single broad diffraction peak of a non-crystalline solid with short range order (Figure 90(a)). When fired at 1,000°C, for 60 minutes, the sol crystallizes to form a mixture of cristobalite and tridymite (Figure 90(b)). This behaviour is unusual as a gel prepared from the sol route usually remains amorphous up to 1,000°C (Section 2.5.6). However, devitrification is catalyzed by the presence of impurity atoms and as Syton X30 contains a relatively large amount of sodium stabilising ions, it is presumed that sodium catalyzes the crystallisation. The effect of sodium will be discussed in more detail in Section 4.3.3.



(a)



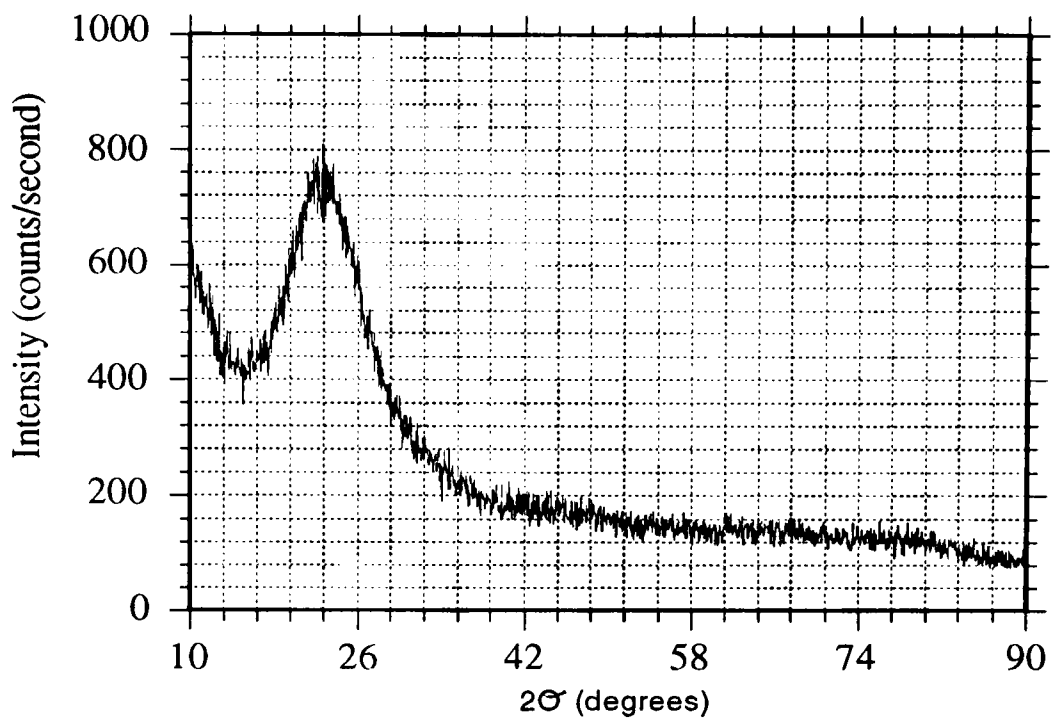
(b)

Figure 90: X-ray diffraction patterns for (a) gelled Syton X30 and (b) Syton X30 fired at 1,000°C for 60 minutes

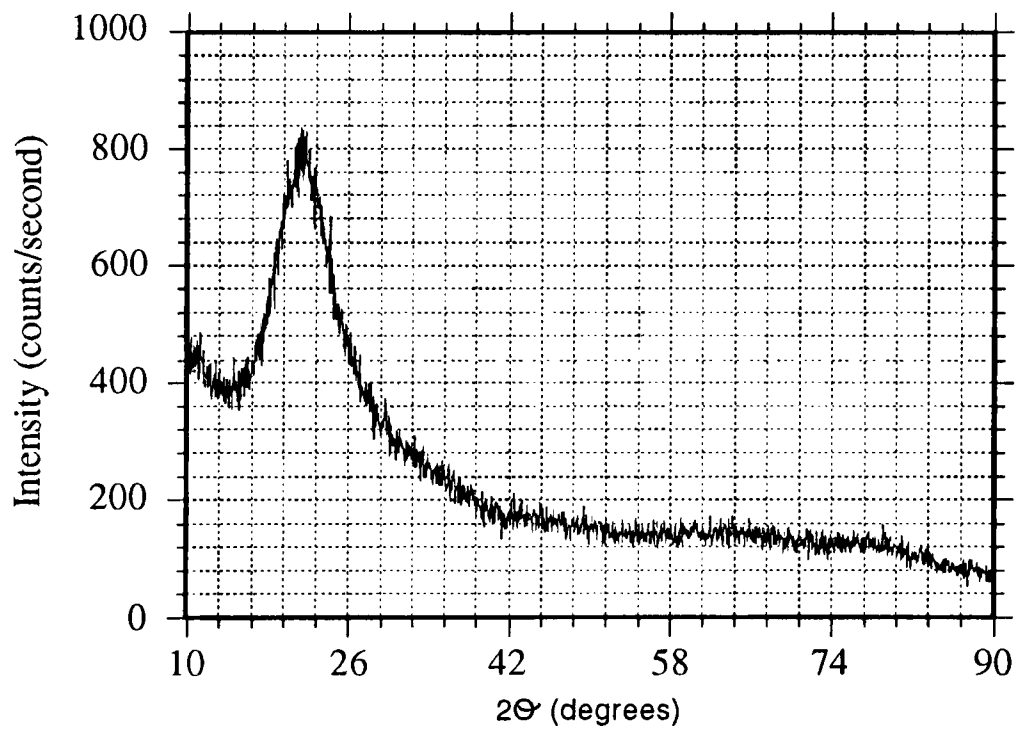
T = S_1 tridymite (low temperature)

C = α cristobalite

Gelled Silester XAR (ethyl-silicate solution) is also amorphous (Figure 91 (a)) and unlike Syton remains amorphous when fired to 1,000°C for 60 minutes (Figure 91 (b)). This behaviour is typical, as most gels derived from an ethyl-silicate base do not crystallise until temperatures of 1350°C and above (Section 2.5.7.2).



(a)



(b)

Figure 91: X-ray diffraction patterns for (a) gelled Silester XAR and (b) Silester XAR fired at 1,000°C for 60 minutes

The composition of the silica binder within a mould sample was investigated using EDX. Examples of two typical traces obtained from an air-cast mould sample are shown in Figure 92. This type of analysis is only qualitative, but the results did serve to highlight the presence of several elements other than silicon and oxygen within the binder phase. The only element that can reasonably be accounted for is sodium, which is present as a stabilisation additive in sol based binders. However, as the lower detection limit for EDX is 0.5% and the maximum level of Na_2O stabiliser is 0.3wt%, the level of sodium detected is still higher than would be expected. Other elements detected, such as Ca, Al, K, Ti and Fe are not present in the original binders (see specifications in Appendix 3).

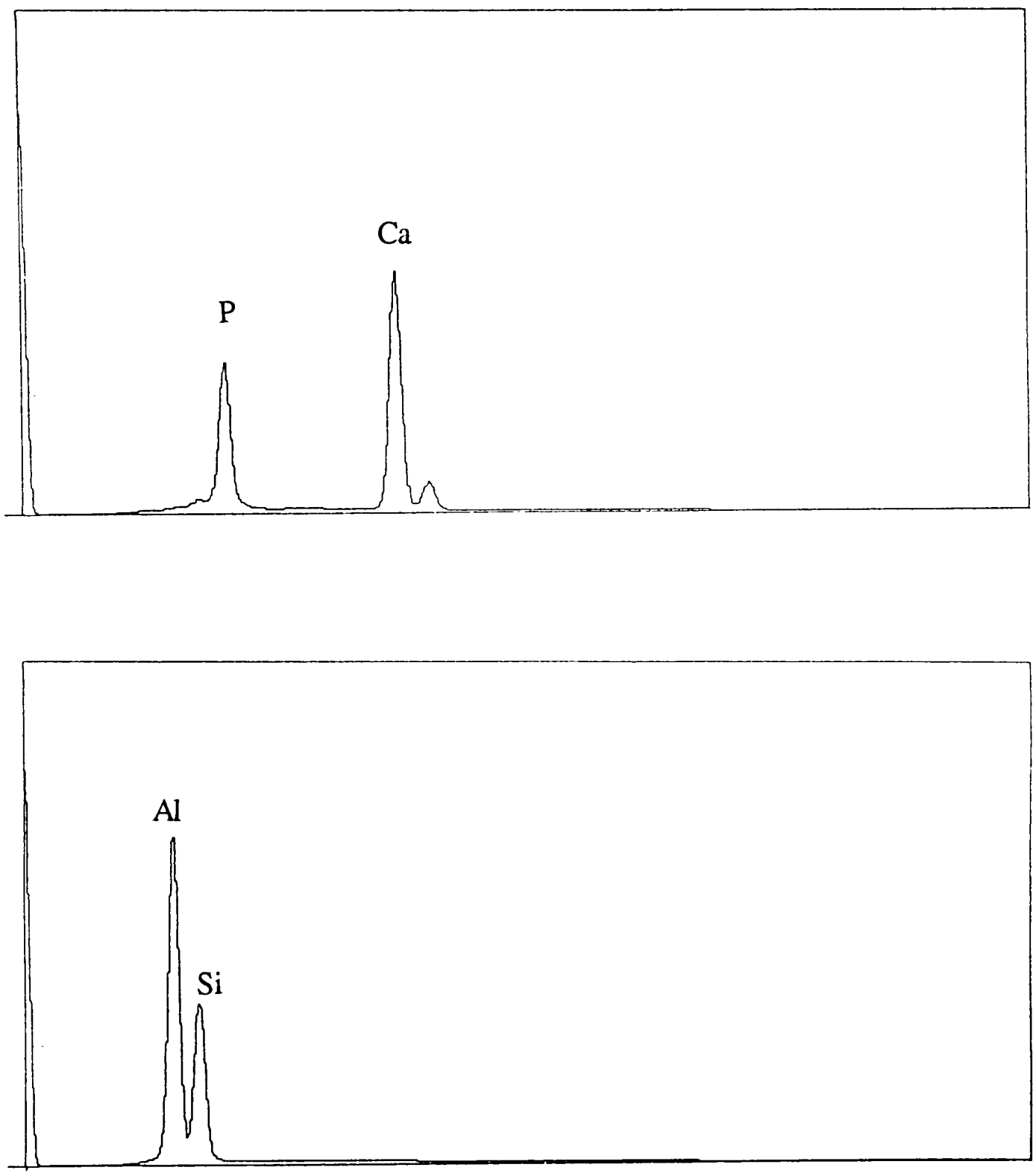


Figure 92: Two typical EDX traces obtained from the binder within a fired air-cast mould

Quantitative binder compositions were determined using EPMA. Many different compositions were found and are summarised in Table 15. It is apparent from these results that the binder composition is variable and unpredictable. Since neither sol or ethyl silicate binders contain these elements prior to slurry production, then the the impurities must have been introduced at some stage during slurry production.

Table 15: Silica compositions within the binder phase of a fired mould determined using EPMA

	Atomic percentages									
	O	Si	Ca	Na	Fe	Zr	Al	K	P	S
Region 1	58.559	39.508	1.393	0.507	-	0.032	-	-	-	-
Region 2	60.768	37.569	0.824	0.424	0.061	0.354	-	-	-	-
Region 3	72.417	27.015	0.144	0.240	0.008	0.041	-	-	-	0.136
Region 4	64.807	33.514	0.029	0.400	0.110	1.140	-	-	-	-
Region 5	62.763	36.021	0.937	0.262	0.013	0.005	-	-	-	-
Region 6	61.270	38.358	0.078	0.182	0.036	0.075	-	-	-	-
Region 7	73.543	25.596	0.213	0.265	-	0.183	-	-	-	0.200
Region 8	61.485	37.971	0.014	0.341	0.058	0.085	-	-	-	-

4.1.5: Summary

An investment casting mould consists of a series of refractory filler particles bound together by a silica binder. The structure has been found to contain a non-uniform filler distribution which gives rise to a variable and unpredictable porosity network. At the high temperature gradients experienced during metal casting this non-uniformity is believed to produce an irregular heat flow, possibly leading to the formation of 'hot-spots' and other weaknesses within the mould section.

The mould also contains a large amount of open porosity within the primary coat of the mould. Porosity provides a direct pathway for liquid metal which, through capillary action, may be drawn

into the mould structure in much the same way as a sponge draws up water. Interaction could increase the silica content of the cast metal surface and also weaken the binder network to such an extent that small sections of the primary coat could be broken away. These would then be incorporated into the metal surface and become primary coat inclusions which require removal prior to casting and may even lead to quality control failure.

Regions of fine filler particles surrounded by silica binder form the main network contact between the refractory particles. Contact between the larger ceramic particles is achieved through small 'bridges' of binder and filler. These thin areas of silica will form the main load bearing points within the mould structure. As such, the overall structural response of the mould will be governed by the response of the binder. Therefore the key to producing an improved mould system lies within a greater understanding of the structure, thermal response and mechanical properties of the binder system.

The phase structure of the silica is determined by the type of binder used. A summary of the phase structures is contained in Table 16. Water based colloidal silica sols when fired to 1,000°C crystallise to form a mixture of phases. Alcohol based ethyl silicate solutions remain amorphous when fired. This leads to the interesting conclusion that the primary coats of the mould are bound by a crystalline network and the secondary coats by an amorphous network which is schematically represented in Figure 93. As such, the thermal and structural response of the mould section will be unpredictable due to the varying responses of the silica.

Binder	Thermal Treatment	Structure
Colloidal silica sol	Gelled and dried at 55°C	Amorphous
Colloidal silica sol	Fired at 1,000°C for 60 minutes	Mainly α – cristobalite with trace amounts of α - tridymite and α - quartz
Ethyl silicate solution	Gelled and dried at 55°C	Amorphous
Ethyl silcate solution	Fired at 1,000°C for 60 minutes	Amorphous

Table 16: Summary of the phase composition of the silica based binders

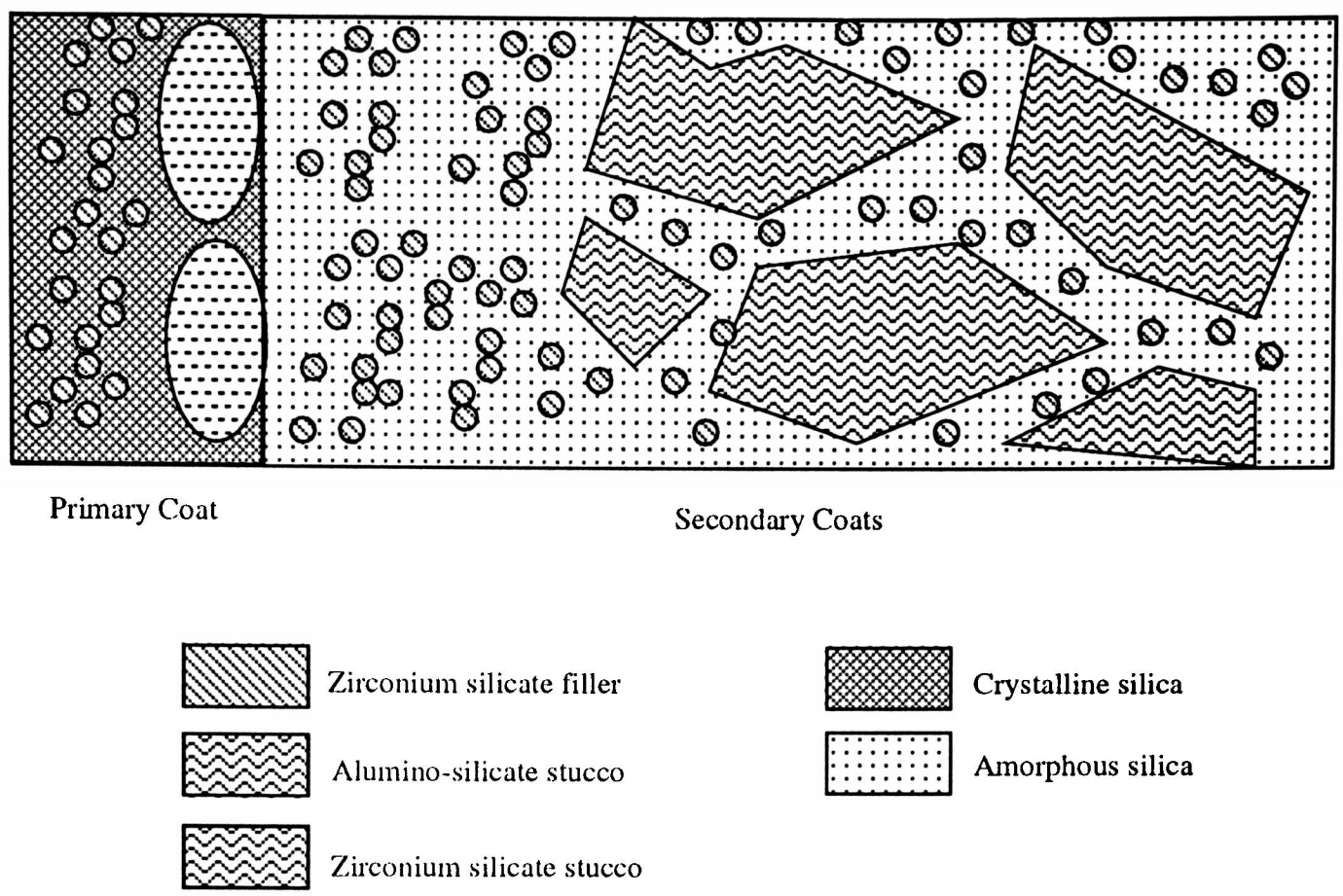


Figure 93: Schematic illustration of the proposed silica phase distribution

The silica binder has been found to contain impurity elements in variable amounts. As such, the binder composition is variable and unpredictable with the type of elements present being similar but in different proportions. The elements appear to have been introduced during slurry/mould processing and their effect, if any, upon the performance of the binder will be investigated in the next section.

4.2: Source of Impurities

4.2.1: Identification of Source

Since the only common factor between a primary and a secondary slurry is the filler material, the investigation into the source of the impurity elements was focused upon this refractory. Investigation of Zircosil filler using SEM and EDX revealed that some of the individual particles consisted of phases other than zirconium silicate (Figures 93 to 97). Phases such as calcium phosphate ($Ca(PO_4)_2$), iron sulphide (FeS) and alumino-silicate ($Al_2O_3.SiO_2$) have been found, the constituents of which are associated with the impurities found in the silica and account for many of the elements in the binder compositions. These phases were easy to distinguish, sometimes without the need for rigorous analysis, since under an SEM the zirconium silicate phase appeared white but the other phases were much darker.

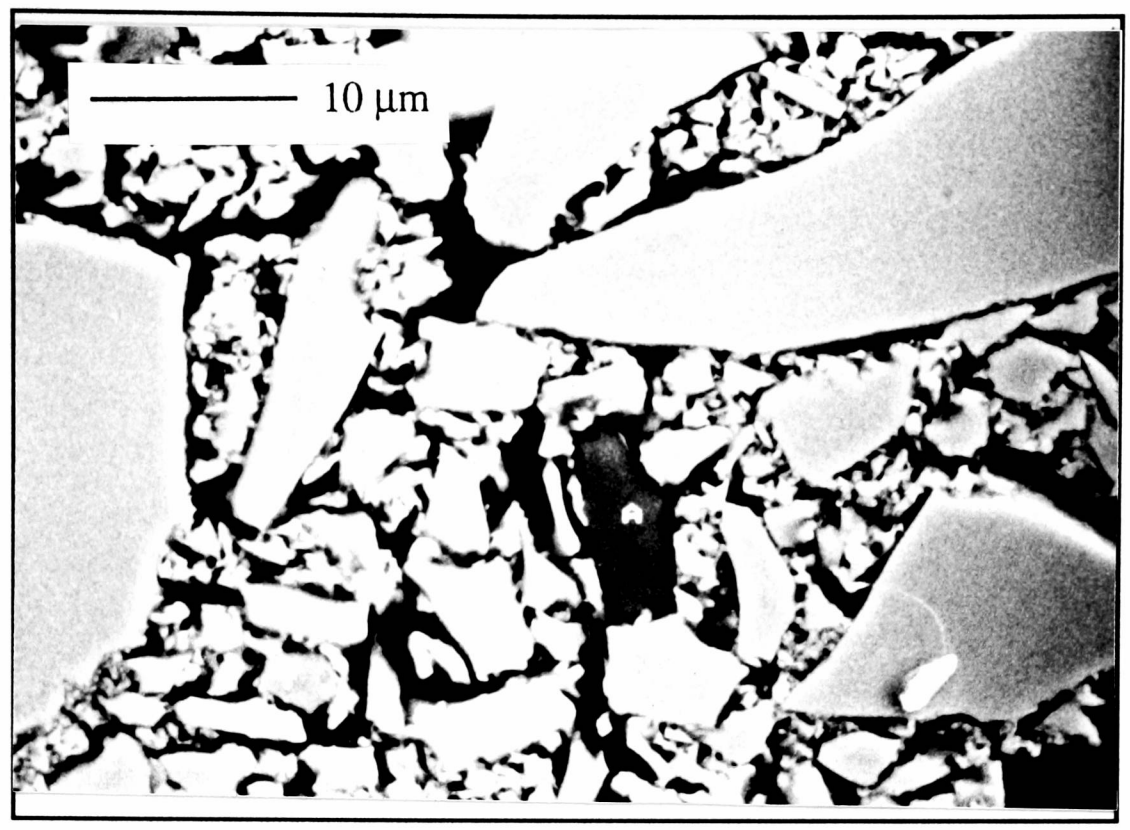


Figure 94: Micrograph of an impurity phase found within Zircosil filler mag = x 2,600
A = SiO_2 B = Ti O_2

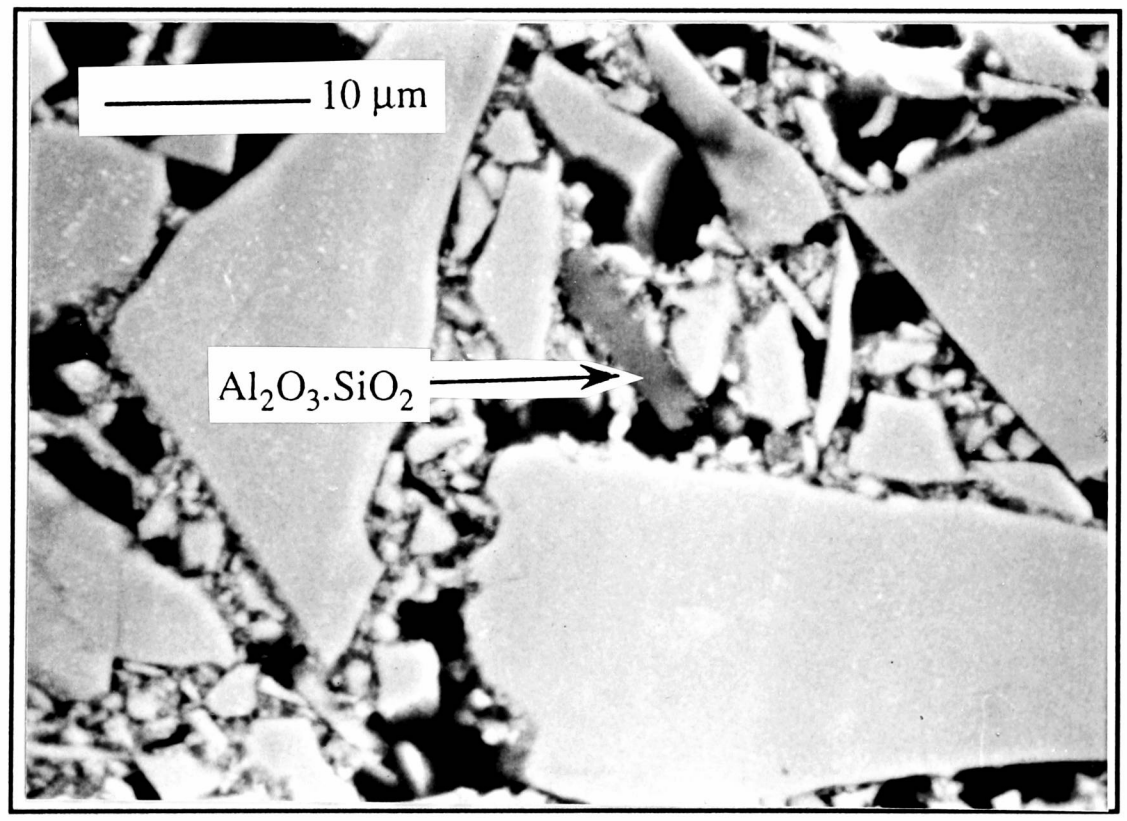


Figure 95: Micrograph of an impurity phase found within Zircosil filler mag = x 2,400

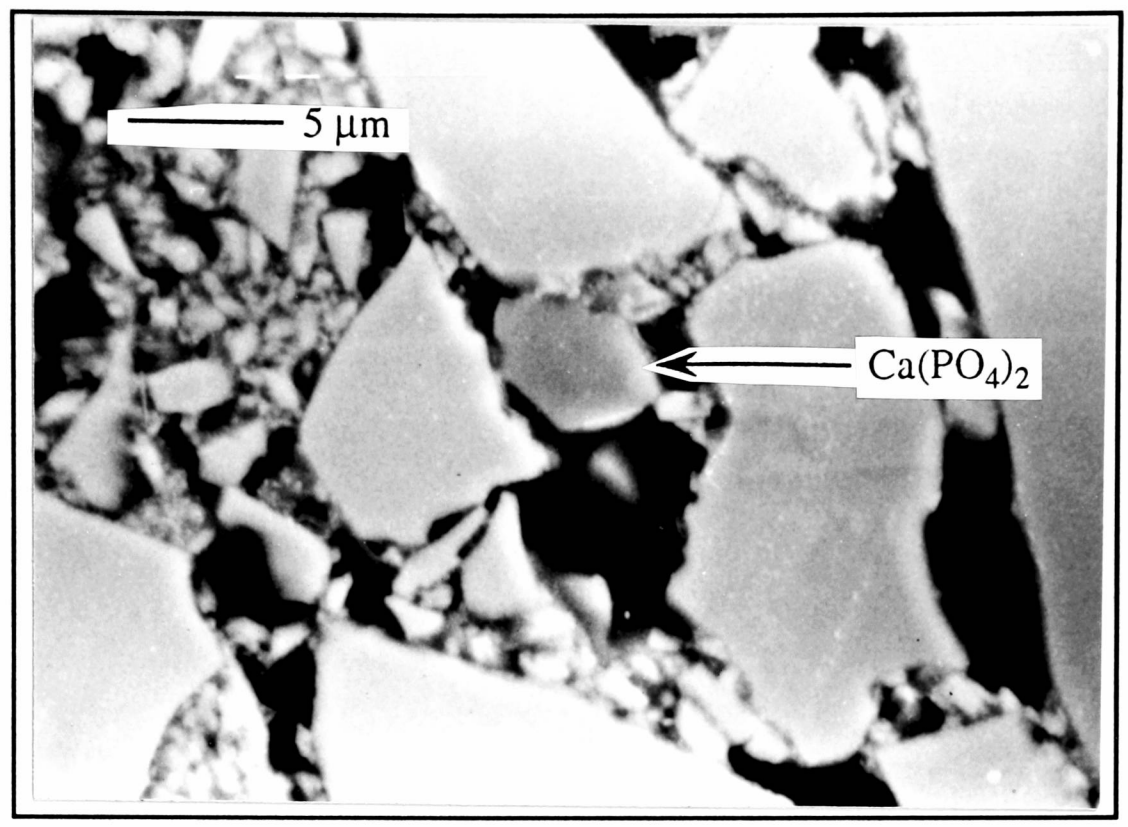


Figure 96: Micrograph of an impurity phase found within Zircosil filler mag = x 3,100

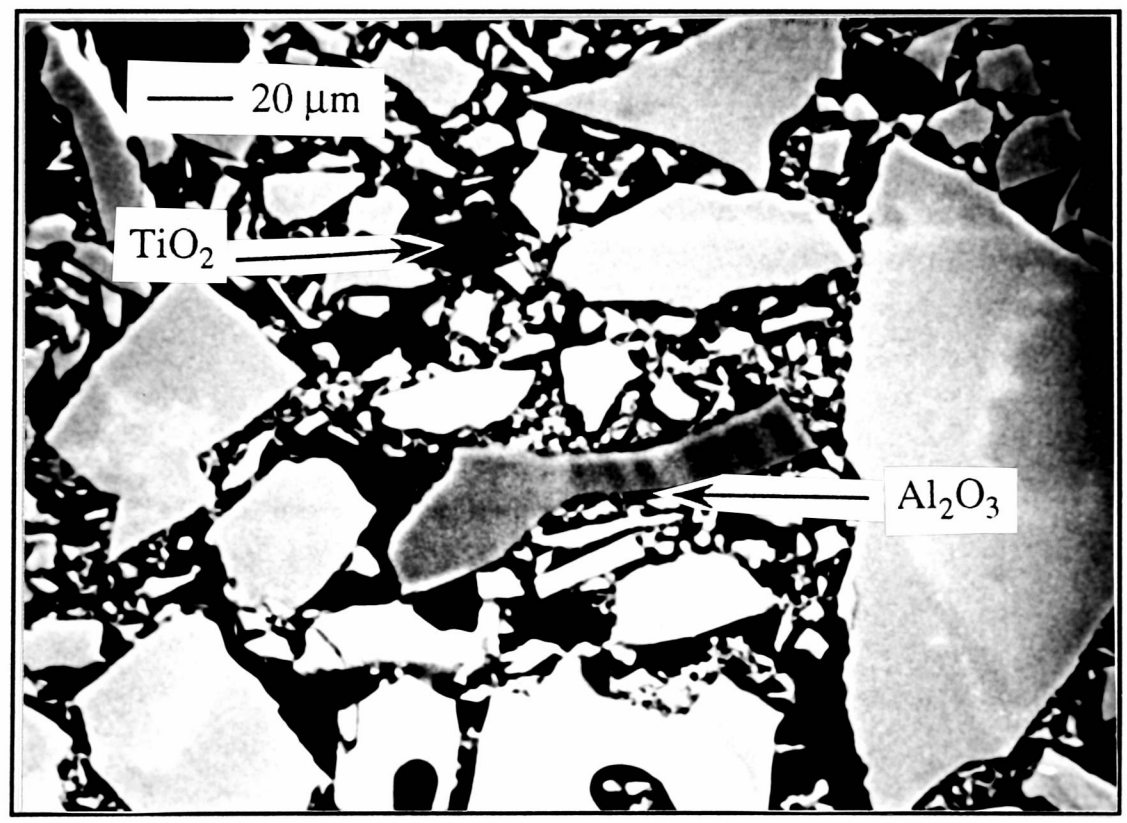


Figure 97: Micrograph of an impurity phase found within Zircosil filler mag = x 2,600

The filler is produced by grinding of the granular zirconium silicate, so the phase separation should be evident in the stucco itself. The micrograph in Figure 98 shows that this is indeed true, with further investigation revealing the presence of similar phase separation within other zircon sand grains (Figures 99 and 100). Note that Figure 98 depicts a grain within an actual mould sample, whereas Figures 99 and 100 are grains which were unused and prepared specifically for microstructural examination. It can be concluded that the source of the impurity phases within the refractory filler is the zircon mineral itself. Though the phases form only a small percentage of the overall section of sand grains, when ground to a finer particle size, they will form Zircosil particles consisting entirely of unwanted phases. The types of phases encountered, such as calcium phosphate, are indicative of fossilised sea shell material. This is consistent with the fact that supplier sources of zirconium silicate are usually from marine sedimentations.

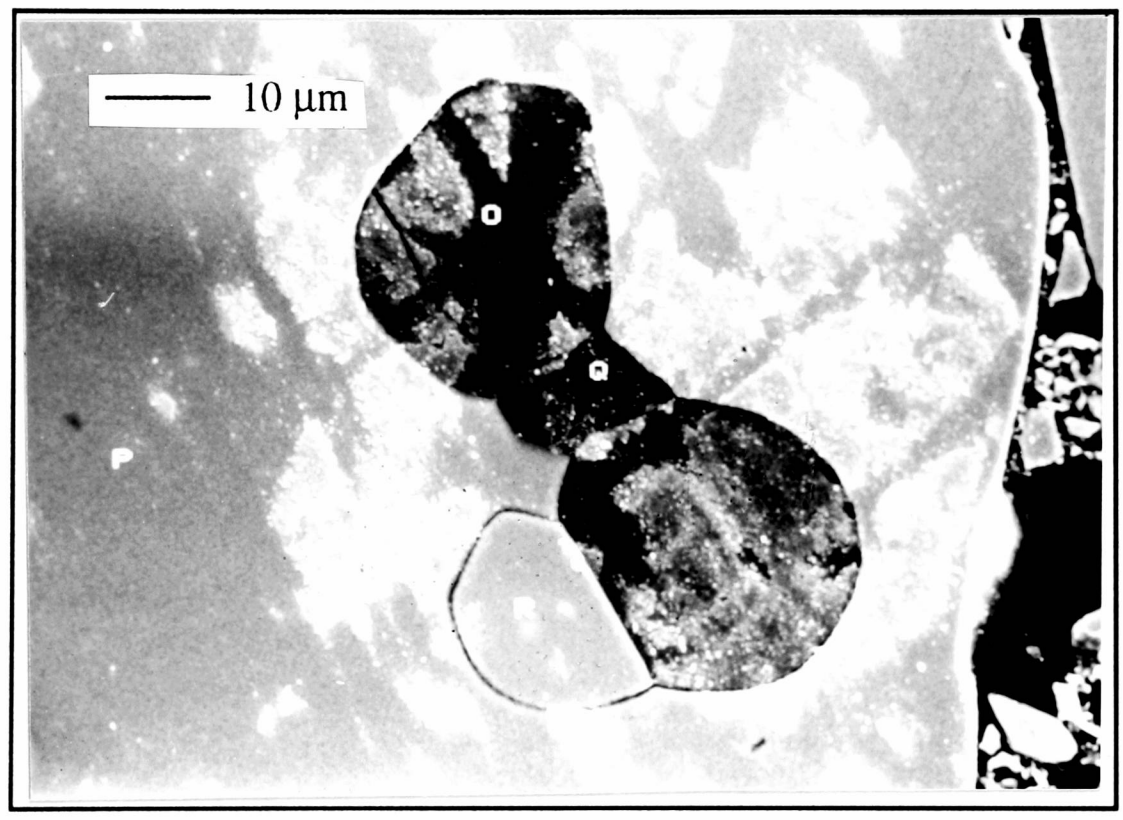


Figure 98: Phase separation within a zircon sand stucco grain (mag x1,050)
O = calcium phosphate
P = zirconium silicate
Q = silica
R = iron sulphide

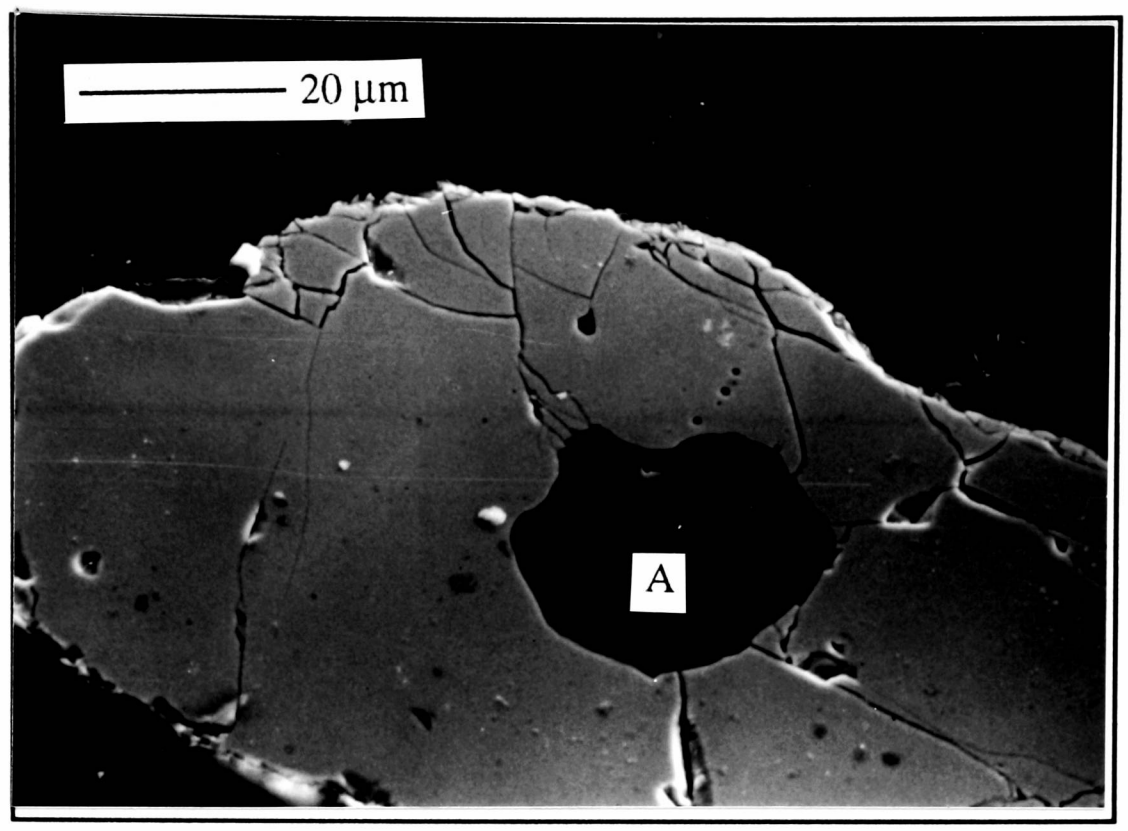


Figure 99: Phase separation within a zircon sand stucco grain mag = x 730
A = alumino-silicate

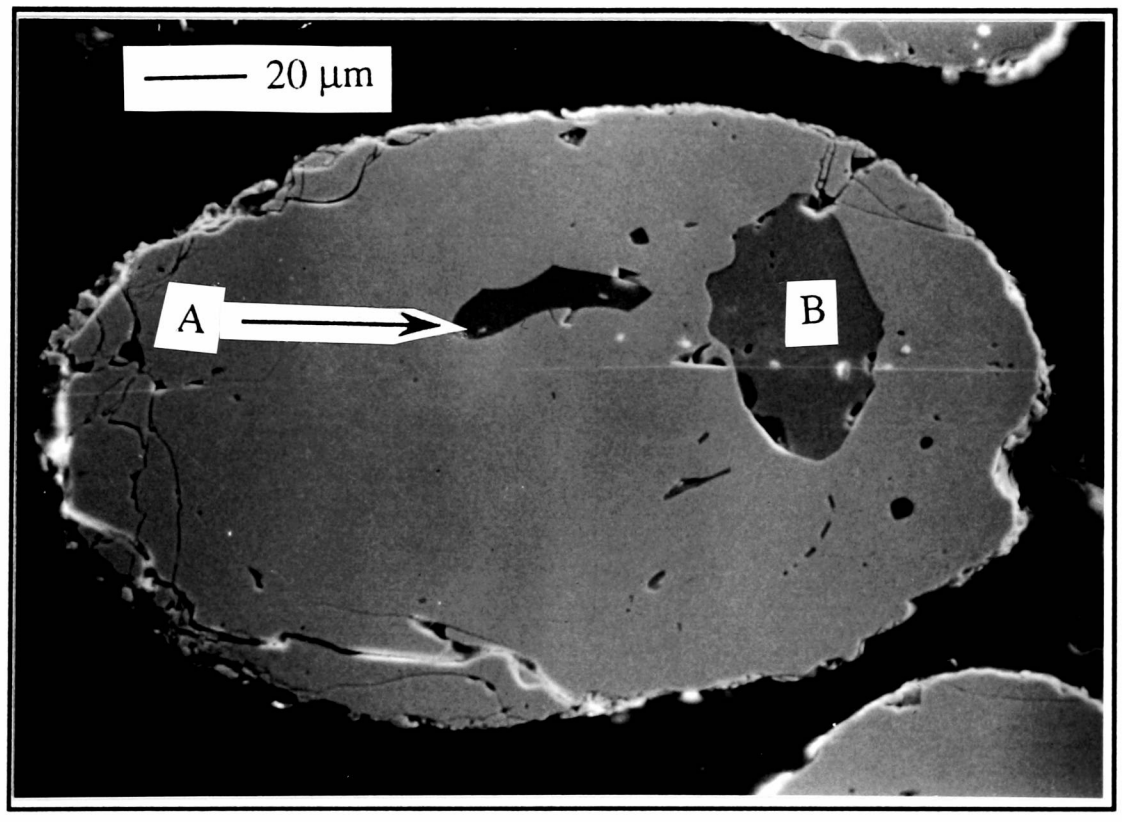


Figure 100: Phase separation within a zircon sand stucco grain mag = x 520
A = silica
B = calcium phosphate

The presence of the separation alone does not prove that this is the source of the elements within the silica binder. Evidence to suggest this is provided by a sample of filler and binder mixed together and fired at 1,000°C for 60 minutes to simulate the firing of the moulds. Analysis of the silica reveals a series of compositions (Table 17) that are comparable with those found earlier within a mould sample. Repeating the same procedure with stucco instead of filler produces no interaction, which indicates that leaching of elements into the binder is controlled by the surface area of phase separation in contact with the silica. The separation within the stucco tends to be enclosed, with very little surface area in contact with the binder. The filler, on the other hand, contains very many small particles in which the entire surface area consists of an unwanted phase in contact with the silica. In this case leaching of the elements is very likely and interaction will take place.

Table 17: Some of the silica compositions found within a mixture of filler particles and colloidal silica binder fired to 1,000°C for 60 minutes

	Atomic Percentage									
Region	Si	O	Ca	Na	Fe	Zr	Al	K	P	S
1	13.451	64.564	0.188	0.540	0.162	0.866	20.186	-	-	0.043
2	25.965	64.757	0.270	0.295	2.611	0.104	5.745	0.112	-	0.140
3	12.607	63.380	0.039	0.075	0.403	0.198	23.268	-	-	0.031

It is assumed that elements leach from the phase separation into the binder. The mould processing stage at which this interaction takes place is a little unclear. A slurry,when left to settle out, will give two distinct layers; one of liquid silica binder and the other of ceramic filler. The binder can be decanted from the surface of the ceramic, gelled, dried and dissolved in concentrated hydrochloric acid to form an aqueous sample which can be analysed for trace elements by Atomic Absorption Spectrometry. Analysis of a secondary slurry binder indicated the presence of nickel (0.045%) and iron (0.13%), but none of the other impurity elements were found. This suggests that the acidic binder may be attacking the stainless steel mixing container but does not seem to be leaching elements from the filler.

The variable composition of the binder phase is also indicative of leaching during the firing of the mould. If elements entered the binder during the slurry stage they would be intimately mixed and dispersed throughout the silica, giving rise to a single composition throughout the mould section. During firing,when the binder has gelled, and is held in a rigid structure, leaching would produce localised and variable binder compositions. As such, transfer of elements appears to take place during the firing stage.

However, though this may well be the case with alcohol based binders, water based binders appear to pick up impurity elements during the slurry stage as well. Samples of Zircosil (150g) were mixed with distilled water (200 ml) and ball milled for 24 hours. The samples were allowed to settle and the water was carefully removed from the surface of the refractory with a syringe before being dried using the application of heat until only a residue was left. This residue was then mounted onto an SEM stub and analysed using EPMA. A summary of the results is shown in Figure 101. Zircosil 200 and 200M are both zirconium silicate refractory flours, the only difference being that 200 is just milled Zircon, whereas 200M is ground from Zircon which has been calcined at high temperatures for a long period of time. Calcination is reputed to remove contaminants and these refractories are used extensively throughout the investment casting industry because in practice they do reduce the incidence of mould failure due to inconsistent structural behaviour. It seems that elements are not leached into an alcohol based binder but do dissolve in a water based binder whilst in the slurry. As such, elements enter the silica matrix of a mould during both firing and slurry production. The route seems to be dependent upon the medium in which the silica is dispersed i.e. alcohol or water.

In this case, although the overall level of contaminants on the surface of the particles seems to have been reduced by calcination, certain elements such as sulphur and calcium have been dramatically increased. This could be due to contamination from the tunnel kiln in which calcination took place, or through interaction with the vessel into which the ceramic must have been placed during firing. It is believed that, though surface contaminants can be reduced to a certain extent, the main body of phase separation will still be present. The elements are present in the form of high temperature oxides which, by their very nature, are less reactive with other substances. As such, using the calcined refractory would marginally improve the performance of the binder but the elements would still be available to leach into the silica, albeit at a slower rate.

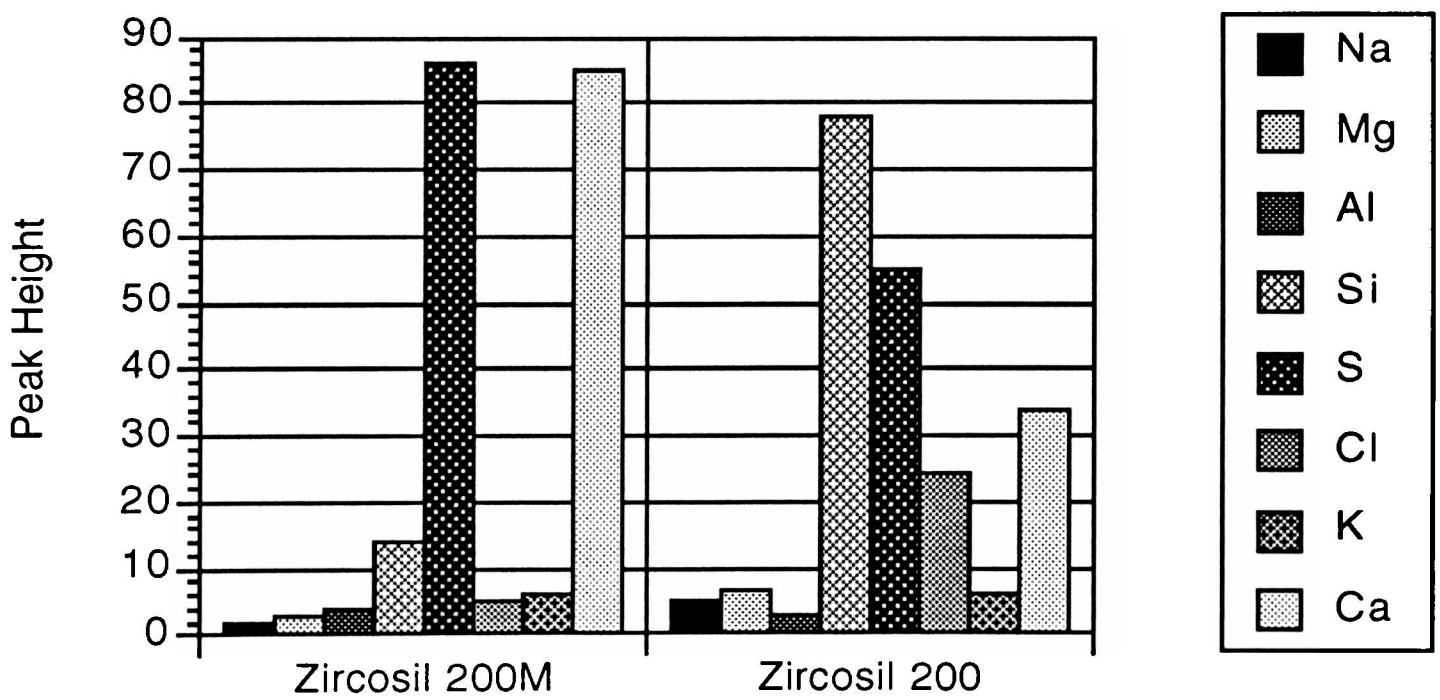


Figure 101: Impurity elements found on the surface of Zircosil refractories

4.2.2: Characterisation of Zircon Sands

The impurity elements found within the silica binder have been shown to originate from the filler and ultimately the stucco material. Since the source of the phase separation is considered to be shell deposits within the zirconium silicate mineral, it follows that refractories from different geological locations may contain differing amounts and even types of deposit. It may be useful to identify the refractory source which contains the least amount of phase separation so that foundries and suppliers are aware of the suitability of this material for investment casting. As such, samples of Zircon Sand from four different locations were obtained and characterised using SEM, EPMA and image analysis.

The samples were donated by a refractory supplier (Cooksons Ceramics Ltd.) and were from the following sources:

Sand A ..... Australia
Sand B ..... Australia
Sand C ..... Australia
Sand N ..... Florida

The only information supplied with the samples was the country of origin, with samples A, B and C coming from three different mineral mines in Australia. The investigation began with a similar experiment to that carried out in Section 4.2.1 to determine the levels of contamination on the surface of the refractory particles. A sand sample (150g), mixed with 200 ml of distilled water, was placed into a plastic container and ball milled (without a milling medium) for 24 hours. The sample was then left to settle and the water decanted from the surface of the ceramic using a syringe before. This water, together with a control sample of distilled water, was dried to a residue by the application of heat. The residue was then mounted as an SEM sample and analysed using EPMA.

The results of this analysis are shown in Figure 102. The water control sample did not leave any residue and analysis of the plastic container showed no evidence of inorganic phases. Similar analysis of the SEM stub revealed only aluminium and a small amount of copper. As such, the elements detected could not have originated from any other source than the stucco. Table 18 shows a summary of the types of phase separation found within the samples. Though the types of phases encountered are similar in all of the sands, there are some notable exceptions. Sands N and C are the only ones which contain what appears to be a Ca_3PO_4 phase and also have relatively large amounts dissolved in the water. Sand A contains a small amount of calcium which is incorporated into other phases. This seems to prevent dissolution and the water contains very little calcium. Sand B has no calcium phases and no calcium ions dissolved in the water. It does however release a lot of silicon and sulphur ions into the water. All sands seem to contain many examples of phase separation which is based on an alumino-silicate system, with various other elements incorporated within the basic structure.

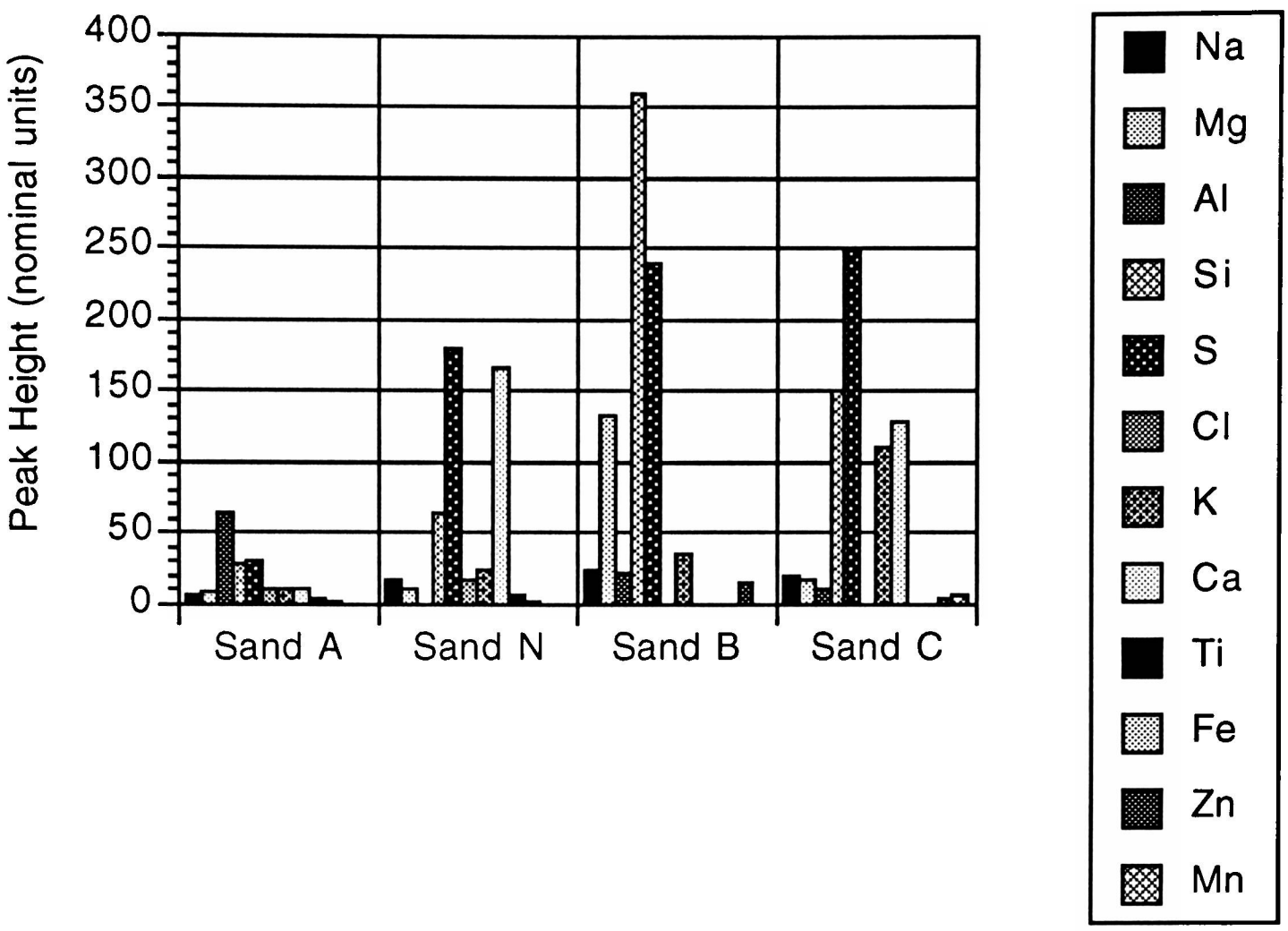


Figure 102: Column chart depicting the elements found on the surface of four Zircon Sand refractories

Table 18: Table showing the elements found in individual occurrences of phase separation within four Zircon Sands

Sand A	Sand B	Sand C	Sand N
Si	Si	Si	Si
Ti	Si/Al	Si/Al	Si/Al
SiP	Si/Al/T	Si/Al/K	Si/Al/K
Si/Al/Ti	Si/Al/K	Si/Al/K/Na	Si/Al/P
Si/Al/P/K	Si/Al/K/Zr	Si/Al/Na/Ca	Si/Al/Mg/K/Ti/Fe
Si/Al/Ti/Fe/K	Si/Al/Ti/Fe	Si/Al/K/Fe	Si/Al/Mg/K/Ti/Fe/P
Si/Al/Na/K/Ca	Si/Al/Ti/Fe/S/K	Ca/P	Si/Al/Na/P/Cl/K/Ca/Fe
Si/Al/Na/K/Cl/S			Si/P/Ca
Si/Al/Na/Co			Ca/P
Si/P/Cl/Co			
Si/P/Cl/Ca			
P/Cl/Ca			

Based upon the evidence so far, it could be stated that sand A contains a lower level of impurities and would be a better refractory choice. However, until now we have only assessed soluble impurity levels on the surface of the particles, and though these may enter the binder during the slurry stage we have also shown that many elements are leached into the silica during firing of the mould. To assess the amount of impurities within the refractory as a whole was a difficult task. Refractory suppliers state that the zircon has been separated from other mineral sands by ore dressing techniques and a chemical analysis is supplied (see Appendix 5). However, this type of analysis does not include some of the other phases such as calcium phosphate and provides little evidence as to the form and distribution of the impurities themselves. Therefore an analysis of the separation was carried out using SEM, image analysis and statistical techniques.

The experimental procedure of the technique has already been covered in Section 3.5.3 and the extensive individual results are to be found in Appendix 2. The results can be combined to give a mean value for the % phase separation (by area) and are shown in Table 19. Sand N now displays the lowest mean impurity level unlike before when sand A appeared the better. The high variances found within the results for sands A and B may be responsible for this result and this high variability (i.e. large spread in the values) is indicative of the fact that the phase separation within these sands tends to exist as very large individual particles as opposed to small areas within the bulk of the zircon grains. As such, fewer impurity elements will dissolve into the water with sand A, not because there is less phase separation, but because the surface area of separation in contact with the water is less. Having suggested that there is a large amount of inherent variability between the four results the question arises as to whether there actually is a difference between the values obtained for phase separation or whether the differences are solely due to the variance. This question can be reasonably answered using the F-Hypothesis test (Appendix 1) from which inferences can be made about the overall populations from which the samples have been drawn. The results of this test are tabulated in Table 20. Since, the tabulated values of the F statistic for both the 90% and 95% confidence limits are numerically larger than the calculated value, it can be assumed that the samples investigated have all been taken from significantly different populations. All four zircon sands have different amounts of phase separation, and the differences in the mean values are not a result of the high variances found in the samples.

Therefore, when choosing a zircon source, both the amount of phase separation and the distribution should be taken into account since both parameters are important. In this case it would appear that sand N displays the best overall characteristics and sand B with the highest impurity level would be the least favourable refractory to use.

Table 19: Statistical interpretation of image analysis results for Zircon Sands

Sample	Values obtained for % phase separation (by area)	Mean	Variance (s^2)	Coefficient of variation
A	0.28, 0.15, 0.23, 0.287, 1.305, 11.65, 5.11, 0.278, 0.826, 0.26, 0.17, 22.08, 52.94, 0.05, 29.4, 0.317, 0.68, 0, 0, 0.317	6.32	185.36	2.15
B	0.9, 1.925, 1.122, 1.655, 3.508, 2.141, 1.45, 3.995, 0.237, 1.247, 2.36, 1.177, 0.381, 1.85, 42.99, 0.386, 67.20, 3.79, 23.586, 0.979	8.55	311.20	2.06
C	1.848, 1.579, 3.124, 3.633, 3.418, 3.145, 4.09, 6.05, 10.44, 8.341, 2.89, 3.72, 4.43, 3.04, 1.696, 7.18, 7.727, 7.694, 7.789, 9.47	5.06	7.58	0.54
N	0.508, 2.17, 1.219, 0.93, 0.625, 2.01, 17.61, 2.026, 0.42, 0.126, 0.587, 1.62, 2.07, 1.513, 0.129, 0.511, 0.101, 0.62, 1.47, 0.645	1.85	14.25	2.04

4.2.3: Summary

Investigation has revealed that the Zircosil refractory filler used in the slurries is phase separated and contains a variety of constituents other than zirconium silicate. This separation is also found in the parent zircon mineral (Zircon Sand) from which the filler is prepared by grinding. The types of phases encountered, such as calcium phosphate, are indicative of fossilised sea shell material. This is consistent with the fact that supplier sources of zirconium silicate are usually from marine sedimentations. Though the separated phases form only a small percentage of the overall cross section of refractory grains, when ground to a finer size they form refractory particles consisting entirely of unwanted phases. The grinding process also significantly increases the surface area of separation in contact with the binder which will make leaching of elements into the silica easier. This is substantiated by the fact that Zircon Sand does not release elements into the binder phase, but Zircosil does.

Table 20: Calculation of the F-statistic for the % phase separation results from four Zircon Sands

Sample Means	6.32, 8.55, 5.06, 1.85
Between column variance (a)	7.8263
Within column variance (b)	5.445
Calculated F statistic (a/b)	1.437
Degrees of freedom (numerator)	3
Degrees of freedom (denominator)	76
Tabulated F statistics	
dx = 0.90	2.18
dx = 0.995	4.73

Samples of filler and binder, mixed together and fired at 1,000°C, reveal the leaching of impurity elements into the silica phase. The processing stage at which the elements enter the silica matrix appears to be determined by the nature of the binder itself such that a water based binder will dissolve impurity elements at both the slurry and the firing stage. Alcohol based binders however contain no elements during the slurry stage and all transfer of material appears to take place during the mould firing stage.

Calcination has been shown to reduce although not entirely eliminate the impurity phases from the filler materials. This is probably due to the fact that firing at high temperatures will cause the phase separation to oxidise and make leaching of individual elements more difficult. The high temperature cycle does not remove the contaminants but instead changes the physical form to some degree. Characterisation of the type and amount of phase separation within Zircon Sands from different global sources has shown that different minerals from different sources contain varying amounts of phase separation.

4.3: Basic Silica Binders

4.3.1: Structure

In order to understand the properties of the mould it was necessary to first establish the phase structure of the two silica based binders currently used in mould production at Deritend Precision castings; Syton X30 and Silester XAR. Full specifications are given for these binders in Appendix 3. Samples of the binders were gelled, dried and fired to 1,000°C for 60 minutes in a platinum crucible. Since the ceramic moulds are subjected to the same thermal treatment, it was assumed that the binder phase structures would be comparable. The phase structures of the individual binders have already been established at 1,000°C (Section 4.1.4), but as a revision Syton X30 is crystalline and Silester XAR is amorphous.

The physical structures of the binders was very different. Silester XAR is a mixture of long chain polysilicate molecules in an alcohol medium. Syton X30 is a colloidal silica sol, consisting of a suspension of discrete silica particles in an aqueous solution. The individual particulate structure can be easily seen in the TEM microscope (Figures 103 and 104). The sol has a very small and uniform particle size distribution of approximately 16 nm as measured from the negative. Since the samples were dried by the application of heat, the agglomeration is due to gellation of the sol.

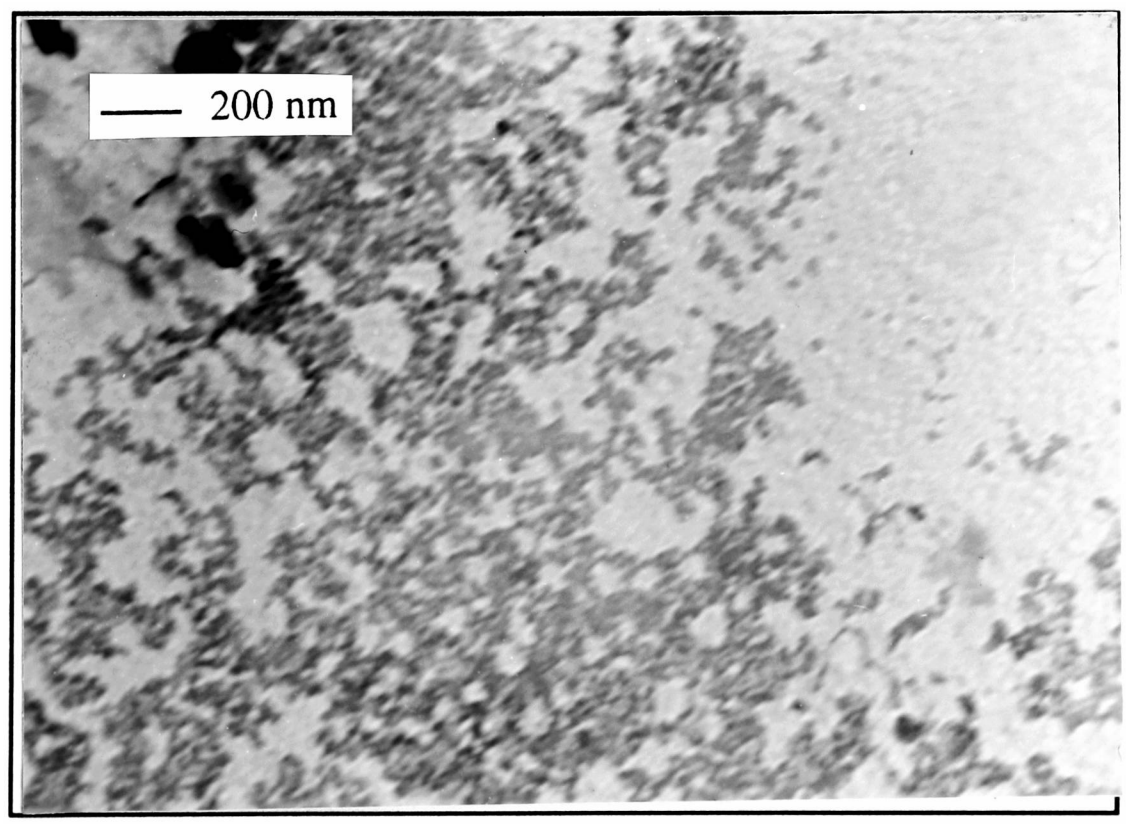


Figure 103: TEM micrograph of Syton X30 mag = x 36,000

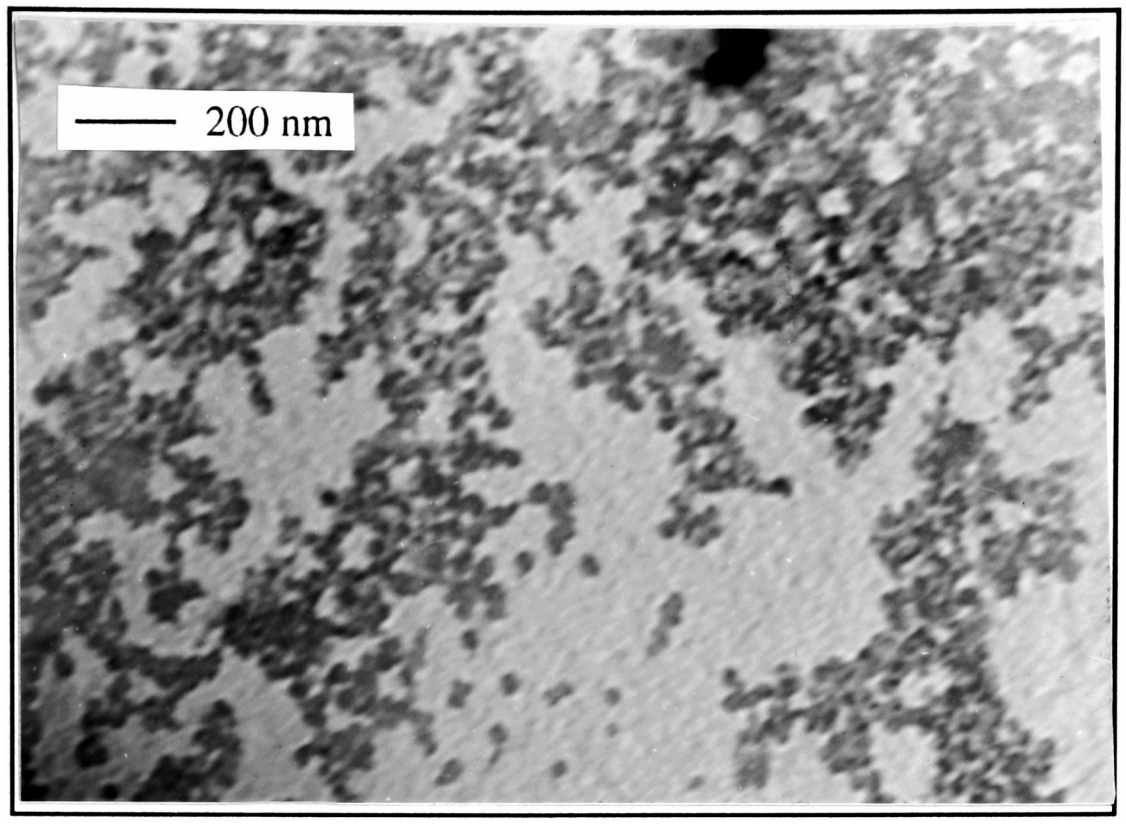


Figure 104: TEM micrograph of Syton X30 mag = x 46,000

4.3.2: Thermal Response

DTA was used to investigate the crystallisation/sintering behaviour of the binders during firing and casting. The samples were subjected to two thermal profiles; the firing schedule to simulate the firing of a mould, and the casting schedule to reflect the casting of metal into the ceramic. It should be noted that the thermal profiles were limited by furnace heating and maximum temperature capabilities.

The firing trace for Syton X30 is shown in Figure 105. During the firing schedule the binder displays a number of exothermic and endothermic peaks up to approximately 500°C. Most of these are due to the displacement of water from the gel structure, since they occur at temperatures which correspond to the volatilisation of water molecules from the surface of the silica and the dissociation temperature for water molecules. The rise in the base line of the plot between 400 and 800°C is due to particle coalescence and the onset of sintering. A sharp exothermic peak at 961°C is indicative of crystallisation and more especially it is the formation temperature for cristobalite. This measured temperature is higher than that at which crystallisation appears to take place in the sol (see Section 4.1.4) because DTA is largely dependent upon the heating rate and differences in this rate will affect the temperatures at which various thermal events occur. Cristobalite formation in silica sol gels is believed to take place because of the presence of the sodium stabilising ions. This concept will be explored further in Section 4.3.3.

This is verified by the presence of an endothermic peak at approximately 240°C on the casting trace (Figure 106), which is the α to β cristobalite transformation temperature. Apart from this phase

transformation the silica binder is relatively inactive during the casting cycle, a situation which is to be expected with a crystalline material. The constraints imposed upon the structure by the presence of crystalline bonds prevents physical or thermodynamic changes from taking place.

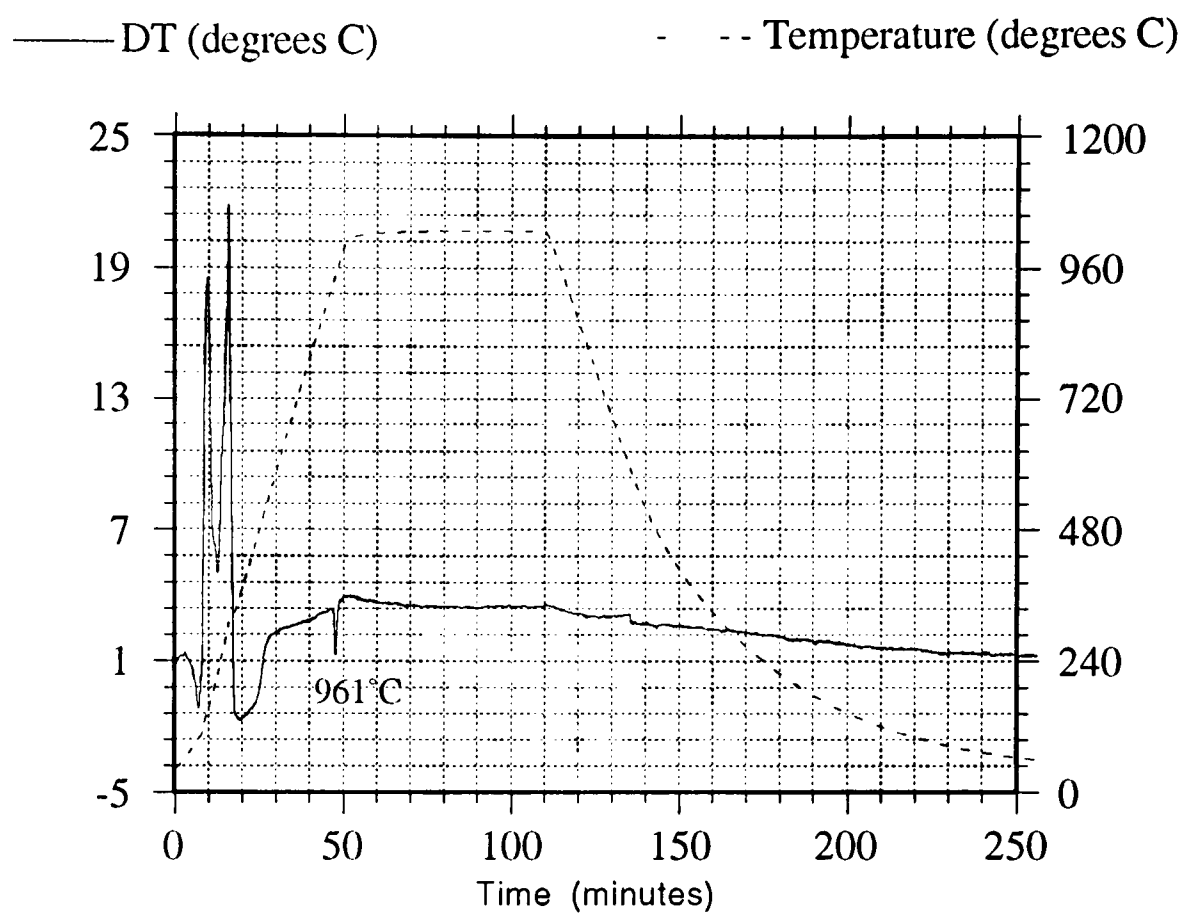


Figure 105: DTA trace for gelled Syton X30 - firing schedule

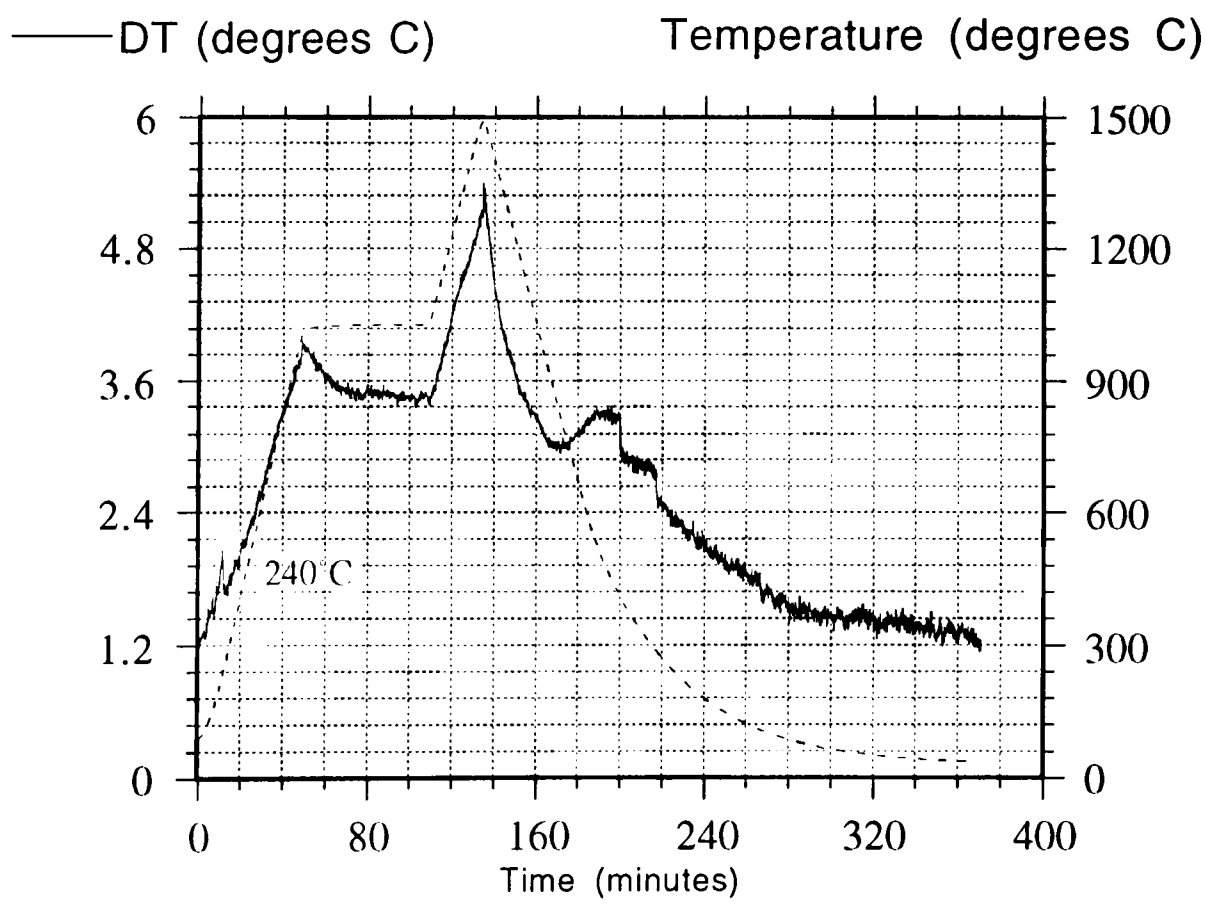


Figure 106: DTA trace for Syton X30 - casting schedule

The volume changes accompanying sintering and phase changes in the silica sol binder can be monitored using dilatometry. As for the DTA experiments, firing and a casting schedules were used to simulate the thermal regimes to which a mould would be subjected during use. In this case, however, equipment limitations meant that the maximum temperature for the casting trace was 1150°C which is considerably lower than that experienced within larger investment casting moulds (see Section 4.6). As such, the values obtained for expansion/contraction were used for comparison purposes only.

The dilatometry firing trace for Syton X30 is shown in Figure 107. Due to particle coalescence and sintering the sample undergoes extensive linear contraction (15%) until approximately 850°C. At this point crystallisation takes place and the crystalline structure remains structurally stable for the rest of the firing cycle. The stability observed in the DTA casting trace is also encountered in the dilatometry casting trace (Figure 108). A linear expansion of approximately 1% occurs at 250°C which is probably due to the α to β cristobalite transformation which is accompanied by a 1.5% volume expansion due to molecular reordering. During the remainder of the cycle the binder remains fairly inactive, with only a small expansion as the temperature is increased to 1150°C.

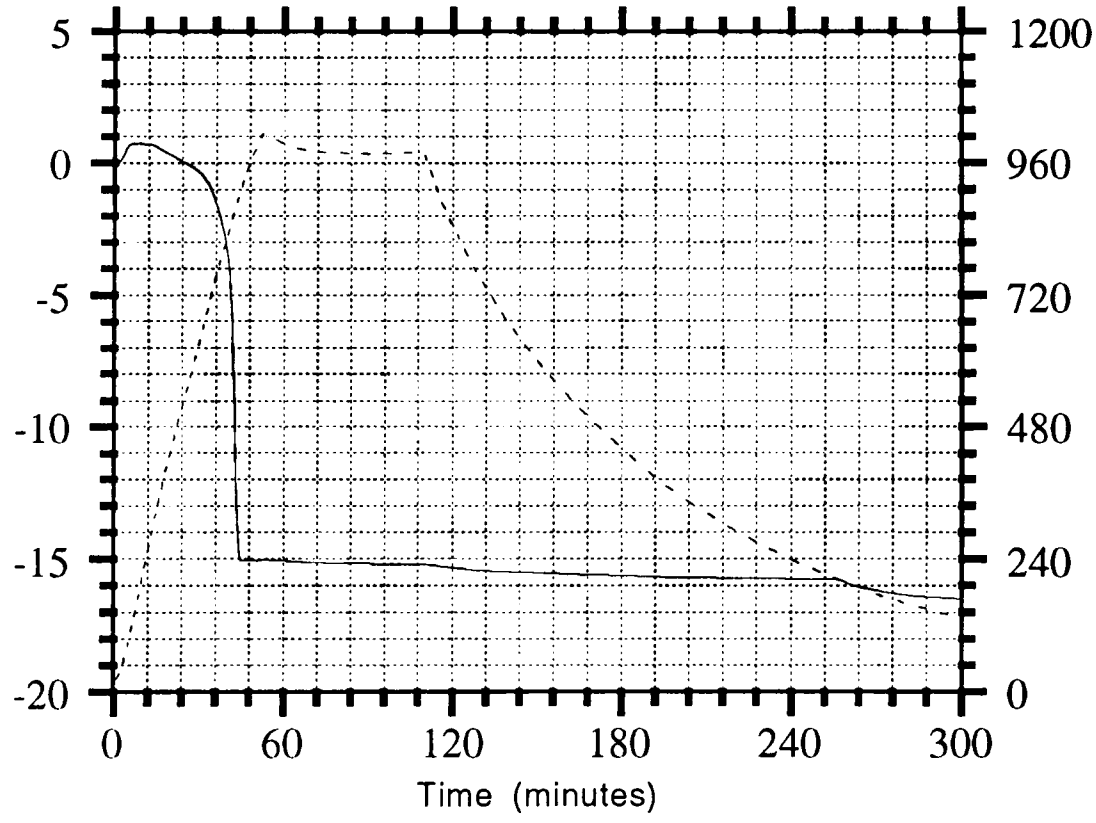


Figure 107: The dilatometry firing trace for Syton X30

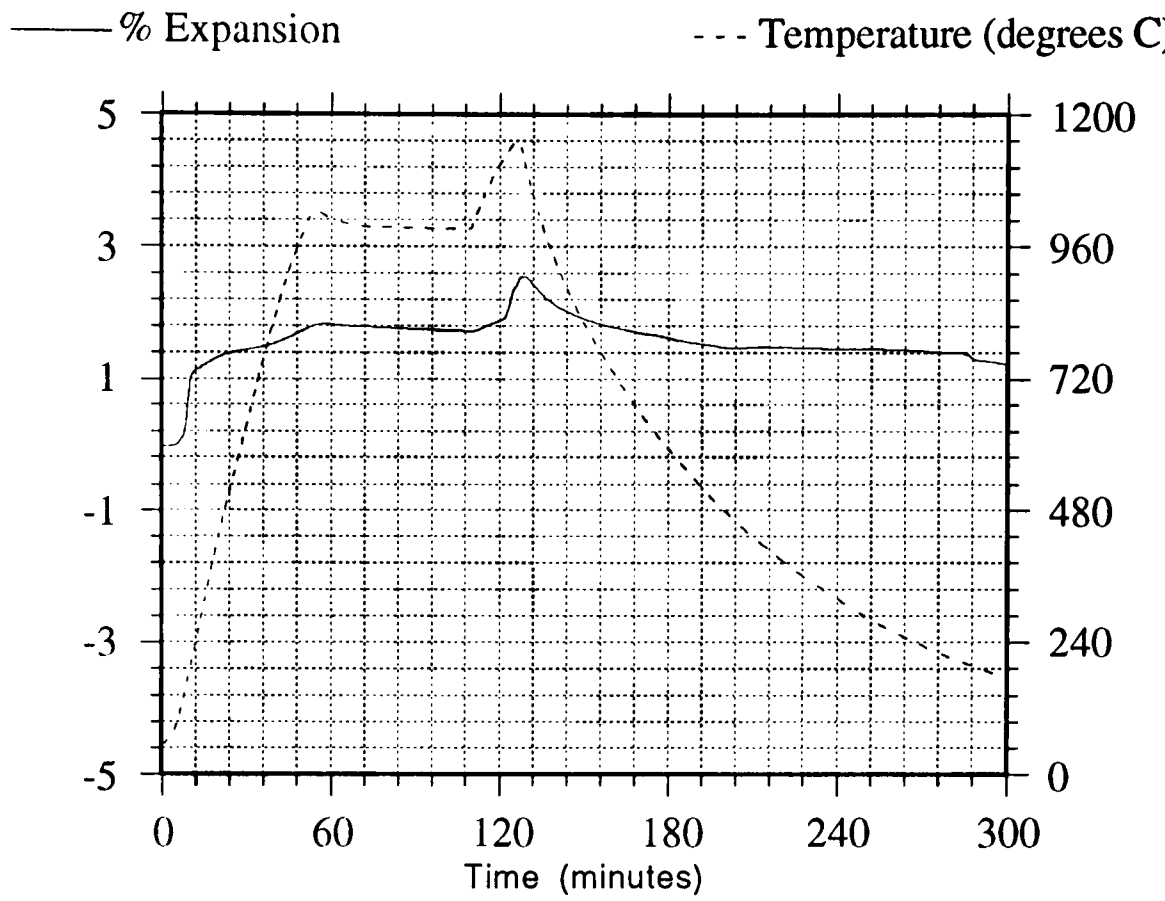


Figure 108: The dilatometry casting trace for Syton X30

The thermal behaviour of Silester XAR is very different. This is due in to the fundamental structural differences between the two binders and also to the different crystallisation behaviour. The DTA firing trace for XAR is shown in Figure 109. The trace also shows a number of exothermic and endothermic peaks up to 500°C, but they are significantly different to those found with Syton X30. These peaks are undoubtably due to the liberation of alcohol from the gel and, as such, each event will occur at different temperatures to the water based gel. All solvent seems to have been removed by 700°C, at which point a rise in the base line of the trace is indicative of coalescence and sintering. The rise in the base line continues until the thermal hold at 1,000°C is reached. Note that there is no exothermic peak at 960°C as for the colloidal sol as crystallisation does not occur in an ethyl silicate gel until 1350°C. The binder is relatively inactive during the remainder of the firing cycle, but this is expected once the sintered amorphous gel structure has been formed.

As with Syton the binder is thermodynamically inactive during the casting cycle (Figure 110). Since cristobalite has not been formed the inversion at 240°C during heating is not present. Apart from changes in the gradient of the base line during thermal cycling, the DTA trace is fairly constant. During the initial reheating of the sample there is a dip in the base line that is probably due to further sintering and reordering of the silica structure. This is more likely to take place with Silester since the silica remains amorphous and is structurally unconstrained.

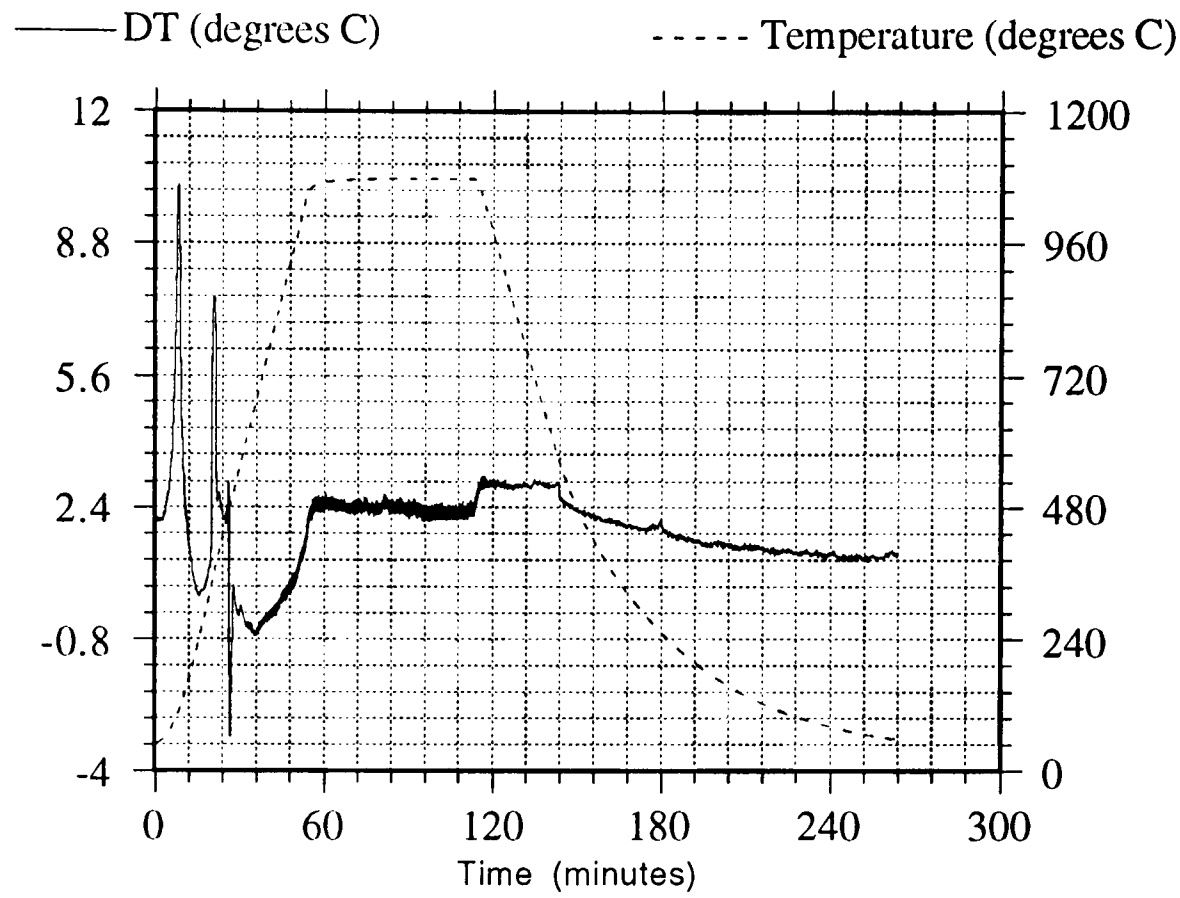


Figure 109: DTA firing trace for Silester XAR

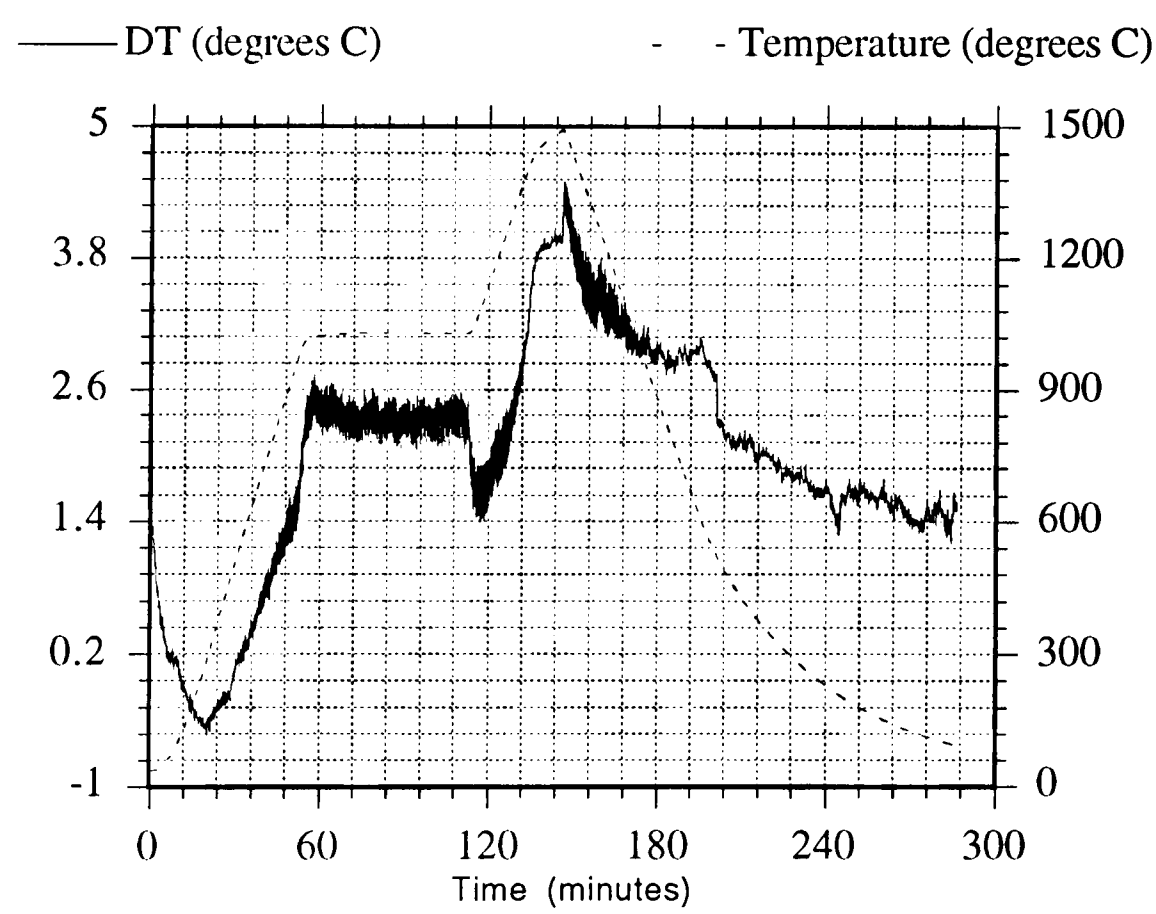


Figure 110: DTA casting trace for Silester XAR

The lack of crystallisation is also apparent in the dilatometry traces for the ethyl-silicate binder. During firing (Figure 111), the binder begins to sinter at 550°C and extensive volume contraction of 17% occurs during heating to 1,000°C. Very little contraction takes place during the isothermal hold and the binder remains structurally stable during cooling. This behaviour is fairly analogous to the firing of the colloidal silica sol, but there is little similarity when the sample is reheated and subjected to the casting profile (Figure 112).

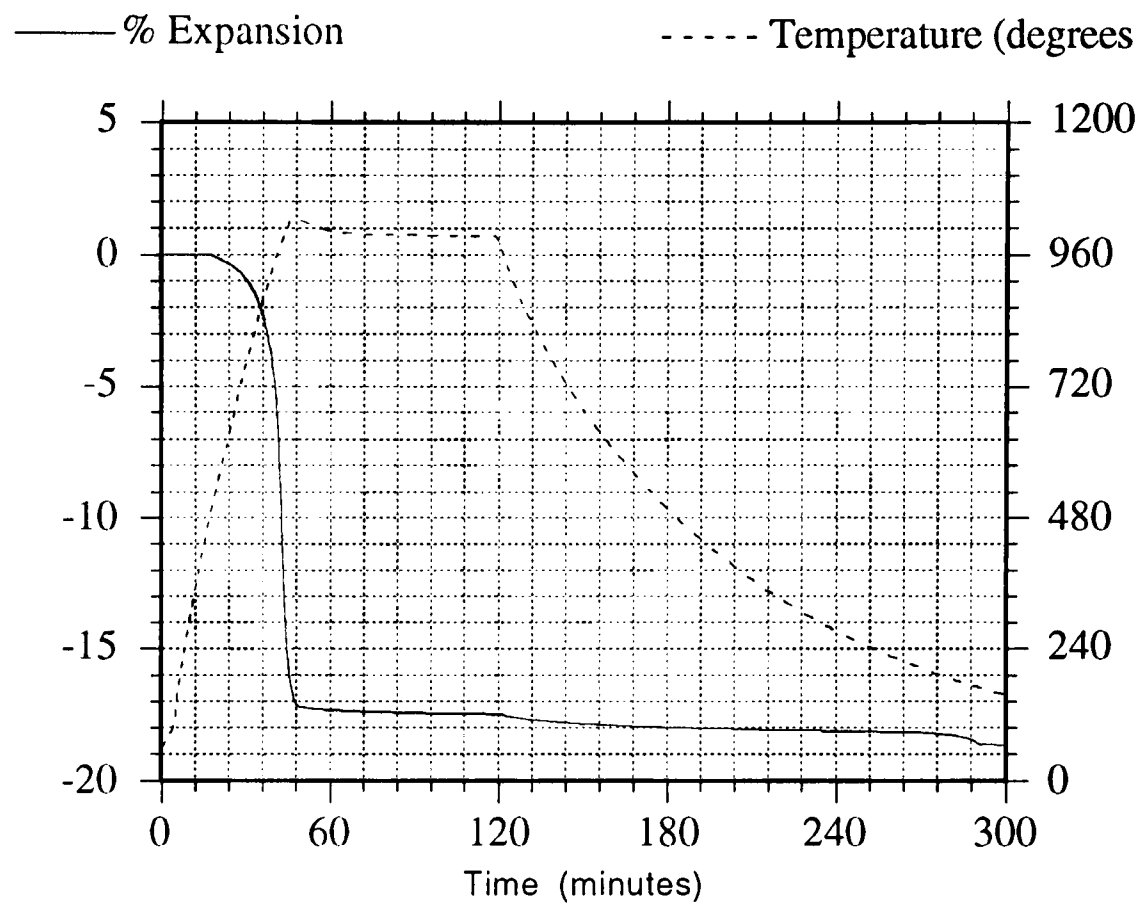


Figure 111: Dilatometry firing trace for Silester XAR

During the initial stages of reheating the sample undergoes a 2% expansion which may be the result of incomplete sintering which leaves pores within the silica structure. These pores contain air which expands during heating, giving rise to the unexpected expansion. At 750°C, however, the expansion is reversed and contraction begins to take place. This contraction continues throughout the remainder of the thermal cycle, resulting in an overall permanent displacement of 7%. The binder remains amorphous throughout and, although sintering and pore removal does take place, the structure never gains the inherent rigidity that the crystalline phase imparts to the colloidal binder. As such, the structure is relatively unconstrained and free to move which appears to be the cause of continued contraction during the casting schedule.

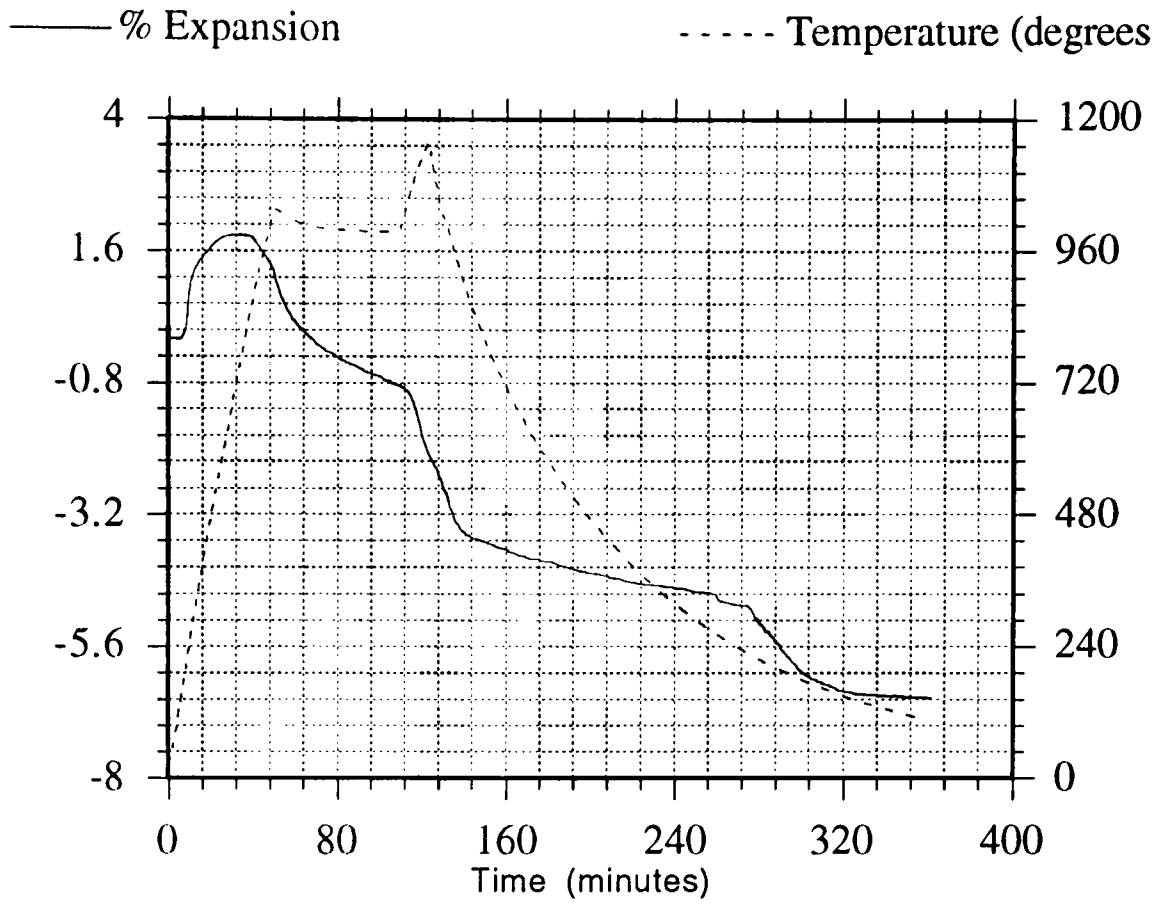


Figure 112: Dilatometry casting trace for Silester XAR

4.3.3: The Effect of Sodium on Colloidal Silica Sols

Most commercially produced silica sols are stabilised with sodium ions to prevent flocculation and gellation which prolongs the shelf-life of the sol. However, differences in the crystallisation behaviour of colloidal sols and ethyl-silicate solutions has highlighted the fact that the presence sodium induces crystallisation at much lower temperatures. Determining the manner in which the crystallisation is controlled by sodium should make it possible to either inhibit or promote a crystalline structure depending upon requirements. This degree of control should improve the performance of the sol in present binder applications.

Three commercially available colloidal silica sols containing differing amounts of sodium stabiliser were gelled, dried, fired and the crystallisation temperature determined by XRD. The results of this investigation, together with the general physical properties of the sols are shown in Table 21. Syton X30, with the highest sodium content, has the lowest crystallisation temperature. The opposite is true of Syton T40 which contains virtually no sodium since the sol is ammonia stabilised. It appears that the presence of sodium decreases the crystallisation temperature by the nucleation of cristobalite at lower temperatures. This lowering of the crystallisation temperature is also noticeable when comparing the phase structure of the binders fired to 1,000°C for 60 minutes (Figures 113, 114 and 115).

Table 21: Specifications and crystallisation temperatures for Syton silica sols (N.B. Syton is the trademark of Monsanto Plc)

SOL	SYTON X30	SYTON W30	SYTON T40 AS
APPROXIMATE PARTICLE SIZE (nM)	15	125	40
STABILISING ADDITIVE	sodium hydroxide	sodium hydroxide	ammonia
SODIUM CONTENT (% w/w sodium oxide)	0.34	0.13	0.08 max
CRYSTALLISATION TEMPERATURE (° C)	840 - 860	870 - 890	970 - 990

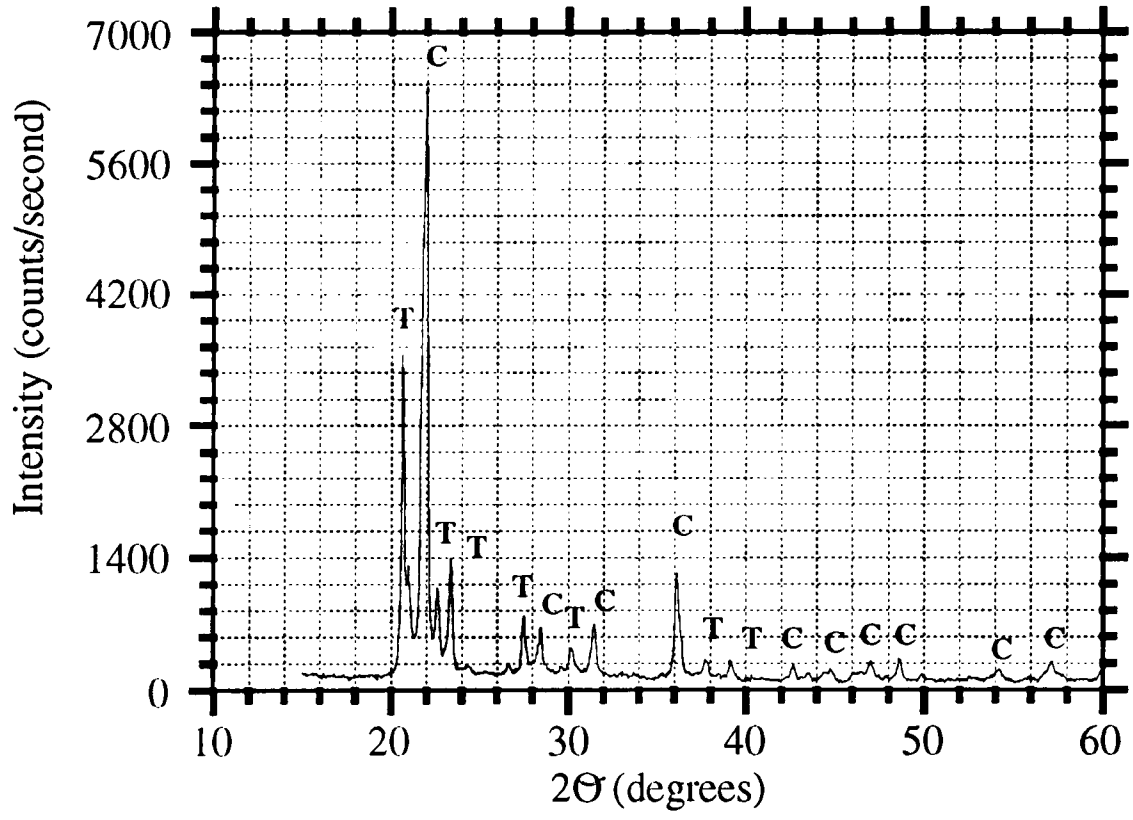


Figure 113: XRD trace for Syton X30 fired to 1,000°C for 60 minutes

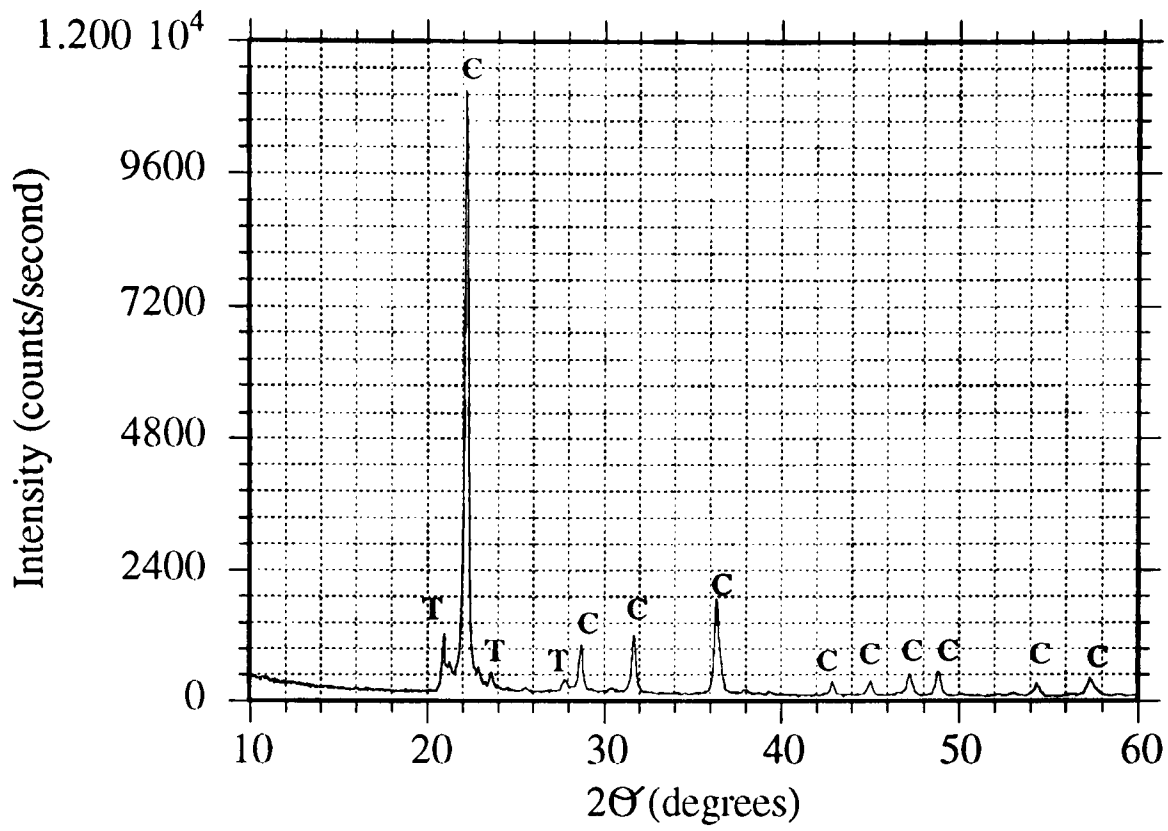


Figure 114: XRD trace for Syton W30 fired to 1,000°C for 60 minutes

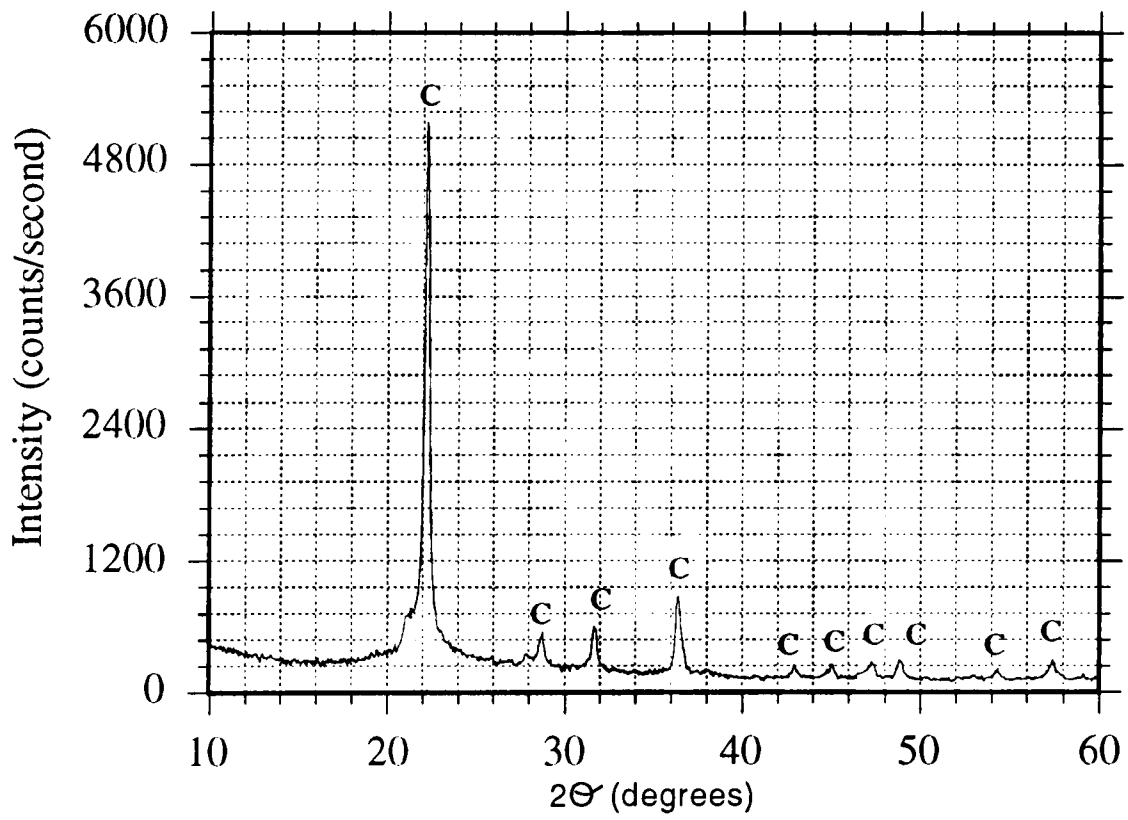


Figure 115: XRD trace for Syton T40 fired to 1,000°C for 60 minutes

At 1,000°C, Syton X30 has crystallised to form a mixture of α-cristobalite and S_1-tridymite. The cristobalite phase was formed at 840°C when the silica crystallised and the tridymite is present as the result of the partial transformation of cristobalite at 870°C (see Section 4.3.3). Full conversion does not take place because the silicate conversions are sluggish and take place only with the application of heat or over long periods of time. Syton W30, with a lower sodium content, crystallises to cristobalite at a higher temperature. The conversion to tridymite is reduced producing a much lower tridymite concentration. The crystallisation temperature of Syton T40 is higher than the other sols because of the absence of sodium. This prevents the conversion from taking place and the fired structure contains only cristobalite.

Therefore it appears that whilst the sodium stabiliser catalyses the formation of cristobalite, large amounts of sodium promote the formation of tridymite. To investigate this theory a series of Syton T40 samples, to which increasing amounts of NaOH had been added, were gelled and fired to 1,000°C for 60 minutes. The relative additions were made according to the calculations contained in Section 8.2.1, and a summary of the compositions are contained in Table 22. XRD was used to determine the phase structure of the samples and a comparison between the relative peak heights provided evidence of the relative amounts of each crystalline phase.

Table 22: Additions of NaOH to Syton T40

SAMPLE	Volume of Syton T40 (ml)	Weight of NaOH Additions (g)	Resulting wt% NaOH
1	20	0.0250	0.1015
2	20	0.0485	0.197
3	20	0.0726	0.295
4	20	0.0999	0.4058
5	20	0.1246	0.5061

Figure 116 shows that cristobalite formation is promoted by additions of NaOH up to 0.3 wt% as sodium acts as the nucleant. However, adding further NaOH reduces the amount of cristobalite because the crystallisation temperature is reduced below 870°C, enabling the conversion of cristobalite to tridymite to take place. This transformation is demonstrated by the fact that there is no tridymite present in the samples below 0.3 wt% NaOH (Figure 117), but above this figure tridymite begins to be produced.Therefore, the sodium content of a sol determines both the crystallisation temperature and the relative amounts of the crystalline phases that are present in the structure.

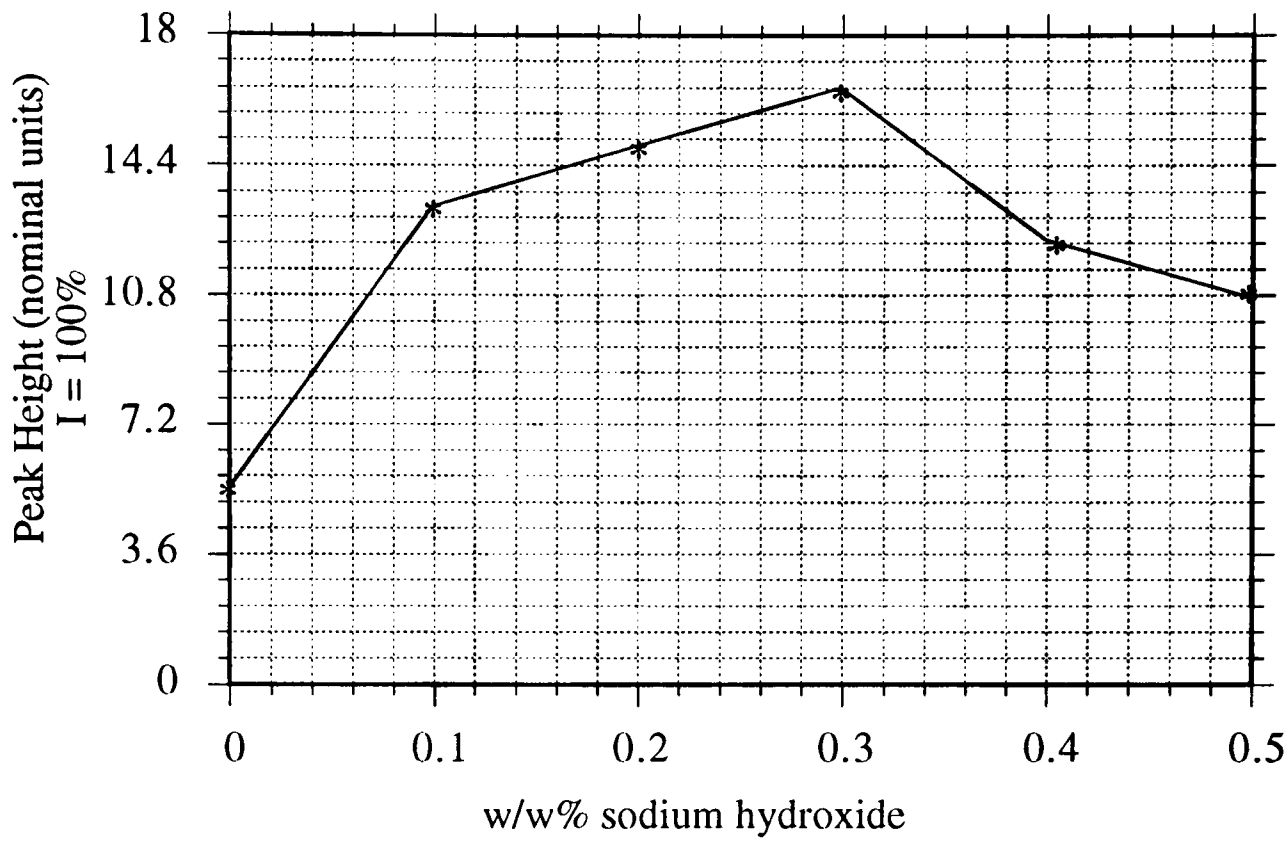


Figure 116: Cristobalite formation in Syton T40 as a function of NaOH content

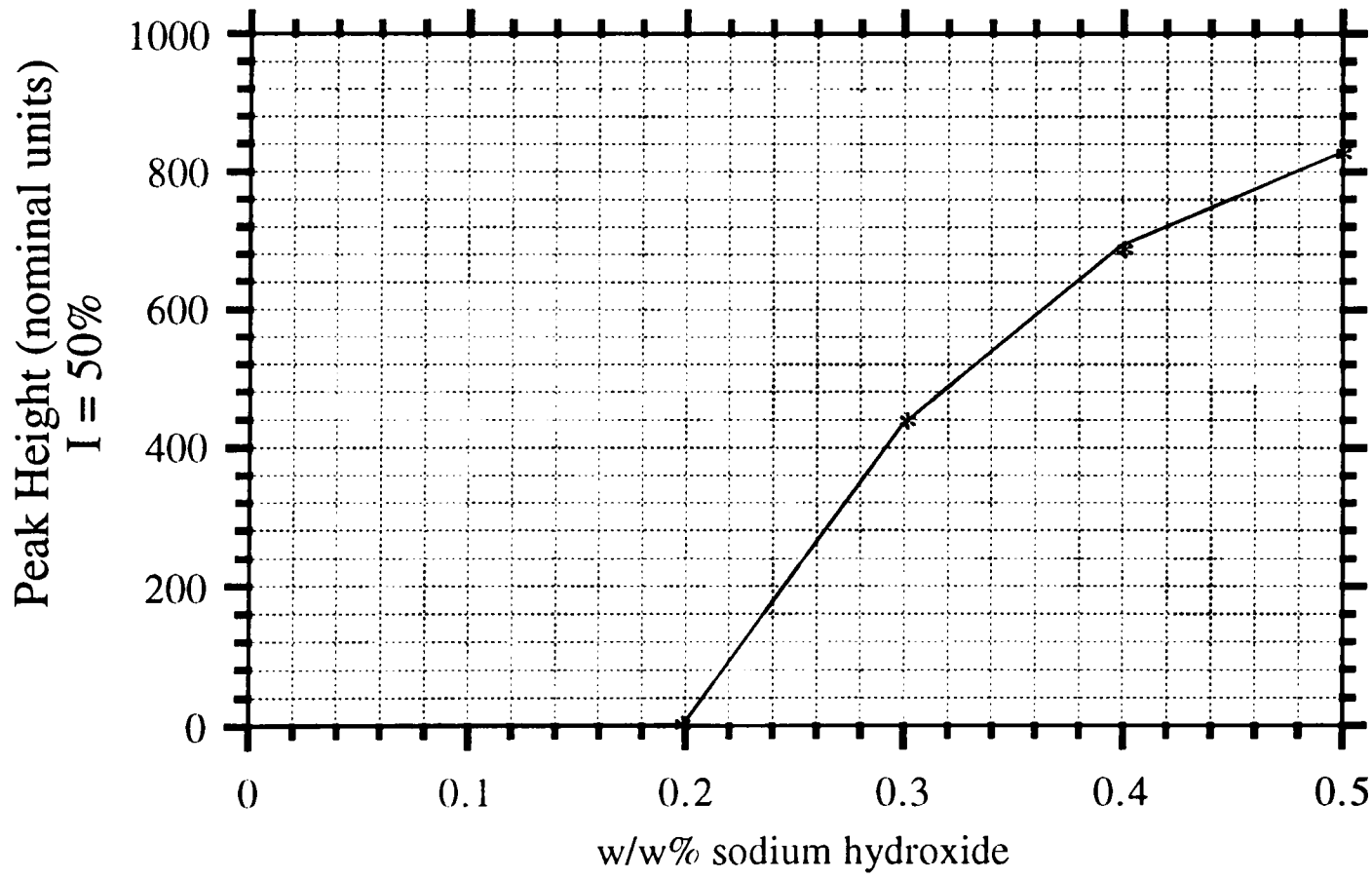


Figure 117: Tridymite formation in Syton T40 as a function of NaOH content

4.3.4: The Effect of Impurities

Having ascertained the presence and source of various impurity elements within the silica binder of an investment casting mould, attention was then turned towards the effect of these elements upon the phase structure and thermal response of the standard silica based binders currently used in mould production. Since it will be difficult to eliminate these impurities, it was necessary to investigate whether the effects, if any, are detrimental to the overall properties of the binders.

4.3.4.1: Phase Structure

The standardised phase structures of both colloidal and ethyl-silicate binders have been reported in Section 4.1.3. To investigate the effect of impurities upon the phase structure one of the silica compositions determined by EPMA of a fired mould was reproduced using gelled binders and controlled additions of appropriate trace oxides. An example of the calculation used to determine the additions is shown in Appendix 10 and the composition used is shown in Table 23. These samples were then fired and the phase structure established using XRD (Table 24).

The phase structure of both binders are affected by impurity elements. The formation of S_1 tridymite is suppressed in the colloidal sol, leading to almost 100% α cristobalite, probably due to raising of the crystallisation temperature. More surprisingly, ethyl silicate binders crystallise to form α cristobalite, suggesting that the impurity elements behave in a similar manner to sodium in sols and nucleate crystallisation at lower temperatures.

Table 23: Silica binder composition determined by EPMA of a fired investment casting mould

	Si	O	Ca	Na	Al
Elemental Composition (atomic %)	13.451	64.564	0.188	0.540	20.186

This leads to the interesting conclusion that, by analogy, the mould is bound by a silica based network consisting of a mixture of crystalline phases in the primary coat and a mainly amorphous secondary coat binder with areas of crystallinity due to the influence of impurity elements. This is summarised in Figure 118 with a revised version of the proposed mould phase structure from 4.4.5.

Table 24: Summary of the effect of impurities upon the phase structure of silica based binders

Binder	Composition	Thermal Treatment	Phase composition
Colloidal Silica Sol	100% SiO_2	Fired at 1,000°C	α cristobalite + small amount α tridymite
Colloidal Silica Sol	32.37% Si 64.74% O 2.485% Ca 0.406% Na	"	α cristobalite
Ethyl Silicate	100% SiO_2	"	Amorphous
Ethyl Silicate	32.37% Si 64.74% O 2.485% Ca 0.406% Na	"	α cristobalite

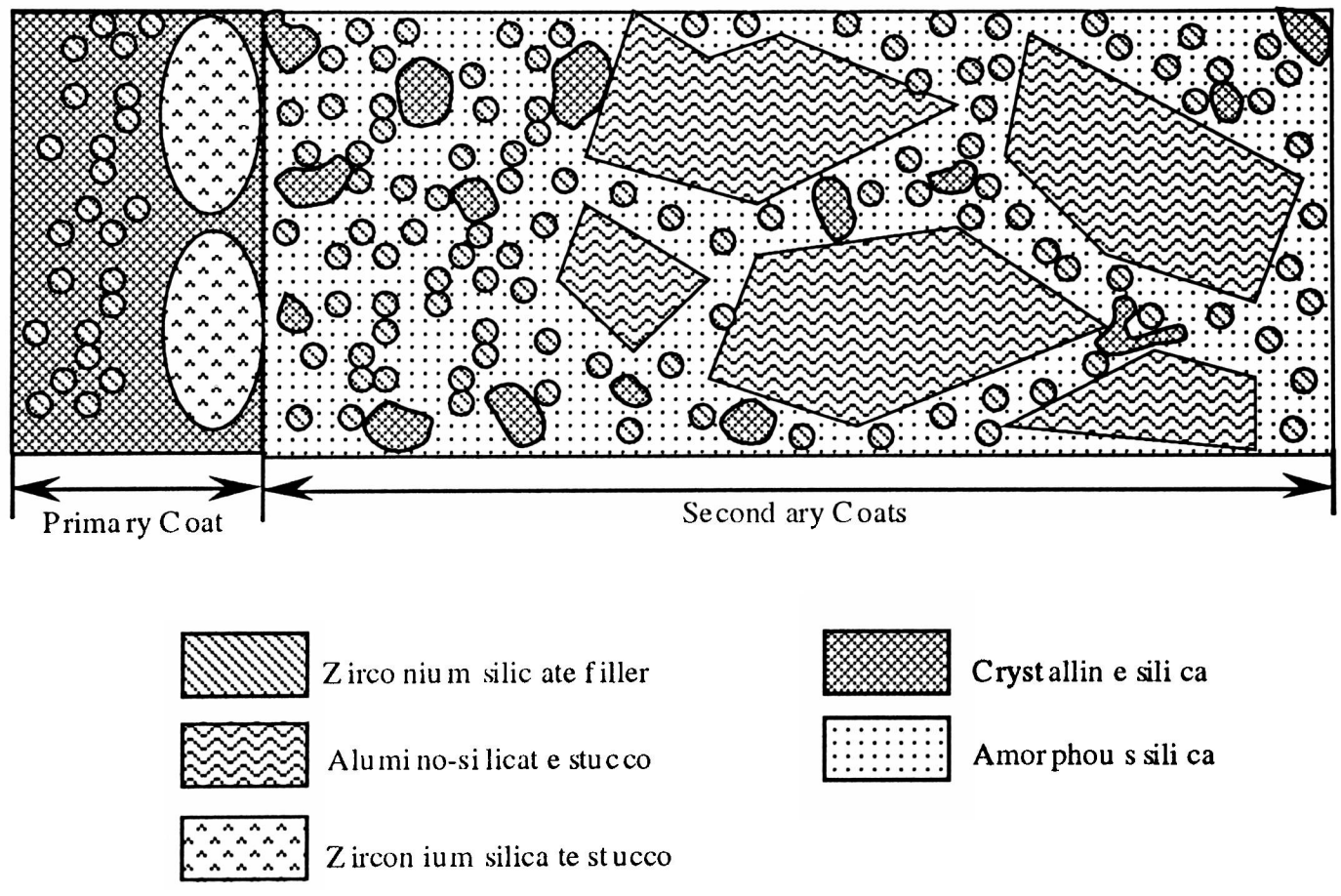


Figure 118: Proposed mould phase structure - revised

4.3.4.2: Thermal Response

Impurities within silica based binders have been shown to affect the phase structure after firing. The same impurities may also affect the thermal response of the binders. In order to investigate this possibility, the silica based compositions from section 4.3.4.1 were made up using fired binder samples. Fired binders were used since it has been shown that most of the leaching of the impurity elements takes place during firing of the mould. Therefore the elements will affect the binder performance during the casting of a mould and as such the sample properties were compared using the thermal profile designed to simulate casting of the mould.

Figures 119 and 120 show the DTA and dilatometry traces for compositions made from fired colloidal silica. When comparison is made with the standard binder response (Section 4.3.2), it can be seen that the impurities do indeed alter the thermal properties. Syton X30 is still reasonably inactive, but is less susceptible to changes in heating rate and there are several extra peaks which may correspond to the formation of glassy phases within the silica. Glassy phases, if formed would have low melting points and a less rigid structure than cristobalite. This could account for the fact that the normally inactive binder is induced to undergo a 17% volume contraction during casting by the presence of the impurity elements.

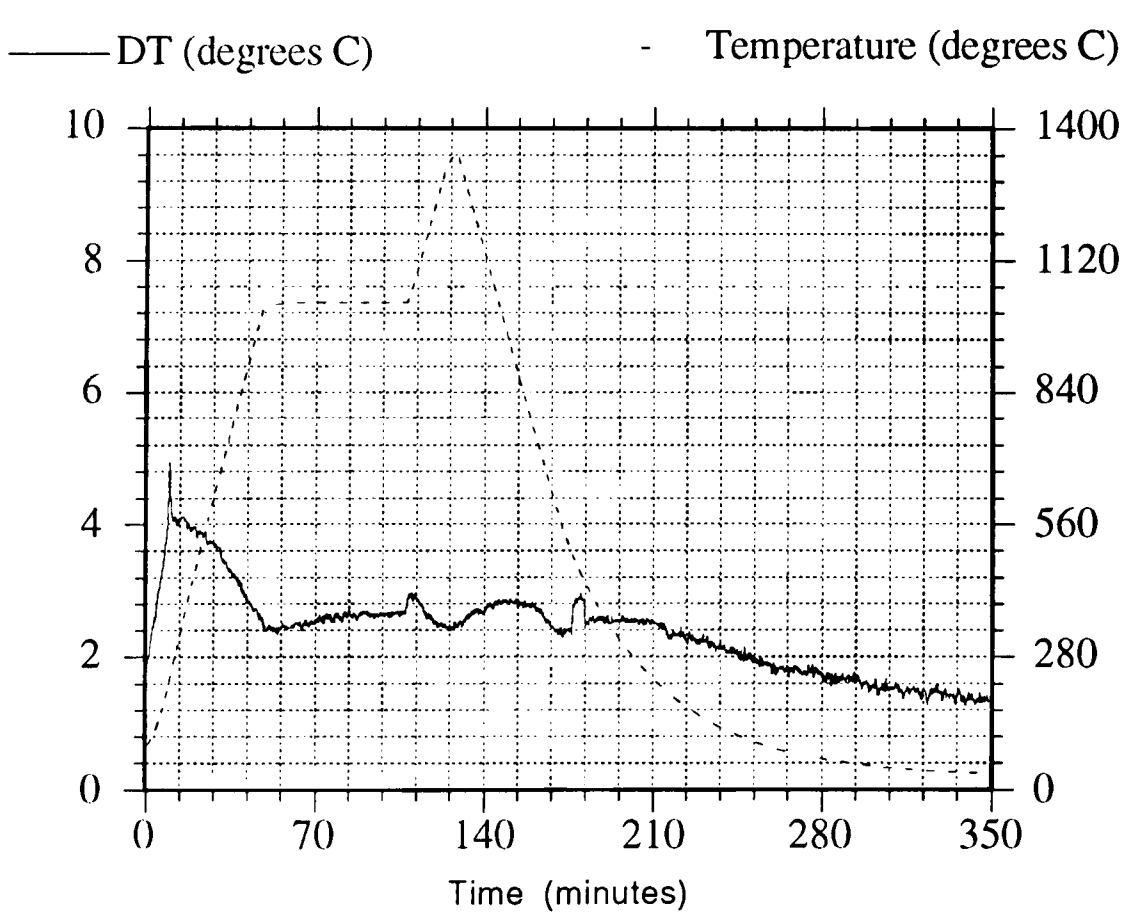


Figure 119: DTA casting trace for Syton X30 + controlled impurity additions

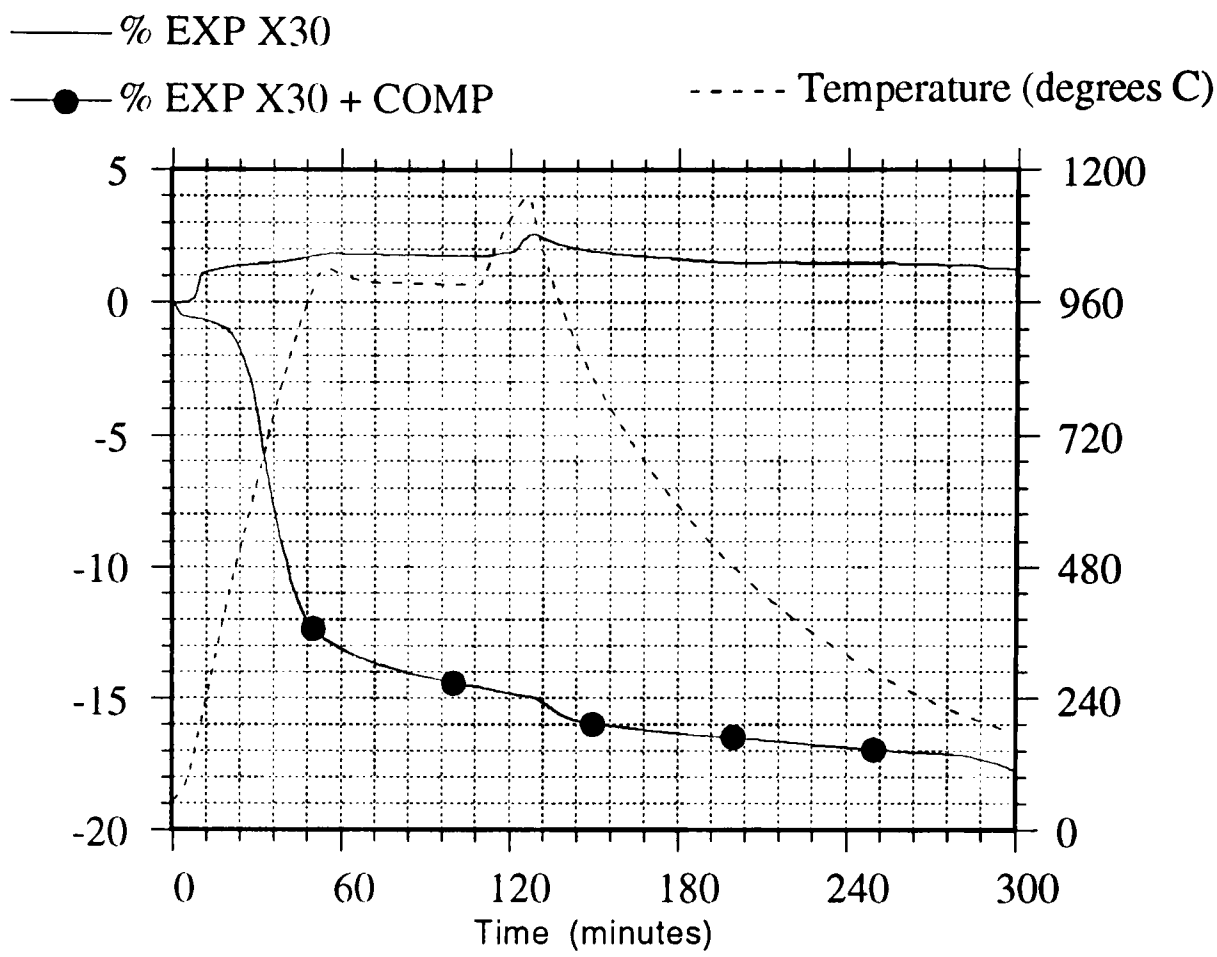


Figure 120: Dilatometry casting trace for Syton X30 and Syton X30 + controlled impurity additions

The thermal properties of Silester XAR are also affected by the presence of impurities. The DTA casting trace (Figure 121) is altered in a similar manner to Syton X30, with extra peaks and less susceptibility to changes in heating/cooling rate. In this case however, the peaks may be indicative of crystallisation, which is the known effect of impurities upon the usually amorphous binder structure. The crystallisation will produce a rigid structure, which seems to be confirmed by the dilatometry casting trace (Figure 122) in which the overall contraction is reduced from 7% to just 1.5%.

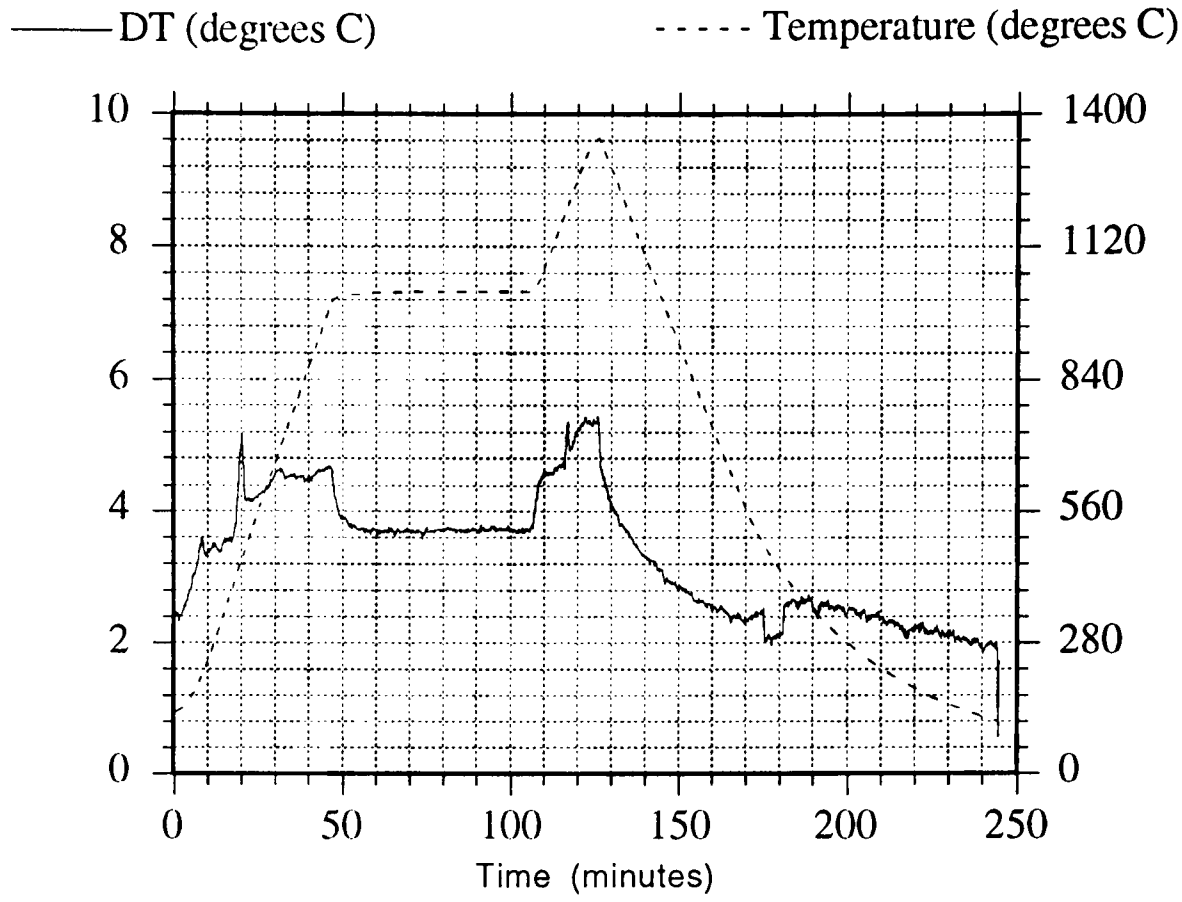


Figure 121: DTA casting trace for Silester XAR + controlled impurity additions

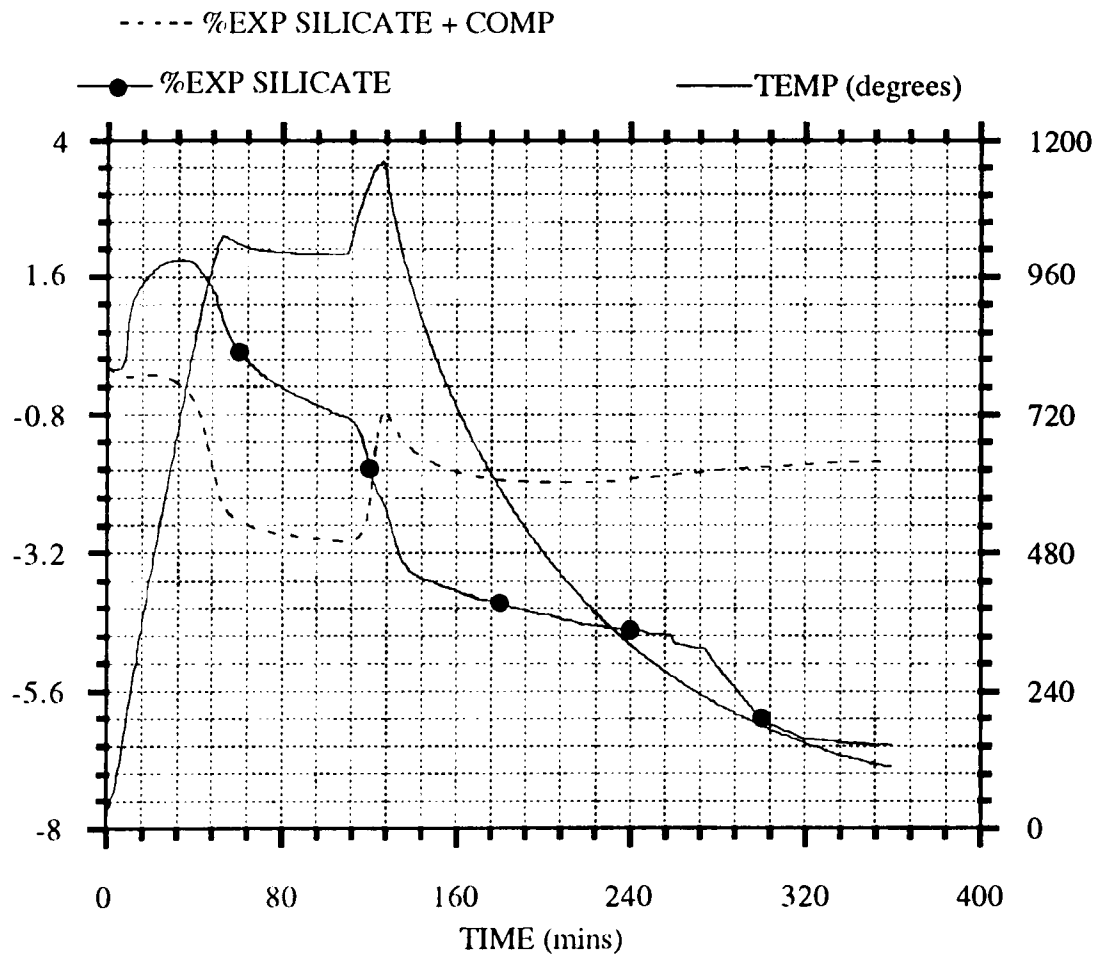


Figure 122: The dilatometry casting trace for Silester XAR and Silester XAR + controlled impurities

4.3.5: Summary

Investigation has revealed that the sintering and firing behaviour of the binder is dependent upon the type. Water based colloidal silica sols crystallise when fired at 1,000°C. This has been shown to be due to the presence of sodium stabilising ions which nucleate the crystallisation to cristobalite at low temperatures. Cristobalite undergoes a phase change at 241°C which is accompanied by a 1.5% volume change. This could produce microcracks which would significantly reduce the strength of the mould during casting of the metal. The crystallisation temperature is also dependent upon sodium, to the extent that a reduction in sodium content will produce a significant increase in crystallisation temperature. The crystalline structure is constrained and rigid which produces a binder which is stable during reheating and cooling of the mould during casting. Alcohol based ethyl silicate binders remain amorphous when fired to 1,000°C and this unconstrained and random silicate structure permits molecular expansions and further contractions up to 7% (linear) during reheating and cooling. It has been proposed that this amorphous binder structure is responsible for mould wall movement and hence high temperature creep of a silica based mould during casting.

Having ascertained the presence and source of various impurity elements within the silica binder of an investment casting mould, attention was then turned towards the effect of these elements upon the phase structure and thermal response of the standard silica based binders currently used in mould production. The phase structure of both binders are affected by impurity elements. The formation of S_1 tridymite is suppressed in the colloidal sol, leading to almost 100% α cristobalite, probably due to raising of the crystallisation temperature. More surprisingly, ethyl silicate binders crystallise to form α cristobalite, suggesting that the impurity elements behave in a similar manner to sodium in sols and nucleate crystallisation at lower temperatures. This leads to the interesting conclusion that, by analogy, the mould is bound by a silica based network consisting of a mixture of crystalline phases in the primary coat and a mainly amorphous secondary coat binder with areas of crystallinity due to the influence of impurity elements.

The alteration of the crystallisation properties of the binders is reflected in the structural performance. The normally inactive and structurally stable sol based binder undergoes a 17% volume contraction during casting. This may be due to the formation of low melting point glasses which have a fundamentally less rigid structure than crystalline silica when heated to high temperatures, due to the random orientation of molecules and the absence of covalent bonds.

In ethyl silicate binders, the presence of impurity elements induces crystallisation which produces a rigid silicate structure as with the sol based binders. This leads to a reduction in volume contraction from 7% to just 1.5% during casting. The fact that the impurities are leached in varying amounts and in various locations throughout the binder system may well be responsible for the inherent variability in the mould properties from one day to the next.

The almost composite structure of the binder phase suggests that the mould will be undergoing a series of vastly different thermal responses during firing and casting, depending upon the type of binder used and the extent of impurity infiltration. Overall this will lead to large stresses and possibly micro-cracking within the mould section which will decrease mechanical strength and lead to mould failure. The large volume contraction experienced by the binders during casting and the mainly amorphous structure of the silica is probably the cause of high temperature creep and hence buckling of larger moulds with higher metal weights.

The overall thermal and mechanical response of the moulds could be improved by altering the crystallisation behaviour of the binders to create a uniform phase structure throughout the mould section. This could be achieved by modifying the binders to make them less susceptible to the presence of stabiliser or impurity elements. Alternatively the source of the impurities could be removed by replacing the filler currently in use with one that is not phase separated or by using an entirely different refractory material that does not interact with the silica binder. However, it may also be necessary to revert to using a binder with greater high temperature and phase stability (e.g. mullite) to improve the failure rates of larger investment casting moulds.

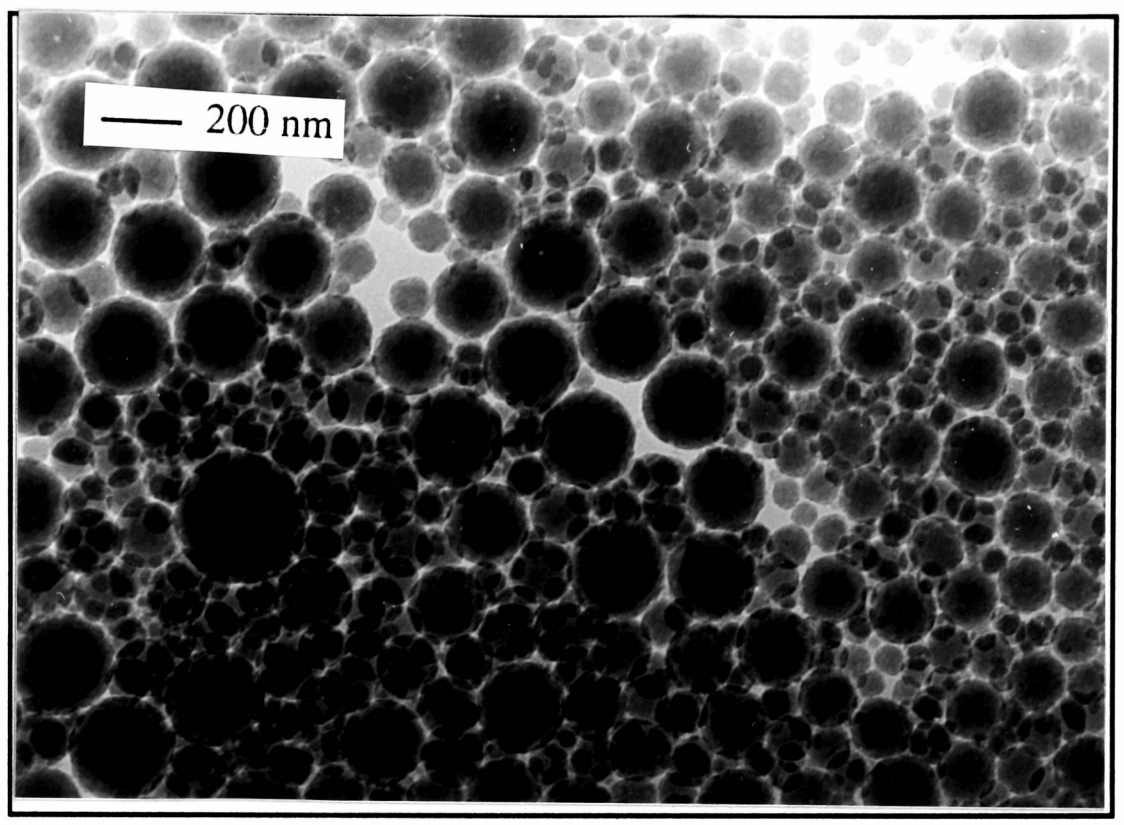


Figure 123: TEM micrograph of Syton W30 mag = x 36,000

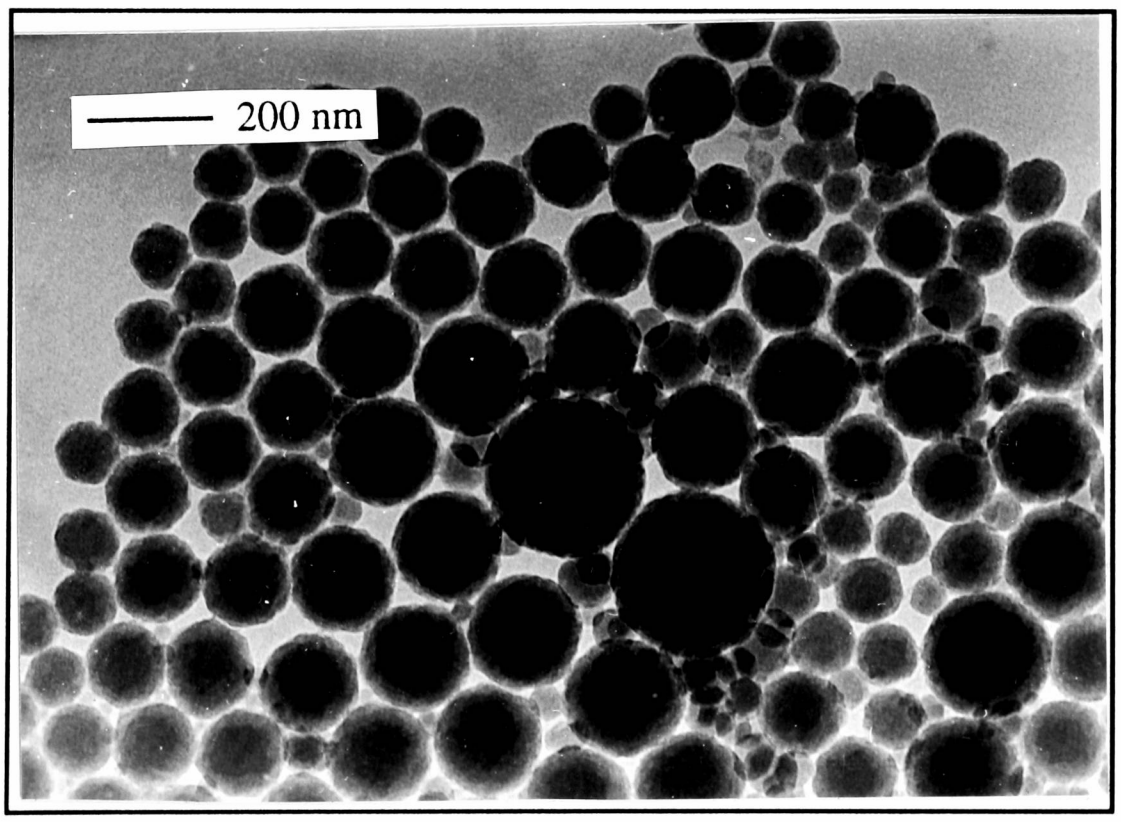


Figure 124: TEM micrograph of Syton W30 mag = x 60,000

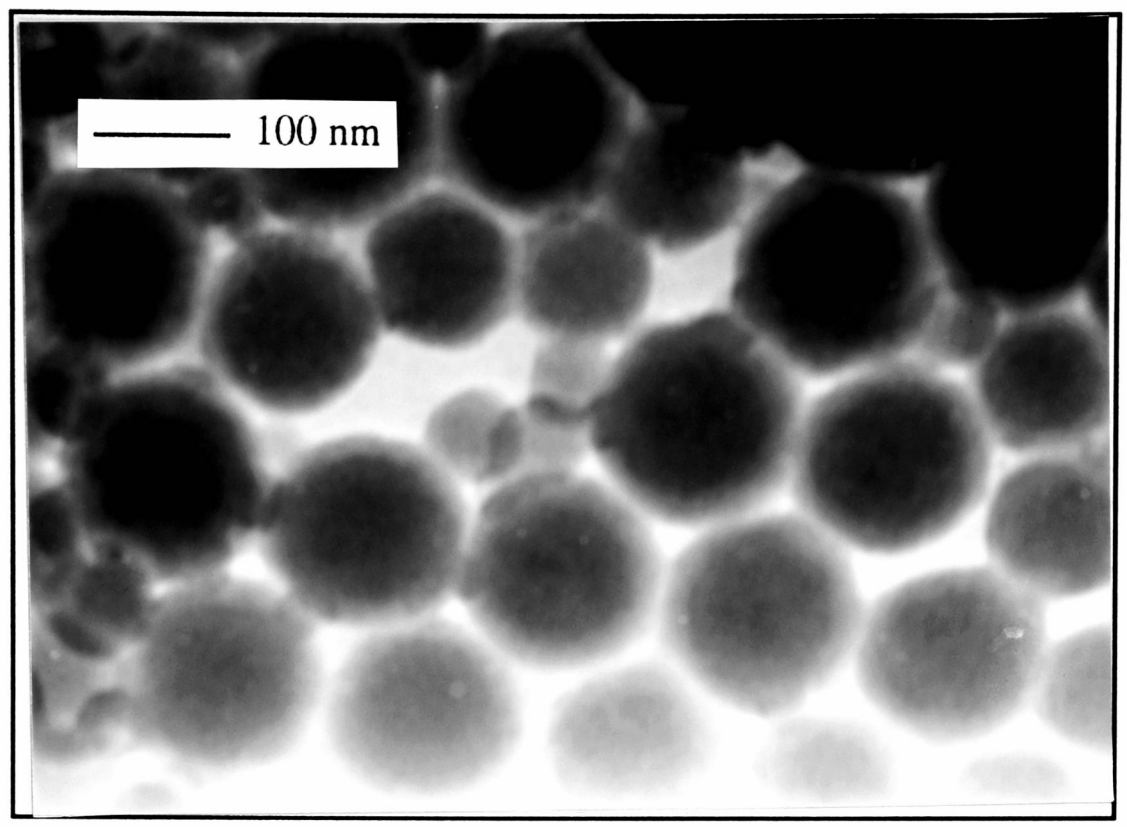


Figure 125: TEM micrograph of Syton W30 mag = x 130,000

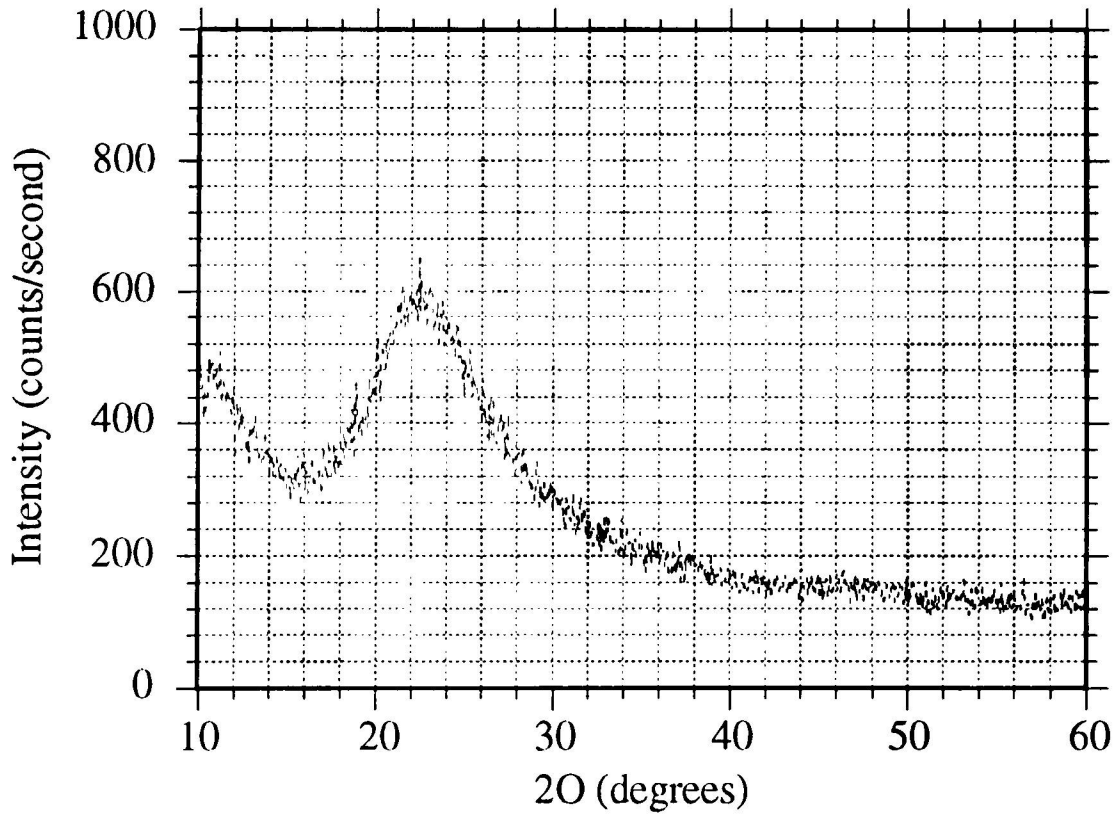


Figure 126: XRD pattern for gelled Syton W30

W30, as with all the water based colloidal sols, can be gelled by solvent evaporation and the gelled structure consists of amorphous silica (Figure 126) displaying the characteristic broad peak. When fired at 1,000°C the structure has crystallised to a mixture of mainly α-cristobalite and a small amount of S_1-tridymite (Figure 127). As has already been discussed in Section 4.3.3, Syton W30 actually begins to form cristobalite at 870-890°C due to nucleation of the crystalline phase by the sodium stabilising ions. The small amount of tridymite in the fired structure is a result of the transformation of cristobalite to tridymite at 870°C.

The thermal response of Syton W30 during firing and casting was investigated using dilatometry. During firing (Figure 128), the binder exhibits the same characteristic features as Syton X30, with a volume contraction of approximately 16% during heating. As the sample is held at 1,000°C and during cooling the volume contraction is unchanged since the binder has sintered and transformed to the relatively constrained crystalline structure. Figure 129 shows the corresponding casting trace for the fired binder. The structure undergoes a small amount of expansion during reheating (1%) but remains fairly stable throughout the whole casting cycle.

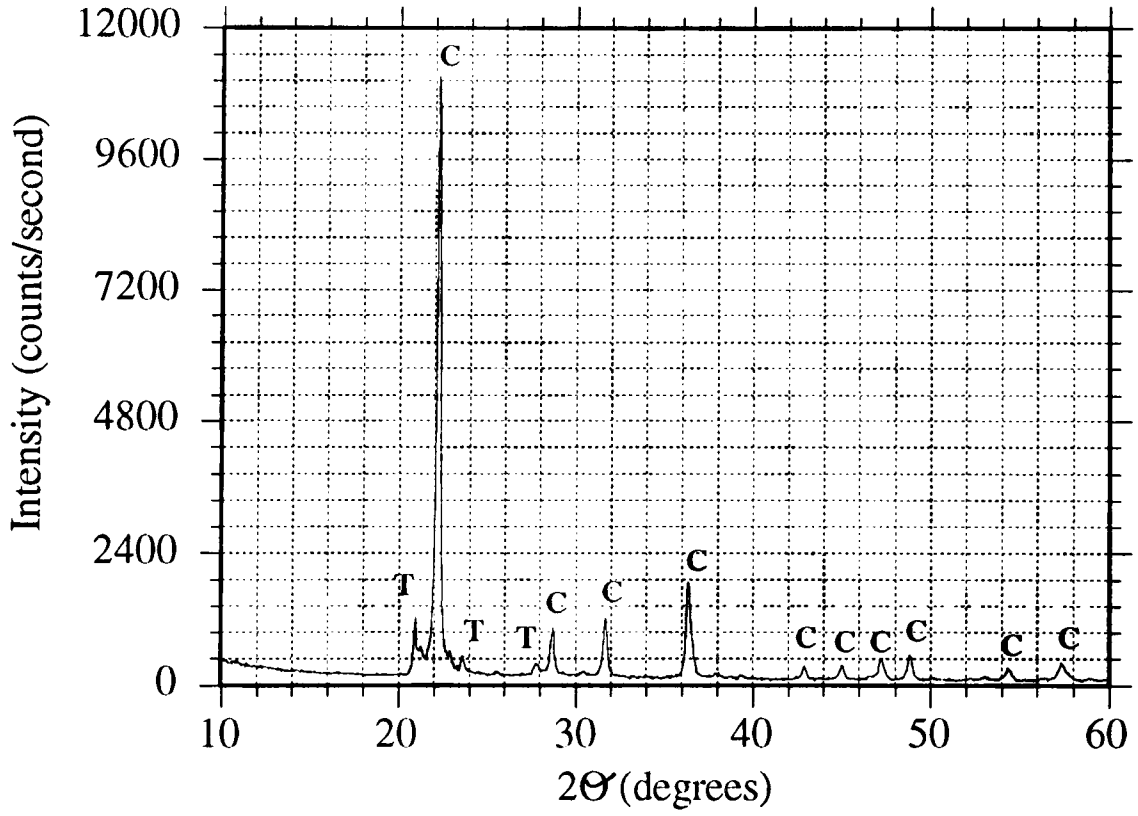


Figure 127: XRD trace for Syton W30 fired to 1,000°C for 60 minutes
C = α-cristobalite
T = S_1 tridymite

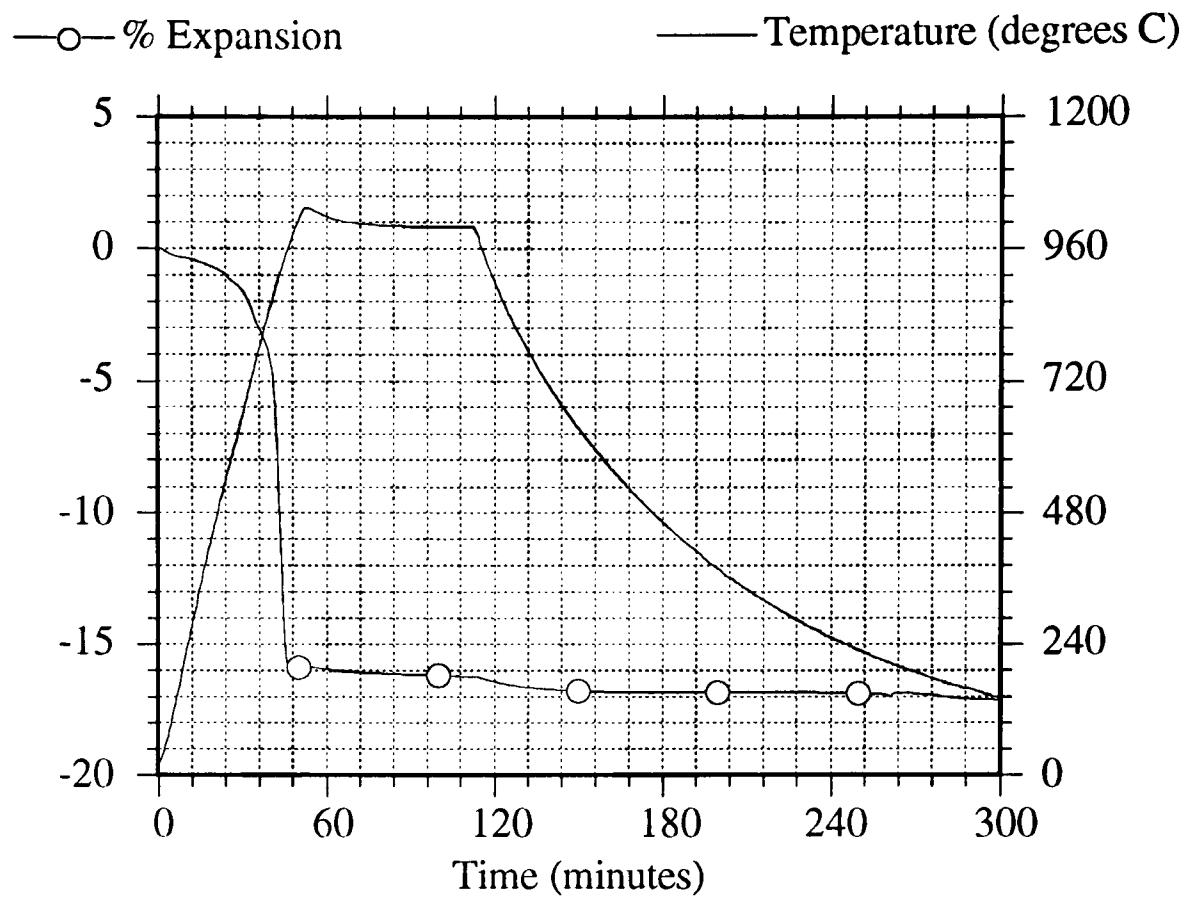


Figure 128: Dilatometry firing trace for Syton W30

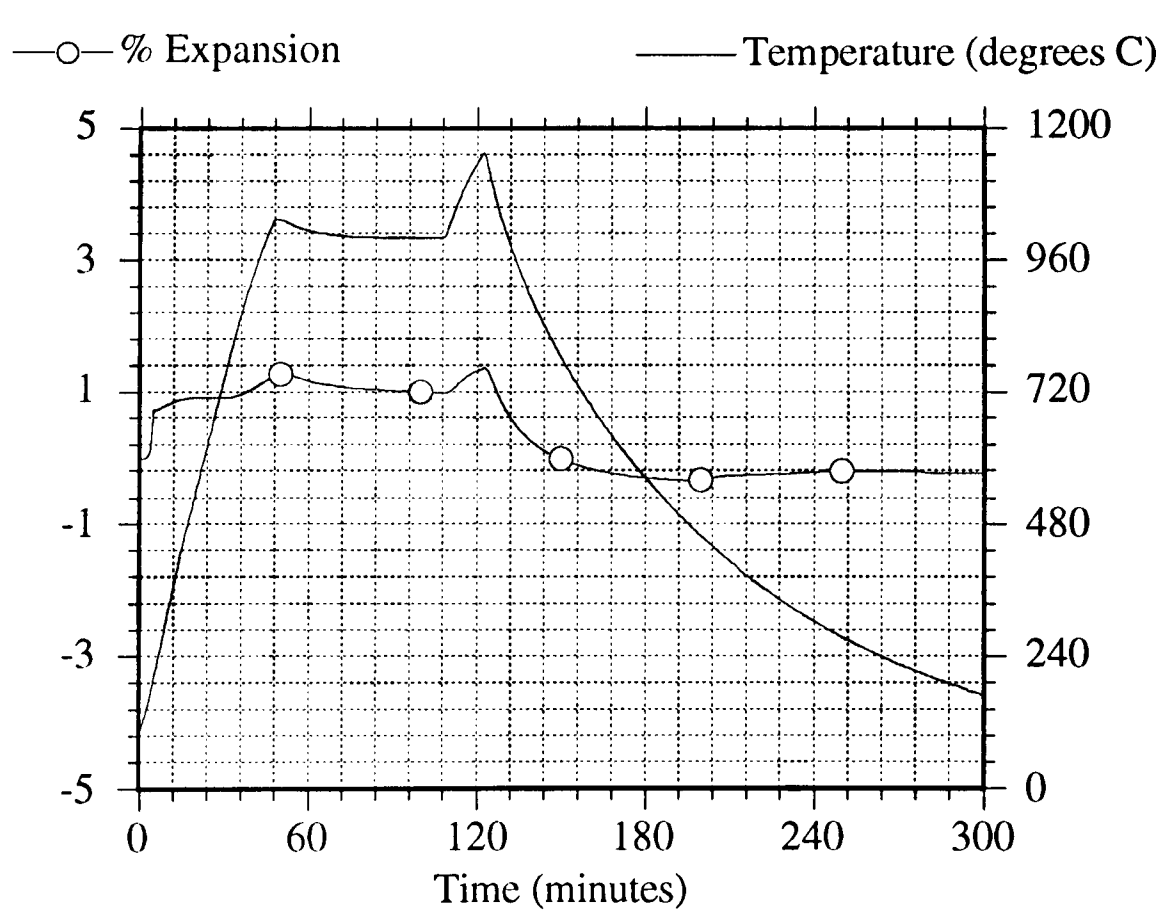


Figure 129: Dilatometry casting trace for Syton W30

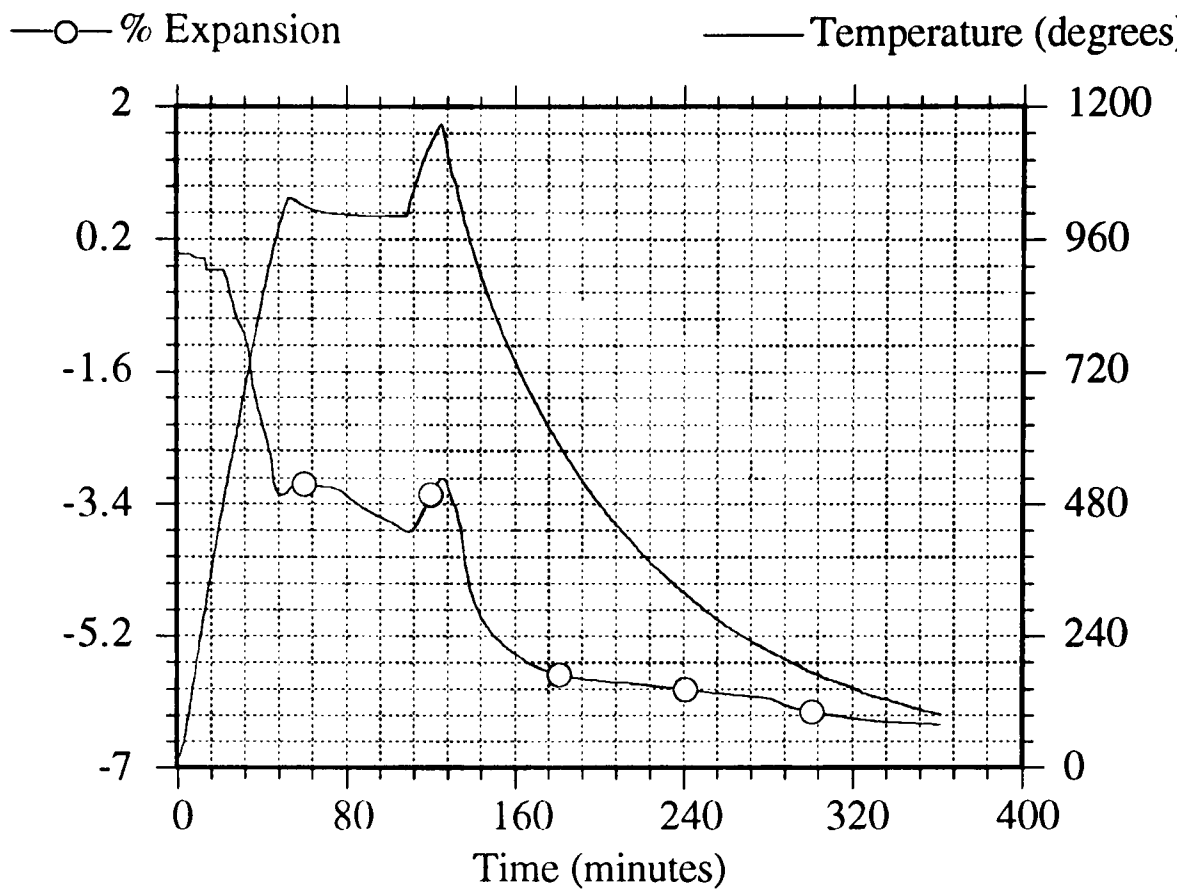


Figure 130: Dilatometry casting trace of Syton W30 + controlled impurity additions

The effect of impurities upon the thermal response was investigated by repeating the casting cycle with a solid state sample made up to represent one of the compositions found within the binder phase of a fired air-cast mould (Table 25). The resulting dilatometry trace is shown in Figure 130. Comparison with the standard binder response in Figure 129 shows that the binder is affected by the presence of the impurity elements. Instead of undergoing a 1% expansion during reheating, the composition sample begins to contract at 500°C and continues to do so until the start of the isothermal hold at 1,000°C. During the hold the sample remains relatively stable, with a small contraction in the latter stages. During the remainder of the thermal cycle further contraction is taking place, so that an overall volume contraction of 6.5% takes place during the casting cycle. As with Syton X30 this behaviour is probably due to the formation of low melting point glasses and the fluxing effect of some of the impurity elements upon the silica structure. The overall alteration in the volume contraction is less than that found with Syton X30 so it appears that the W30 is less susceptible to the presence of impurity elements.

Table 25: Composition used to prepare dilatometry samples (see Section 3.8.3.2 for details)

Element	Si	O	Ca	Na	Al
Atomic %	13.451	64.564	0.188	0.540	20.186

2. Primcote

Primcote is a water based colloidal silica sol manufactured by Ransome and Randolph. The binder is for use in the primary coats of moulds and is unique in the fact that it contains a proprietary colour change component which changes colour when the slurry coat has dried sufficiently for the application of the next. When gelled and dried the silica is amorphous (Figure 131) and when fired to 1,000°C for 60 minutes a crystalline structure is formed (Figure 132). The small amount of tridymite present indicates that the temperature at which crystallisation takes place is higher than Syton X30, but still below 1,000°C.

The volume changes during firing (Figure 133) and casting (Figure 134) are very similar to those in Syton X30 which is to be expected with the structures being so similar. During firing, however, Primcote binder only undergoes a 9% volume contraction as opposed to 17% detected in the standard Syton sols. This could be due to the presence of several other proprietary ingredients, such as the drying indicator, which may alter the sintering properties of the colloidal network. There also appears a slight and sudden volume contraction around 200°C during cooling which could be attributed to the α - β cristobalite transformation. Unfortunately, computer failure meant that the data concerning a composition made with this binder was lost.

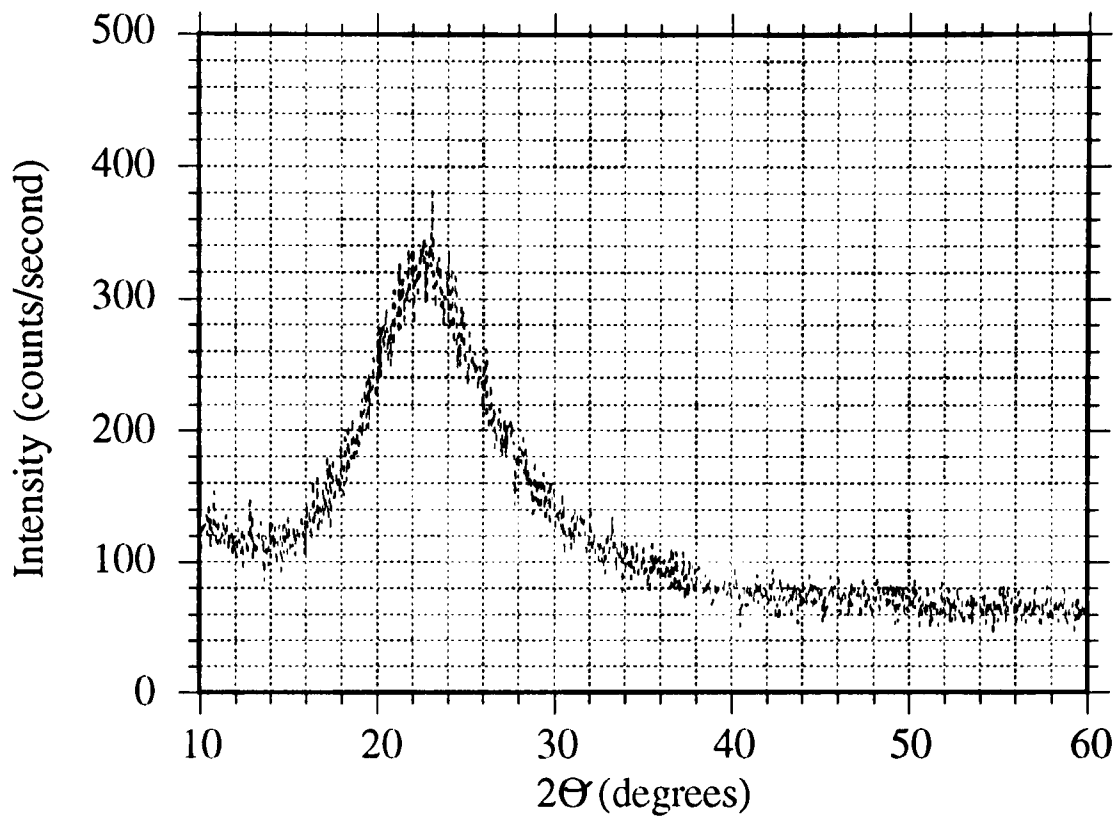


Figure 131: XRD pattern for gelled and dried Primcote binder

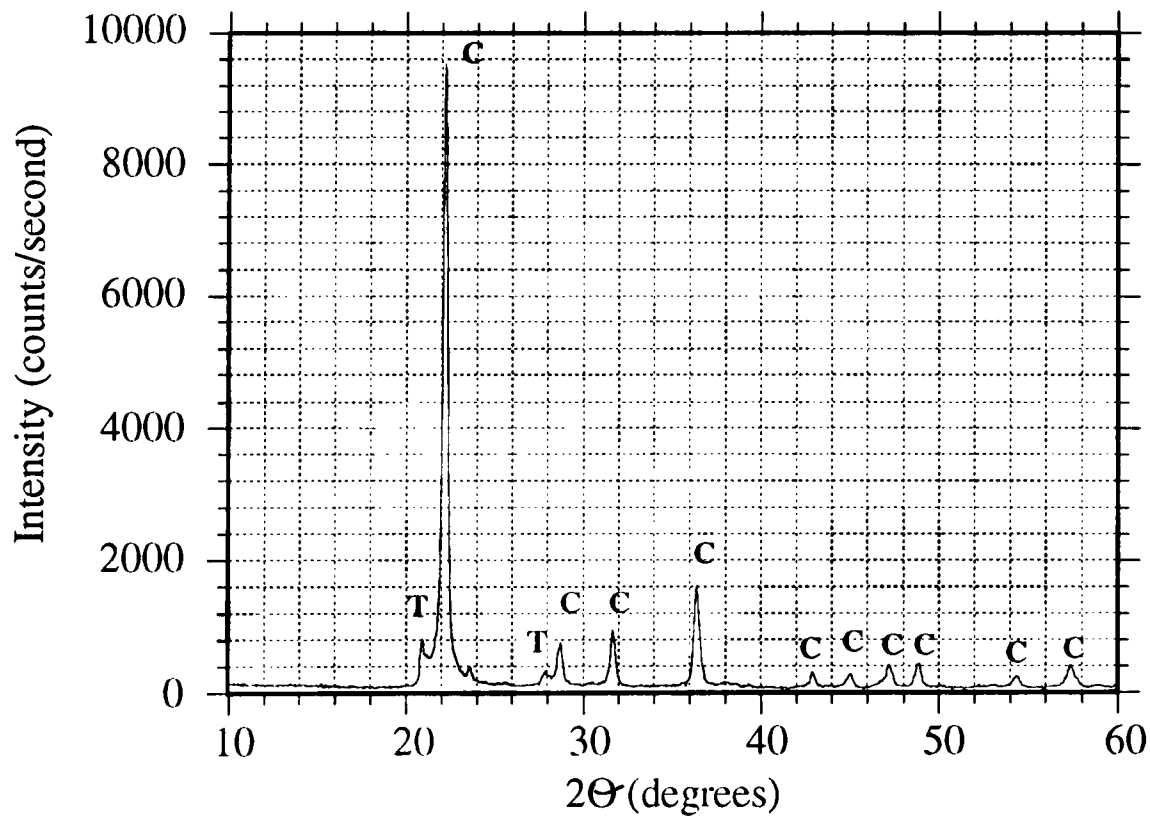


Figure 132: XRD pattern for Primcote binder fired to 1,000°C for 60 minutes
C = α-cristobalite
T = S_1 tridymite

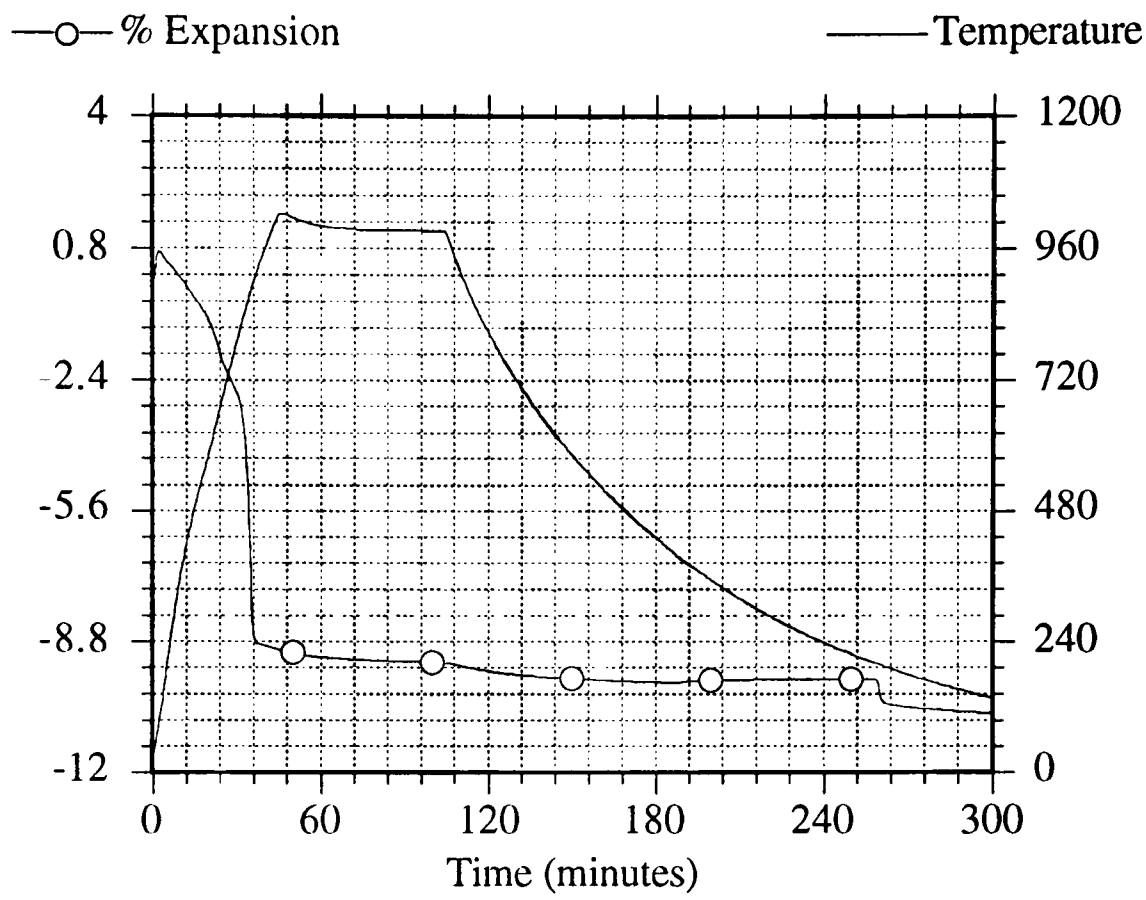


Figure 133: Dilatometry firing trace for Primcote binder

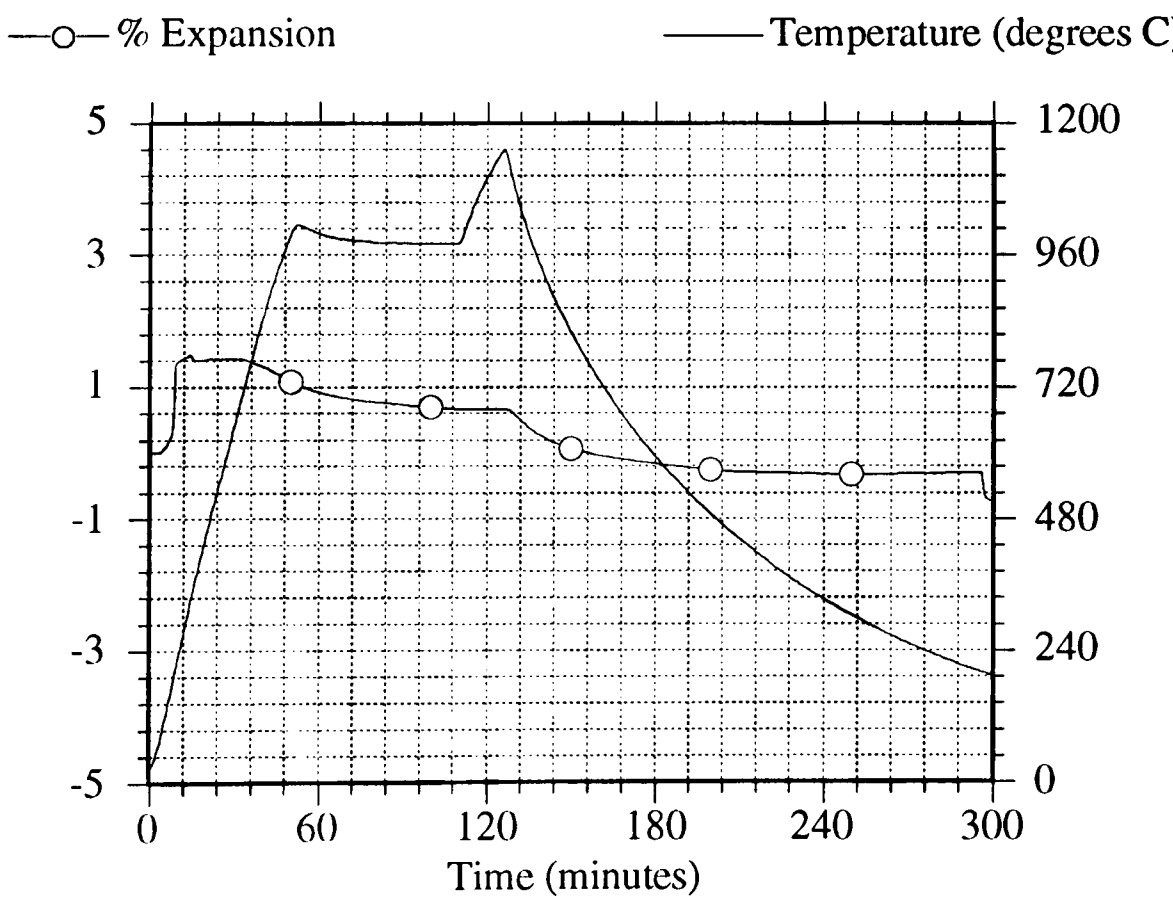


Figure 134: Dilatometry casting trace for Primcote binder

3. Fascote

Fascote is another colloidal silica sol binder which contains a dryness indicator to assess the rate of water loss from the slurry coat. Most colloidal silica binders are used solely for the production of primary coat slurries, but this binder was developed to be used as a silica binder for secondary coat applications. When gelled (Figure 135) the binder exhibits the usual amorphous gel structure, and when fired the silica has crystallised (Figure 136). Again the relative amounts of tridymite and cristobalite in the crystalline mixture suggests that the silica has crystallised at a higher temperature than Syton X30.

The firing trace (Figure 137) shows a very high volume contraction of 24% during firing. This is much higher than both Syton X30 and the counterpart Primcote binder and begins to suggest that this binder may have additives that modify the binder responses to match those of more traditional secondary coat binders. The casting response (Figure 138) follows the general trend for colloidal silica sols in that a small expansion occurs during reheating, followed by an equal contraction during cooling of the sample.

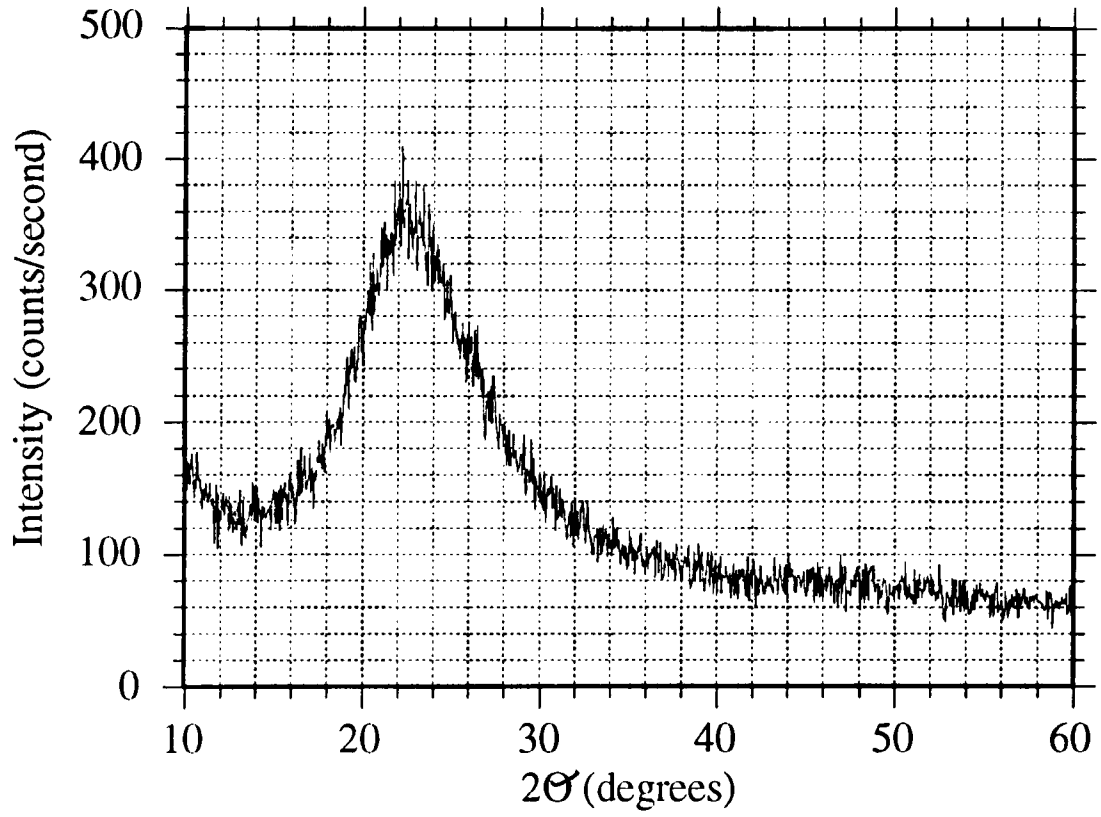


Figure 135: XRD trace for gelled and dried Fascote binder

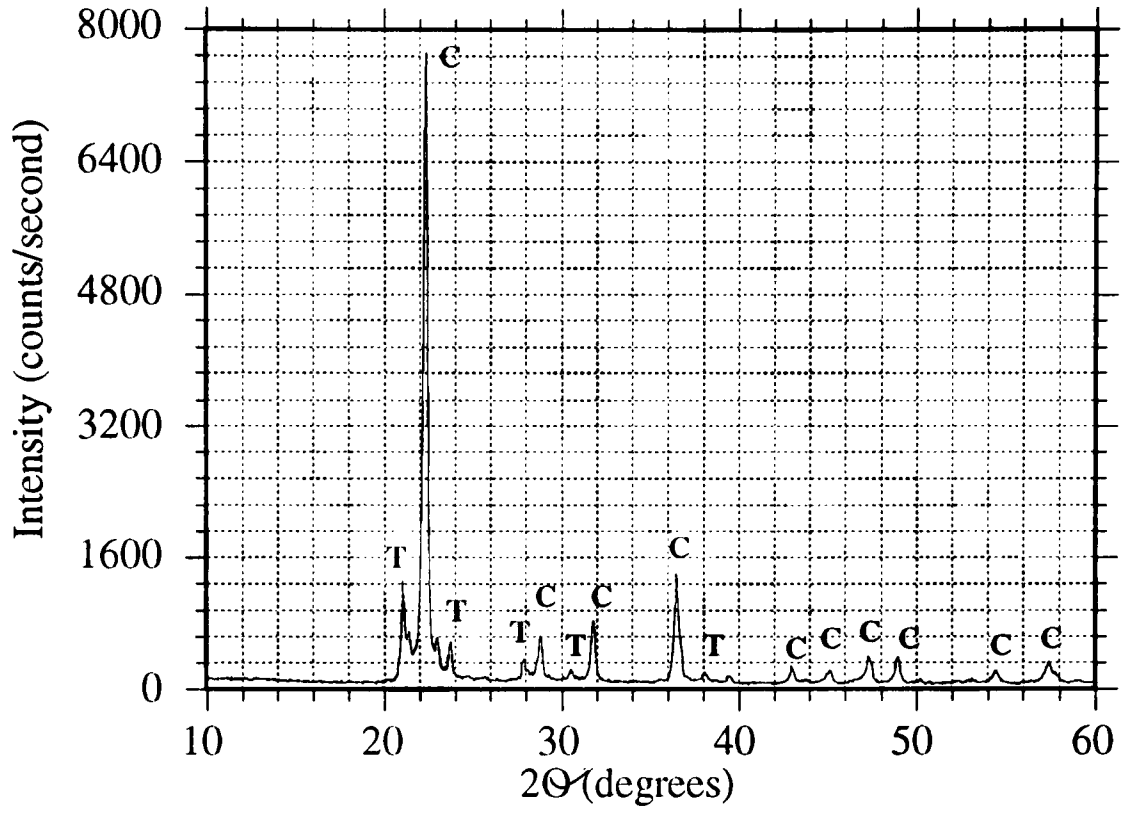


Figure 136: XRD trace for Fascote binder fired at 1,000°C for 60 minutes

C = α-cristobalite

T = S_1 tridymite

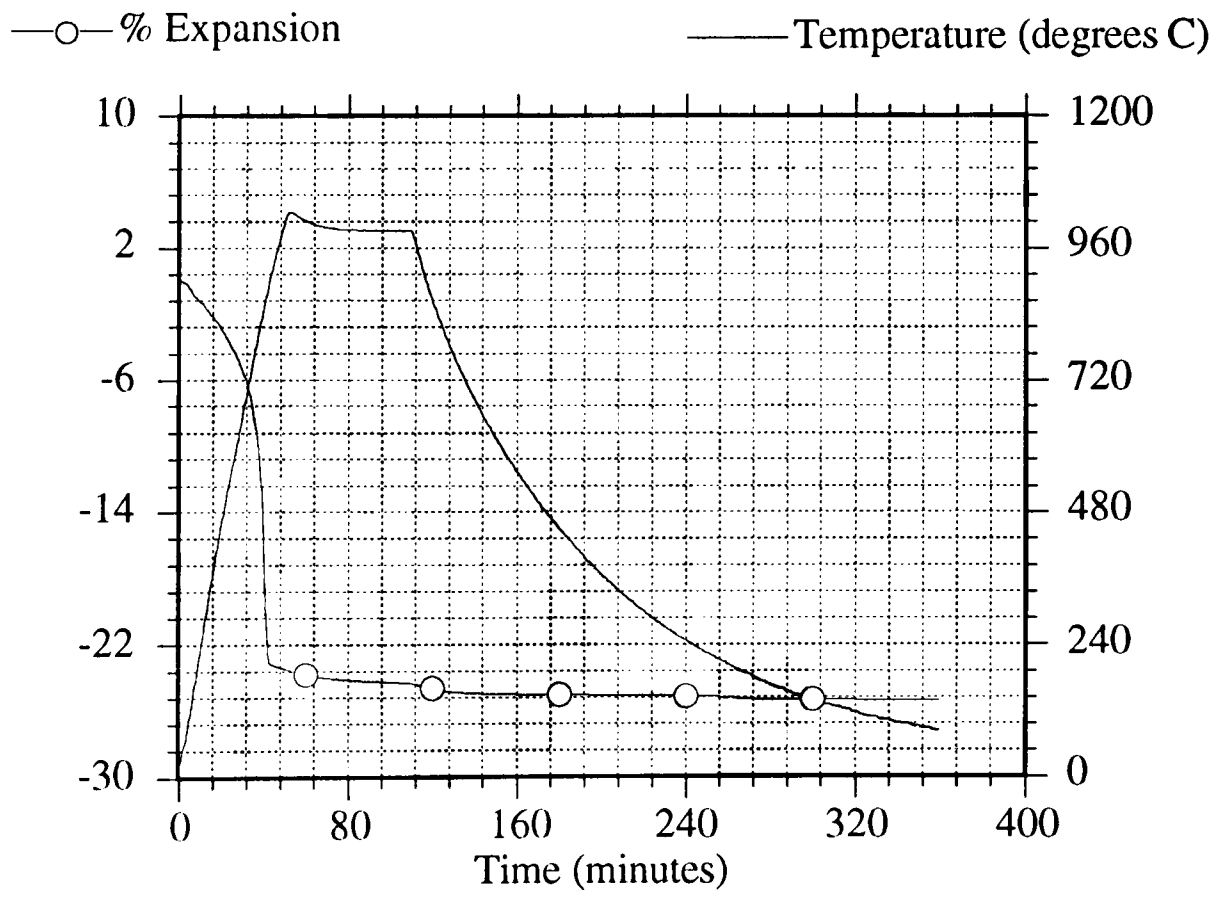


Figure 137: Dilatometry firing trace for gelled Fascote binder

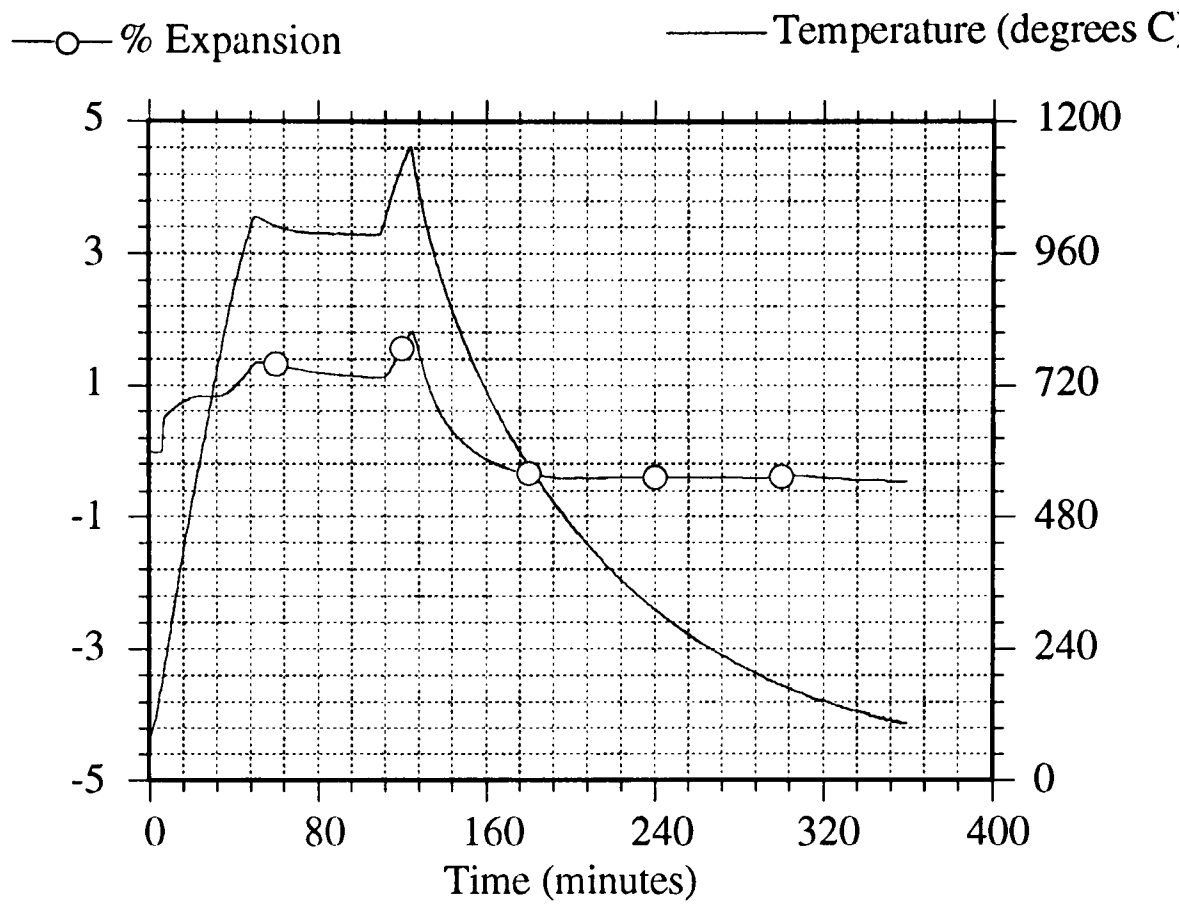


Figure 138: Dilatometry casting trace for Fascote binder

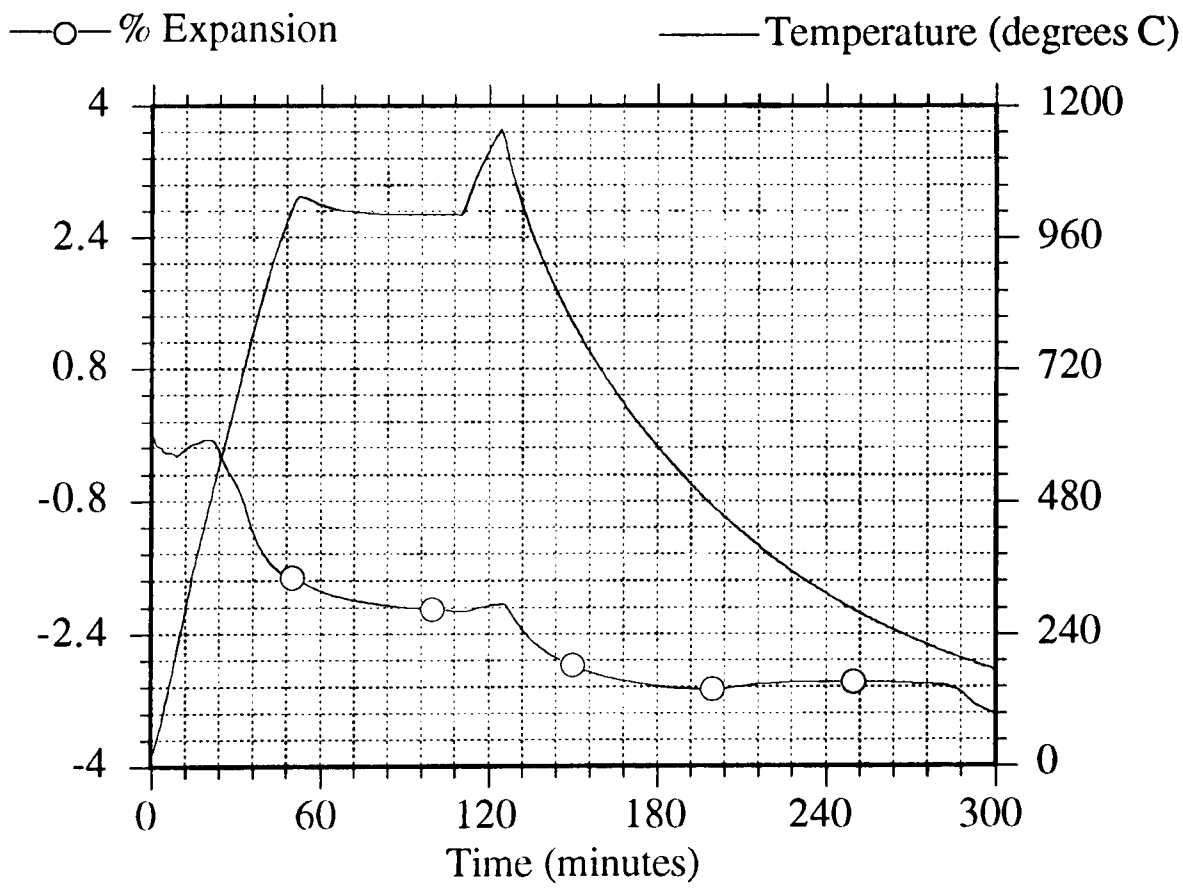


Figure 139: Dilatometry casting trace for Fascote binder + controlled impurity additions

The effect of impurities upon the thermal response of the binder was again investigated by making up the composition in Table 25 using fired Fascote binder. The casting trace is shown in Figure 139 and it can be seen that the binder response is again modified by the incorporation of other elements into the silica network. It should be noted that the induced volume contraction is only 4% which suggests that, of the alternative colloidal systems investigated, Fascote appears to be the least affected by the presence of impurity elements.

4.4.2: Ethyl Silicate Based Binders

1. Silester OS

Silester OS is an ortho-silicate mixture, supplied in the unhydrolysed form to the foundry industry. In-House acid based hydrolysis is used to produce a mixture of poly-silicate in an acidic alcohol based medium. This liquid is then used as a secondary coat silica binder in the same manner as Silester XAR. However, binders like XAR are hybrids, containing both ethyl-silicates and sol particles which impart long-term stability to the mixture. Silester OS contains no sol particles and tends to produce slurries with much shorter life spans. When gelled the structure is amorphous, and when fired to 1,000°C the binder remains amorphous which is standard behaviour for an ethyl-silicate based system (Figure 140).

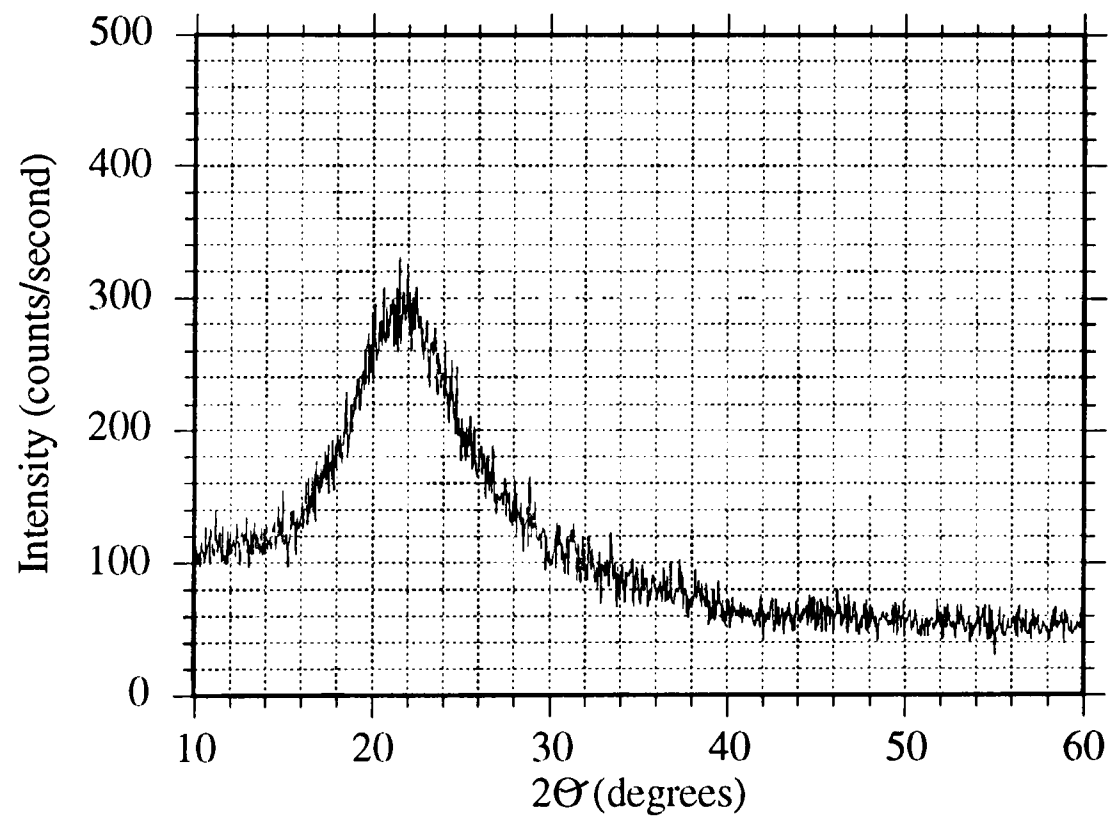


Figure 140: XRD trace for Silester OS fired to 1,000°C for 60 minutes

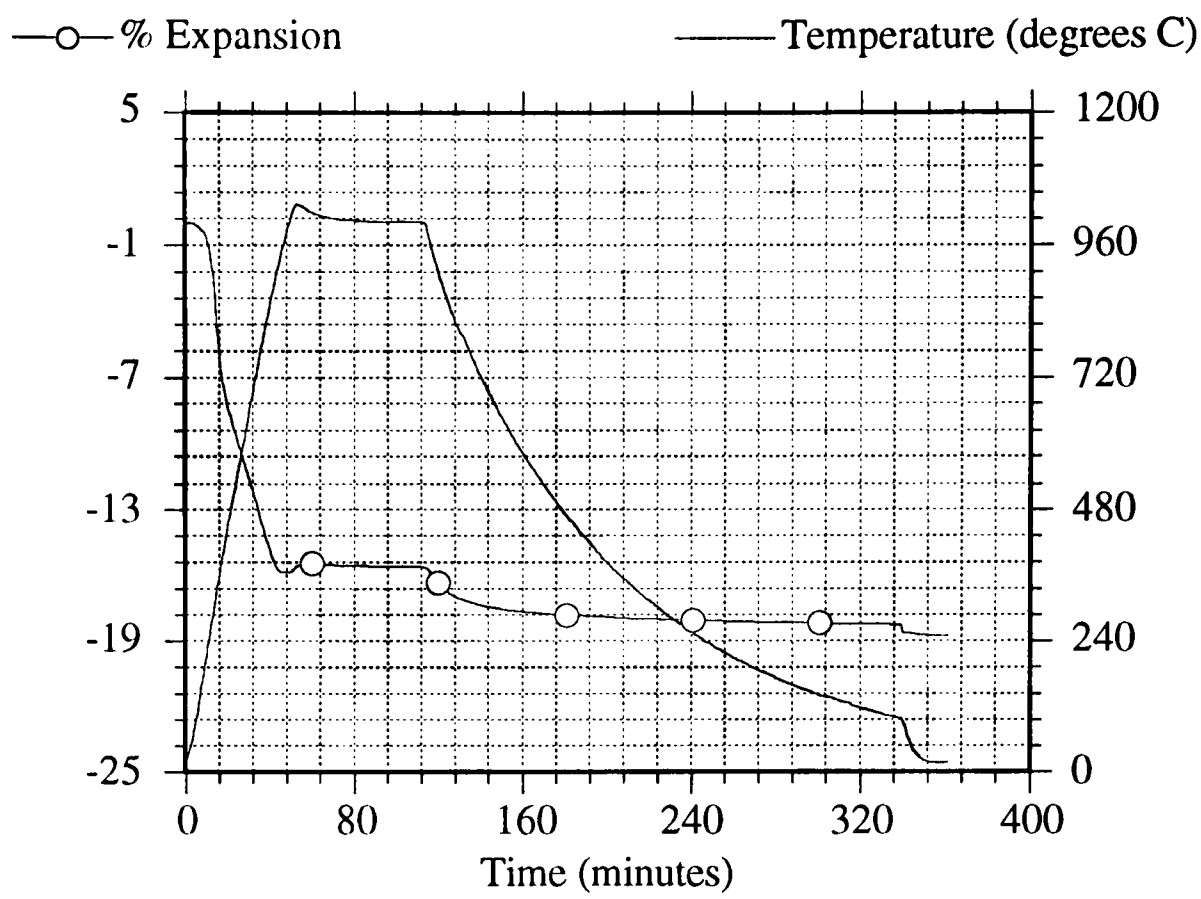


Figure 141: Dilatometry firing trace for Silester OS

When fired the dilatometry trace (Figure 141) shows that extensive volume contraction brought about by coalescence and sintering takes place. The dilatometry casting trace (Figure 142) is a little surprising as the binder appears to be fairly inactive and only undergoes a 1% volume contraction throughout the temperature cycle. Other ethyl silicates, because of the amorphous structure, are free to move and sinter further during the casting cycle. As such, volume contractions of around 6% are usually observed. The fact that Silester OS does not behave in the same manner could be due to the fact that this is not a hybrid binder and the thermal response is influenced by the absence of sol particles in the structure.

This apparent difference between the thermal response of Silester OS and the hybrid ethyl-silicate binders is reflected in the apparent effect that impurity elements have when the binder is mixed together to form a silica composition sample. The resultant dilatometry casting trace (Figure 143) shows that impurity elements instigate a 9% volume contraction during casting. Silester XAR, when subjected to this thermal regime in the presence of impurity elements (Table 25), will crystallise and the volume contraction is reduced rather than increased. It is difficult at this stage to propose reasons why Silester OS has apparently unorthodox thermal responses, but the fact that the binder does not contain sol particles and is hydrolysed in a reasonably uncontrolled manner may be contributing to the surprisingly different responses.

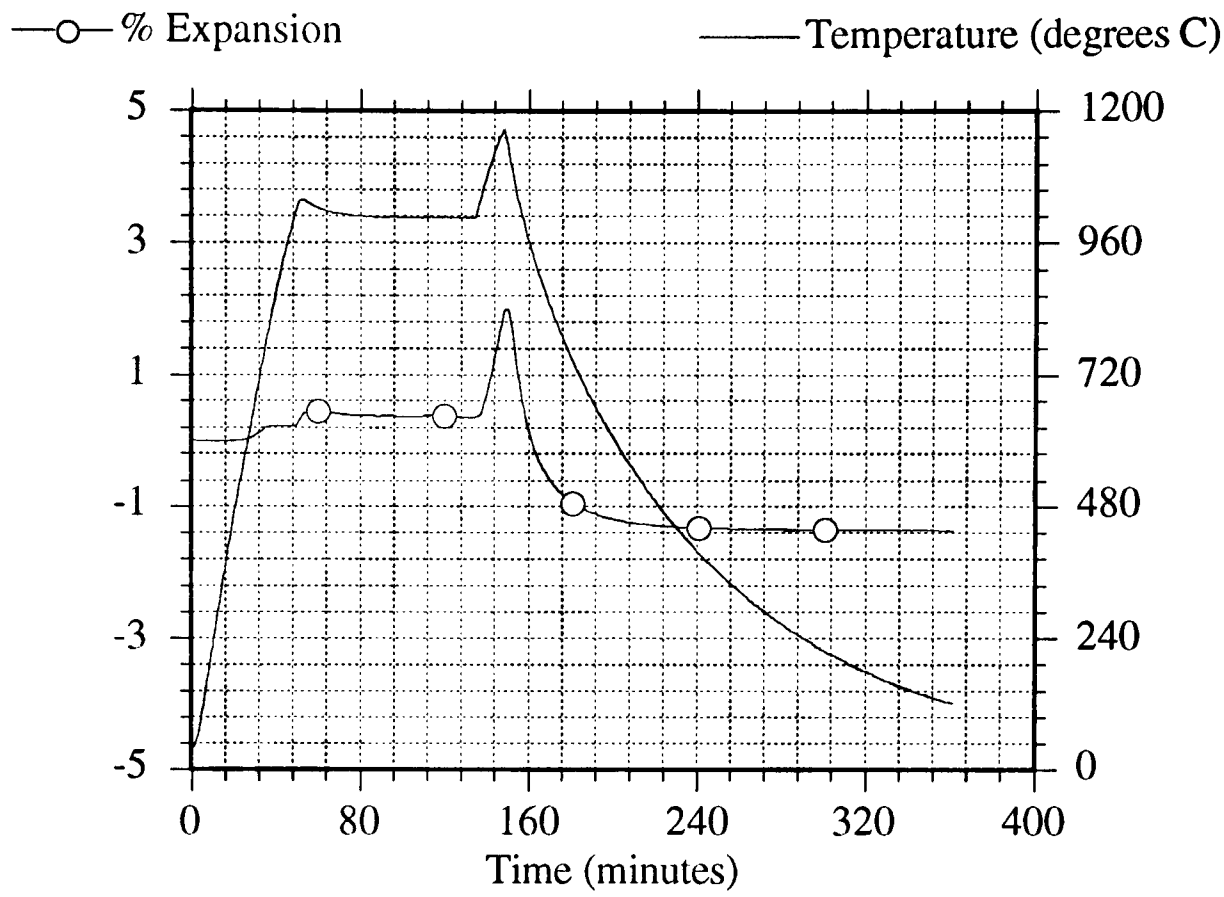


Figure 142: Dilatometry casting trace for Silester OS

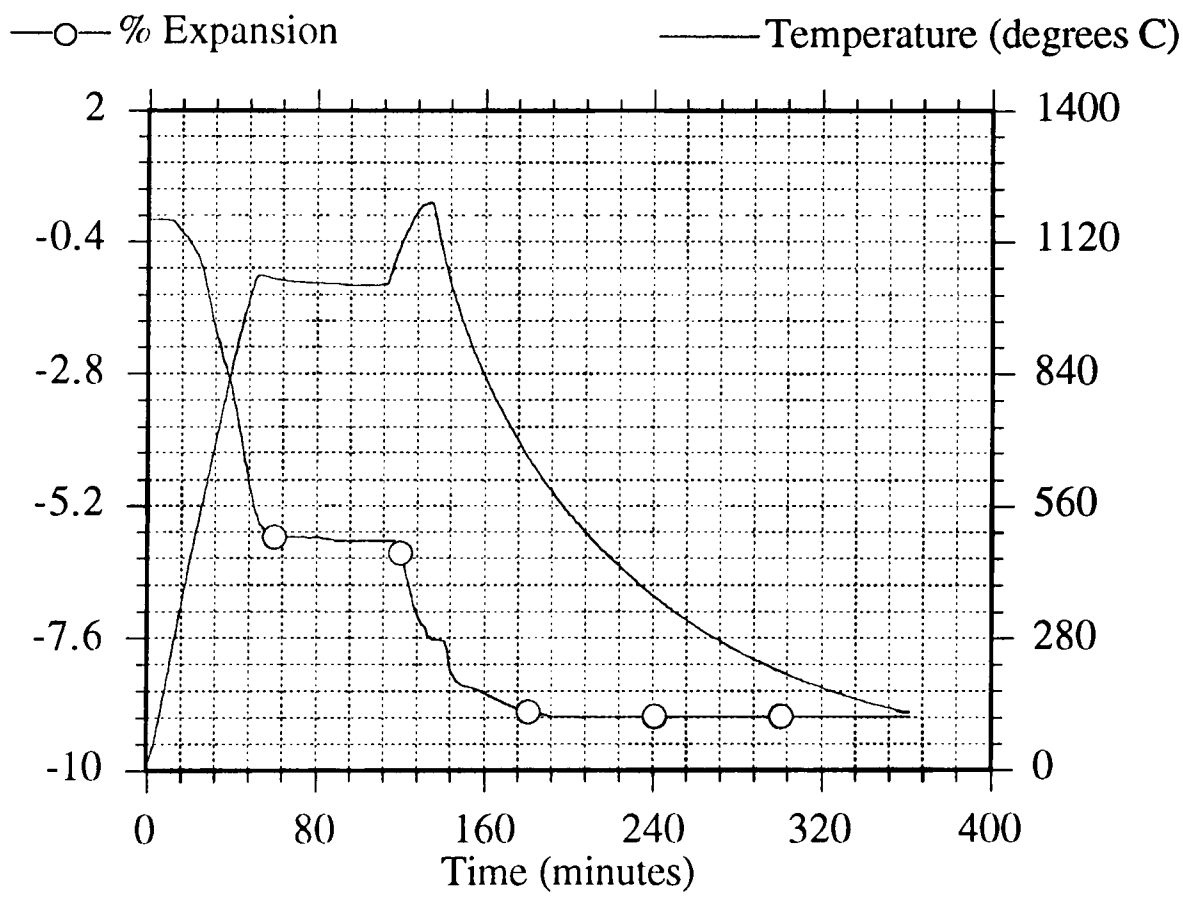


Figure 143: Dilatometry casting trace for Silester OS + controlled impurities

2. Ethyl Silicate AAZ

Ethyl Silicate AAZ is a standard hybrid ethyl silicate binder containing 18.5 wt% silica. The manufacturer indicates that this is a good binder for investment casting applications as improved bonding power can be achieved in both the green and fired ceramic states. This improved strength is due to the fact that when fired at 1,000°C the binder has begun to crystallise to a-cristobalite (Figure 144). This crystallinity will undoubtably impart rigidity to any ceramic body prepared using this binder.

The dilatometry firing trace (Figure 145) is similar to all ethyl-silicate binders, in that sintering begins at approximately 400°C and results in an overall volume contraction of 19% during the firing schedule. However, the fact that the binder has crystallised produces a casting trace that is similar to those obtained from colloidal silica systems, in which the structure is also crystalline at around 1,000°C (Figure 146). Very little further contraction is evident and the binder is reasonably structurally stable. The presence of controlled impurities (Figure 147) produces a 4% volume contraction during the casting cycle. Again, as with colloidal sol samples, the impurity elements may act as fluxing agents or even produce low melting point glasses which will be less rigid than the crystalline state leading to volume contraction when placed under load at higher temperatures.

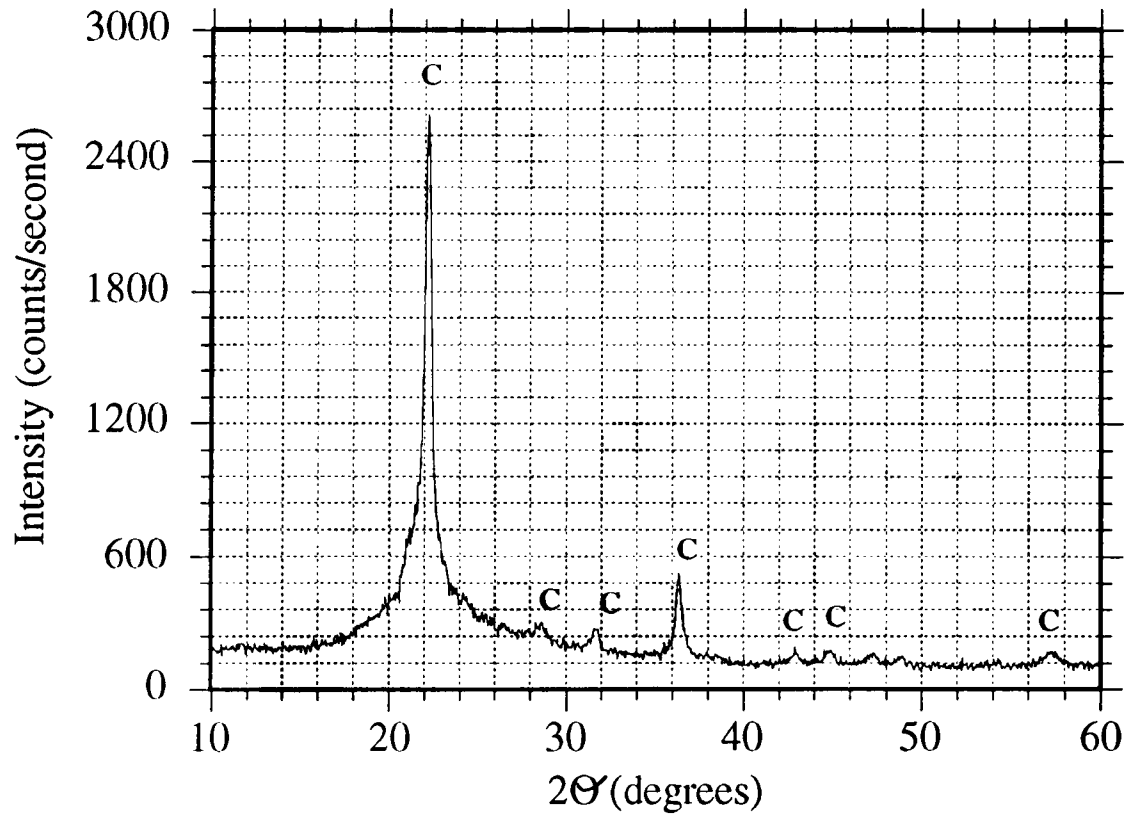


Figure 144: XRD trace for Ethyl Silicate AAZ fired to 1,000°C for 60 minutes
C = α cristobalite

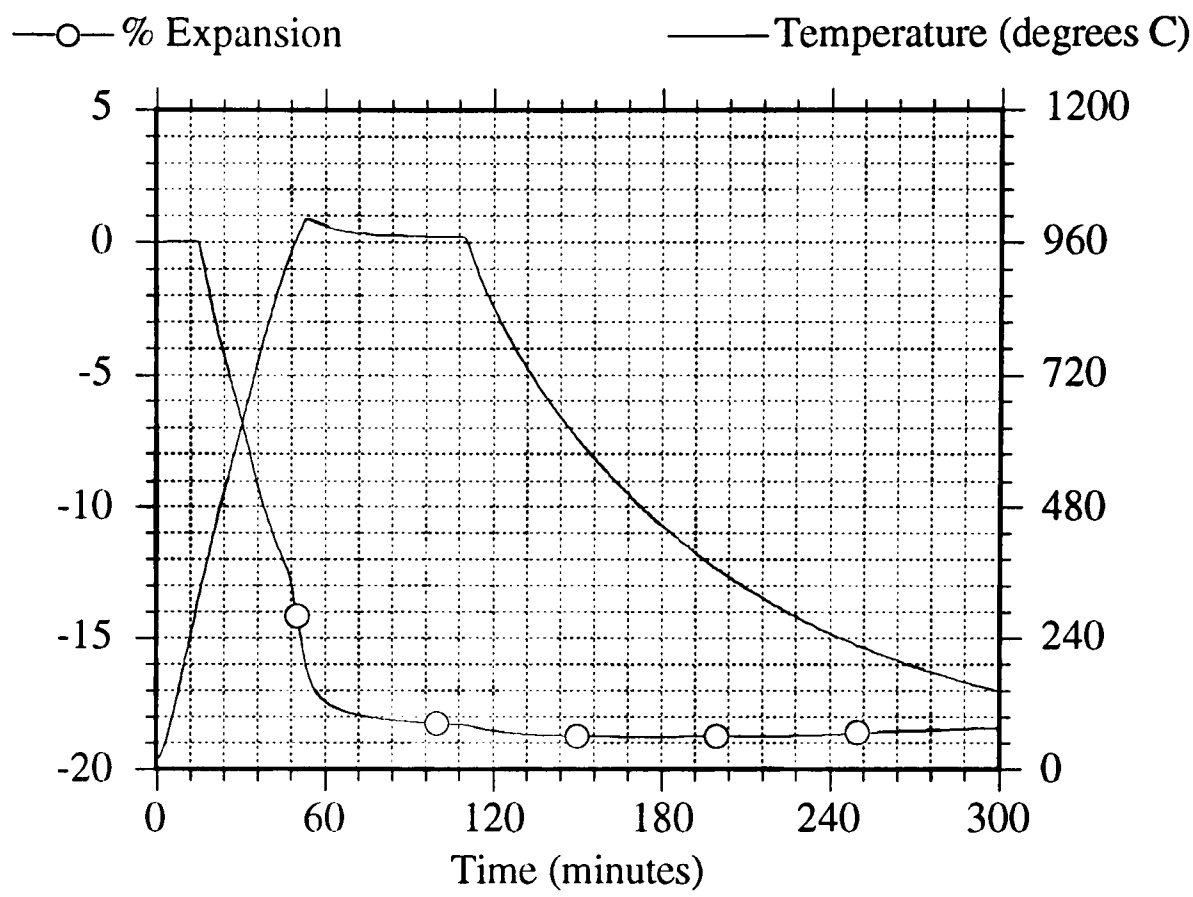


Figure 145: Dilatometry firing trace for Ethyl Silicate AAZ

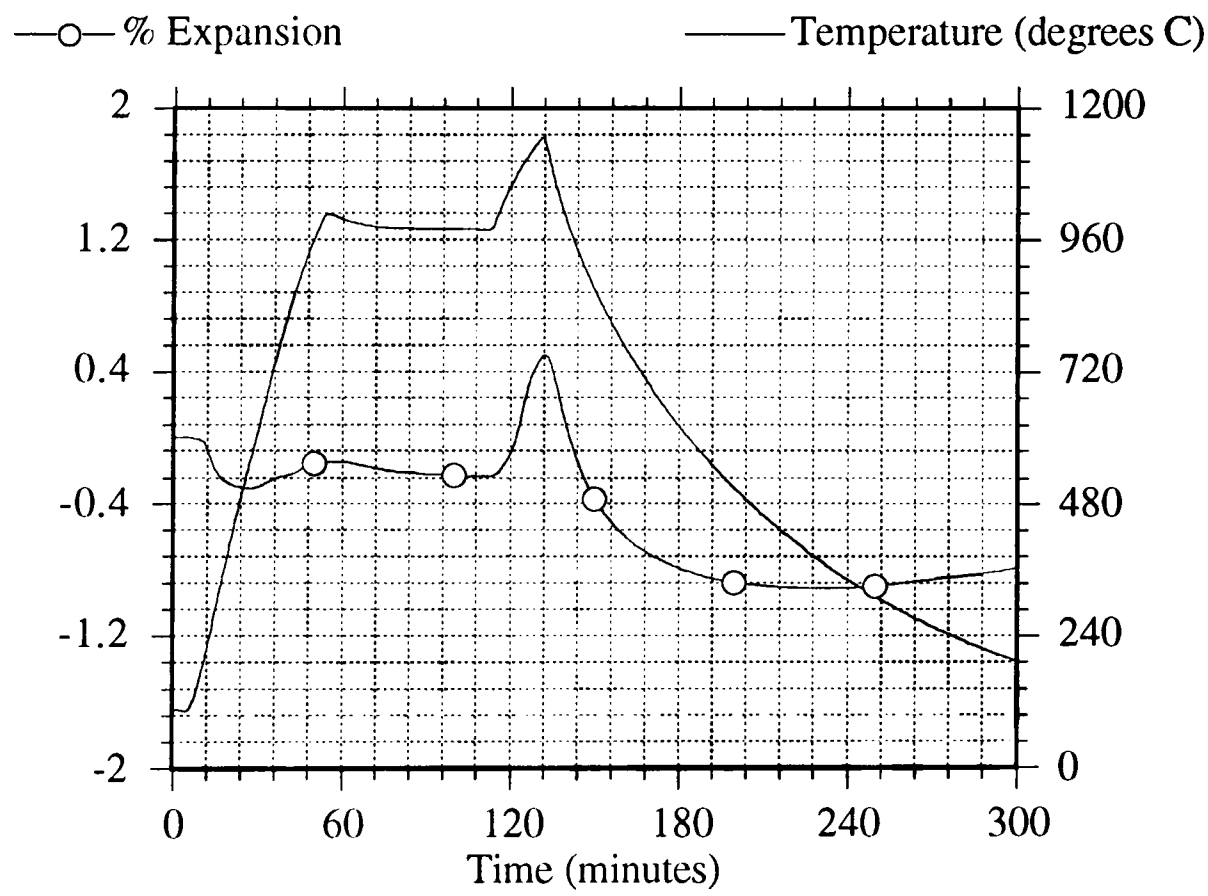


Figure 146: Dilatometry casting trace for Ethyl Silicate AAZ

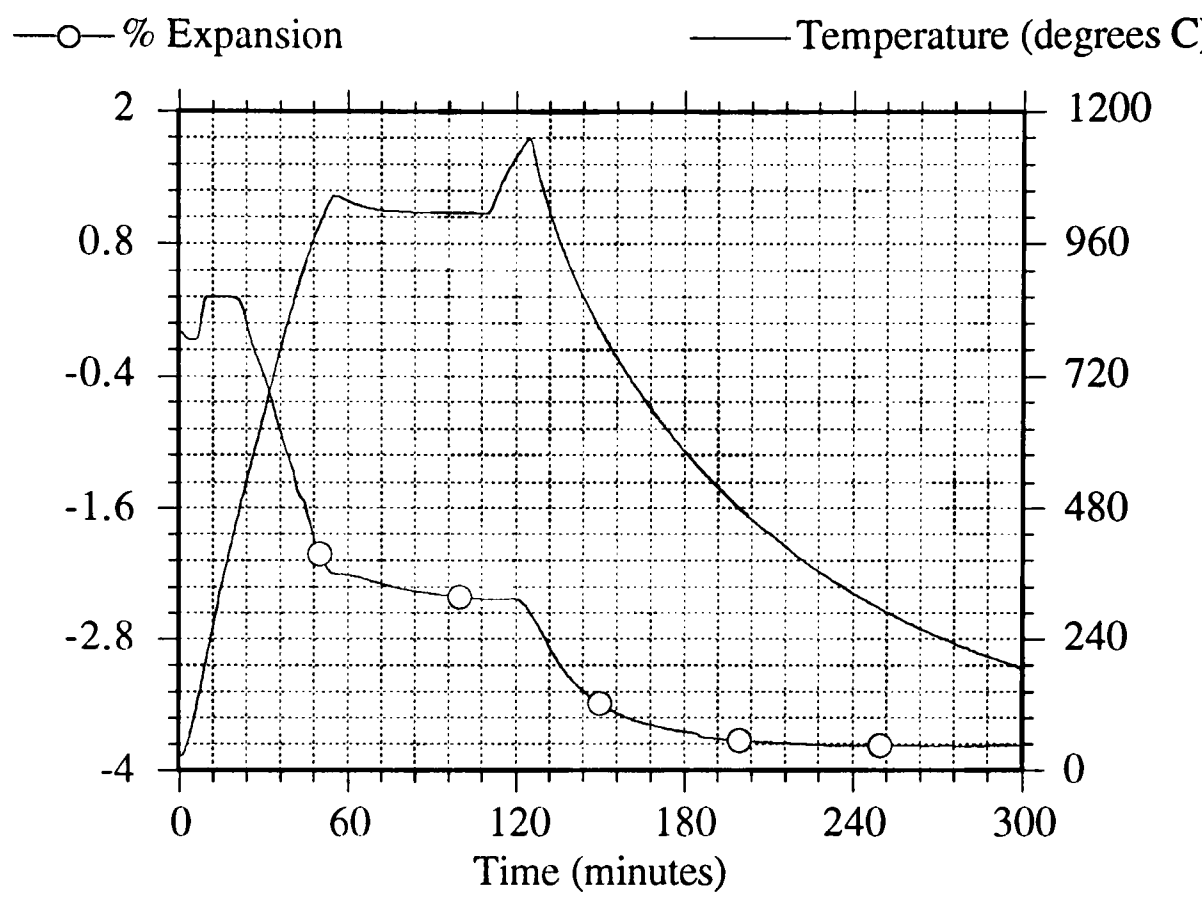


Figure 147: Dilatometry casting trace for Ethyl Silicate AAZ + controlled impurities

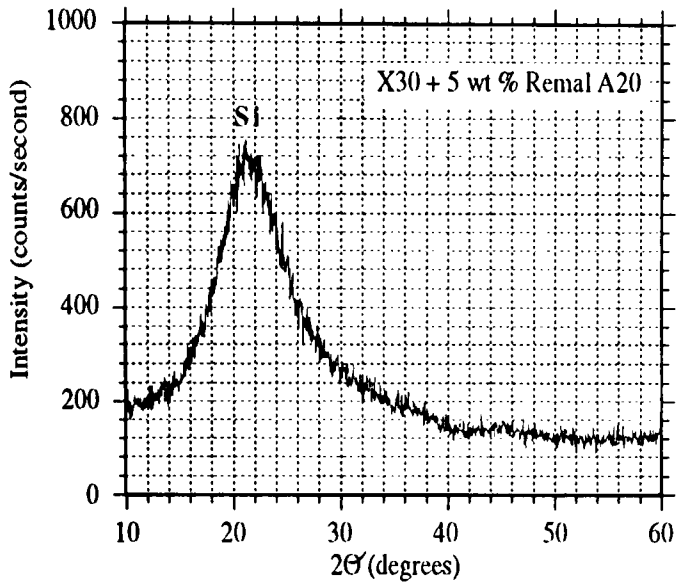
4.4.3: Mixed Systems

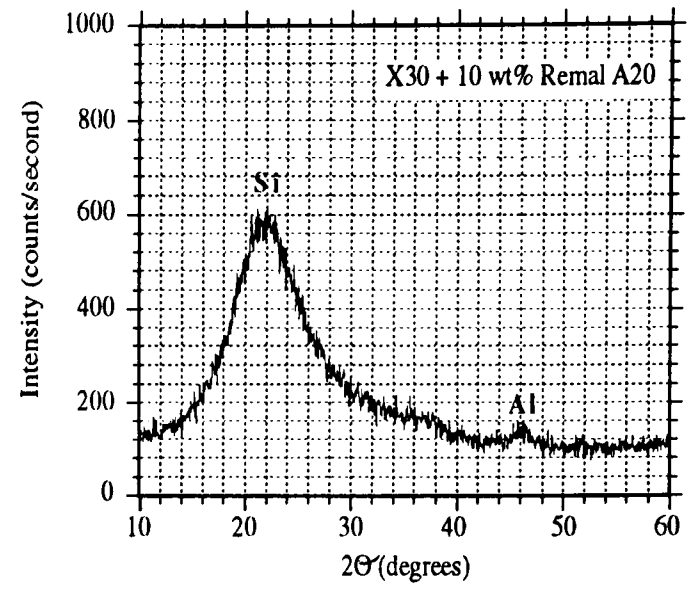
Some of the thermal responses of colloidal silica sol binders, such as the crystallisation temperature and the effect of impurity elements, could be modified by the addition of other basic constituents. Research carried out by Miao[134] et al, showed that when a mixture of alumina and silica sol particles are mixed together, the crystallisation behaviour is altered. A silica sol in the presence of a small amount of alumina will experience a raising of the crystallisation temperature due to the influence of the alumina particles upon the system as a whole. Therefore, an investigation was carried out which monitored the effect of mixing silica and alumina sols together.

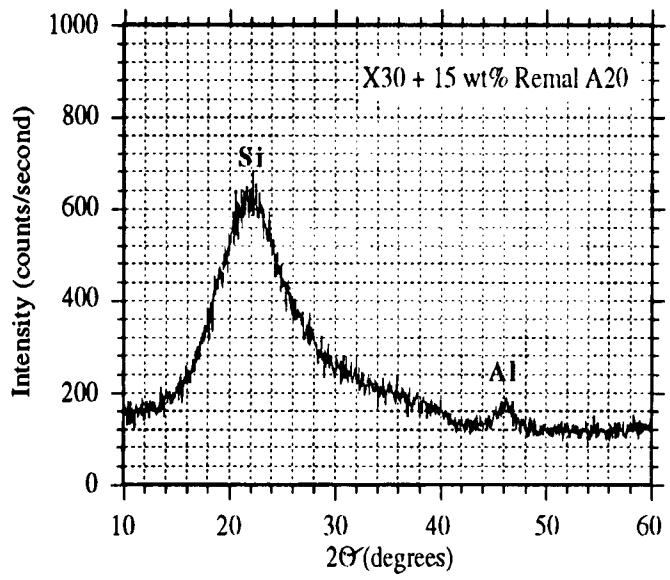
Syton X30 and Remal A20*

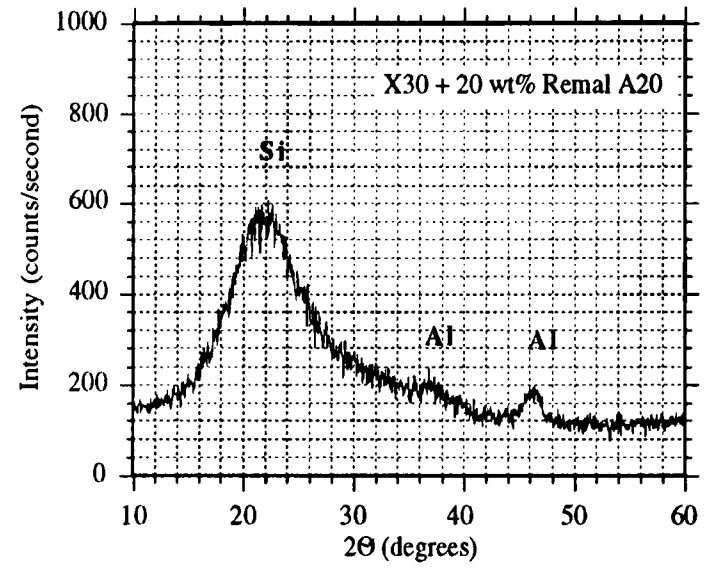
Additions (by weight) of the alumina sol Remal A20 were added to Syton X30. Since the alumina sol was acidic and the silica sol was alkaline, straight additions of one to the other cause instant gellation. Alumina based sols are only stable when acidic but silica sols are stable over a range of pH values including both acidic and alkaline. It was necessary, therefore, to alter the pH of the silica sol to approximately 2 with dilute hydrochloric acid before the addition of the alumina sol.

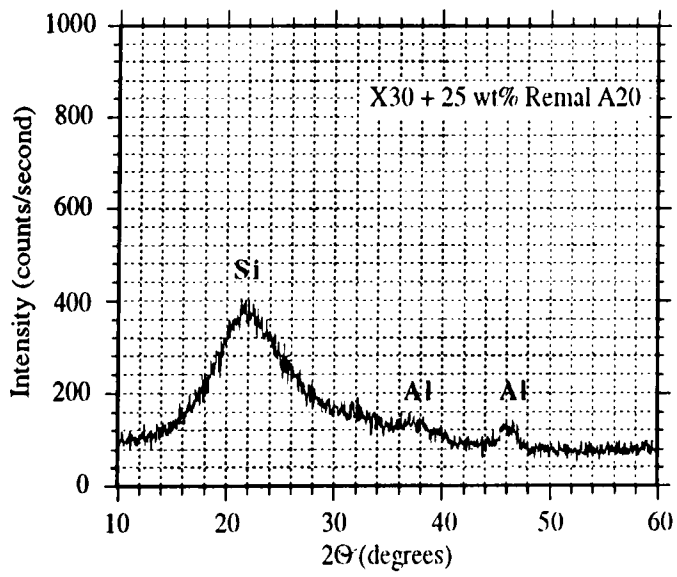
* see Appendix 4











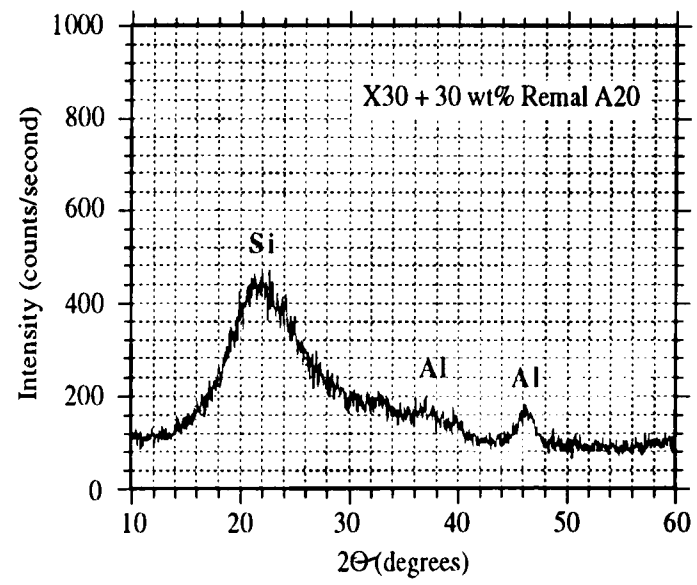


Figure 148: XRD traces for Syton X30 + various Remal A20 additions fired to 1,000°C for 60 minutes

Figure 148 shows the XRD patterns for Syton X30 + various alumina additions fired to 1,000°C for 60 minutes. The first point to note is that the binder no longer crystallises, but remains amorphous at 1,000°C. The alumina sol particles must be influencing the behaviour of the silica sol, and it seems likely that the presence of the relatively large positive alumina particle may attract the negatively charged silica particles to such an extent that any reaction requiring molecular movement, such as crystallisation, will be prevented. It is also feasible that alumina could have a fluxing effect on the silica which produces a glassy, and hence amorphous structure. Alumina is not detected when in low concentrations (5 wt%) but above this amorphous alumina is present on the XRD traces.

The addition of a large amount of alumina produces a sol system which is very unstable and gells rapidly. Since a small amount of alumina appears to affect the crystallisation behaviour in the same manner as a large amount, the sample containing the smallest percentage of alumina was chosen as the one upon which further work was carried out. When fired to 1,200°C (Figure 149), a mixture of Syton X30 and 5 wt% Remal A20 is just beginning to crystallise, with cristobalite being the evident silica phase. So we can see that the addition of a small amount of alumina to a colloidal silica sol will increase the crystallisation temperature from 840°C to 1,200°C.

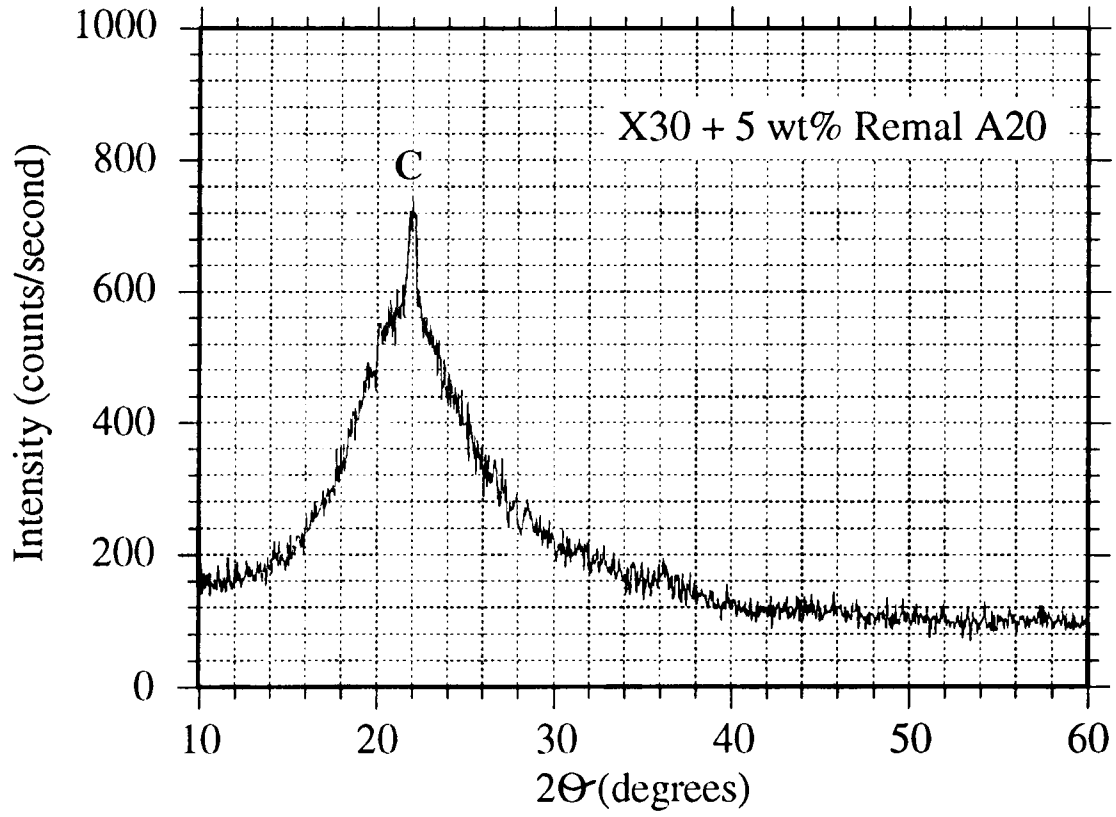


Figure 149: XRD pattern for Syton X30 + 5 wt% Remal A20 fired to 1,200°C for 60 minutes
C = α-cristobalite

The effect of impurity elements upon the phase structure of this mixed sol system was investigated using a sample made to represent a composition found within the silica binder of a fired investment casting mould (Table 25). The XRD pattern for the sample fired at 1,000°C is shown in Figure 150. It can be seen that the impurity elements have initiated the crystallisation of the alumina sol particles to the alpha alumina phase, but the silica base has remained amorphous. This would produce a system that contained a little more structural rigidity than a fully amorphous one, but the thermal response would be unpredictable as different impurity levels would produce different phase structures.

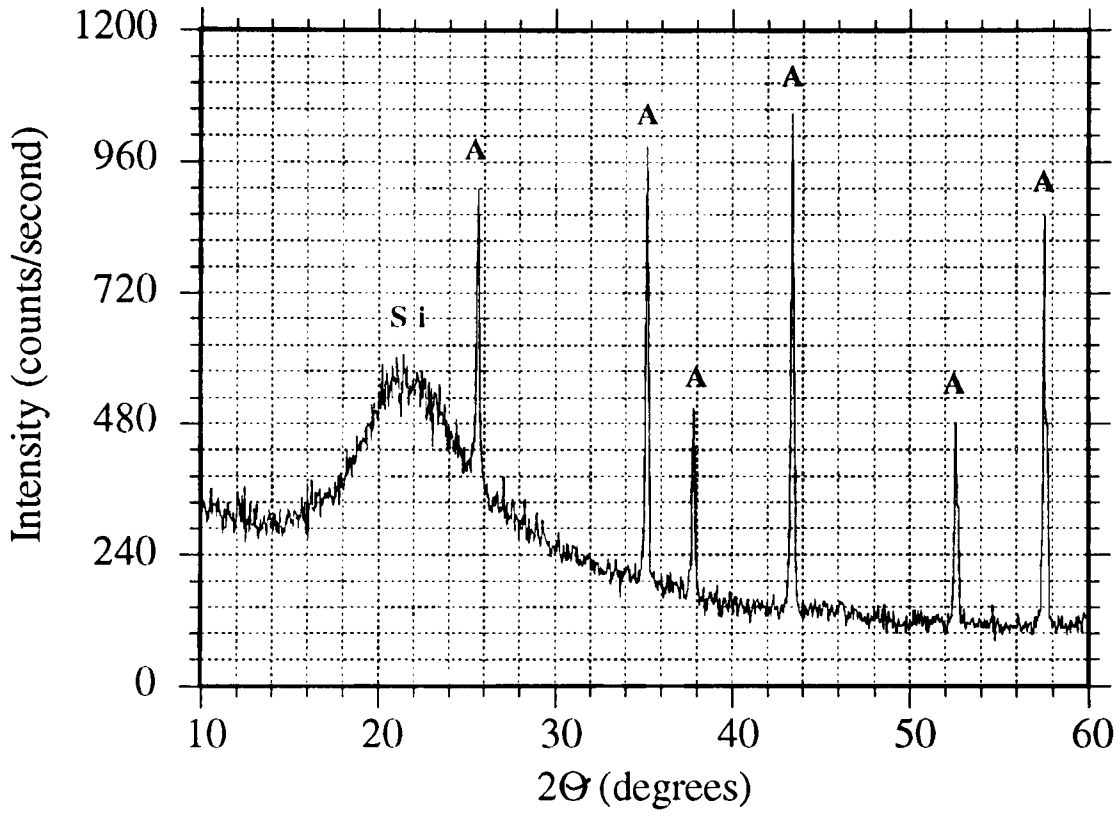


Figure 150: XRD pattern for (Syton X30 + 5 wt% Remal A20) + controlled impurity additions
Si = amorphous silica A = α Al_2O_3

The presence of crystalline alumina in amorphous silica base should have an interesting effect upon the thermal responses of the sample. The DTA firing and casting traces for the mixed system are shown in Figures 151 and 152 respectively. The peaks below 500 °C are identical to those found with Syton X30 and correspond to the removal of water from the sol system. The trace does not contain a crystallisation peak at 961°C because cristobalite is not formed and the system remains amorphous when fired at 1,000°C. The DTA casting trace is very similar to that of X30 and shows no reactions are taking place during reheating of the structure. There is a slight difference in the fact that the base line of the trace seems less dependent upon the heating rate of the sample at low temperatures (i.e. the two lines do not mirror one another).

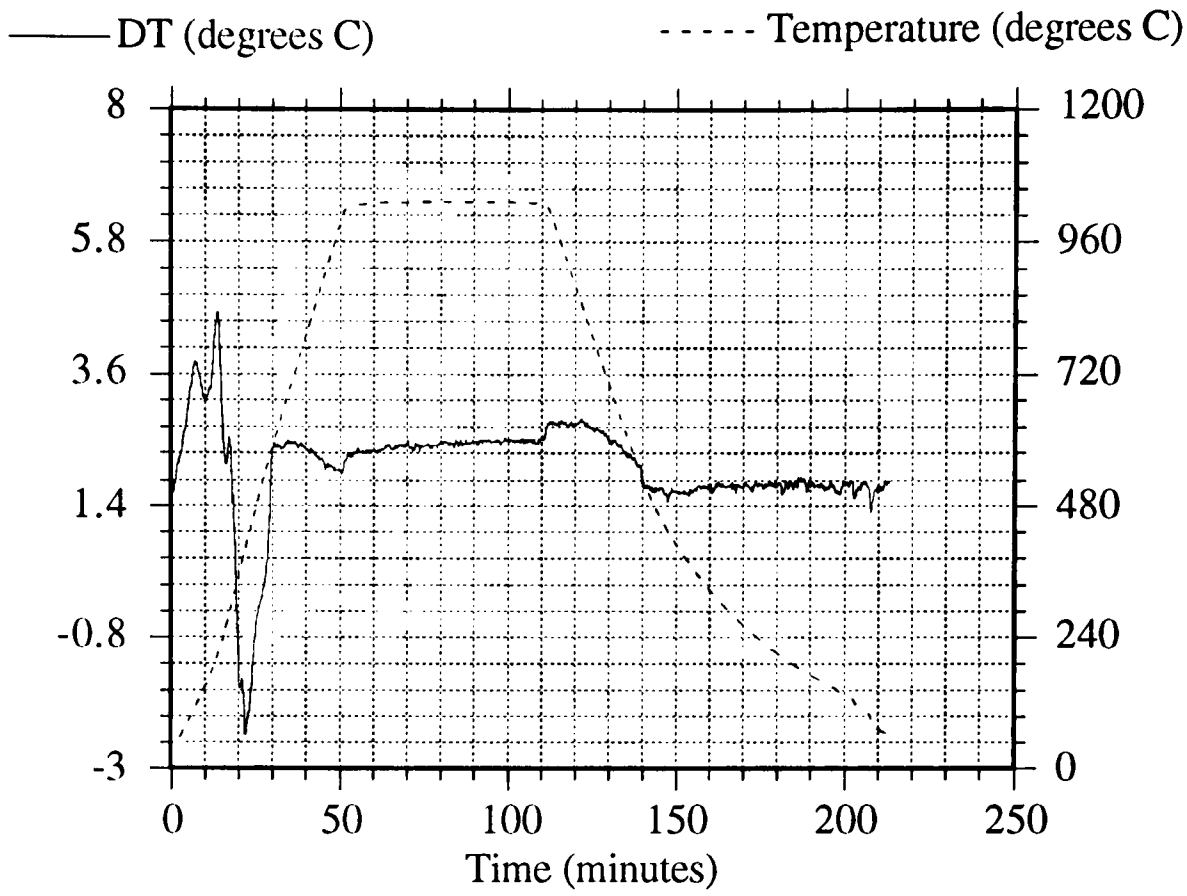


Figure 151: DTA firing trace for Syton X30 + 5 wt% Remal A20

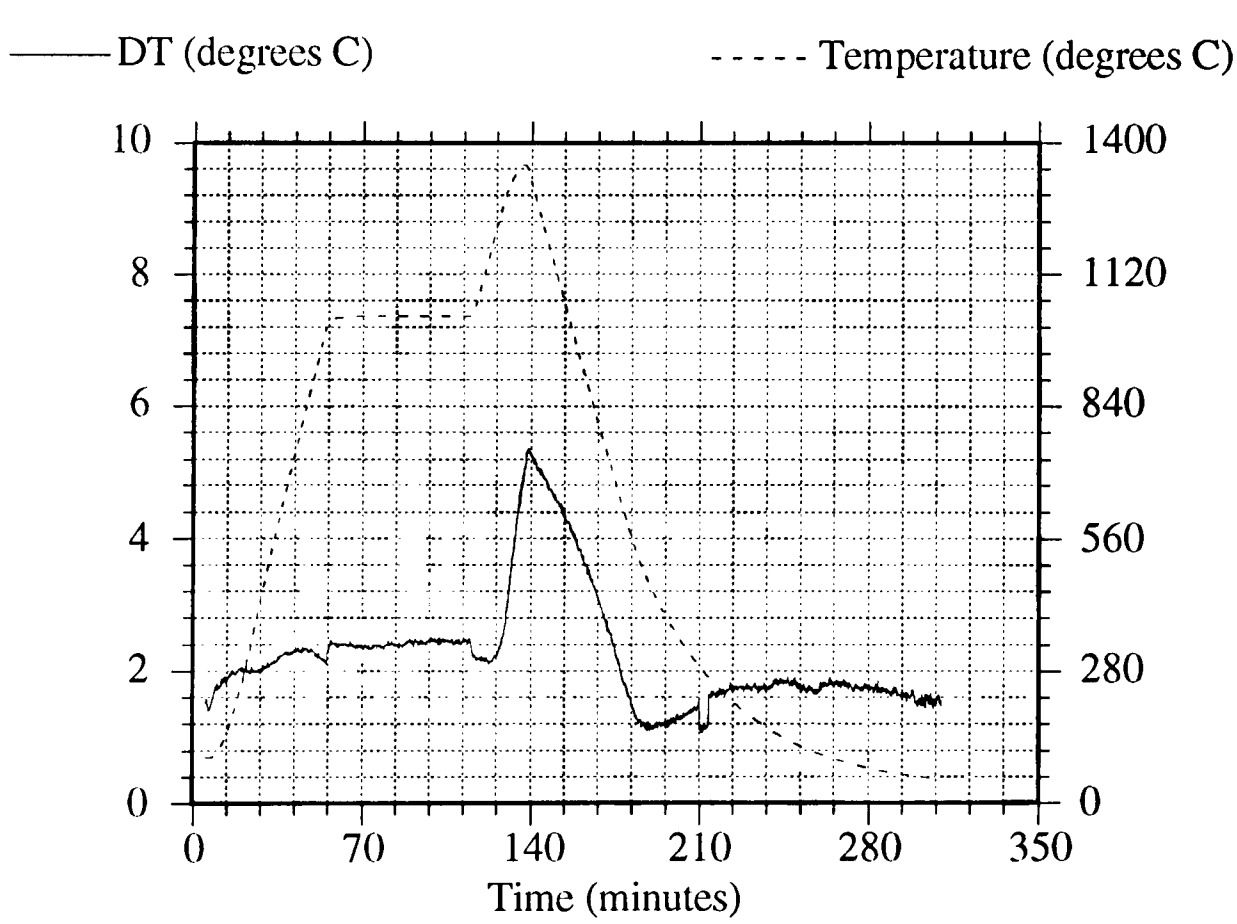


Figure 152: DTA casting trace for Syton X30 + 5 wt% Remal A20

The dilatometry firing and casting traces (Figures 153 and 154 respectively)) show an initial sintering contraction of 14.5% during firing, followed by a further 5% contraction during casting due to the fact that the structure is amorphous. The presence of alumina within the silica network seems to have little effect, other than the prevention of crystallisation, upon the thermal response of the silica sol. The behaviour during casting is very similar to that of an ethyl-silicate binder because the structures are essentially identical.

The dilatometry casting trace for the mixed system incorporated into a silica based composition (Table 25) is shown in Figure 155. As has been shown, the presence of impurity elements crystallises the relatively small alumina portion of the sample, leaving the majority of the structure as amorphous silica. Therefore, the system ceases to behave as a ethyl-silicate and undergoes a volume contraction of 5% during casting.

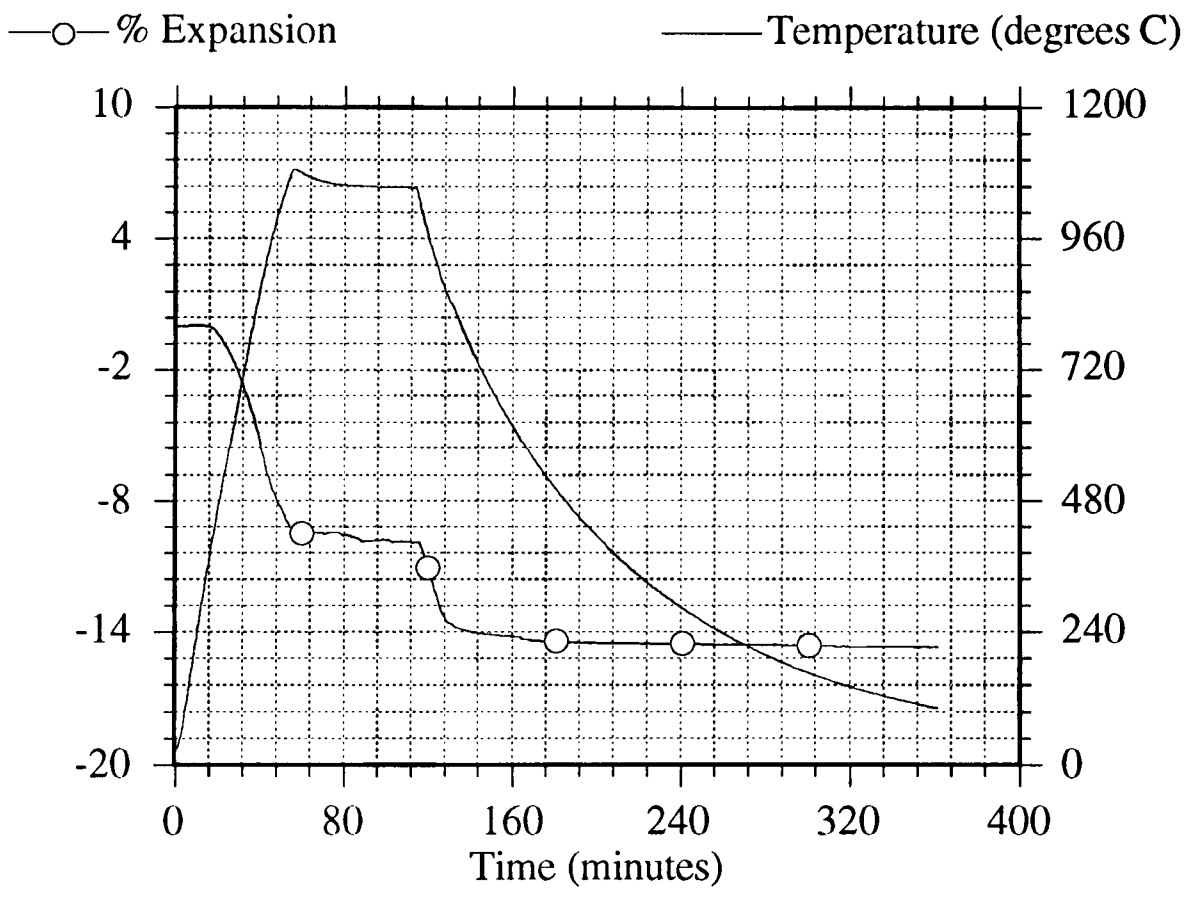


Figure 153: Dilatometry firing trace for Syton X30 + 5 wt% Remal A20

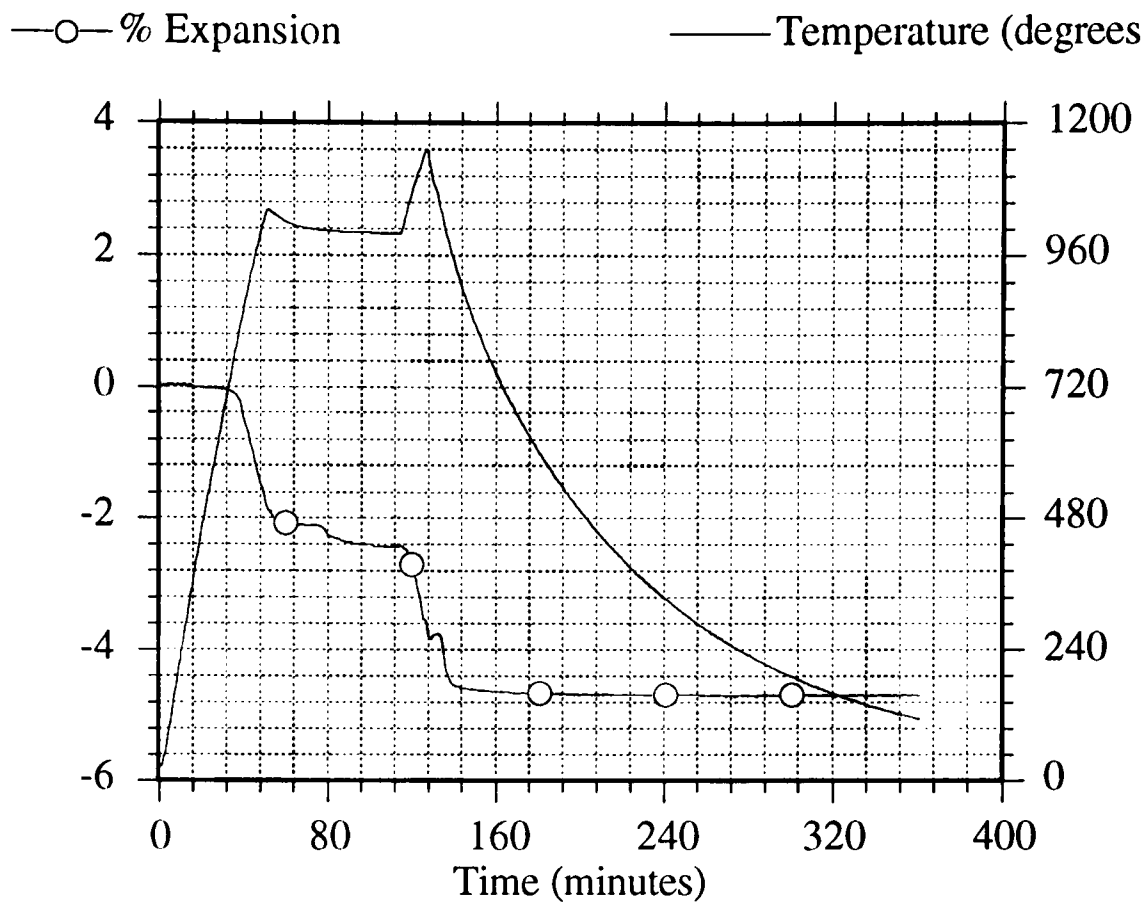


Figure 154: Dilatometry casting trace for Syton X30 + 5 wt% Remal A20.

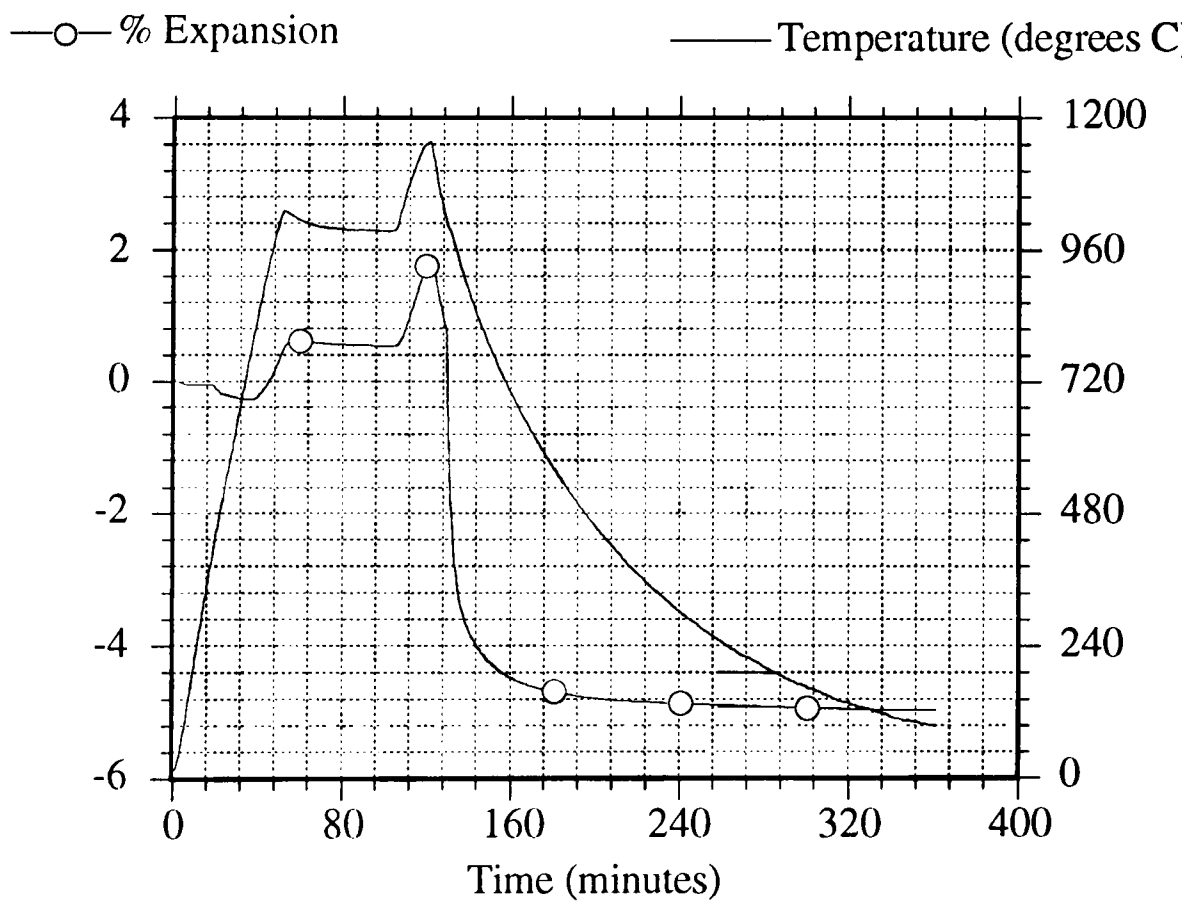


Figure 155: Dilatometry casting trace for (Syton X30 + 5 wt% Remal A20) + controlled impurity additions

4.4.4: Summary

It has been shown that the phase structure and thermal response of the binders currently used in the production of investment casting moulds are affected by the presence of impurity elements leached from within the ceramic fillers. Since the filler phase currently in use contains the lowest level of impurities and the best overall thermal properties of all the refractories currently available, it seems better to replace the binder rather than the refractory. As such, several alternative water and alcohol based binders were obtained and investigated.

Three alternative colloidal silica based binders were investigated. Syton W30 is very similar to Syton X30, except for differences in the particle size and level of sodium stabiliser. The crystallisation temperature of the sol is 870 -890°C and the first phase to be formed is cristobalite. As with other colloidal systems, once initial particle coalescence and sintering has taken place during firing the binder is fairly stable throughout the whole of the casting cycle. In the presence of impurity elements the binder undergoes a 6.5% volume contraction during the casting cycle. As this is less than with Syton X30 it appears that W30 is less susceptible to structural modifications brought about by unwanted elements in the structure and may be an alternative to X30 in the production of an investment mould. Primcote is a colloidal silica binder, incorporating a dryness indicator, which is manufactured to be used in the primary coats of a mould. The binder contraction is less than X30 during firing and the crystalline structure is inactive during casting. Unfortunately, computer failure meant that data concerning the effect of impurities upon the binder was lost, and no comment as to the suitability of the binder as a replacement can be made at this stage. Fascote is a very similar water based binder, manufactured by the same company, but intended to be used in the secondary coats of a mould. The overall contraction during firing is greater than X30 but the inactivity during casting is similar. Volume contraction induced by the presence of impurity elements is only 4% overall which means that on the basis of initial research it can be predicted that Fascote may be a good alternative binder as far as structural properties are concerned. However, other factors have to be taken into account when considering a binder for mould applications, as the crystalline structure of this binder may prove to possess a greater strength than is needed. High mould strength tends to lead to hot-tearing problems and difficulties in removing the mould once casting is complete.

Two alternative alcohol based ethyl-silicate binders were investigated. Silester OS is a binder which consists of an ortho-silicate mixture which is acid hydrolysed by the customer to form a mixture of poly-silicate chains in an acidic alcohol based medium. When gelled and fired, the binder behaves in a similar manner to Silester XAR except that, although the structure is amorphous, the sample undergoes very little volume contraction during the casting cycle. The fact that Silester OS has a different structural response could be due to the absence of sol particles which are incorporated into prehydrolysed binders to increase the stability. The apparent structural differences are also mirrored in the effect of impurity elements. The induced volume contraction of OS during casting is larger than

that in a standard hybrid binder which imparts greater structural instability in the presence of impurities. It is difficult at this stage to propose reasons why the binder possesses the apparently unorthodox thermal responses, but it can be seen that the binder would not make a good alternative to Silester XAR in the production of an investment mould due to instability. Ethyl silicate AAZ is a hybrid binder manufactured as a binder for the investment industry. This binder crystallises below 1,000°C which is unusual for an ethyl-silicate system and may be due to the fact that the binder has not been prepared under the correct conditions or contains elements which catalyse crystallisation. As a crystalline structure, the binder is stable during the casting cycle but is susceptible to the influence of impurity elements and undergoes volume contraction. As such, this binder would not make a good replacement system as the responses are unpredictable and more likely to cause mould wall movement than the binder currently in use.

Some of the thermal responses of colloidal silica sol binders, such as the crystallisation temperature and the effect of impurity elements, could be modified by the addition of other basic constituents. Research carried out by Miao[133] et al, showed that when a mixture of alumina and silica sol particles are mixed together, the crystallisation behaviour is altered. A silica sol in the presence of a small amount of alumina will experience a raising of the crystallisation temperature due to the influence of the alumina particles upon the system as a whole. Therefore, an investigation was carried out which monitored the effect of mixing silica and alumina sols together. The crystallisation temperature of Syton X30 can be raised above 1,200°C by the addition of just 5% (by weight) of alumina sol to the system. As an amorphous system the binder undergoes volume contraction during the casting cycle and even further contraction in the presence of impurity elements. As such, the phenomena of raised crystallisation temperature has many potential applications, but as an investment casting mould binder the mixed system would be more likely to produce mould wall movement and creep during the casting of a large metal weight component.

4.5: Alternative Non-Silica Based Binders

It has been shown that the phase structure and thermal response of the binders currently used in the production of investment casting moulds are affected by the presence of impurity elements leached from within the ceramic fillers. Since the filler phase currently in use contains the lowest level of impurities and the best overall thermal properties of all the refractories currently available, it seems better to replace the binder rather than the refractory. As the maximum temperature that investment casting moulds have to tolerate is increasing with the production of larger components, it is becoming clear that silica may no longer possess adequate physical properties. Some other refractory materials, such as alumina or zirconia, have greater strength and structural stability than silica at higher temperatures. Therefore, several non-silica water based binders were obtained and investigated. Full specifications for the binders can be found in Appendix 4.

4.5.1: Zirconia Based Binders

Zirconia is a refractory material with a high melting point (2590°C)[38] which has recently become available in colloidal form. It is this high melting point which makes zirconia binders an attractive alternative to silica.

1. Remet Zirconia Sol

This sol is an acetate stabilised, aqueous dispersion of amorphous zirconia particles. When gelled the binder exhibits an amorphous structure (Figure 156) with broad diffraction peaks. When fired at 1,000°C the zirconia has crystallised and is present as monoclinic zirconia (Figure 157).

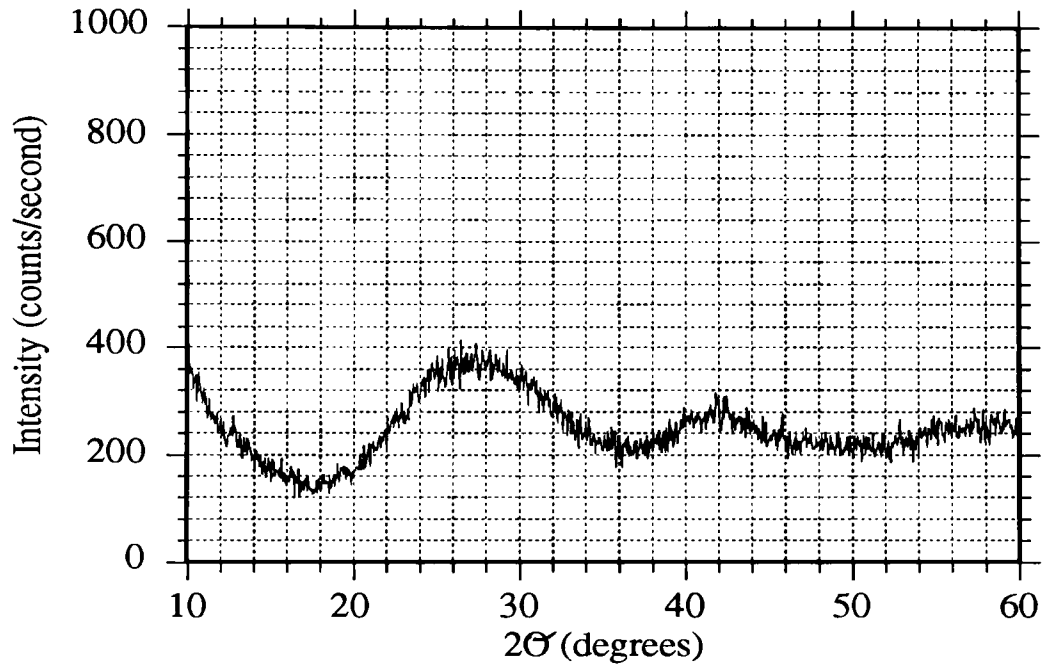


Figure 156: XRD pattern for gelled and dried Remet zirconia sol

The dilatometry casting trace for the sol is shown in Figure 158. The gelled structure undergoes a 40% volume contraction during heating to 1,000°C after which the fact that the structure is crystalline means that no further contraction takes place during cooling. The large contraction during heating is due to the very small particle size (2 nm). This makes the entire system highly reactive because of the relatively large amounts of surface area available for reaction. Therefore, when heated, the sol particles react strongly together and sintering is extensive. This may be a limiting factor in the production of investment casting moulds as the structure is self-supporting and may be unable to accommodate large contractions in the binder system.

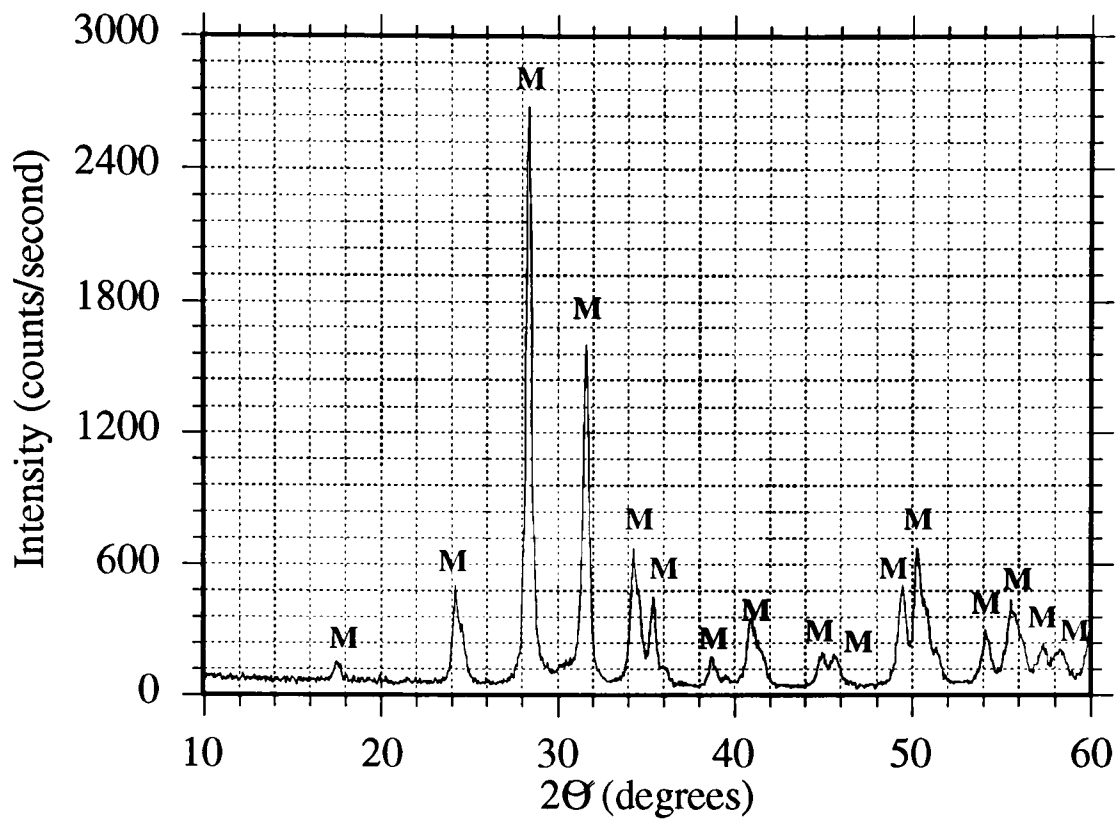


Figure 157: XRD trace for Remet zirconia sol fired at 1,000°C for 60 minutes

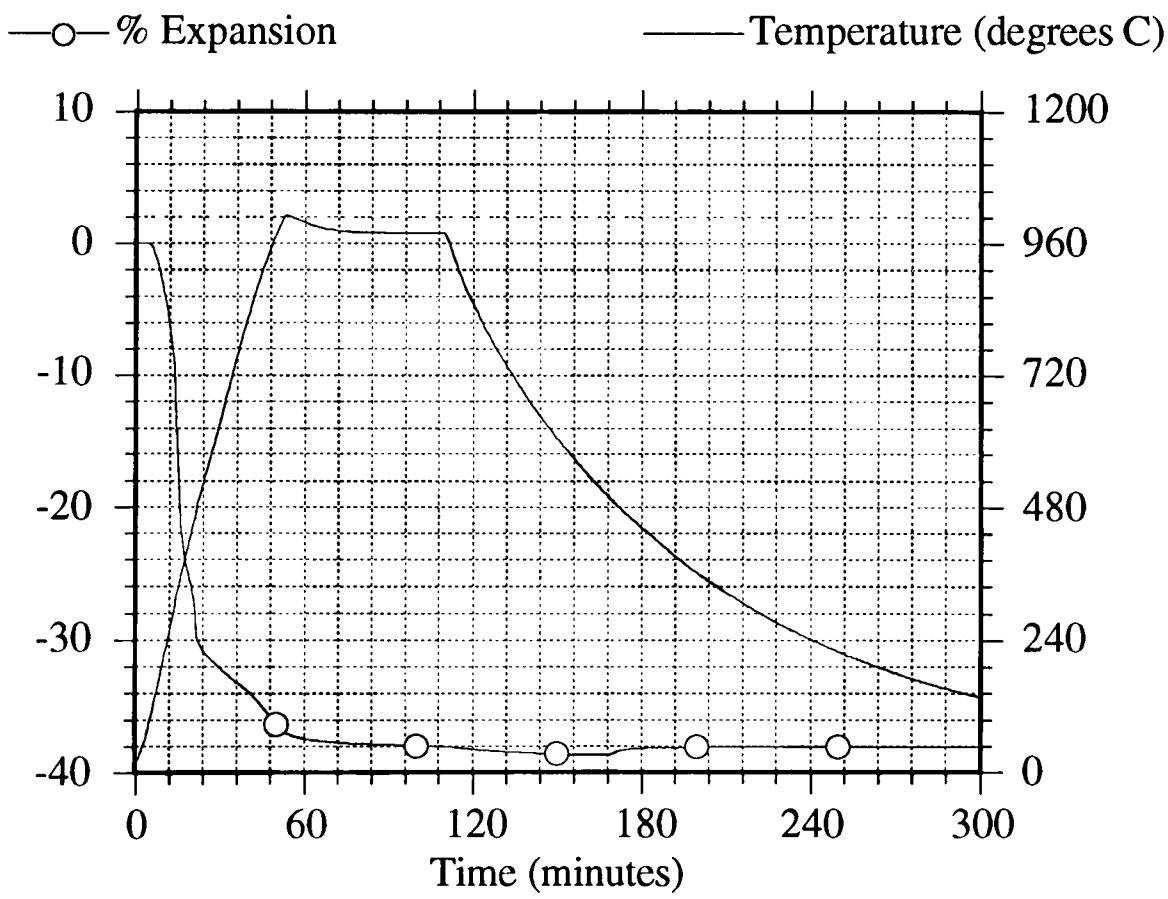


Figure 158: Dilatometry firing trace for Remet zirconia sol

Though the binder structure is monoclinic when fired at 1,000°C, this may not be the case when the sample is heated above this temperature. Zirconia undergoes a series of polymorphic transformations: monoclinic up to 1,170°C, tetragonal up to 2370°C and cubic at higher temperatures[135]. The transformation from monoclinic to tetragonal zirconia is accompanied to by a 3-5% volume contraction because the tetragonal phase has a much greater density. This volume contraction is catastrophic to the structure of most ceramic bodies and failure usually occurs. In order to use zirconia in an application which requires heating above the transformation temperature, the structure must be stabilised as either the monoclinic or the tetragonal phase to prevent the transformation from taking place. Oxides such as CaO, Y_2O3 and MgO[135] can stabilise the structure and this must not be confused with the fact that acetate is quoted as the stabilising agent.

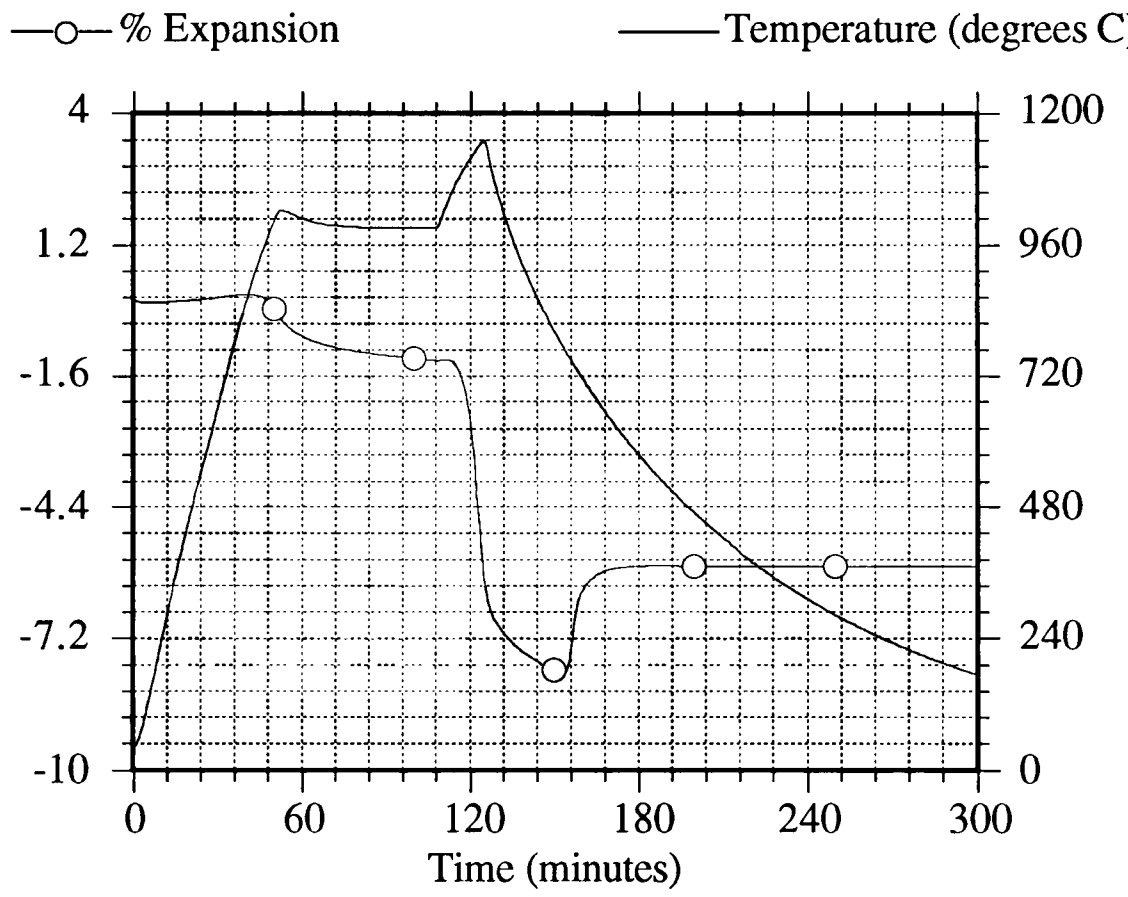


Figure 159: Dilatometry casting trace for Remet zirconia sol

During the firing cycle (Figure 159), the monoclinic phase is free to transform to the tetragonal structure since the phases are not actually stabilised. During reheating to 1,000°C the sample is fairly stable, but once above this temperature contraction begins again. This is expected, as densification will take place at a greater rate as the sample nears the transformation temperature. During cooling there is an abrupt volume expansion of around 3% at 900°C which is almost certainly due to the tetragonal phase transforming to monoclinic. The temperature is lower than would be expected; possibly due to the hysteresis effect observed in many zirconia systems[13].

To investigate the effect of impurity elements upon the thermal response, a composition found within the binder of a mould was recreated (see Section 4.4.1 for details). The casting trace for the modelled composition (Figure 160), has the same overall form but much less volume contraction is observed. Elements such as calcium have a stabilising effect upon zirconia and though the tetragonal-monoclinic transformation still takes place, it may only be happening in isolated regions of the binder where elements are not present. As such, the overall contraction is reduced during the casting cycle.

The uncontrolled phase changes which take place in the structure will be detrimental to the stability of the mould both during firing and casting. This binder, in its present unstabilised form, would not make a good alternative to silica in an investment casting mould.

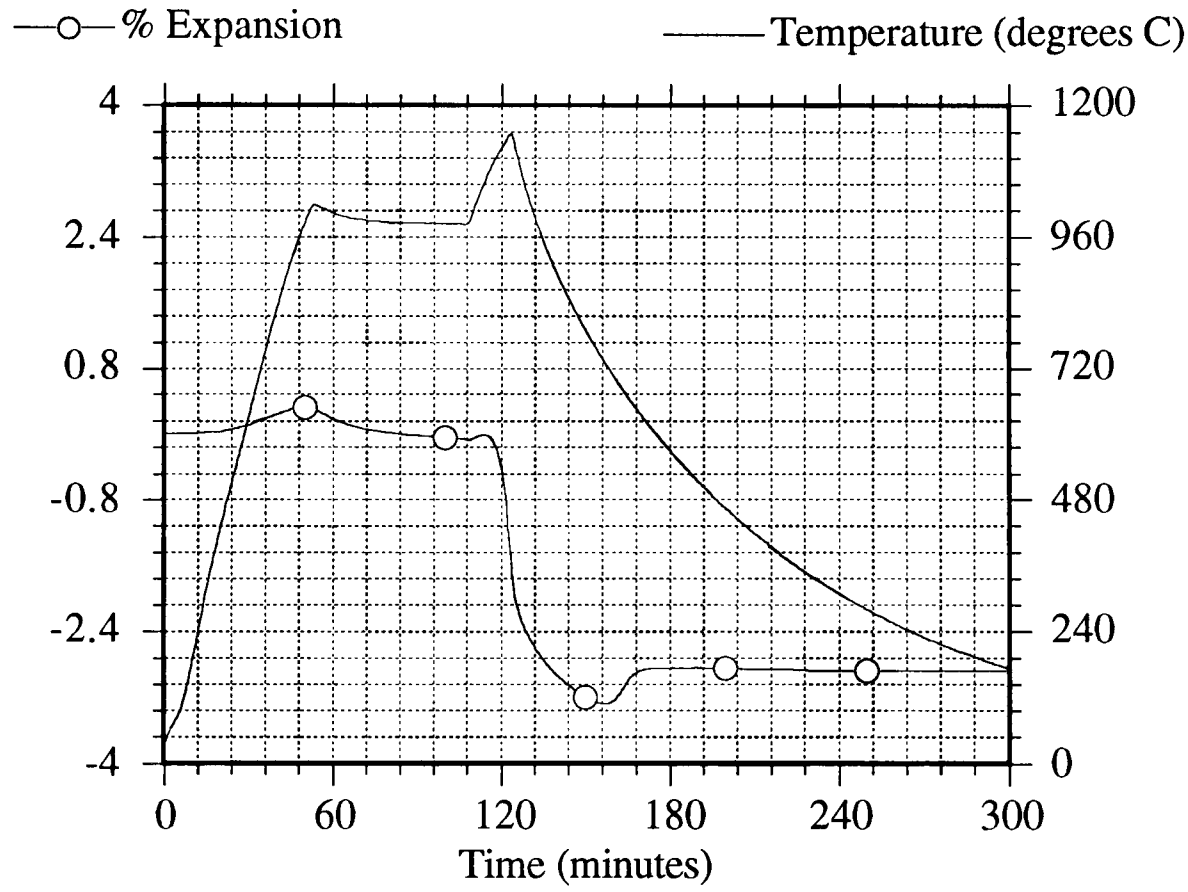


Figure 160: Dilatometry casting trace for Remet zirconia sol + controlled impurity additions

2. Magnabond Z

This is a water based zirconia binder which is similar to the Remet sol but the manufacturer does not quote a stabilising agent since the structure may not be sol based. The gelled structure (Figure 161) appears to be based upon an amorphous zirconia background with a small amount of crystallinity which cannot be identified as any particular zirconia phase. The crystalline peaks could be due to the fact that the binder is not sol based and may contain polycrystalline or even organic material. When fired, however, any unidentified material is removed and the structure is completely monoclinic (Figure 162).

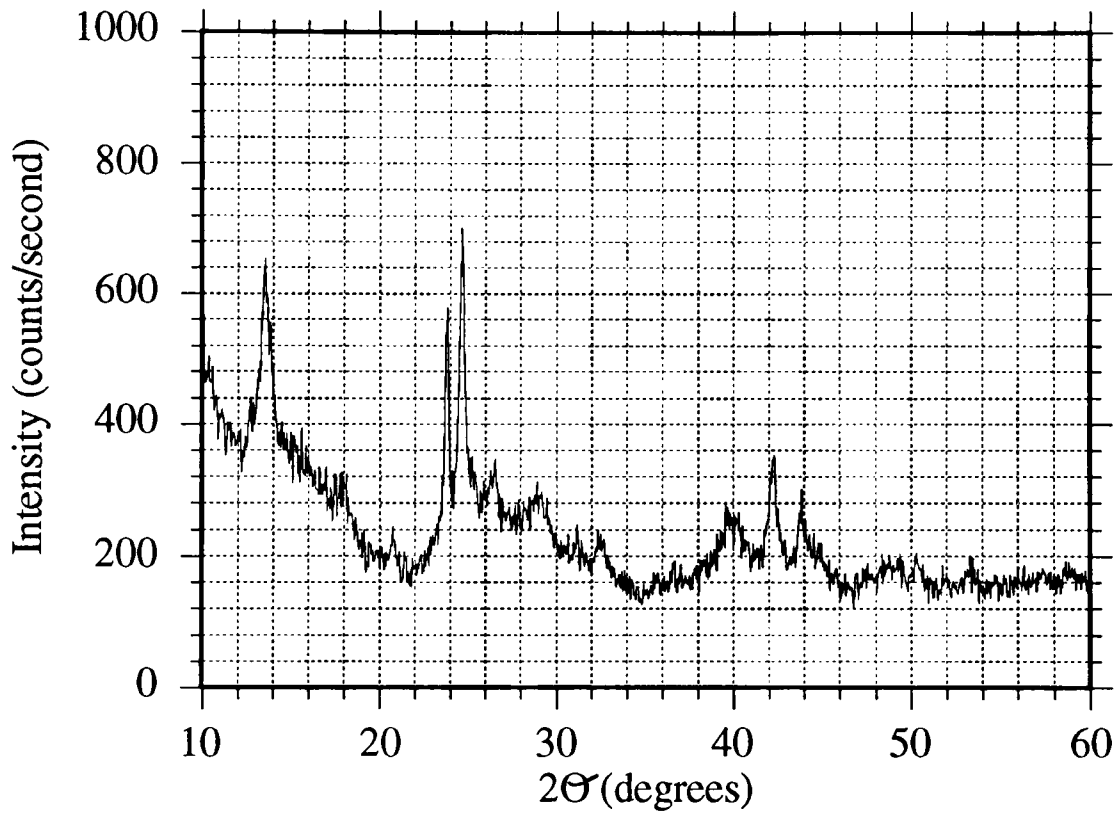


Figure 161: XRD pattern for gelled Magnabond Z

The dilatometry firing trace is shown in Figure 163. Extensive contraction indicates that the zirconia is a reactive system and undergoes extensive sintering during firing. Since the zirconia is unstabilised and monoclinic in nature, the casting trace (Figure 164) is similar to that of Remet zirconia sol except that the overall amount of volume contraction is less. The volume expansion at 900°C, due to the tetragonal-monoclinic phase transformation, is less abrupt, less extensive, and occurs slowly over a range of temperatures. The alteration in the thermal properties may have something may be due to the absence of acetate ions within the system or to the action of other constituents which are not named in the customer specifications but are visible as crystalline phases in the gelled structure.

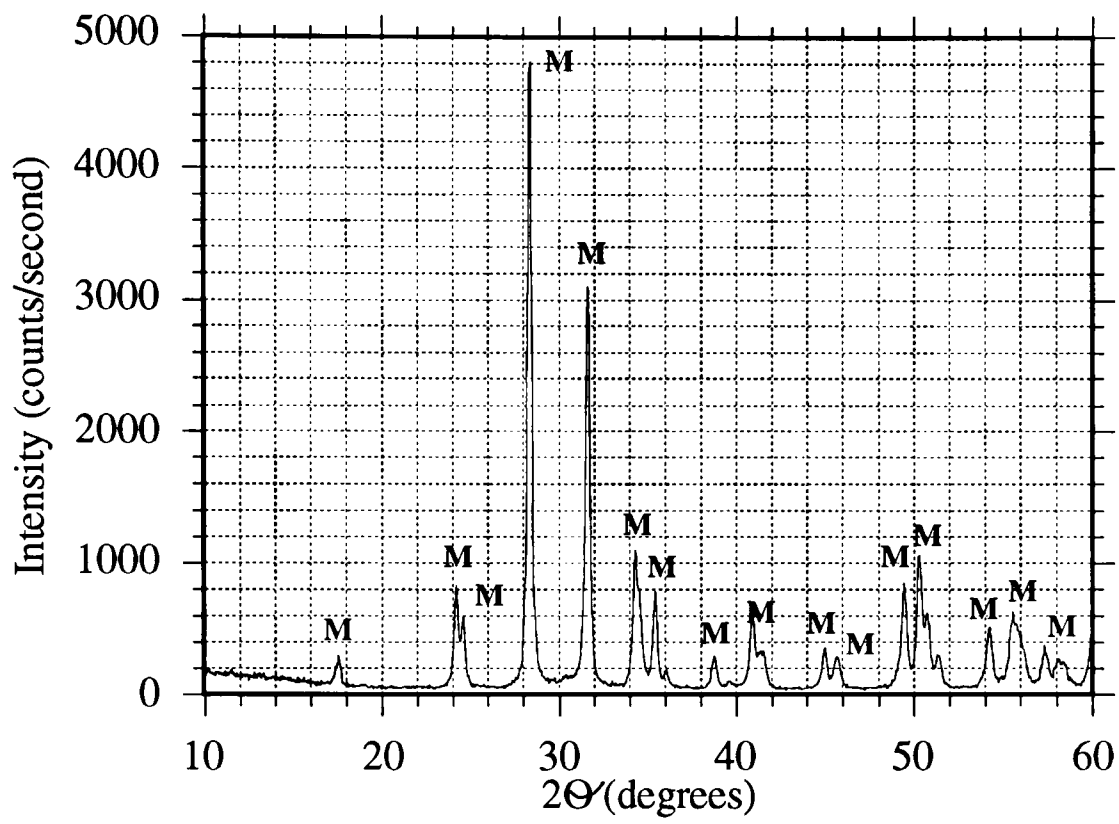


Figure 162: XRD pattern for Magnabond Z fired to 1,000°C for 60 minutes

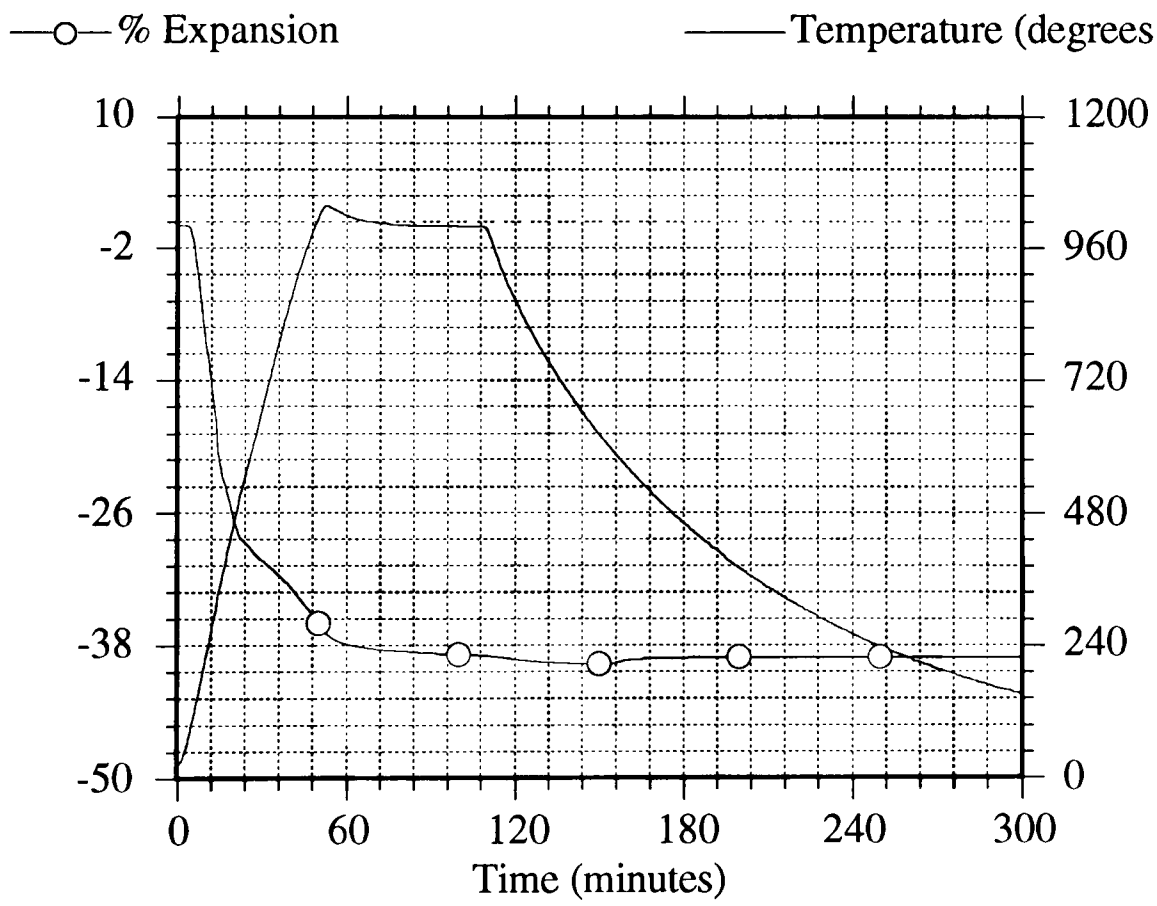


Figure 163: Dilatometry firing trace for Magnabond Z

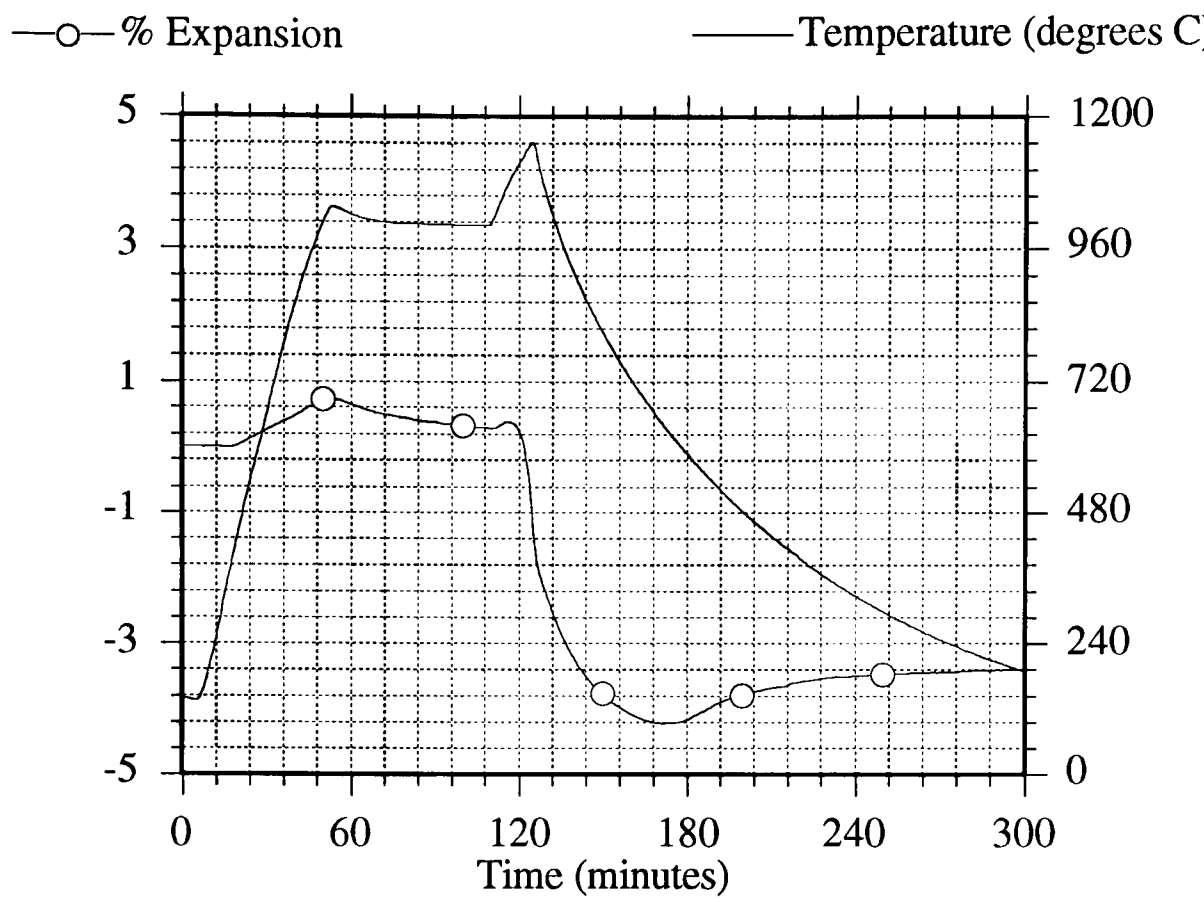


Figure 164: Dilatometry casting trace for Magnabond Z

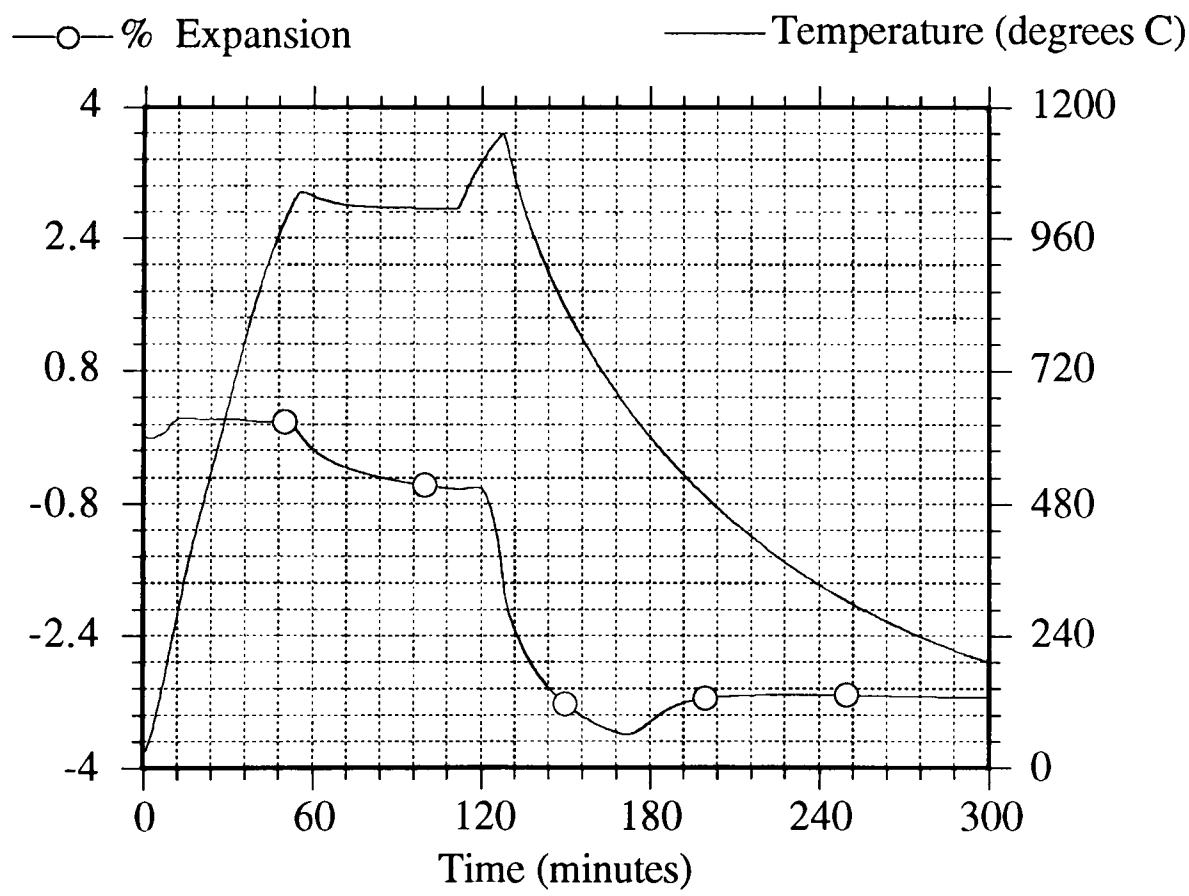


Figure 165: Dilatometry casting trace for Magnabond Z + controlled impurity additions

The dilatometry casting trace, after the addition of controlled impurity elements, is shown in Figure 162. Comparison with the standard trace shows that the two are identical and it seems that the impurity elements have no effect upon the thermal response of the binder. This immunity to the influence of impurity elements would be desirable in an investment mould binder, but the phase changes, extensive contraction during firing and volume changes would limit the use of the binder for this application.

4.5.2: Alumina Based Binders

1. Remal A20

This is a colloidal alumina binder consisting of small pseudo boehmite particles suspended in an aqueous medium. The XRD trace for the gelled binder showing the boehmite phase is displayed in Figure 166. Boehmite is a form of aluminium hydrate which has a specific transformation sequence when sintered in air (Figure 167). When fired at 1,000°C for 60 minutes the structure transforms to θ alumina (Figure 168). This phase usually develops at 1,050°C but here it is formed during an isothermal hold at temperatures around that of the transformation.

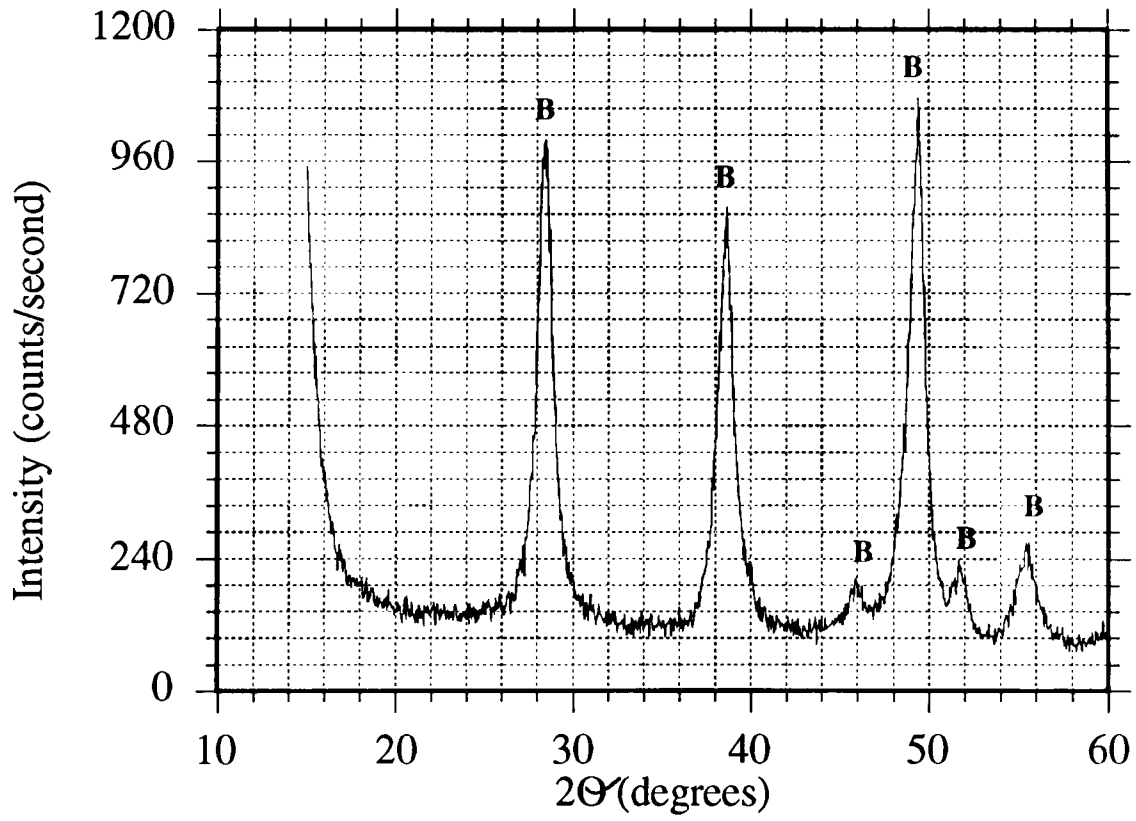


Figure 166: XRD trace for gelled Remal A20
B = boehmite

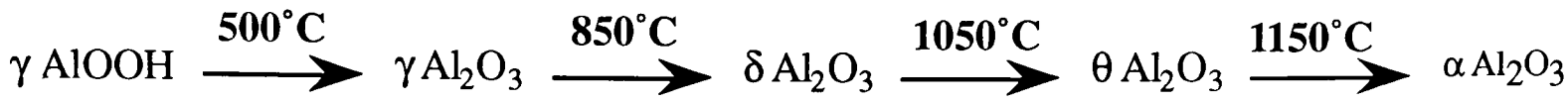


Figure 167: Reaction sequence for alumina based sols[136]

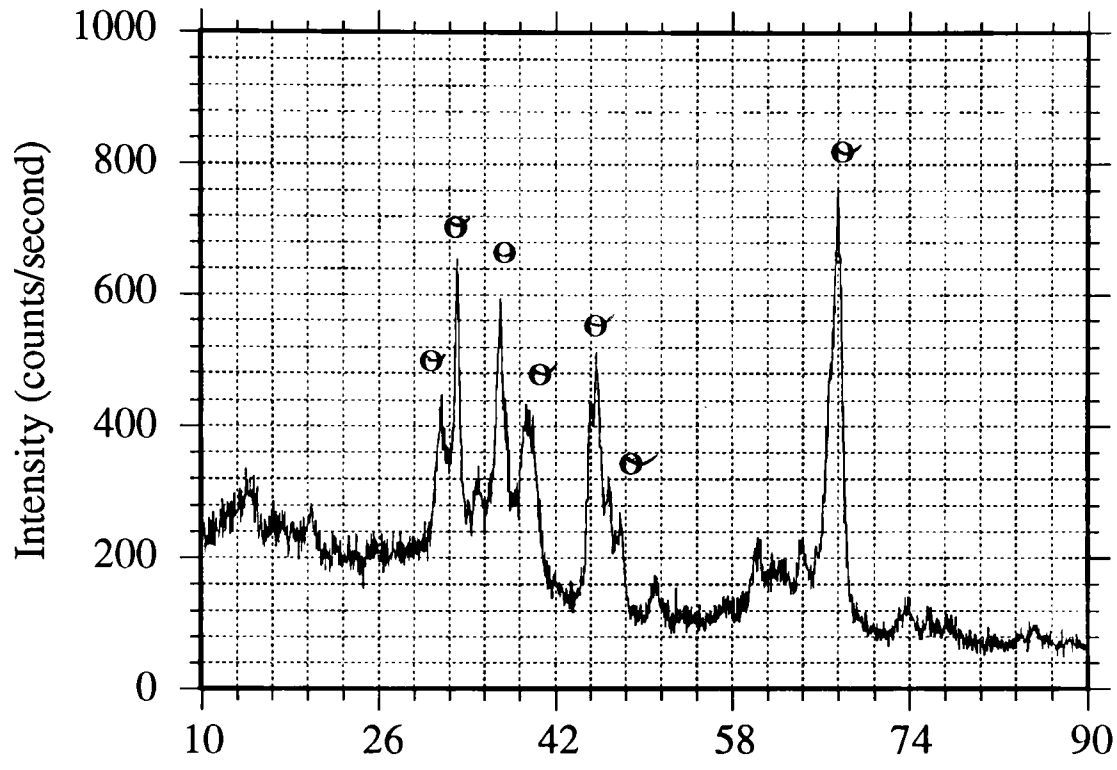


Figure 168: XRD trace for Remal A20 fired to 1,000°C for 60 minutes

The dilatometry firing trace (Figure 169) shows a 9% volume contraction due to sintering during heating of the sample to 1,000°C. A small inflection in the curve at 500°C is due to the transformation of boehmite to γ-alumina. At 1,000°C the sample consists of δ-alumina, which transforms to θ-alumina during the isothermal hold. Once the crystalline structure has been established the sample undergoes very little contraction or expansion during cooling and reheating during the first stages of the casting cycle (Figure 170). A small amount of contraction occurs during the isothermal hold which is due to further transformation of residual theta phase. As the sample approaches 1150°C another transformation, this time to the α-alumina phase, takes place and extensive sintering takes place (12% overall). This indicates that the alpha phase is considerably less dense than the theta phase.

Incorporation of impurity elements into the structure causes a 1% volume expansion during reheating to 1,000°C (Figure 171). This is followed by a reduction in the extensive contraction during heating to 1,150°C and cooling by as much as one half, with the overall contraction being reduced to 6%. It is possible that the impurity elements partly inhibit the transformation from theta to alpha alumina and this reduces the overall contraction during the casting cycle.

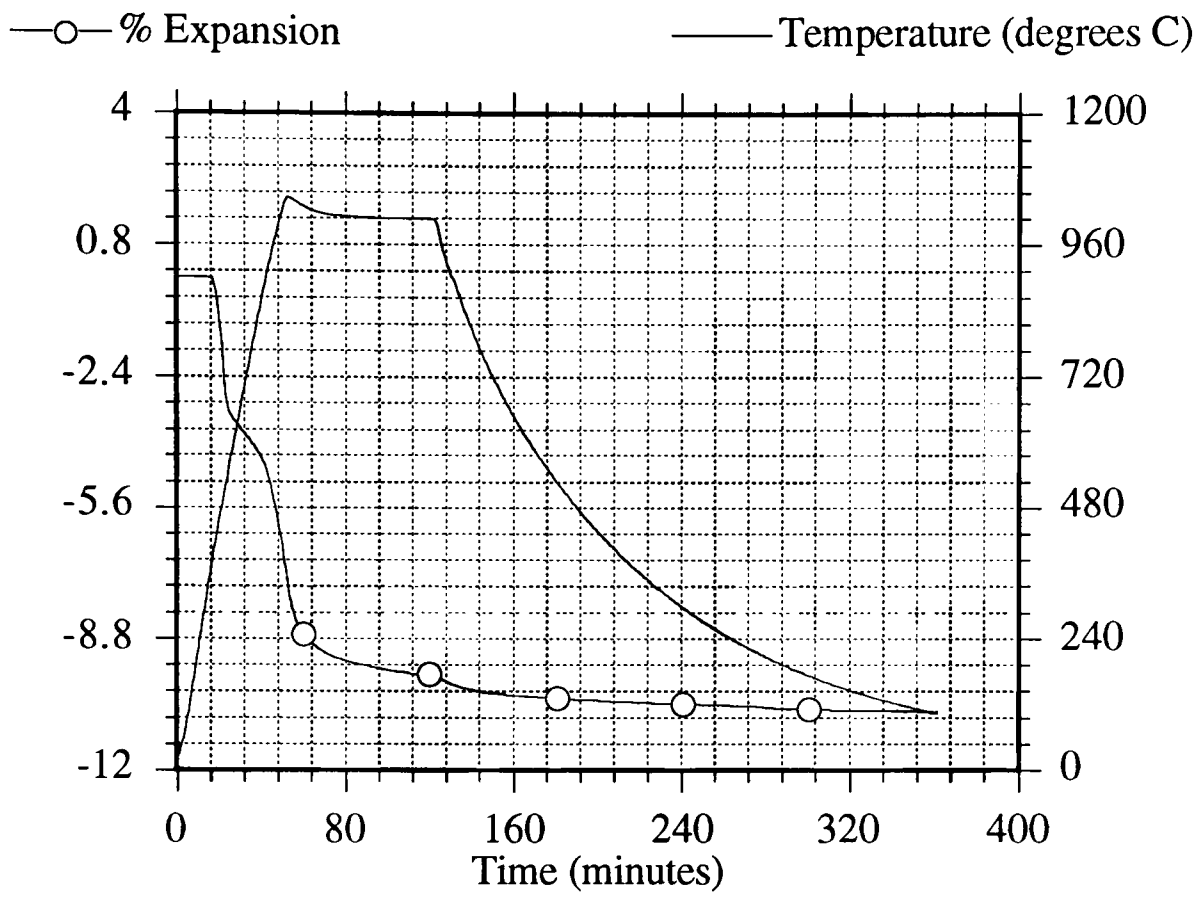


Figure 169: Dilatometry firing trace for Remal A20

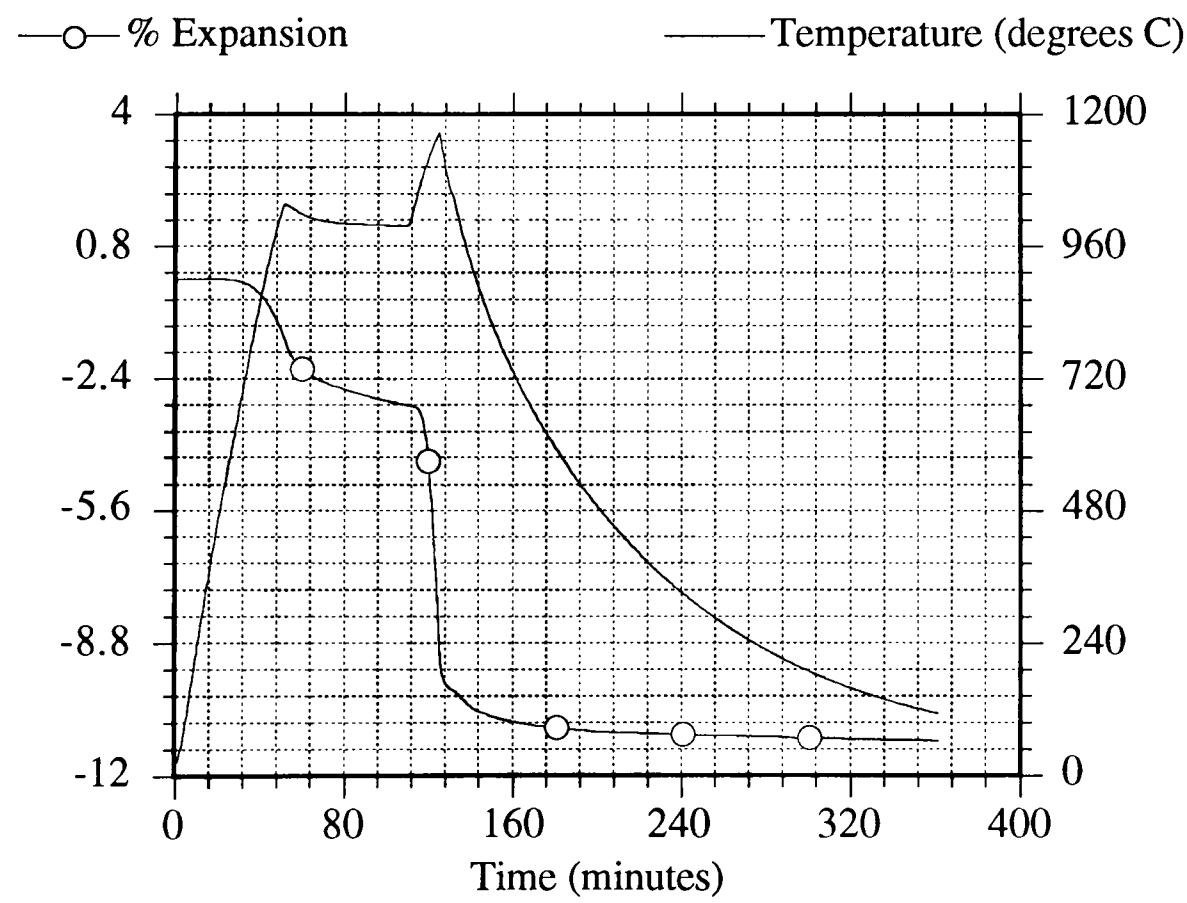


Figure 170: Dilatometry casting trace for Remal A20

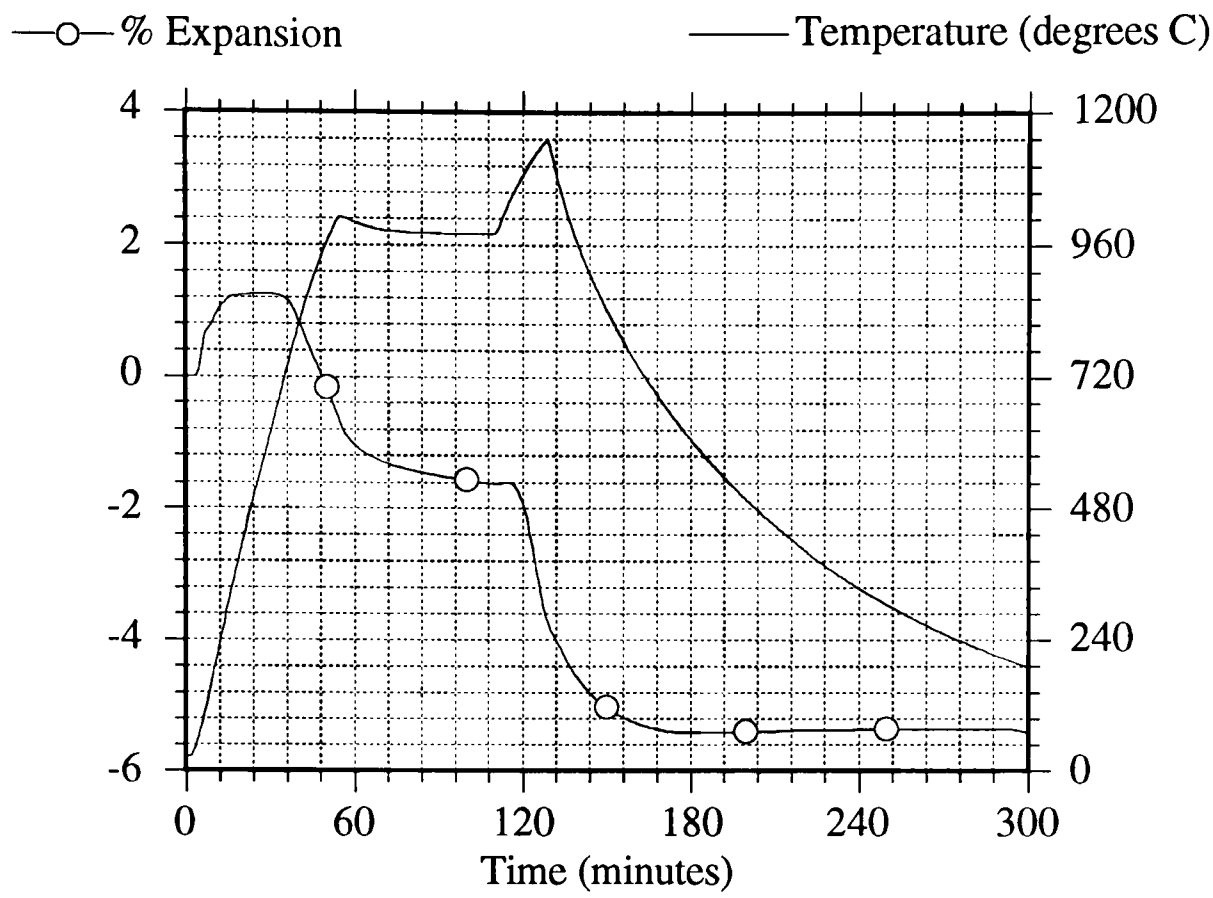


Figure 171: Dilatometry casting trace for Remal 20 + controlled impurity additions

2. Bacosol 2A and 3A

Bacosols are a series of alumina sols which are produced in both anionic and cationic forms. Due to computer error the data for Bacosols 2C and 3C, which are the low sodium binders, was lost and the research therefore concentrated upon the anionic (2A) and the cationic (3A) versions of the high sodium sol. Both binders produced the same gelled structure when investigated using XRD (Figure 172). The gelled structure consists of mainly boehmite and an amorphous matrix, but there are some small crystalline peaks which cannot be identified. These may be crystalline phases that are incorporated into the mineral source or may be constituents that have been added to the sol system at a later stage in manufacture. When fired to 1,000°C the binders transform to a mixture of an amorphous matrix with a small amount of δ-alumina (Figure 173). This is different to Remal 20 which transforms to θ-alumina which is the next reaction product in the sequence. The unidentified crystalline phases may be responsible for inhibiting the transformation at 1,050°C, which prevents the formation of theta alumina.

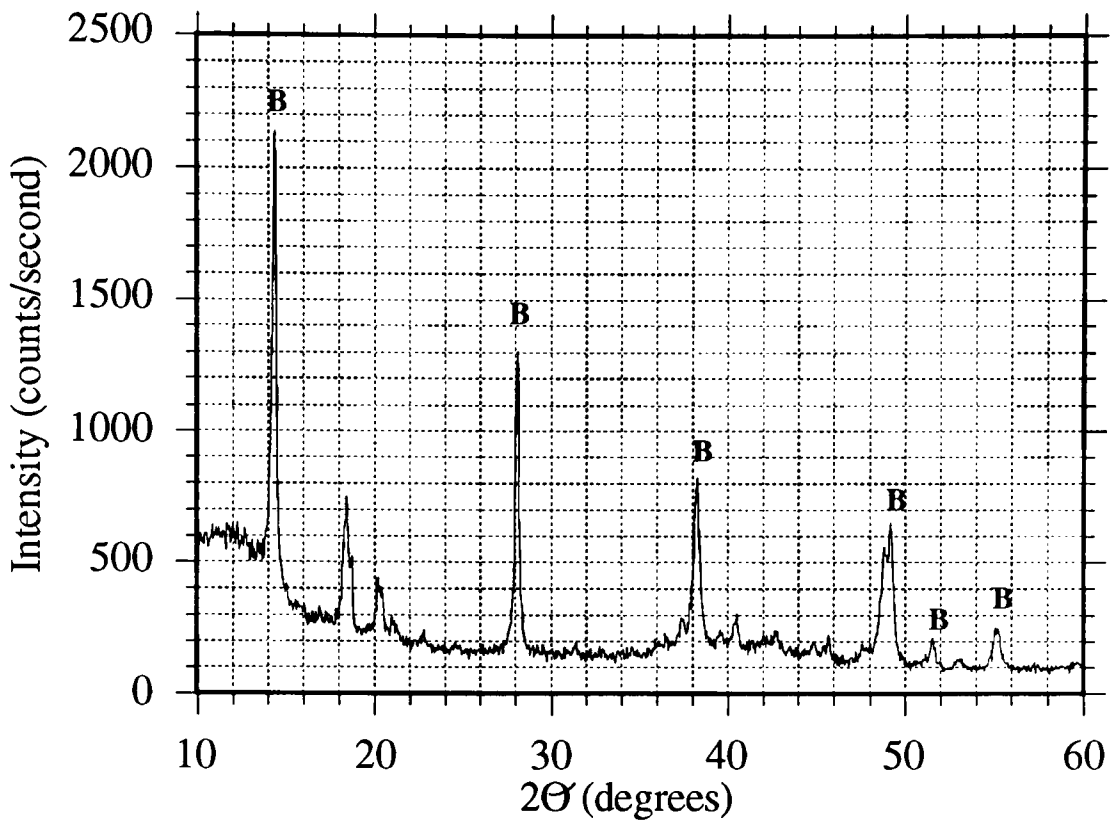


Figure 172: XRD trace for gelled Bacosols 2A and 3A
B = boehmite

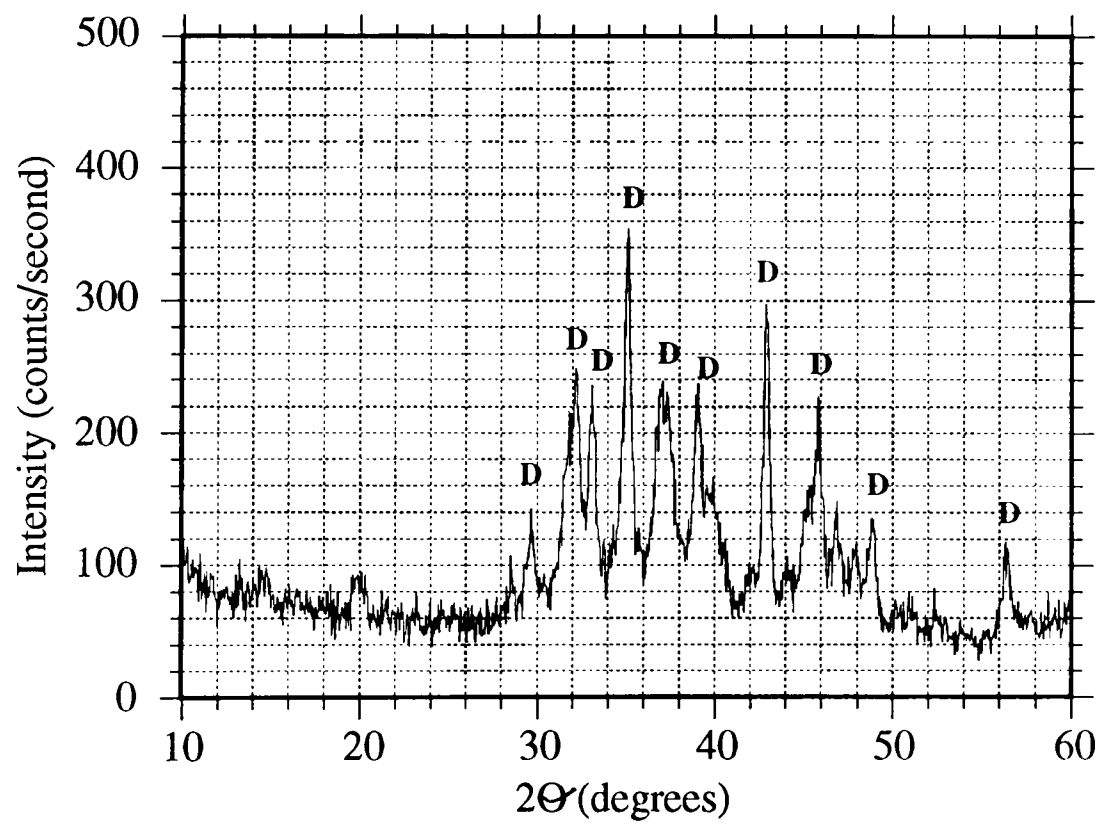


Figure 173: XRD trace for Bacosols 2A and 3A fired to 1,000°C for 60 minutes
D = δ alumina

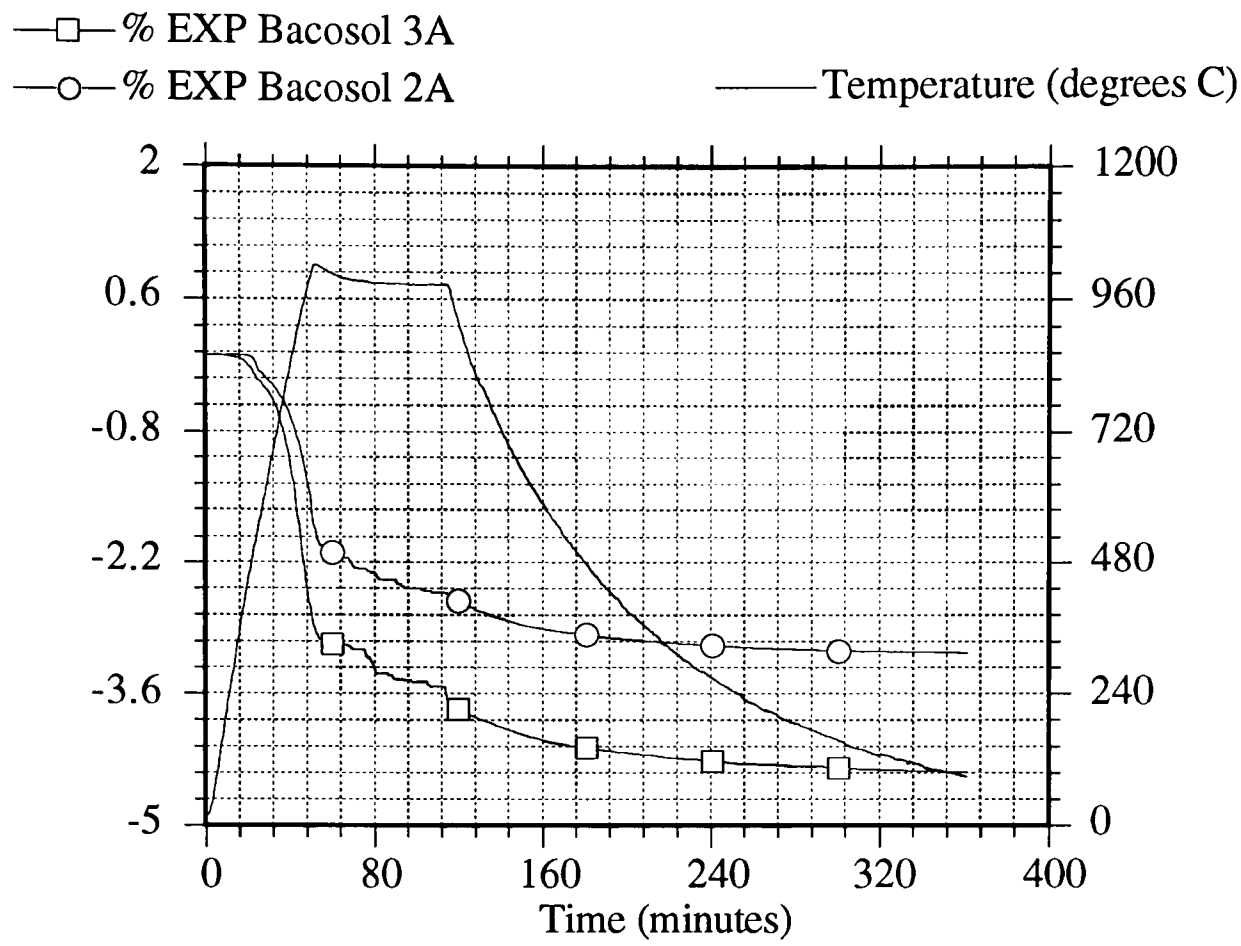


Figure 174: Dilatometry firing traces for Bacosols 2A and 3A

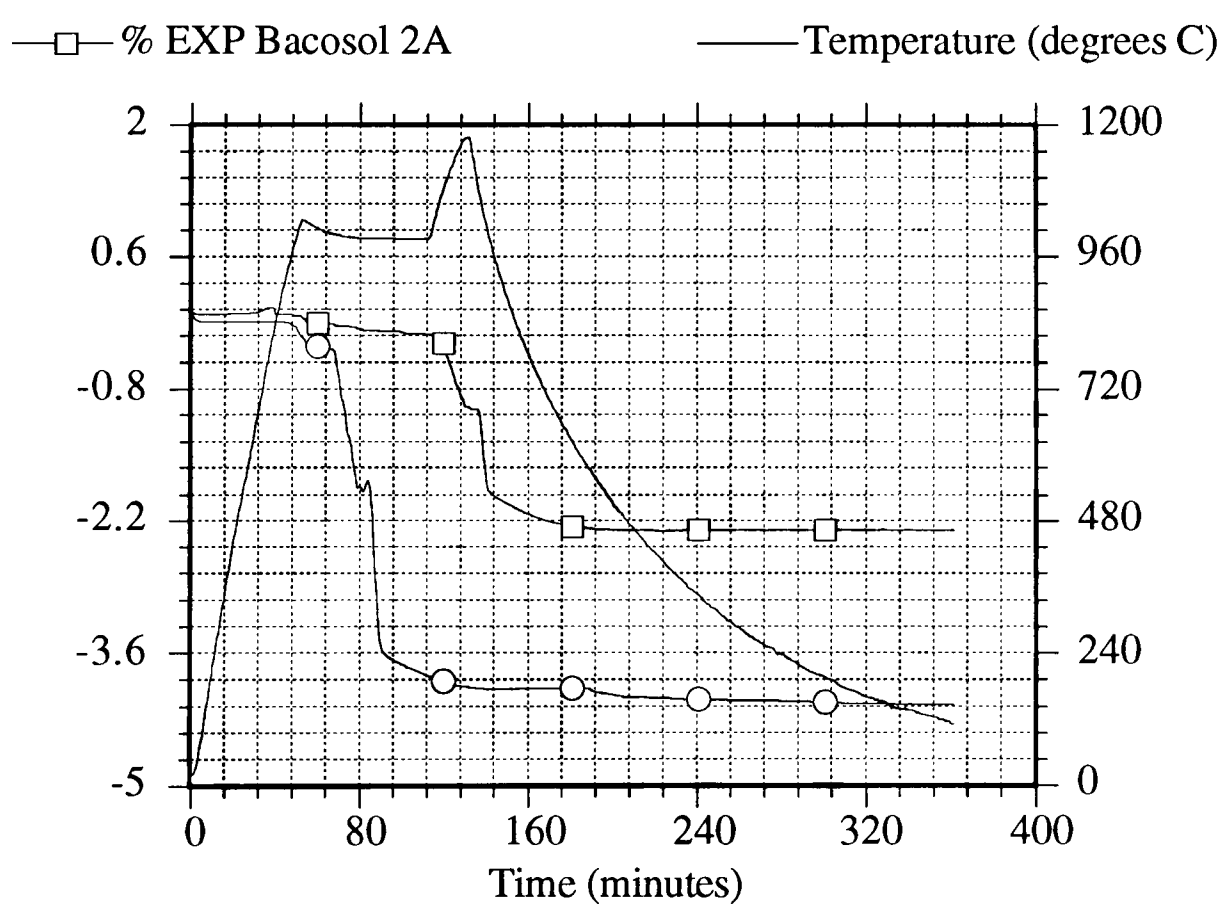


Figure 175: Dilatometry casting traces for Bacosols 2A and 3A

Both sols undergo only small volume contractions during firing (Figure 174) with Bacosol 2A contracting the least. This situation is reversed during the casting cycle (Figure 175) when Bacosol 2A displays the most contraction. Since the samples consist of the δ-alumina phase at 1,000°C, the volume contraction which is initiated during the heat to 1,150°C is probably due to a transformation to θ-alumina at 1,050°C.

In the presence of impurities, the thermal response of the individual binders is dramatically different. Figure 176 shows the dilatometry casting traces for the binders with controlled impurity additions. In Bacosol 2A any sintering or phase transformation is inhibited and the binder is inactive during the casting schedule. Impurity elements in Bacosol 3A initiate a volume contraction of 15% which is three times as much as would be expected. So it appears that the binders are affected differently by the presence of impurity elements, with Bacosol 2A showing the favourable response with regards to an investment casting mould.

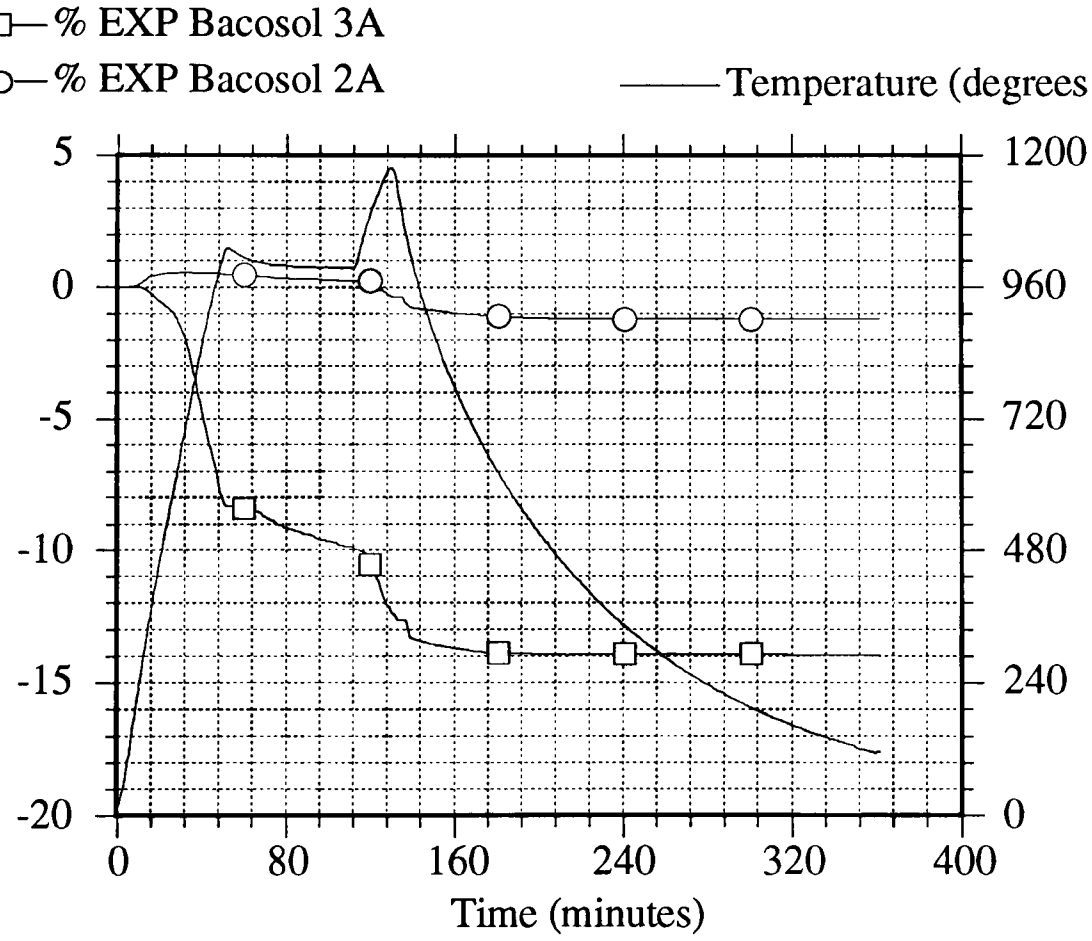


Figure 176: Dilatometry casting traces for Bacosols 2A and 3A + controlled impurity additions

4.5.3: Alumino-Silicate Based Systems

Alumina and silica particles can be mixed together to form a composite sol which will form a variety of alumino-silicate bonds when fired, depending upon the ratio of alumina to silica in the original mixture. When mixed in the ratio $72Al_2O_3$ / $28SiO_2$ the binder should form mullite when heated to the correct temperature. Since alumino-silicates, and especially mullite, have excellent refractory properties, several mixed sols were obtained and investigated.

1. Magnabond B

Magnabond B is a proprietary binder which consists of a mixture of alumina and silica sol particles in a water base. The proportion of constituents is such that the fired refractory should have an alumina/silica ration of 5/17. When gelled the structure is non-crystalline, with broad diffraction peaks corresponding to amorphous silica and alumina. When fired at 1,000°C for 60 minutes the sample consists of a mixture of amorphous silica, cristobalite and mullite. It appears that the alumina and silica have reacted together to form mullite and any excess silica remaining in the structure has either remained amorphous because of the influence of the alumina or crystallised to form cristobalite. This mixture of reacted and unreacted phases could prove detrimental to the structural stability of the binder during thermal cycling.

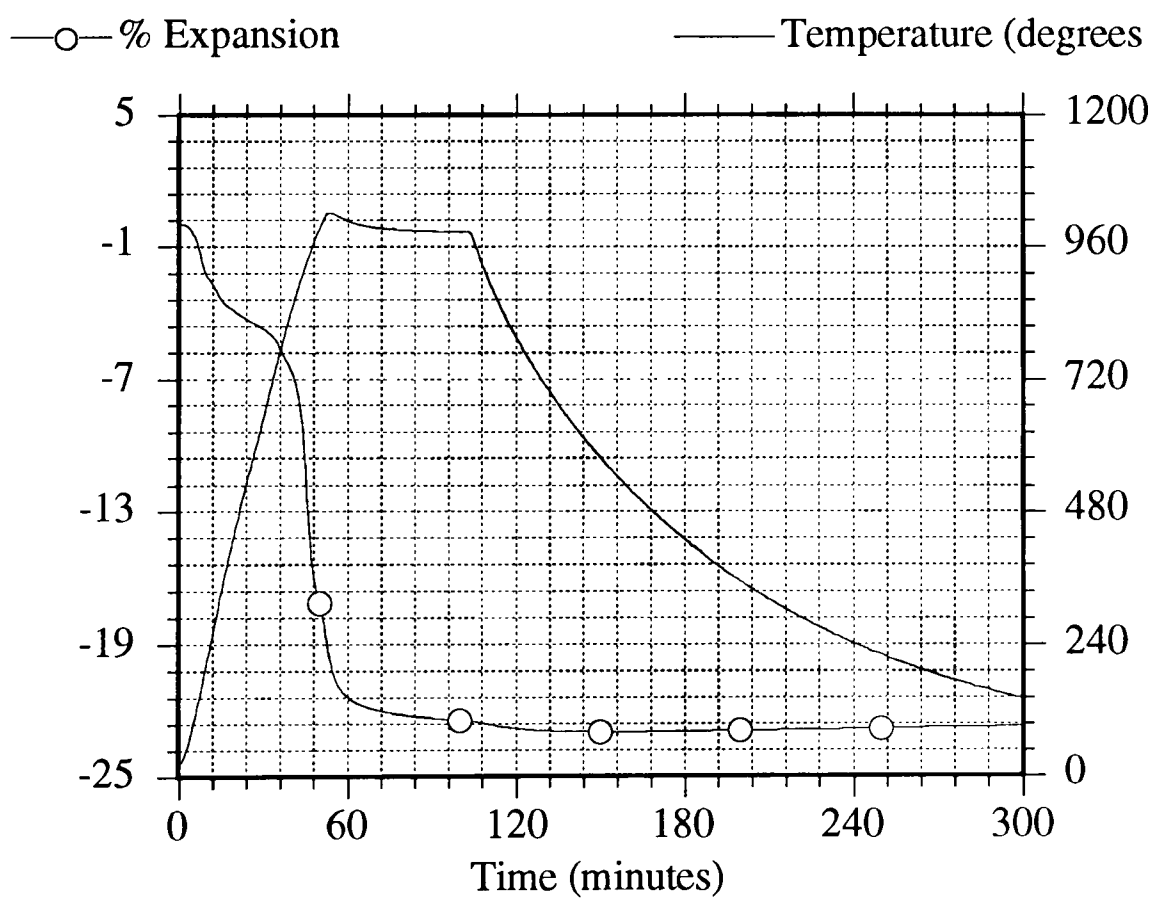


Figure 177: Dilatometry firing trace for Magnabond B

The dilatometry firing trace (Figure 177) shows that the binder undergoes extensive volume contraction (approximately 23%) during firing. This is due to transformation of the alumina portion of the structure, which can be seen as an inflection in the plot at 500°C when gamma alumina is formed. After this, and up to 1,000°C, the silica and alumina particles are reacting together to form mullite which promotes sintering and produces a rapid volume contraction. During cooling the binder remains inactive and stable. The mixture of phases in the fired structure does produce an unstable binder during the casting process (Figure 178). Further sintering takes place during the isothermal hold which could be due to the continuing reaction of alumina and silica. However, as the sample approached 1,150°C, a reaction takes place which causes immediate volume contraction. This contraction continues throughout the remainder of the cooling cycle and may be due to the initiation of high temperature creep within the amorphous portion of the sample, or could be the result of further transformation of the mixture to mullite.

Incorporation of impurity elements into the structure (Figure 179) promotes a greater volume contraction during the casting cycle. This could be due to the formation of silicate and alumino-silicate based glasses which will be unstable at high temperatures. The reaction at 1,150°C which causes an abrupt volume change is still present, but the extent of contraction is lessened in the presence of other elements.

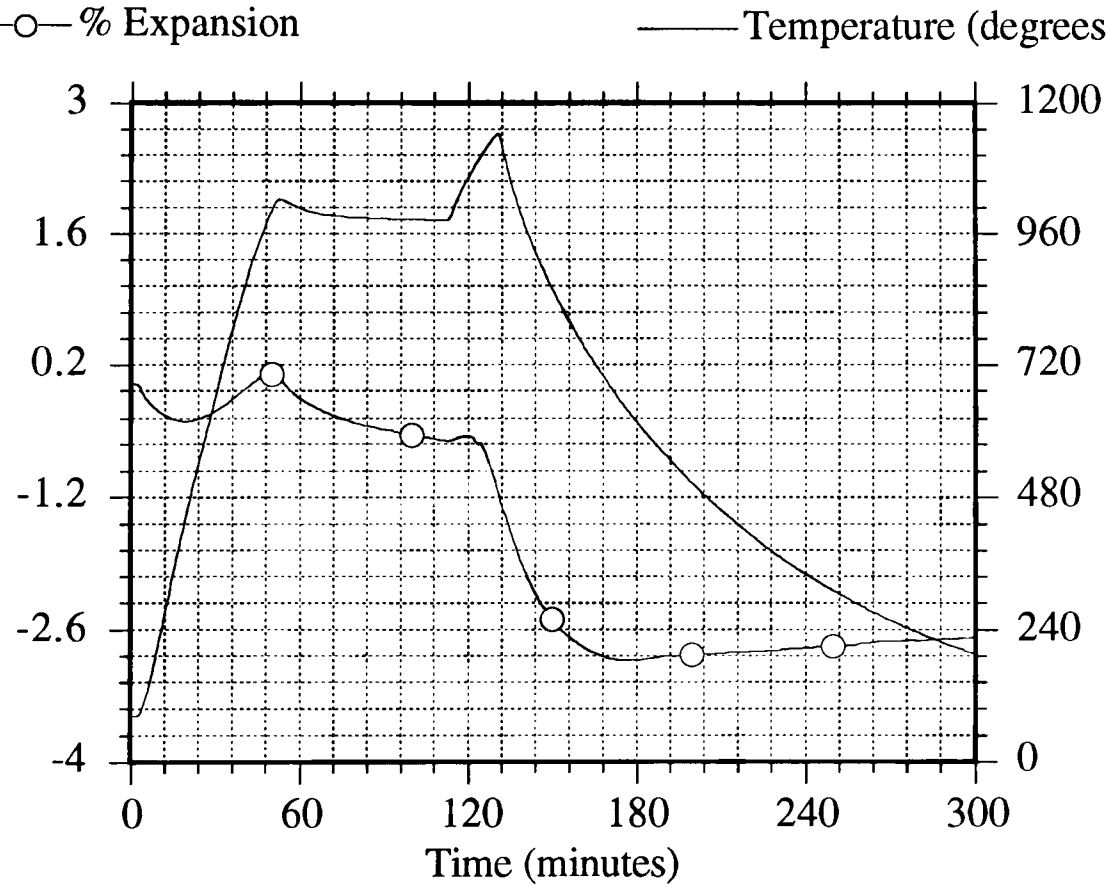


Figure 178: Dilatometry casting trace for Magnabond B

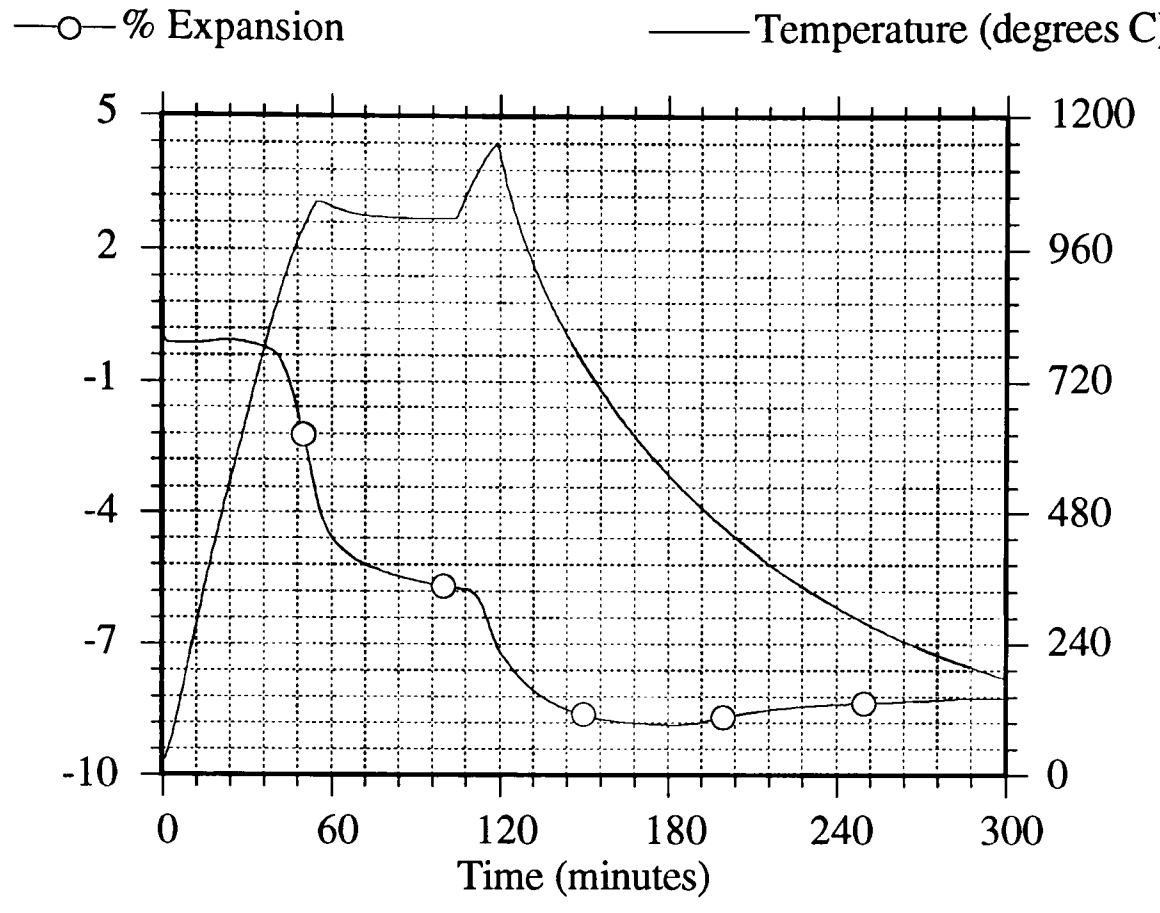


Figure 179: Dilatometry casting trace for Magnabond B + controlled impurity elements

2. Magnabond A

Magnabond A is very similar to B in the fact that it consists of a mixture of alumina and silica sol particles in a water base, but this time the ratio of constituents is 72/28 and the binder should form mullite when fired. When fired at 1,000°C for 60 minutes (Figure 180) mullite has just begun to form but the reaction is by no means complete and the sample still contains a small proportion of amorphous silica and alumina. The dilatometry firing trace (Figure 181) is similar to that of Magnabond B, with the alumina inflection at 500°C and an overall volume contraction of 22%. After firing at 1,000°C the sample is fairly inactive during cooling and remains so during the reheat and isothermal hold at 1,000°C during the casting cycle (Figure 182). However, the sample is affected as the temperature approaches 1,150°C, and abrupt contraction occurs. Since the mullite phase is stable at these temperatures, this contraction must be due to the creep of unreacted silica or to the completion of the transformation to mullite. This does suggest that the binder will not be stable until complete mullitisation has occurred which will leave the structure devoid of free silica. As such, the binder should be fired at temperatures in excess of 1,150°C if the structure is to be stable enough for use in an investment casting mould. The presence of impurity elements (Figure 183) induces a small amount of expansion during reheating and a little contraction during the isothermal hold. The structure is still susceptible to abrupt volume contraction at 1,150°C but the overall amount is reduced from 8 to 4% when other elements are present in the sample.

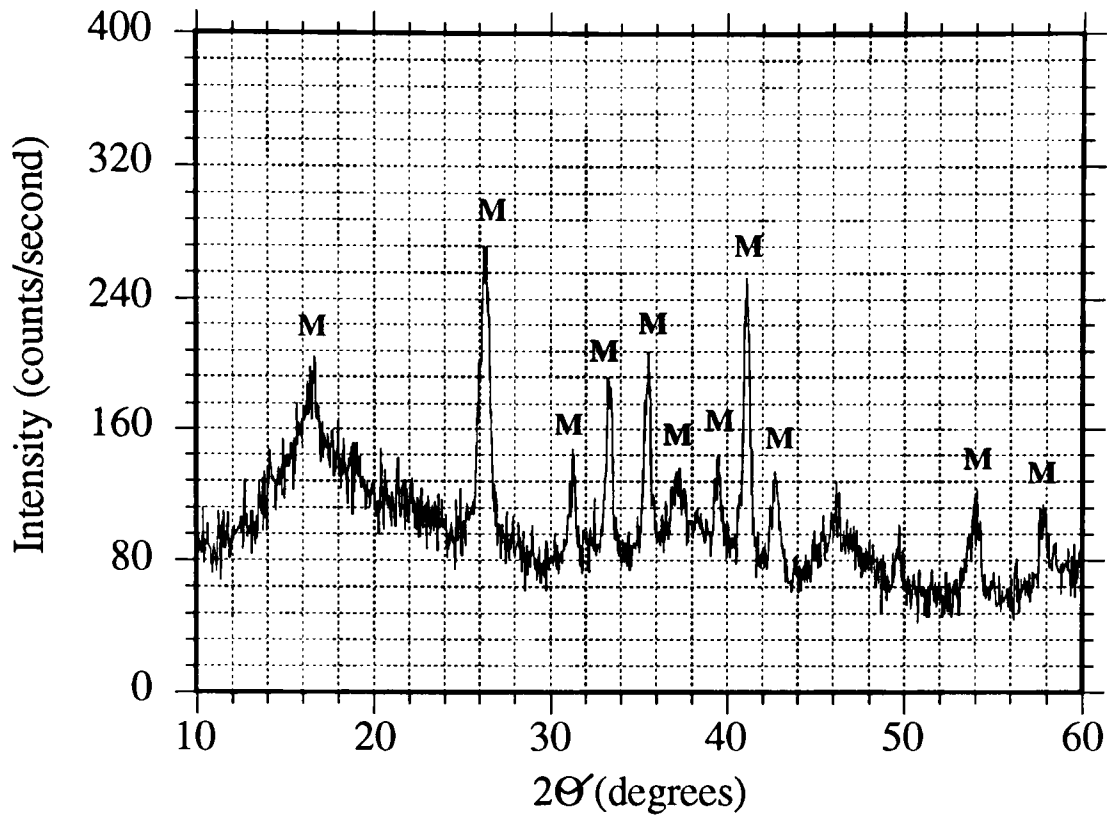


Figure 180: XRD trace for Magnabond A fired to 1,000°C for 60 minutes

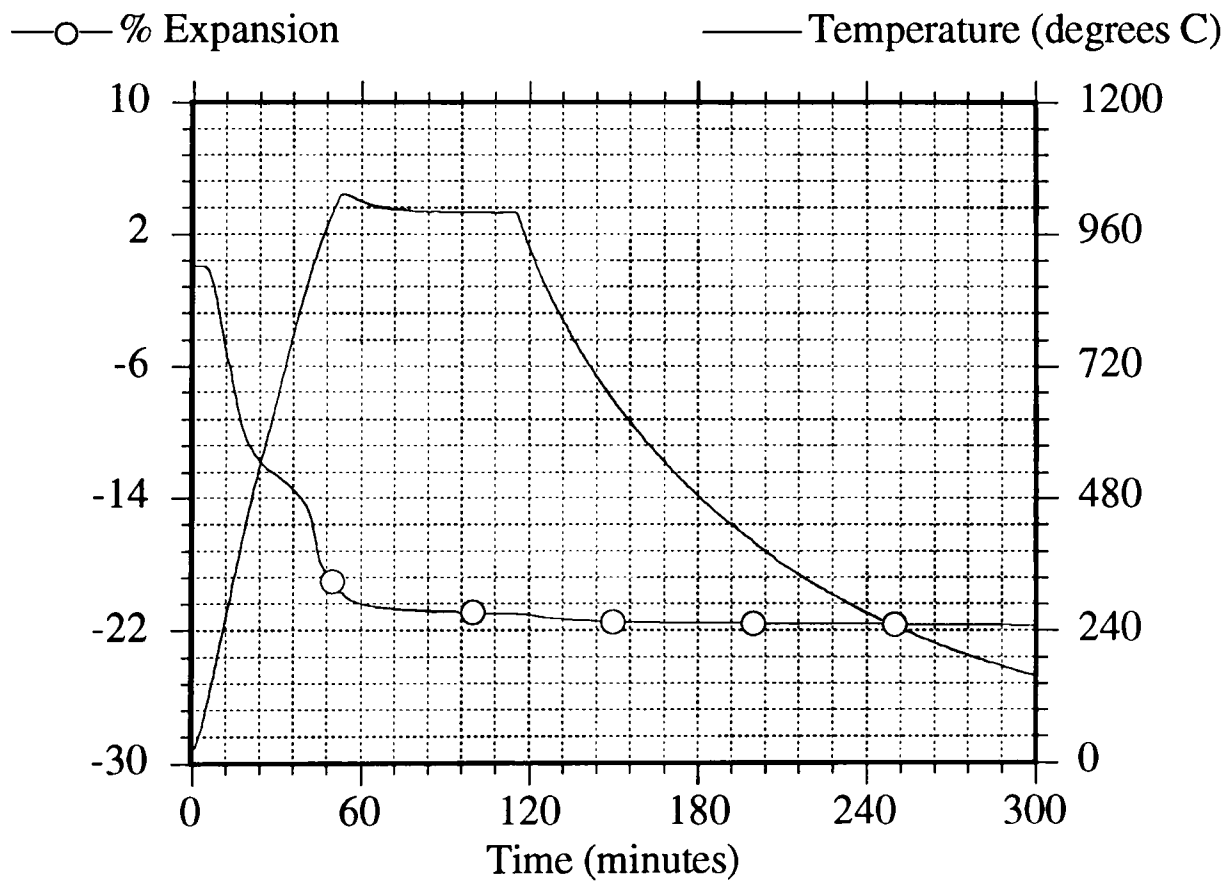


Figure 181: Dilatometry firing trace for Magnabond A

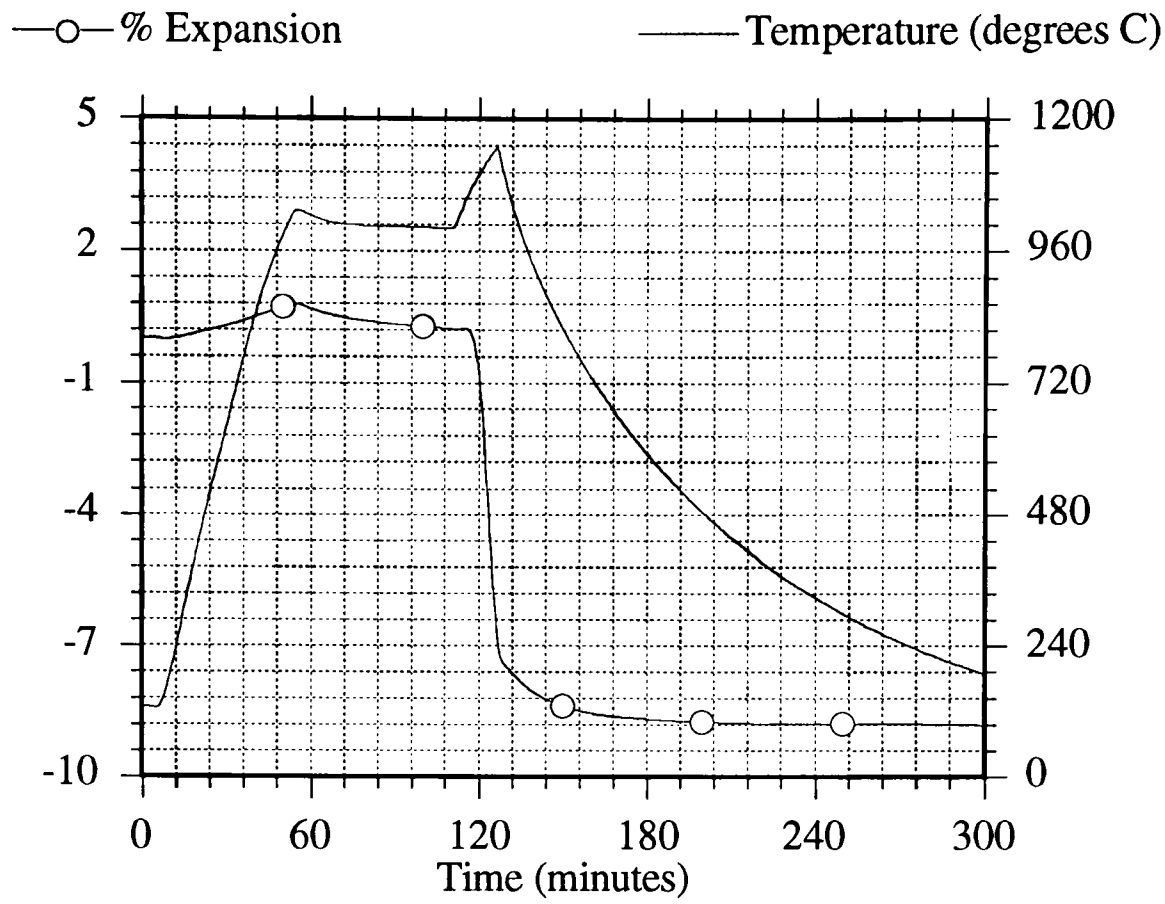


Figure 182: Dilatometry casting trace for Magnabond A

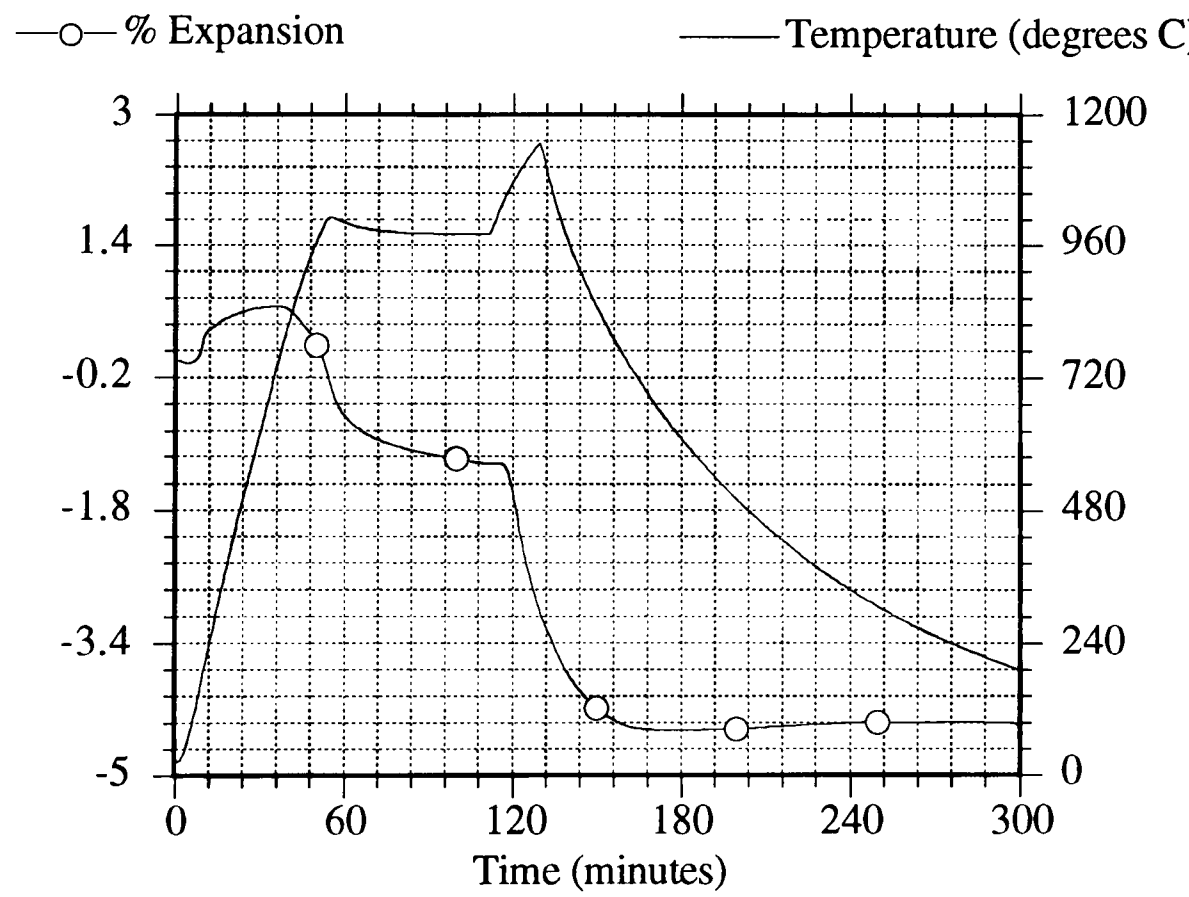


Figure 183: Dilatometry casting trace for Magnabond A + controlled impurity additions

4.5.4: Summary

Several non-silica binders were obtained and the thermal properties investigated, with a view to finding an alternative water based binder system to be used with larger investment casting moulds. Zirconia binders are prone to extensive contractions of the order of 40% during firing. This is due to the relatively small particle size, which increases the surface area of the solid material, and greatly increases the reactivity of the system as a whole. The binders crystallise to form monoclinic zirconia but, since the zirconia does not contain a stabiliser, the phase is free to transform to tetragonal zirconia and vice versa during heating and cooling. This transformation is accompanied by a 3% volume change which will produce microcracks in the binder. These will seriously undermine the strength of any refractory body produced using an unstabilised zirconia system. The presence of impurity elements actually seems to have a beneficial effect upon the binder, reducing the overall contraction and the extent of the volume changes during the monoclinic to tetragonal phase change. The uncontrolled phase changes which take place in the structure will be detrimental to the stability of an investment casting mould made using a zirconia binder system. The binders, in their present unstabilised form, will not make good alternatives to silica. With the incorporation of stabilising agents such as yttria or calcium oxide, it may be possible to remove the phase changes from the system and produce a stable binder with good high temperature properties.

Several alumina based binders, both cationic and anionic, were investigated. Due to a reaction sequence, alumina sols go through several phase transformations up to 1150°C. As such, since the high temperature phase is dense, the binders are susceptible to abrupt and extensive contraction at temperatures around 1,150°C. This could be prevented by increasing the firing temperature above 1,150°C which will produce a monophase (α alumina) system which should be stable during thermal cycling. The presence of impurity elements reduces the overall contraction in the system.

Mixtures of alumina and silica sol particles when fired form a variety of materials which are dependent upon the initial ratio of the constituents. A binder containing an alumina/silica ration of 5/17 will produce a mixture of mullite and cristobalite when fired at 1,000°C. This system would not make a good binder for an investment mould because the presence of free silica induces a sudden and extensive volume contraction at temperatures above 1,000°C. The system is also affected by impurity elements which may produce low melting alumino-silicate glassy phases which are susceptible to volume contractions during temperature cycling. A binder containing an alumina/silica ratio of 72/28 begins to form mullite at 1,000°C. Unfortunately, when heated above this temperature the mullitisation reaction continues and the sample suddenly contracts by as much as 8%. However, the extent of this contraction is reduced by 50% when impurity elements are added to the system. Therefore, if the binder were fired to a particular temperature above 1,150°C for an appropriate duration so that complete mullitisation takes place, the system could make a good alternative to silica as the high temperature refractory properties of mullite are superior to silica.

4.6: Thermal Profiles of Investment Casting Moulds

The fundamental requirement of any solid vessel designed to contain a liquid is to hold that liquid within specified boundaries for the required period of time. An investment casting mould not only has to hold liquid metal, it also has to retain integrity and specific dimensions during a prolonged high temperature cycle. The structural integrity and resistance to high temperature deformation of a mould directly determines the quality of the finished metal casting. It has been shown that the major load bearing points within the structure of a mould are formed by the binder phase. Therefore, the physical properties of a mould at high temperatures will be directly dependent upon those of the binder, which in turn are determined by the temperature cycle imposed upon the structure.

Most adhesive links are designed to be as strong, if not stronger than the material which is being held together. However, when the structural and thermal properties of the adhesive are inferior then the concept of teh binder as the weakest link can be considered. This is especially relevant when considering a silica based mould since the onset of viscous flow for the silica binder is only 1200°C[136] compared with temperatures in excess of 1700°C[137] for the other refractory constituents.

Moulds, although identical in composition and structure, are subjected to a wide range of load and temperature regimes due to the relative size of the components produced. The same basic system is therefore required to withstand very different thermal environments to produce a sound casting. As the mould capacity increases, the weight of metal poured to produce the final component will also increase, though not necessarily in proportion since larger castings often require a heavier and more intricate runner system. An increase in metal mass produces a slower cooling rate, which means that the mould is subjected to higher temperatures for longer periods of time. This change may be sufficient to alter the structural response of the mould to such an extent that failure may occur. In order to examine the relationship between mould capacity and maximum temperature generated in the ceramic, two different sized moulds were produced and the temperature attained across the mould section monitored as a function of time.

4.6.1: Thermal Profile of a 5 kg Capacity Mould

Martensitic stainless steel, at a metal pouring temperature of 1580°C, was cast into the unbacked 5 kg mould. Full compositional specification of the metal can be found in Section 3.10.1.2 and the relative thermocouple positions in Section 3.10.1.1. As the mould was relatively thin, the thermocouples were positioned after adjacent coats throughout the complete mould section. Thermocouple 7 displayed no output, possibly due to an incomplete connection, and so was discounted. The remaining thermocouples did display an output and this was monitored using the data analysis computer throughout the casting procedure. A large volume of data was collected which, when displayed on a single graph is confusing, with the layout making it difficult to distinguish individual

thermocouple traces. Therefore the data was divided and displayed separately on two graphs: one showing the thermocouple data from the metal, the primary coat and the outer coat to give a view of the thermal gradient across the mould section, and the other showing the data collected from the thermocouples placed in the inner coats of the mould.

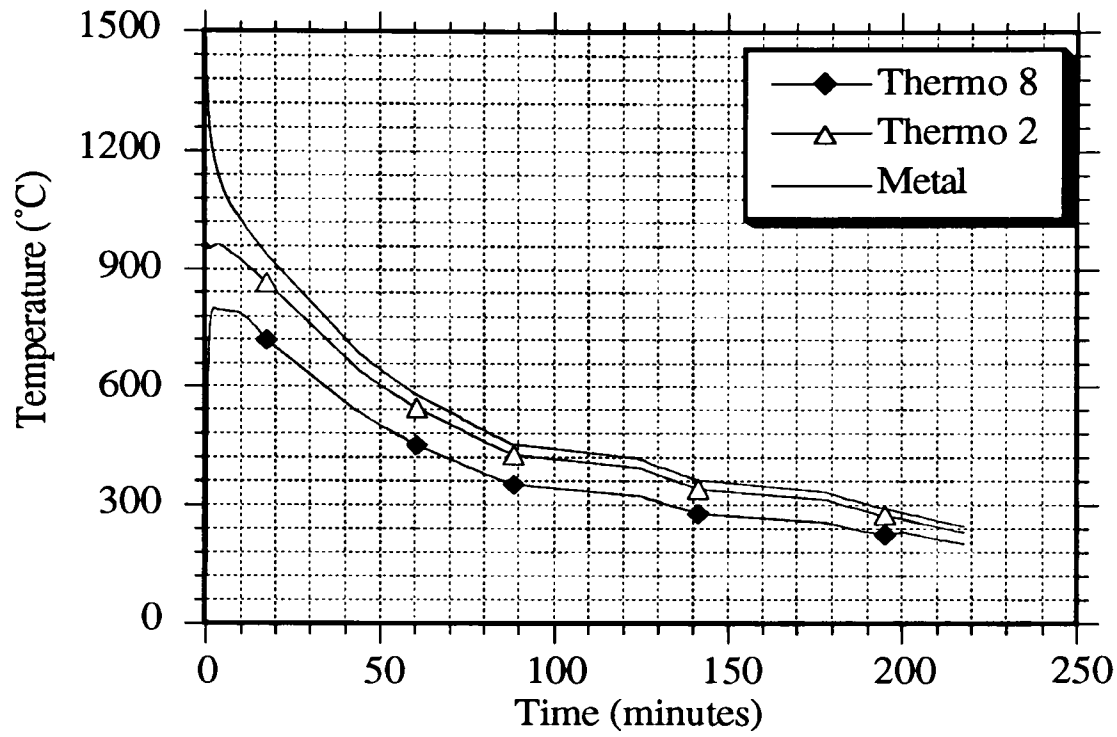


Figure 184: Thermal profiles obtained from the metal, the primary coat (Thermo 2) and the outer coat (Thermo 8) of a 5 kg capacity mould cast with martensitic stainless steel

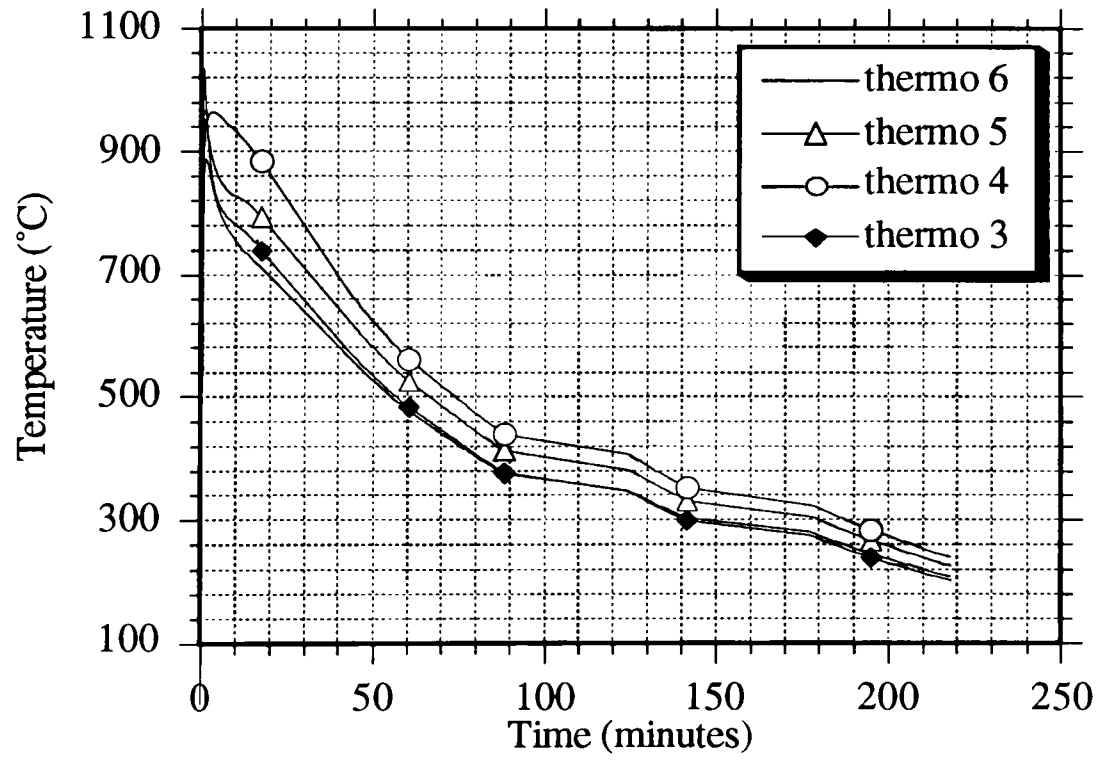


Figure 185: Thermal profiles obtained from the thermocouples placed in the inner section of a 5 kg capacity mould cast with martensitic stainless steel.

Figure 184 shows the thermal profiles obtained from the metal, the primary coat and the outer coat thermocouples. Figure 185 shows the data obtained from the remaining thermocouples positioned in the central region of the mould section. Though poured at an initial temperature of 1580°C, the metal appears to have cooled considerably during the pouring process and only achieves a maximum temperature of 1485°C when in the mould cavity. Almost immediately the metal begins to cool at a very rapid rate until after 5 minutes it settles to a steady rate of approximately 12°C / minute. Throughout the casting process the metal maintained a higher temperature than the mould reaching thermal equilibrium at 20 minutes, after which a constant 20°C difference between the metal and the primary coat was established. The rapid cooling rate of the metal is undoubtably due to the fact that the mould was unbacked and the entire surface area of the mould, through which the heat will be lost, is exposed to the atmosphere.

It appears from the profiles that the temperature regime within the ceramic is directly dependent upon the rate of heat loss from the metal, to the extent that any change in cooling rate within the metal will be mirrored in the ceramic. As such, it would be wise to consider the metallurgical aspects of solidification when choosing a mould system in which to cast a particular metal alloy. A metal does not solidify instantaneously but instead there is a period of time in which part of the metal is solid and the other part is still liquid, known as the solidification range. Thermodynamic forces induce other areas of the metal to solidify, which in turn produces small amounts of heat since this is an exothermic reaction. The cooling rate of the metal is reduced which in turn reduces that in the ceramic which could lead to the equivalent of an isothermal hold, which will continue until all of the metal has solidified. All metals do not have identical solidification ranges: differences occur in the temperatures at which solidification takes place and in the duration of the solidification. Since the ceramic cooling rate is dependent upon the metal it would be unwise to cast a metal possessing a high temperature and long duration solidification into a mould which is susceptible to binder creep over long periods of time. Most investment foundries use the same mould system, irrespective of the alloy being cast, and this may be responsible for the inability to achieve dimensional tolerances with some of the metals that are cast.

The mould cools fairly rapidly, possibly due to the small volume of metal, relatively thin shell used (7 completed coats) and again the fact that the mould was unbacked. Since refractories exhibit a low thermal transfer rate, this lack of section thickness must also be responsible for both inner and outer coats reaching maximum temperature almost immediately after the metal was poured. The maximum temperature reached within the primary coats was 980°C compared with 800°C within the outer coats. However, the coats do not remain at the higher temperatures for long as cooling begins almost immediately at a reasonably high rate. The inner coats begin to lose heat first , with the outer coats slower to respond, but thermal equilibrium between the coats is reached after 10 minutes. A steady thermal gradient of 100°C is then maintained across the mould section for the remainder of the cycle.

These results indicate several reasons why the failure of small investment cast components is rarely due to mould creep, even though most of the moulds are unbacked and unconstrained. Creep and structural instability in silica based systems will tend to occur where there is a combination of high temperature and high loading over prolonged periods of time. These conditions are not found in the smaller moulds. The metal weights used are low and the highest temperature attained in the ceramic is less than 1,000°C, which is not maintained for any significant length of time as the mould and metal cool rapidly after casting.

4.6.2: Thermal Profile of a 60 kg Capacity Mould

Low alloy steel, at a metal pouring temperature of 1580°C, was cast into the fully backed 60 kg capacity mould. Backing was used since most moulds above 50 kg in weight are routinely cast in this manner by the foundry industry. Full compositional specification of the metal can be found in Section 10.1.2 and the relative thermocouple positions in Section 10.2.1. As the data analysis equipment had the capacity for only eight thermocouples, it was not possible to position a thermocouple after adjacent slurry coats as for the 5 kg mould. A thermocouple was placed to monitor the metal temperature and the remainder were placed between alternate coats of the mould section. It should be noted that the inner mould thermocouple is actually positioned after the 3rd ceramic coat, and not after the primary coat as for the smaller mould. For interest a photograph of the mould, with backing and thermocouples attached is shown in Figure 186. Again the large volume of data was divided into two and displayed in separate graphs.

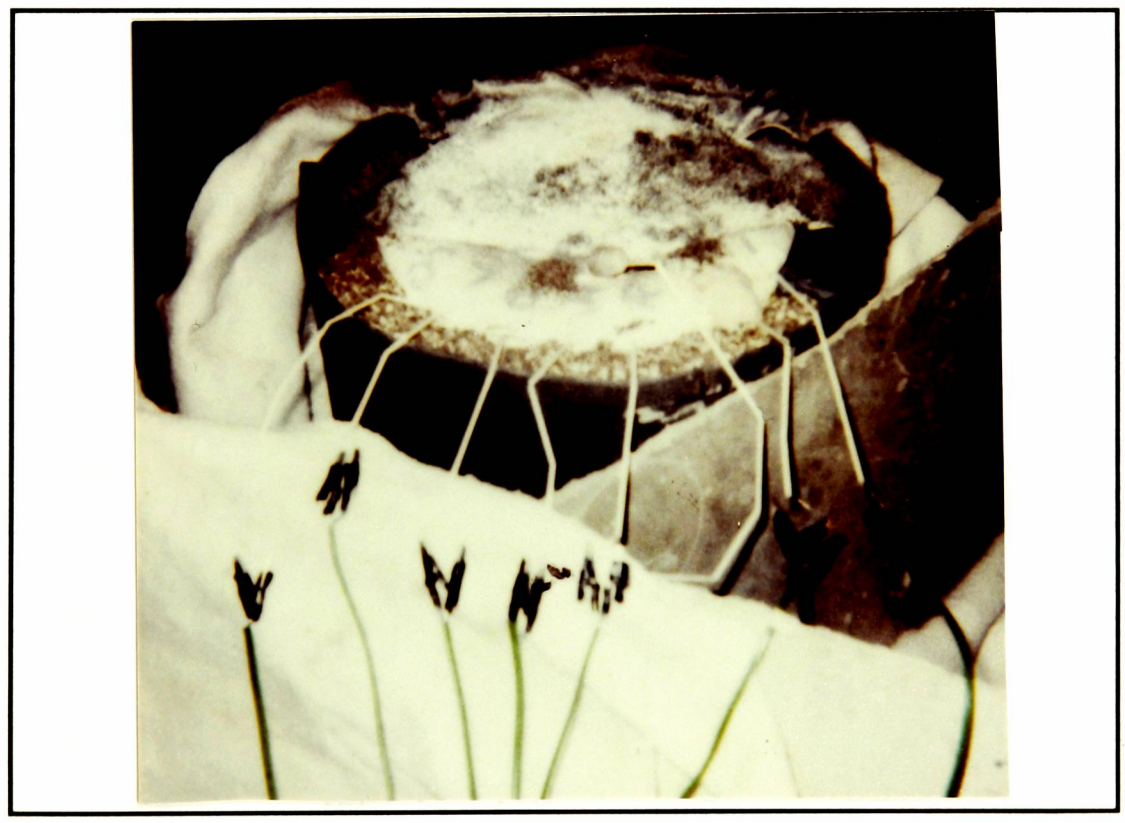


Figure 186: The 60 kg mould with thermocouples attached after being cast at Deritend Precision Castings

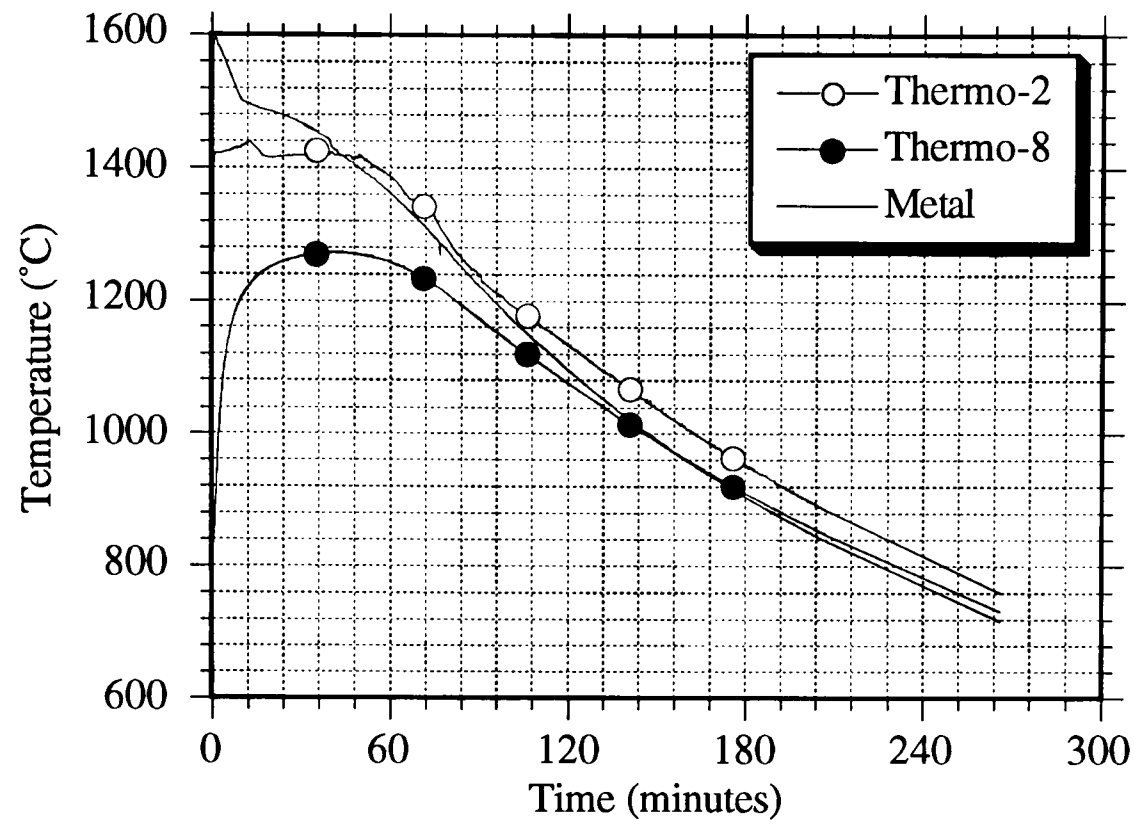


Figure 187: Thermal profiles obtained from the metal, the primary coat (Thermo 2) and the outer coat (Thermo 8) of a 60 kg capacity mould cast with low alloy steel

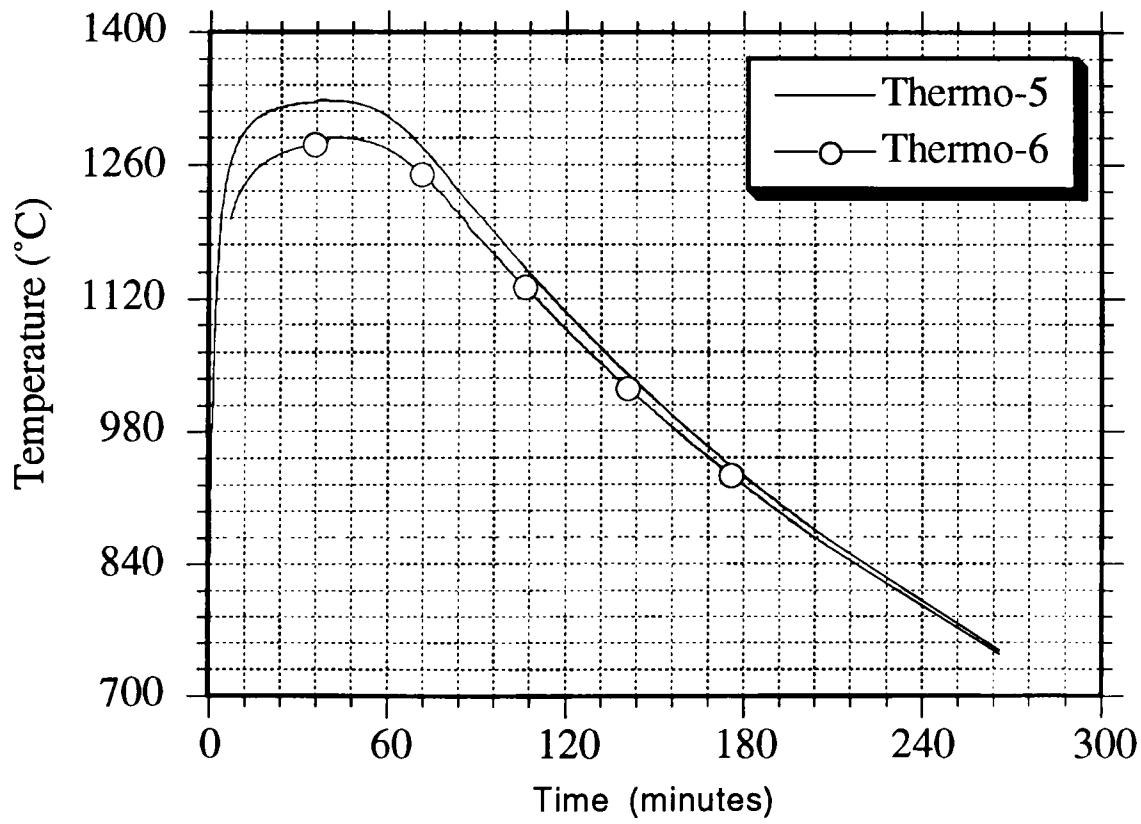


Figure 188: Thermal profiles obtained from the thermocouples placed in the inner section of a 60 kg capacity mould cast with low alloy steel.

Figure 187 shows the temperature data gained from the thermocouples in the metal, the inner coat and the outer coat of the mould. Figure 188 shows the remainder of the thermocouples in the central portion of the mould section. Note that thermocouples 3,4 and 7 failed to give an output and had to be discounted from the profile. The metal achieves a maximum temperature of 1594°C which is approximately 100°C higher than that obtained in the 5 kg mould. This could be due to the relative metal weights, with the larger mass of metal retaining more heat during the pouring stage. Initial metal cooling is rapid but after 10 minutes a steady and relatively slow rate of 4°C/minute is maintained throughout the rest of the solidification process. This slow cooling rate may be due in part to the way in which heat is lost from a large body with more external surface area, and also to the fact that the mould is fully backed with refractory material which will act as insulating material, reducing the thermal gradient between the metal and its surroundings. Unlike the smaller mould, the metal temperature only remains higher than the rest of the mould for the first 40 minutes. After this, just prior to the commencement of cooling within the mould itself, the metal temperature drops below than that in the primary coats and remains so throughout the rest of the experiment. Again this could be another representation of the effect that backing has on the thermodynamics of the whole system. This effect could also be due to a high rate of heat loss from the large surface of metal which is exposed to the air at the top of the casting. Indeed, after 150 minutes the temperature is surprisingly very similar to that of the outer mould coat and at least 20°C lower than the inner coats.

Like the smaller mould, the inner coats reach maximum temperature (1420°C) almost instantaneously, but cooling is delayed and this temperature is maintained for approximately 50 minutes. Note the fact that, since the first thermocouple is placed after the third mould coat, it is almost certain that the primary coat of the mould reaches a temperature well in excess of 1420°C. Being a much thicker mould section (16 completed coats), thermal transfer is slow and the outer coats attain a maximum temperature of 1273°C after 40 minutes. This temperature is not maintained as, once the outer coats have reached maximum temperature and a steady thermal gradient is produced, the entire mould section begins to cool at a slow rate. The mould is less dependent upon the cooling rate of the metal since the whole thermodynamic system has been altered by the presence of the backing material. Thermal equilibrium across the mould section takes approximately 100 minutes to be established, after which a steady temperature difference of 58°C is maintained between the inner and outer coats. This lower temperature gradient of 3°C/minute is due to the greater section thickness, the higher temperatures and slower cooling rates generated by a much greater mass of metal and again the presence of the backing material.

These results indicate several reasons why larger investment casting moulds tend to suffer from mould wall movement during casting. Creep and structural instability in silica based systems will tend to occur where there is a combination of high temperature and high loading over prolonged periods of time. The mould system is experiencing all of these factors, with the inner coats of the mould reaching and maintaining 1420°C for at least 50 minutes.

4.6.3: Summary

Thermal profiles across sections of a 5 kg capacity and a 60 kg capacity mould cast with metal at 1580°C were measured and compared. The 5 kg mould instantaneously reaches a maximum temperature of 980°C in the primary coat and 800°C in the outer coat. Both of these temperatures are not maintained as cooling is rapid, with a large temperature difference of 100°C across the mould section. The rapid cooling is due to the relatively small mass of metal, the thinness of the ceramic shell and the fact that the mould is unbacked. These results indicate several reasons why the failure of small investment cast components is rarely due to mould creep, even though most of the moulds are unbacked and unconstrained. Creep and structural instability in silica based systems will tend to occur where there is a combination of high temperature and high loading over prolonged periods of time. These conditions are not found in the smaller moulds. The metal weights used are low and the highest temperature attained in the ceramic is less than 1,000°C, which is not maintained for any significant length of time as the mould and metal cool rapidly after casting.

The 60 kg mould achieves and remains at a temperature of 1420°C for 50 minutes in the third coat of the section. This implies that the primary coat will be subjected to even higher temperatures. Cooling is slow and does not begin to take place until the remainder of the mould coats have achieved maximum temperature of 1273°C. The slow cooling rate is due to the relatively large mass of metal which retains heat for longer periods of time, the thickness of the mould section and the fact that the mould is fully backed with refractory material. This insulates the outer coat of the mould, prevents heat loss into the atmosphere and reduces the temperature difference to 58°C between inner and outer coats of the mould. These results indicate several reasons why larger investment casting moulds tend to suffer from mould wall movement during casting. The onset temperature for creep within a silica system is 1200°C and, as the entire mould section is above this temperature for at least 80 minutes, we can assume that creep is initiated within the binder system. The high temperatures coupled with the high loading due to a larger mass of metal will produce mould wall movement in the larger moulds even if they are backed with refractory material.

The thermal regime that a ceramic shell is subjected to during casting is determined by the mass of metal used and the ceramic section thickness. The higher the metal weight, the greater the maximum temperature attained and the lower the thermal gradient. It appears that the temperatures experienced within the ceramic when larger components are cast are above those that can be tolerated by a silica based system.

4.7: Metal Mould Interaction

The structural integrity and resistance to surface interaction of an investment casting mould directly determines the quality of the finished metal casting. The extent of metal mould interaction is determined by many factors such as the refractory and the type of metal being cast and also by the mechanism of metal to ceramic contact. It is also possible that the temperature of casting and the weight of metal may affect the interaction since, as was shown in Section 4.6, the maximum temperature and thermal profile to which a mould section is subjected is determined by the size of the casting. An examination of both refractory and metal surfaces of the 5 kg and 60 kg thermal profile moulds was undertaken using microstructural and compositional analysis. This will lead to a better understanding of the mechanisms of interaction and allow comparisons to be made between the interaction observed in small and large cast components.

4.7.1: 5 kg Investment Mould

Martensitic stainless steel, at a pouring temperature of 1580°C, was cast into a 5 kg investment mould made using standard zirconium silicate refractory and silica binder. Experimental procedures together with compositional analysis of the metal can be found in Section 3.10. After cooling, samples from both the mould and metal casting were sectioned and mounted for SEM analysis.

4.7.1.1: Mould Surface

The micrograph of a section through the primary coat of the mould is shown in Figure 189. Metal appears to have interacted with the primary edge of the mould and left behind a layer adhered to the surface after mould removal. This layer is shown in greater detail in Figure 190 as region A. Analysis of the layer suggests that it consists of only iron instead of the mixture of iron and alloying elements present in the original metal specification. However, some of the alloying elements may still be present in small amounts, since the detection limit for EPMA analysis is only 0.5%. It can be stated that the layer consists of iron with the possibility of alloying elements in concentrations below 0.5%.

Some of the alloying elements appear to have leached or diffused further into the mould structure via the silica binder (Figure 190 - region B), possibly through melting of the binder followed by capillary action in much the same way as a sponge draws up water. The interaction occurs to an average depth of 85μm after which the structure is unaffected by the metal (region C). The basic structure of both the refractory filler and stucco does not appear to have been affected by the metal and no interaction between refractory and metal appears to have occurred.

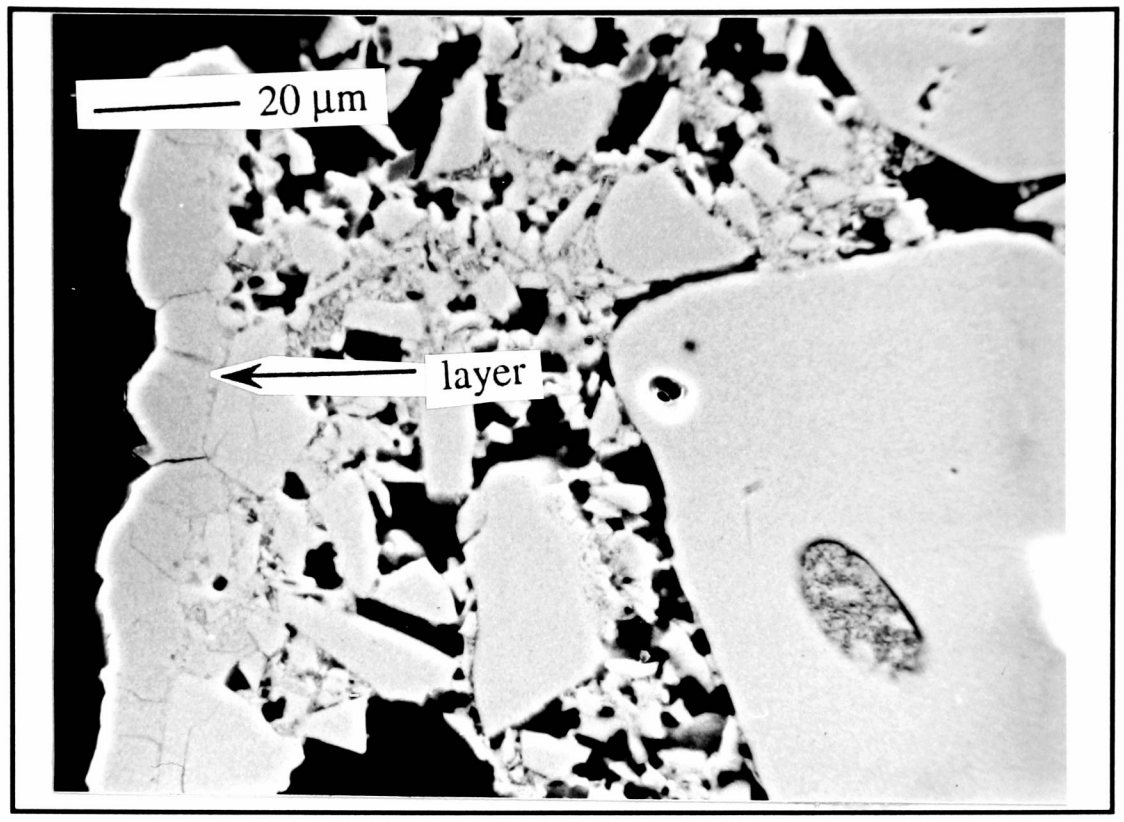


Figure 189: Section through the primary coat of a 5 kg silica based mould cast with martensitic stainless steel mag = x 660

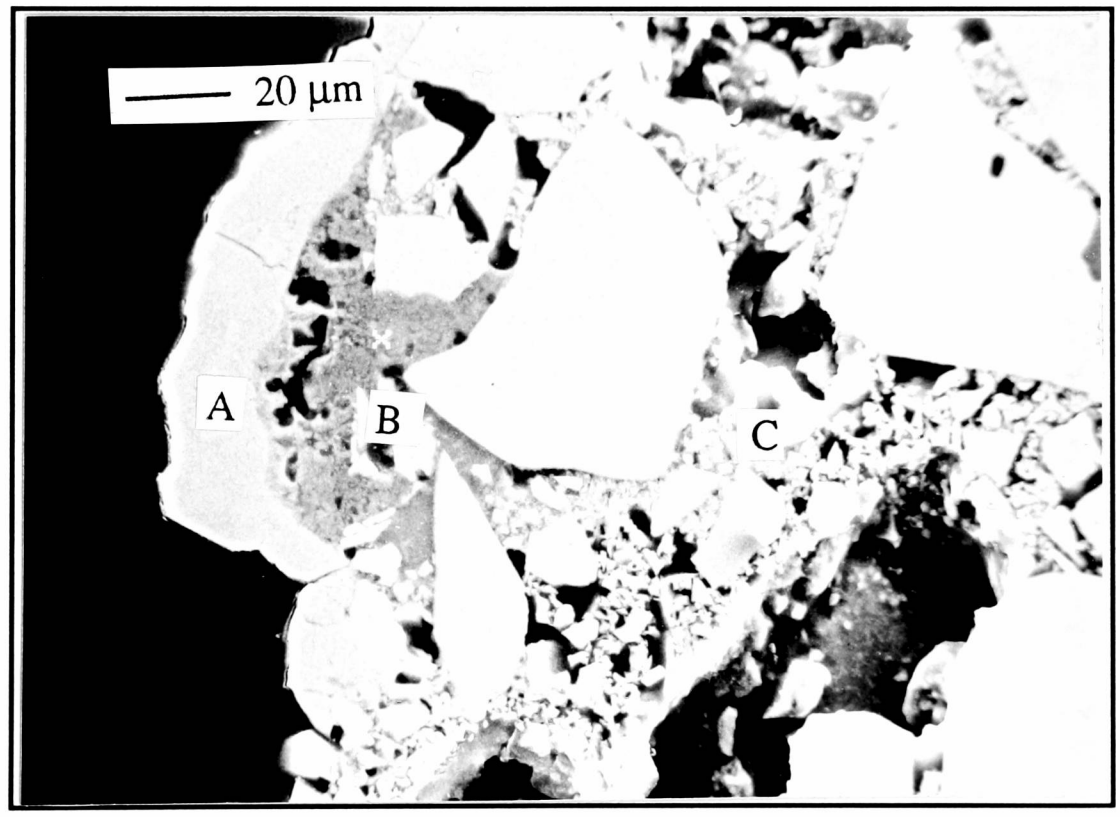


Figure 190: Section through the primary coat of a 5 kg silica based mould cast with martensitic stainless steel mag = x 490

A = metal layer

B = Al/Si/Cr/Mn/Fe

C = unaffected mould structure

The primary layer also contains many holes (20 - 25µm in depth) from which ceramic constituents have been removed. Refractory particles may have interacted with the metal surface and, since the binder appears to have melted or softened, it seems likely that this has allowed these refractories to be pulled out or dissolved from the mould and into the metal itself. As alloying elements can be detected in the binder phase surrounding these holes it seems unlikely that these particles have been removed by polishing.

4.7.1.2: Metal Surface

A micrograph through a section of the metal casting in contact with the mould can be seen in Figure 191. It can be seen that the surface of the metal has reacted with the mould to form an oxide layer which is divided into three areas (Regions 1, 2 and 3). Region 4 is the untouched metal structure.

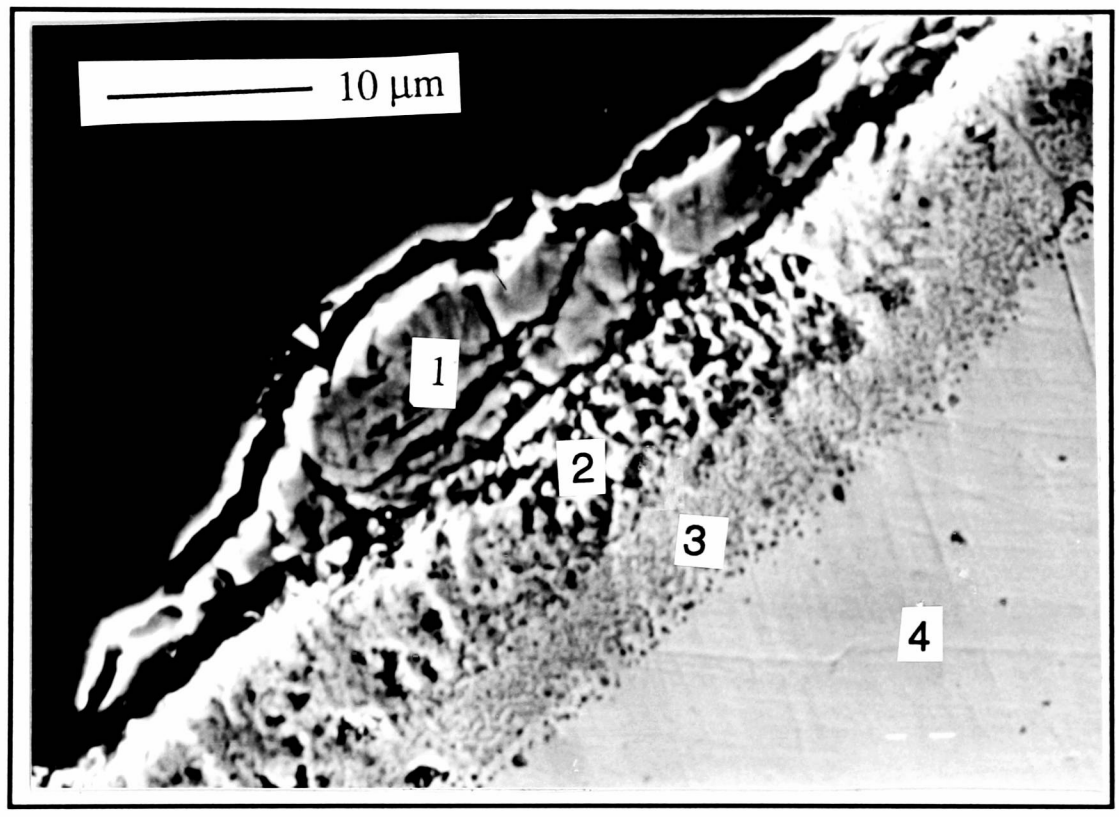


Figure 191: Section through the metal surface of a 5 kg martensitic stainless steel casting (silica based mould) mag = x 1,700

The layers of oxide contain different amounts and types of porosity with the outside layer (Region 1) appearing to be a scale on the surface. Region 2 is a highly porous layer containing large pores, which are randomly spaced throughout the structure giving the appearance of low density. Region 3 consists of an oxide layer which contains a large amount of very fine porosity which is evenly spaced throughout the structure. This high density of pores can be viewed at higher magnification (Figure 192).

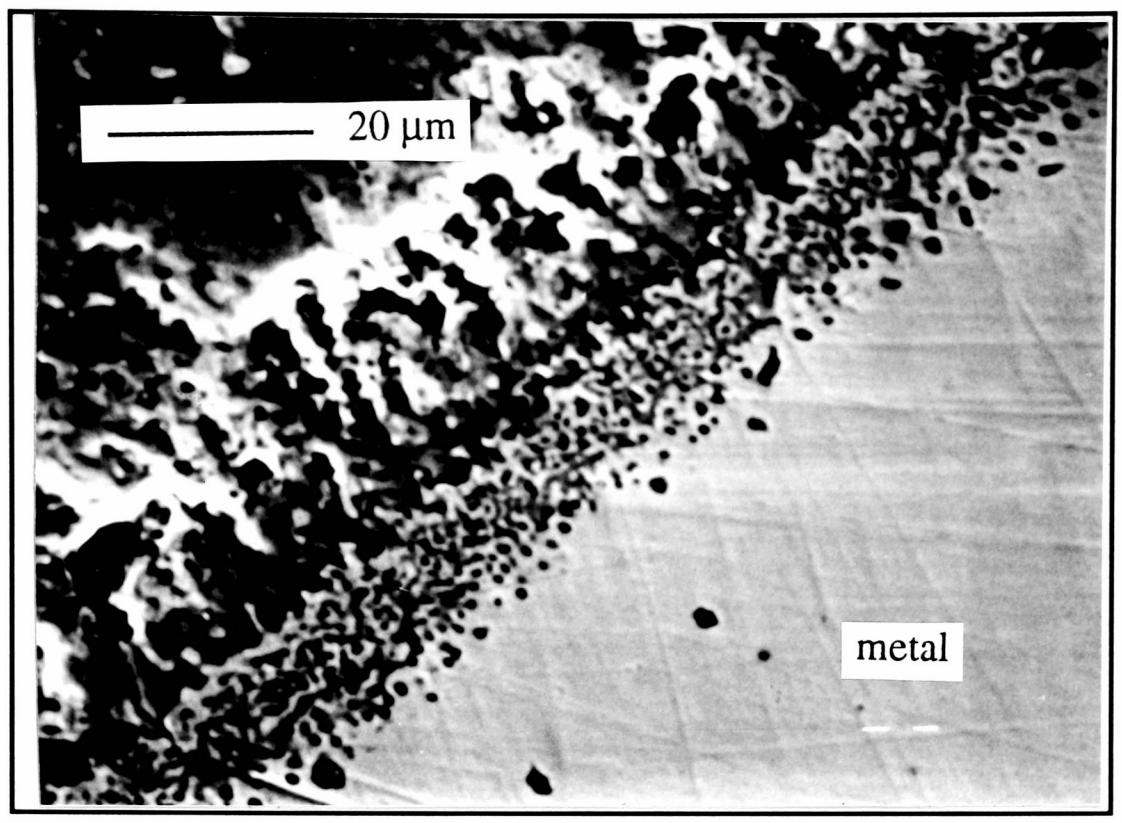


Figure 192: Section through the metal surface of a 5 kg martensitic stainless steel casting (silica based mould) mag = x 2,500

EPMA was used to analyse the layers and the metal in order to determine the basic constituents. Analysis of the basic metal structure revealed the presence of Fe, Si, Cr, Mn, and Ni. These are all alloying elements which are present in varying amounts in the original metal composition. The elements C, S, P and Mo were not detected, but this is not surprising as the relative amounts in the original specification are all below the detection limit of 0.5%. The elements Fe, Si, Cr and Al were detected in varying amounts in the oxide layers. Note that Al is not an element which is present in the original metal composition. Since Al is added as deoxidant it can be concluded that this is the source. By a comparison of the relative element peak heights on the EPMA traces, a compositional profile of the cast metal surface was constructed (Figure 193).

The metal composition is contained in the bar chart for region 4. The amount of Fe present in the oxide decreases in the outer layers but the amount of Cr increases. This could due to the fact that the outside layers of the metal, in contact with the surface of the mould, are Cr enriched. This is possible when considering the fact that chromium ions have a greater thermodynamic affinity for oxygen than Fe and are susceptible to diffusion. The likelihood of diffusion is increased when there is a difference in oxygen partial pressures. It is safe to assume that the partial pressure of oxygen in the metal is much lower than that in the mould and therefore chromium ions will migrate toward the surface of the metal.

The increase in Al content in the outer layers is considered to be due to the fact that this metal is deoxidised with Al powder. Incomplete removal of this element from the melt will leave a high Al content in the liquid metal which will then diffuse towards the surface in the same way as the chromium ions. This theory also helps to explain the pore structure seen within the metal surface. When ions diffuse from one place to another they do so by a number of means, one of which involves the movement of vacancies in the opposite direction. When there is an unequal rate of ion movement the equilibrium is unbalanced and a supersaturation of vacancies condense to produce voids in the structure. This phenomenon has been observed in the Kirkendall Experiment[140] where voids are formed in the copper rich side of a copper/nickel joint. It is possible that a vast number of vacancies left in the metal after the preferential diffusion of Al and Cr ions to the surface have produced the observed structure. It is therefore postulated that the phase which reacts with the mould surface is not the original metal, but a layer of oxide 'slag' consisting of an Al/Cr oxide containing small amounts of other elements such as Si, Mn and Fe. This accounts for the fact that these are the elements found within the binder phase of the corresponding mould section.

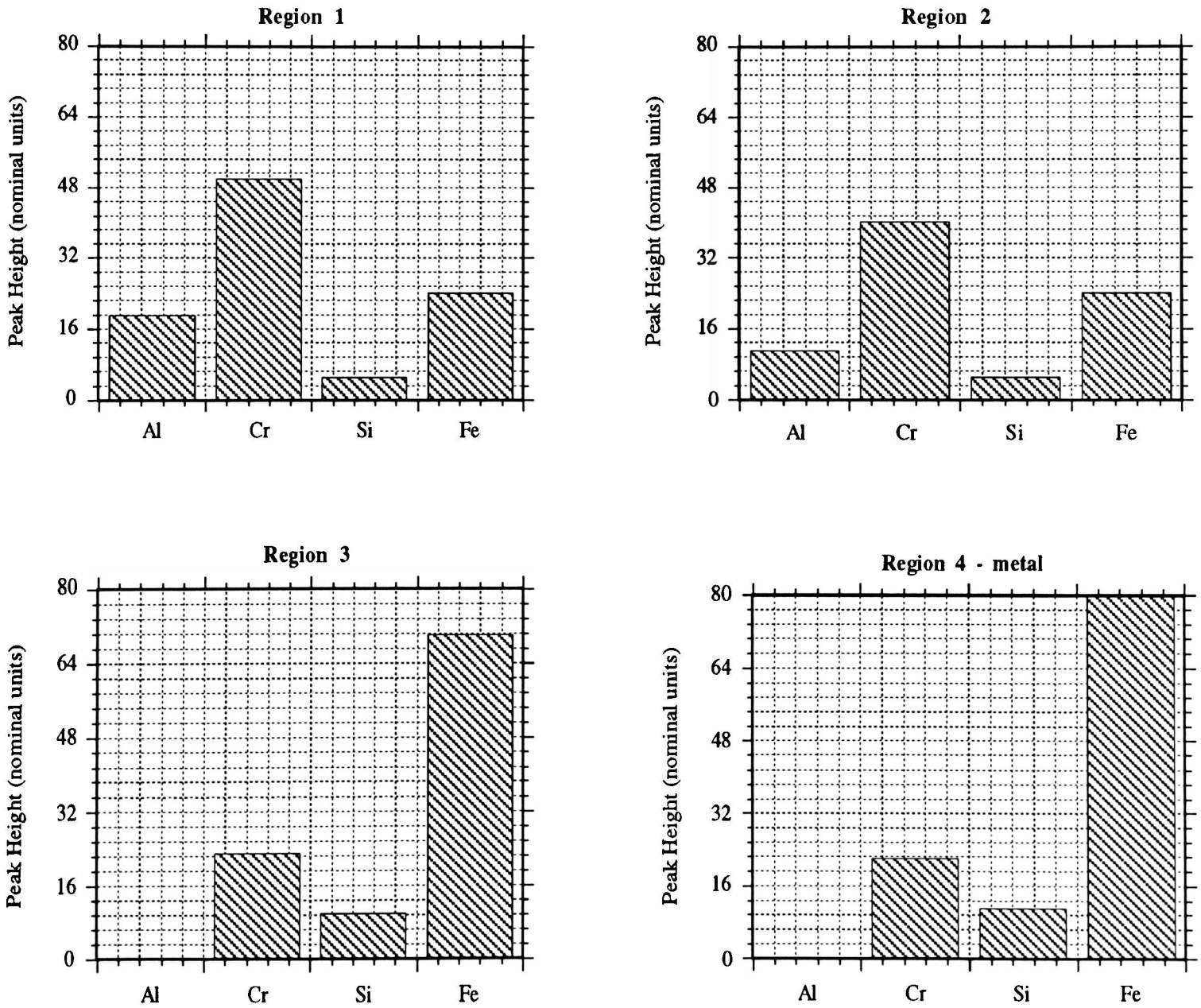


Figure 193: EPMA compositional profile for regions 1 to 4 (Figure 191)

4.7.2: 60 kg Mould

Low alloy steel, at a pouring temperature of 1580°C, was cast into a 60 kg investment mould made using standard zirconium silicate refractory and silica binder. Experimental procedures together with compositional analysis of the metal can be found in Section 3.10. After cooling, samples from both the mould and metal casting were sectioned and mounted for SEM analysis.

4.7.2.1: Mould Surface

The low magnification micrograph of a section through the primary coat of the mould is shown in Figure 194. Instead of a layer of metal, the primary surface has a layer of an aluminium compound attached to it (region 1), which has a composition resembling that of the deoxidant (Figure 195). Other elements present in the layer such as Na, S, K and Fe have originated from the metal itself. As with the smaller mould, it is the deoxidant that is attacking the mould surface, but in doing so it is removing elements from the melt, changing the metal specification and leaving a layer attached to the surface of the mould.

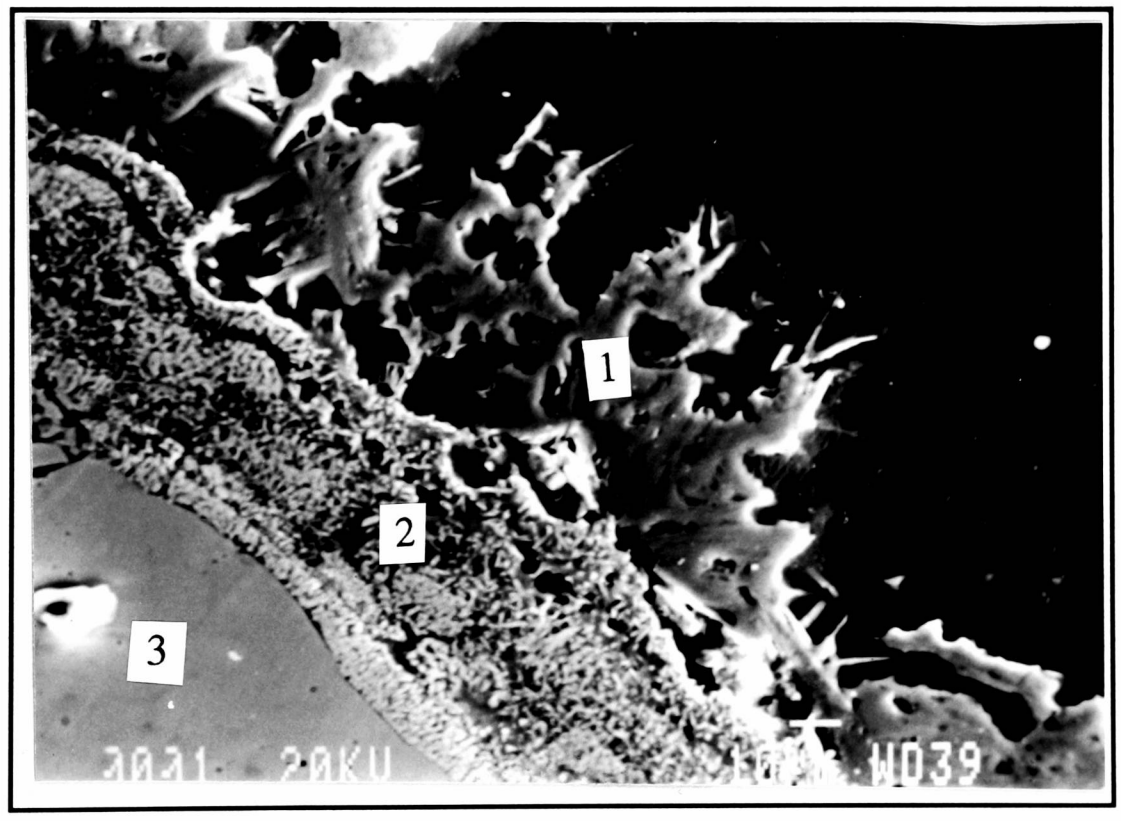


Figure 194: Section through the primary coat of a 60 kg silica based mould cast with low alloy steel mag = x 550

Interaction of the deoxidant 'slag' with the mould has continued deeper into the mould in region 2. The structure of the refractory constituents has been totally altered (Figure 194). A binder network still exists but no longer consists of silica alone; elements such as Zr, Al, Fe and Na are present in large amounts. The refractory particles themselves appear to have been broken up into rod shaped pieces, possibly by partial melting, to an average depth of 75μm. This structure is very similar to that of plasma sprayed zircon, which has been in contact with steel fluxes, and has undergone dissolution at low temperatures. After this, during cooling, recrystallisation under the influence of a thermal gradient produces the rod-like structure. It is very possible that this is a similar phenomena, since other elements are in contact with the refractory particles and the temperature within the primary coats of this moulds has risen above 1,400°C for a prolonged period of time (see Section 4.6).

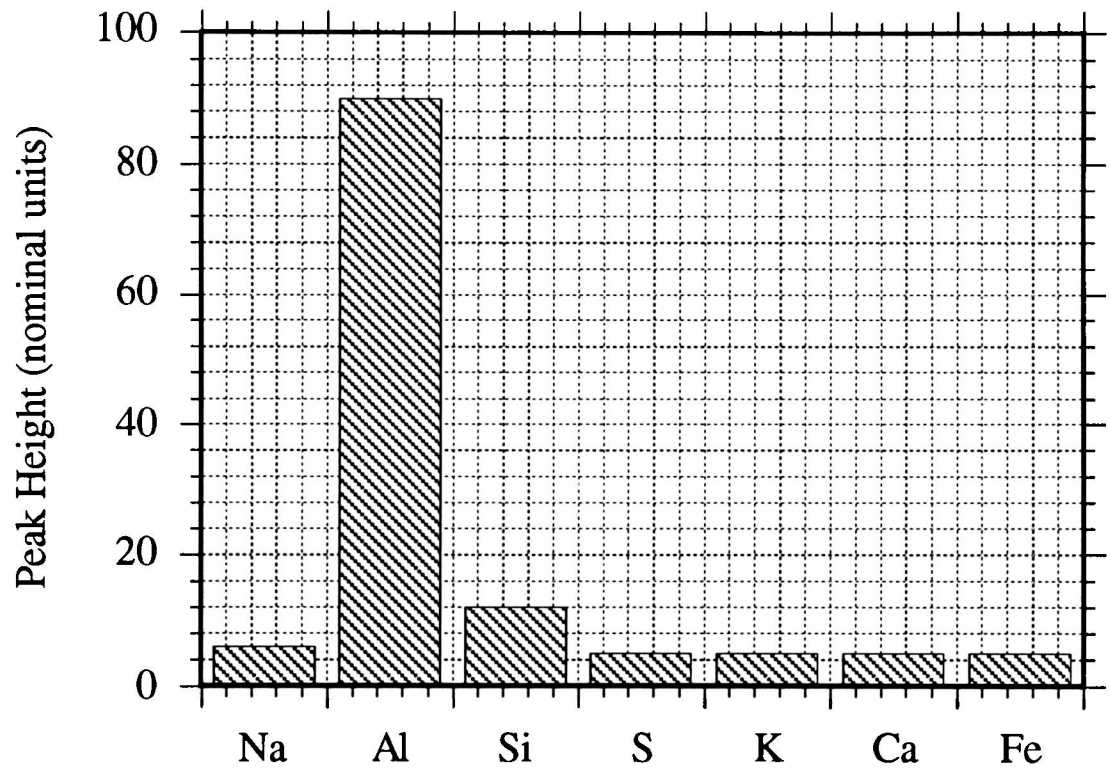


Figure 195: EPMA composition of region 1 (Figure 194)

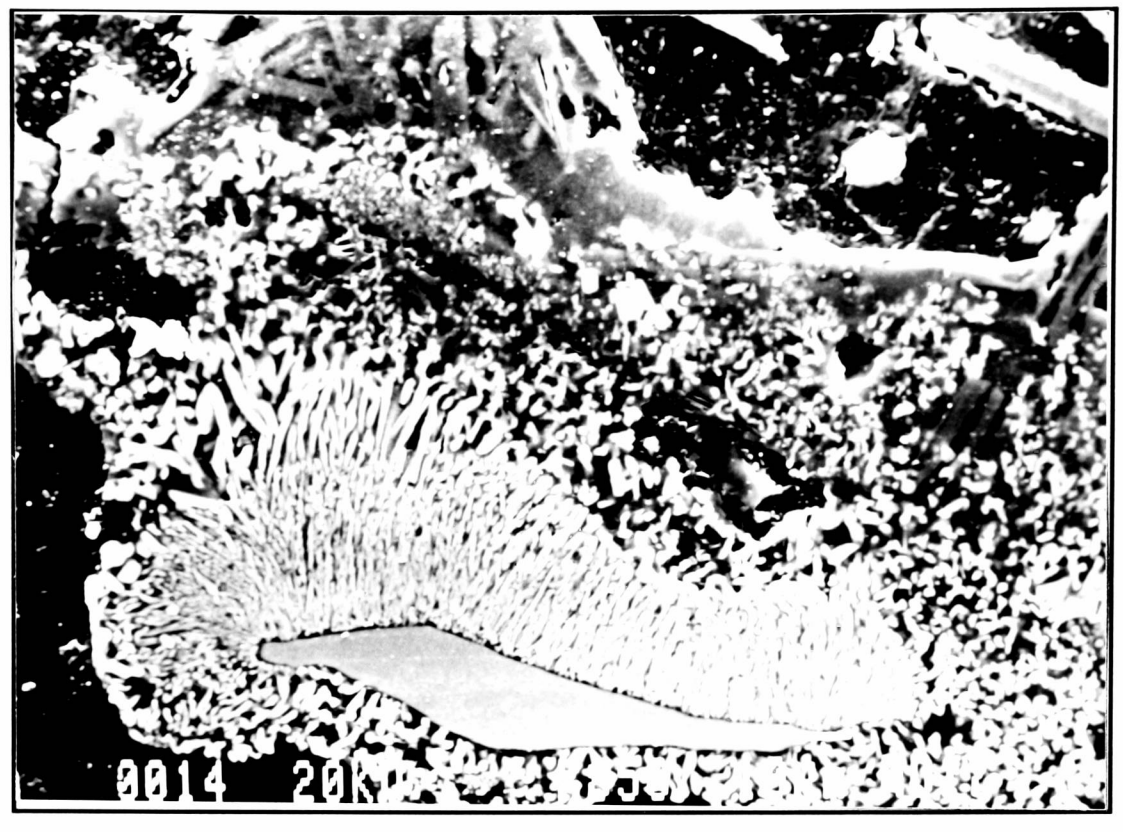


Figure 196: Higher magnification micrograph of region 2 showing the partial recrystallisation of a Zircon Sand stucco particle mag = x 850

Further into the mould section the mould structure is normal (region 3) apart from the presence of large cracks across both the binder phase and the ceramic particles themselves (Figure 197). Cracking of this nature is typical during the creep of ceramic particles at high temperatures (Section 4.8).

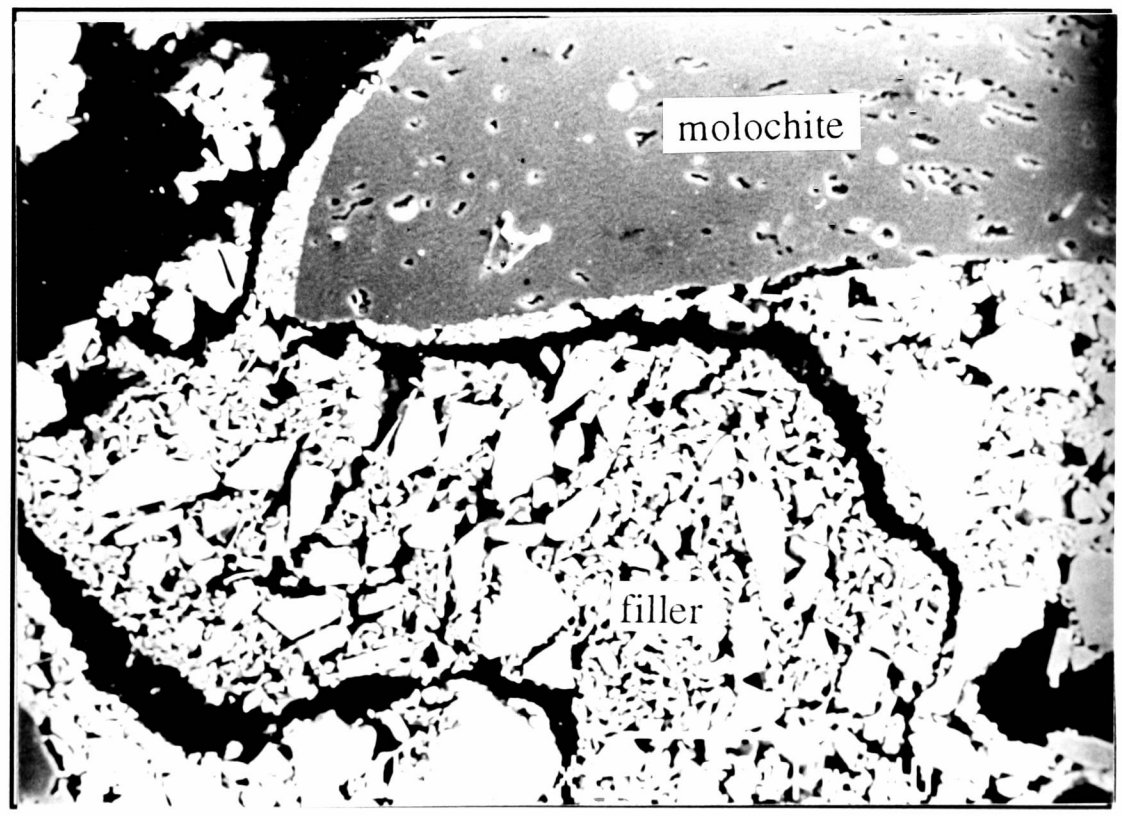


Figure 197: Micrograph of region 3 showing the cracks in the mould structure mag = x 250

4.7.2.2: Metal Surface

To obtain a sample through the outer section of a 60 kg casting proved to be difficult since the casting itself was very large and the metal could not be cut be conventional methods. The sample that was eventually used for analysis came from a piece of metal which flaked away from the surface of the casting in the riser section of the component. Before sectioning, the sample was mounted and the surface examined using SEM (Figure 198). The white inclusions embedded into the surface of the metal could not be analysed using EPMA because the technique requires an optically flat surface which this sample did not possess. However, visual examination reveals an angular morphology which suggests that these inclusions are ceramic in nature and may be small filler particles from the primary coat of the mould.

This conclusion is further substantiated by the micrograph of a section through the metal sample (Figure 199). Region 1 is low alloy steel which has penetrated into the primary coat of the mould. The remaining structure is that of refractory materials, some of which have been partially melted (Figure 200), enclosed by a alumino-silicate matrix containing large amounts of Mn and Fe. It appears that metal and the metallic 'slag' has penetrated throughout the primary coat of the mould via the silica network, which has reacted with the aluminium oxide to form an alumino-silicate binder matrix. This matrix, in the presence of fluxing agents such as Fe and Mn, is probably a glass which will produce a brittle layer between the metal and the mould. When the mould material is removed from the casting this brittle phase may have fractured and produced a metal casting with a layer of refractory inclusions on the outer surface.

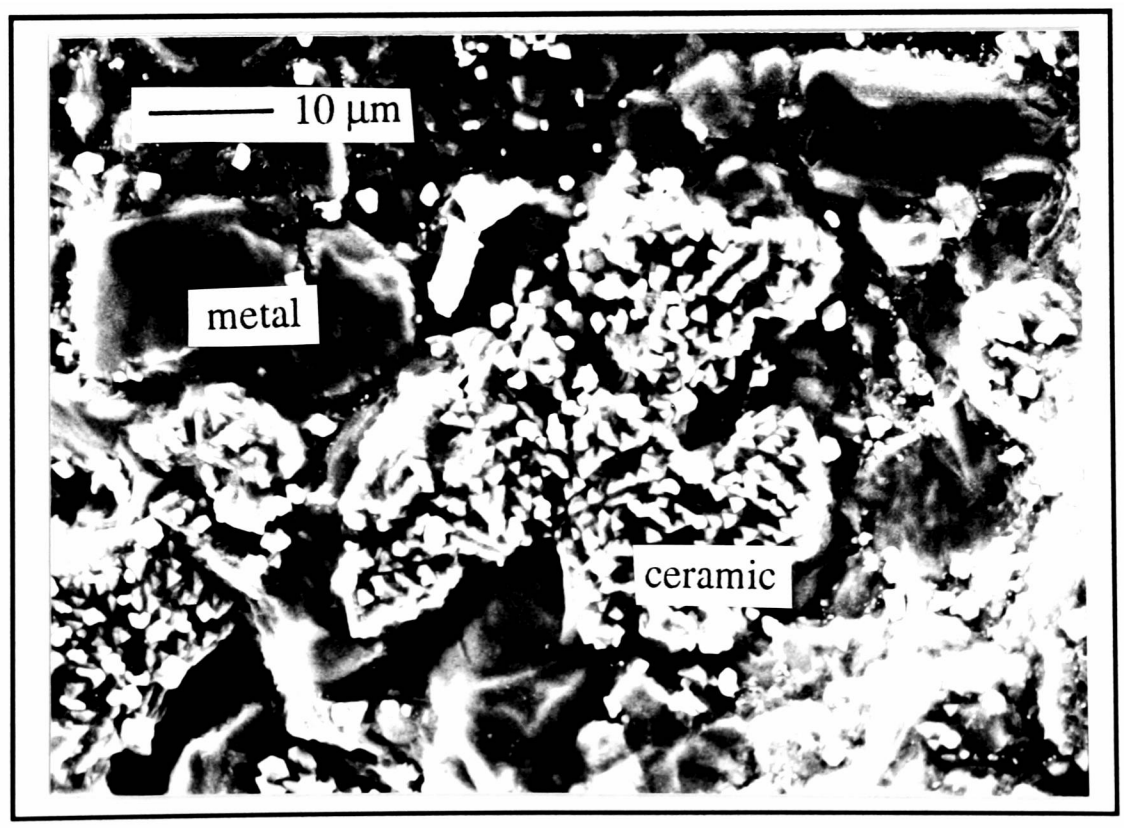


Figure 198: Micrograph of metal flake from the surface of the 60 kg casting

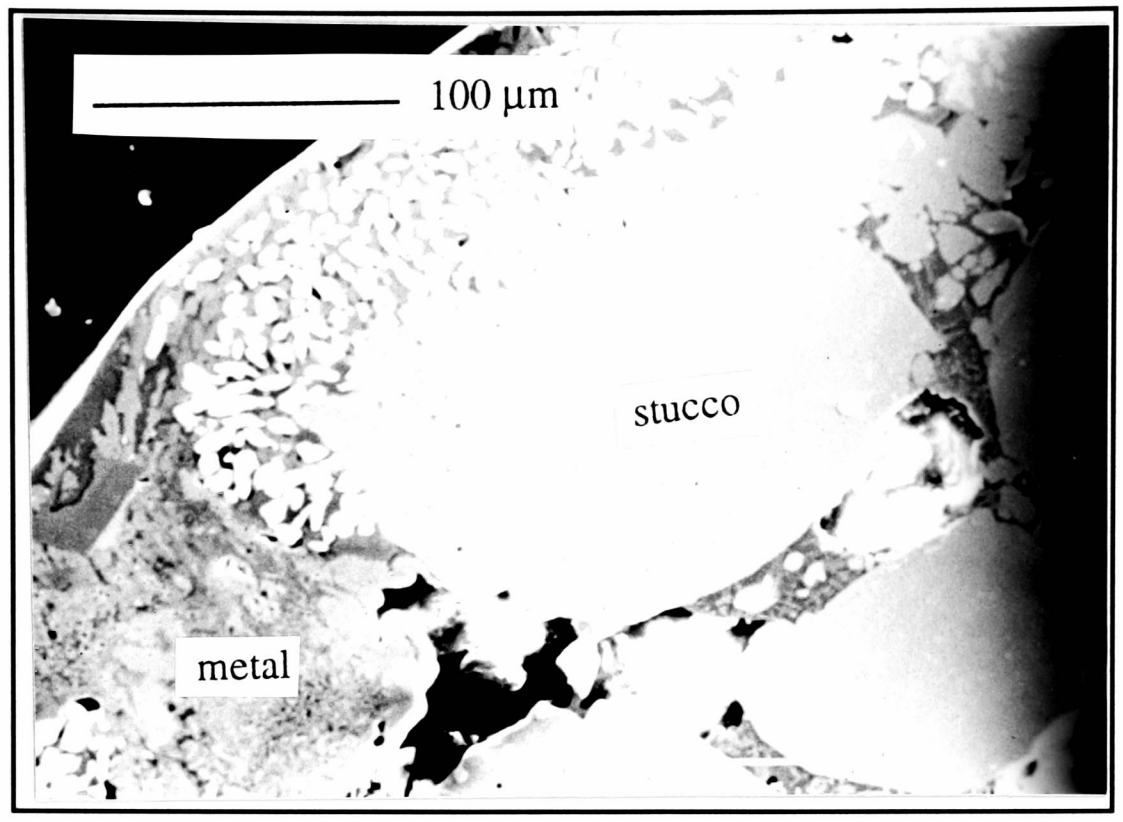


Figure 199: Section through the metal sample from the surface of the 60 kg mould

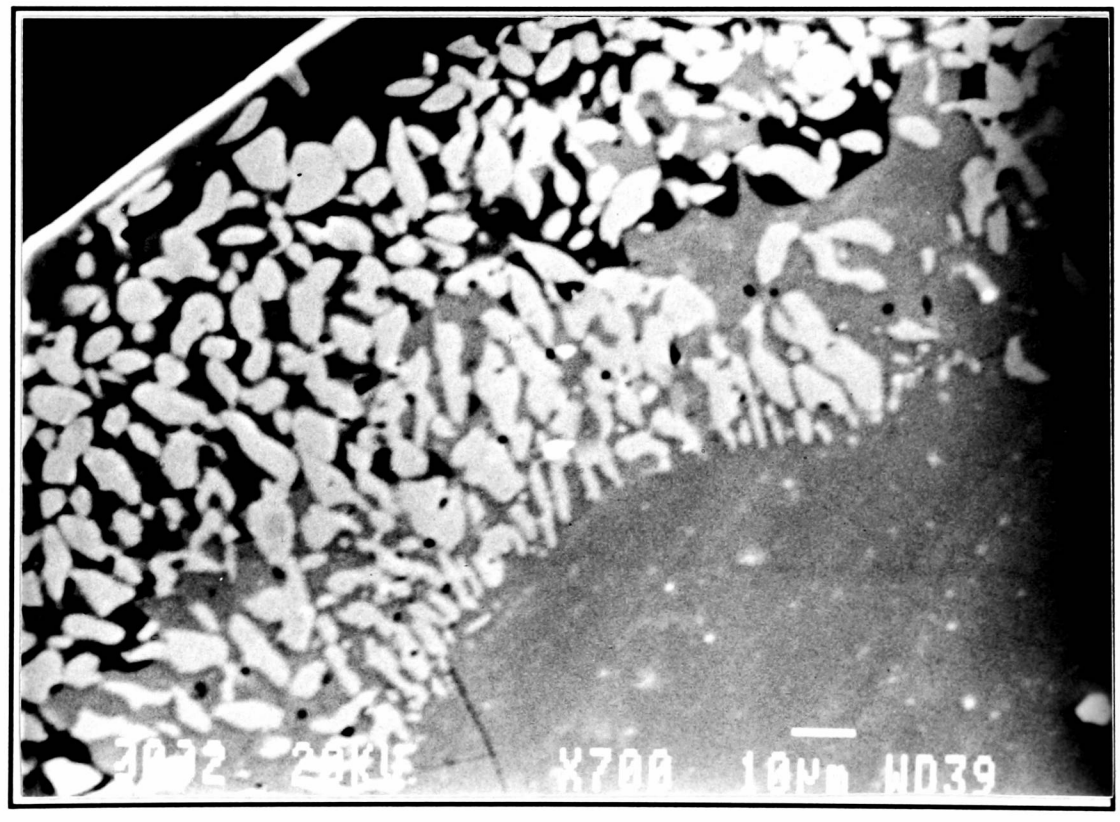


Figure 200: Partial reaction and melting of a Zircon Sand grain in the metal surface of a 60 kg mould cast with low alloy steel mag = x 700

The extent of interaction between the metal surface and the refractory mould is much greater than in the smaller mould. This is due to the fact that the primary layers of the large mould are subjected to higher temperatures for longer periods of time. As the temperature is approaching the melting point of the silica binder it is not difficult to understand why, in the presence of fluxing agents, the binder matrix appears to have melted and allowed the influx of liquid metal and slag into the pore network of the mould section. The metal in intimate contact with the larger refractory particles has reacted and produced a rough casting surface with inclusions of primary coat refractory particles which have broken away and embedded into the metal. As such, quality control failure of larger castings due to surface roughness and inclusions is more likely than with smaller components.

4.7.3: Summary

Martensitic stainless steel interacts only slightly with the surface of the small mould, leaving behind a layer of iron from which the alloying elements have been removed. These elements appear to have diffused farther into the primary coat, possibly through melting of the binder followed by capillary action, and have combined with the silica binder. The presence of these elements, some of which are fluxing agents for silica, probably means that the binder in this interaction layer has been converted to a silicate based glass. The interaction with the binder occurs up to an average depth of 85μm after which the structure is unaffected by the metal.

The basic structure of both filler and stucco does not appear to have been affected. Holes in the primary edge of the mould, within this interaction range, suggest that filler particles have been pulled out or dissolved and may well have been combined with the 'slag' which interacts with the metal surface to produce a layered oxide structure into which varying amounts of alloying and deoxidiser elements have been incorporated. However, apart from this oxide scale the interaction appears to have been light and this is due to the fact that the metal/refractory interface in the smaller mould only reaches 980°C for a short period of time.

The primary layers of the 60 kg mould are subjected to temperatures in excess of 1,400°C for relatively long periods of time. As such, the extent of interaction with the mould is much greater and this is due to the fact that temperatures experienced are close to the melting point of the silica binder. Again it appears that the metal oxide slag, combined with deoxidant material, is attacking the surface of the mould. This is to be expected as corrosive slags are usually responsible for the deterioration of other refractories such as furnace and ladle linings used in the casting industry.

The mould has a layer of deoxidant material attached to it which has attacked the mould structure to an average depth of 75μm. Alloying elements, iron and deoxidant constituents have reacted with the binder to form a silicate network which is possibly glassy in nature. This network has probably been

formed by the fact that the silica binder has melted and the deoxidant/oxide material has infiltrated the pore network. The glassy network is probably responsible for the fact that the metal surface contains primary coat refractory particles. When the mould is removed from the casting after cooling, this brittle phase may fracture, leaving the interacted areas of the mould embedded in the surface of the metal. Unlike the smaller mould, the interaction has continued into the larger refractory particles which appear to have been fluxed, melted and recrystallised by the alloying elements which are in intimate contact with the refractory particles.

4.8: Creep Tests

The structural integrity of the mould section is directly dependent upon the mechanical response and resistance to creep of the ceramic constituents when subjected to various loads and temperatures. Large silica bound moulds are more prone to excessive creep due to the fact that temperatures in excess of 1200°C (the softening temperature of silica) are easily achieved and maintained for long periods of time. This creep is believed to be responsible for the bulging of large mould sections which leads to dimensional inaccuracy and ultimately failure at the quality control stage. Since the maximum temperature that an investment mould is required to withstand is directly dependent upon the component size, it may be necessary to replace the silica binders with alternatives which are not prone to creep at higher temperatures. Therefore the creep response of various silica and non-silica based mould systems was investigated.

Mould samples were prepared according to the schedule contained in Appendix 9 and the experimental procedures are detailed in Section 3.12. Note that extra samples were made at the same time and used as a basis for the physical property evaluation tests (Section 4.9). The thermal profile used throughout the creep testing was based upon that obtained in the inner coats of the 60 kg mould (Figure 201) cast with low alloy steel (Section 4.6.2), in order to determine the properties of the mould system under the worst case scenario. all samples were fired prior to testing at temperatures determined using expansion/contraction tests (Section 4.9.1). Samples were heated to 1,000°C without the application of a load and held at this temperature for 1 hour to simulate preheating of the mould. After this the temperature was raised to 1,420°C as quickly as the equipment would allow, in this case only 400°C/hour. As soon as the maximum temperature was reached, the load was applied to simulate pouring of the metal into the mould.

Creep testing was carried out at the National Engineering Laboratory in Scotland. During casting the metal weight acts upon the primary coat of a mould producing compression within the inner coats and tension within the outer. Samples were tested in the three point bend mode so that the stress distribution was analogous.

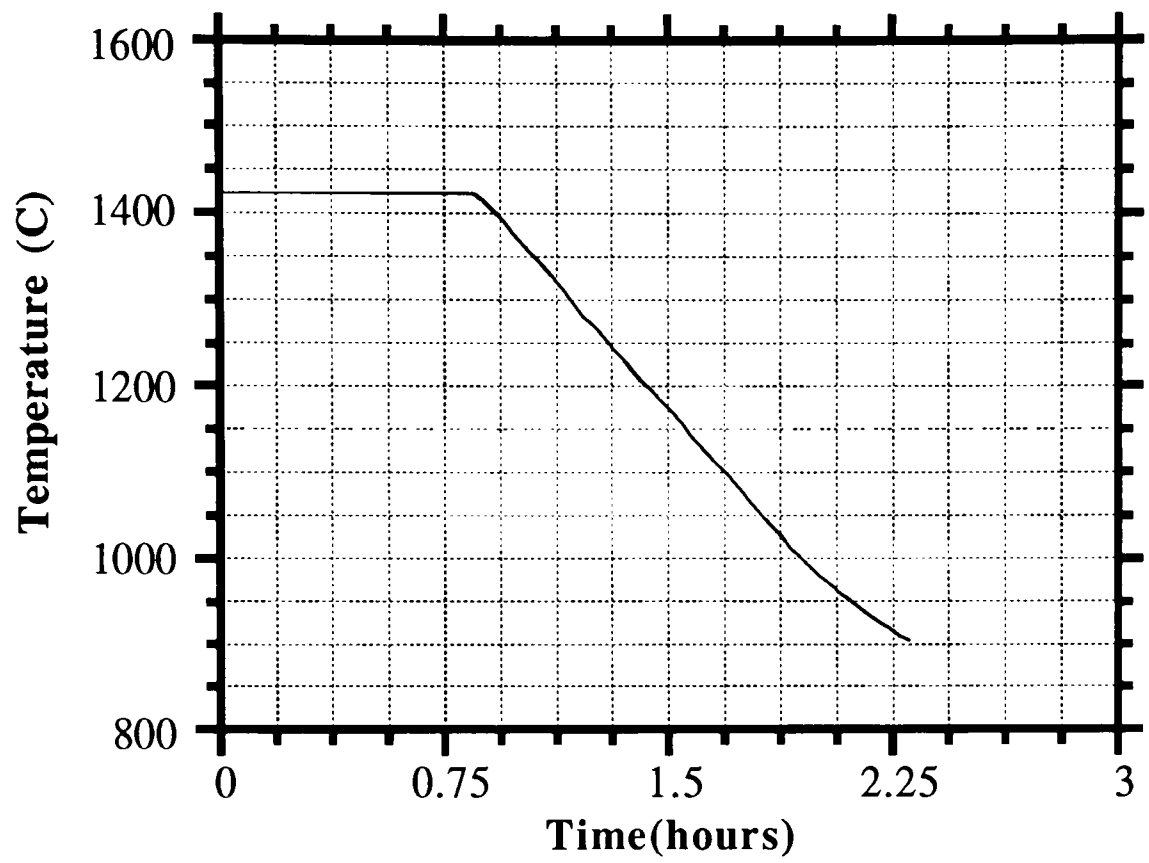


Figure 201: Thermal profile used for creep testing of mould samples

4.8.1: Mould System With Silica Binder

These samples were made using a water based primary coat and alcohol based secondary coats and are the standard silica based mould system used at Deritend Precision Castings. Investment casting shell samples, though produced under identical conditions, have an inherently variable structure. In order for any measurement to be considered absolute, several samples must be tested and the results statistically combined. As such, eight shell samples were produced and tested, giving rise to the results displayed in Figure 202. Note that the standard shell system was the only one which was tested using a 200g load and that the system is fairly consistent as 100% of the samples survived until completion of the test.

All of the samples underwent linear deflection during the hold at 1420°C followed by no further movement during cooling. The extent of the deflection ranged from 0.2 to 1.35 mm with a calculated mean deflection of 0.75 mm ($\sigma_{(n-1)}$ = 0.36 mm). The quoted surface tolerance of a 100 mm metal section cast using the investment technique is 0.35 mm[139]. According to these results, 87.5% of castings produced using these shell samples would have not met the tolerance specification and could be considered casting failures.

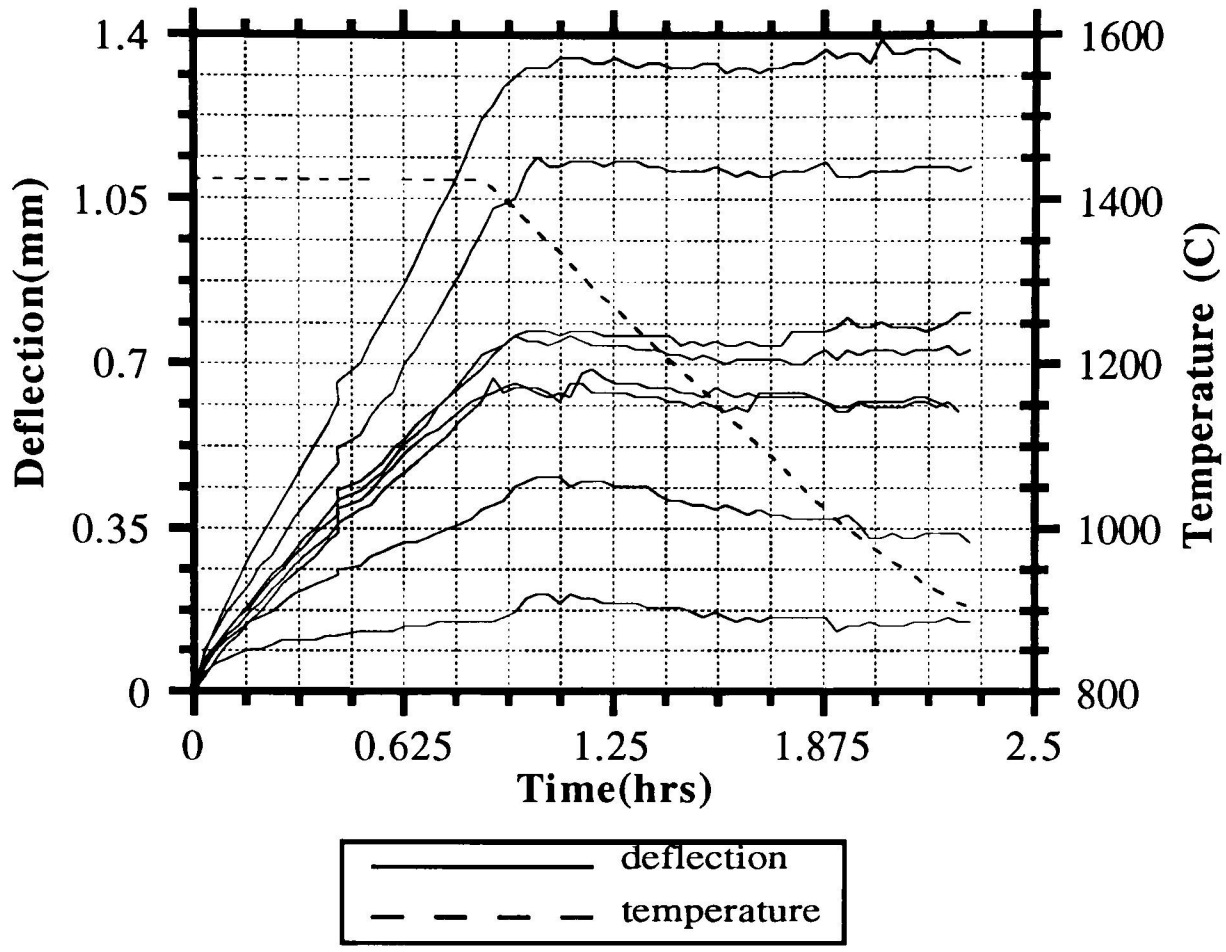


Figure 202: Creep test results for the standard silica based shell used at Deritend Precision Castings

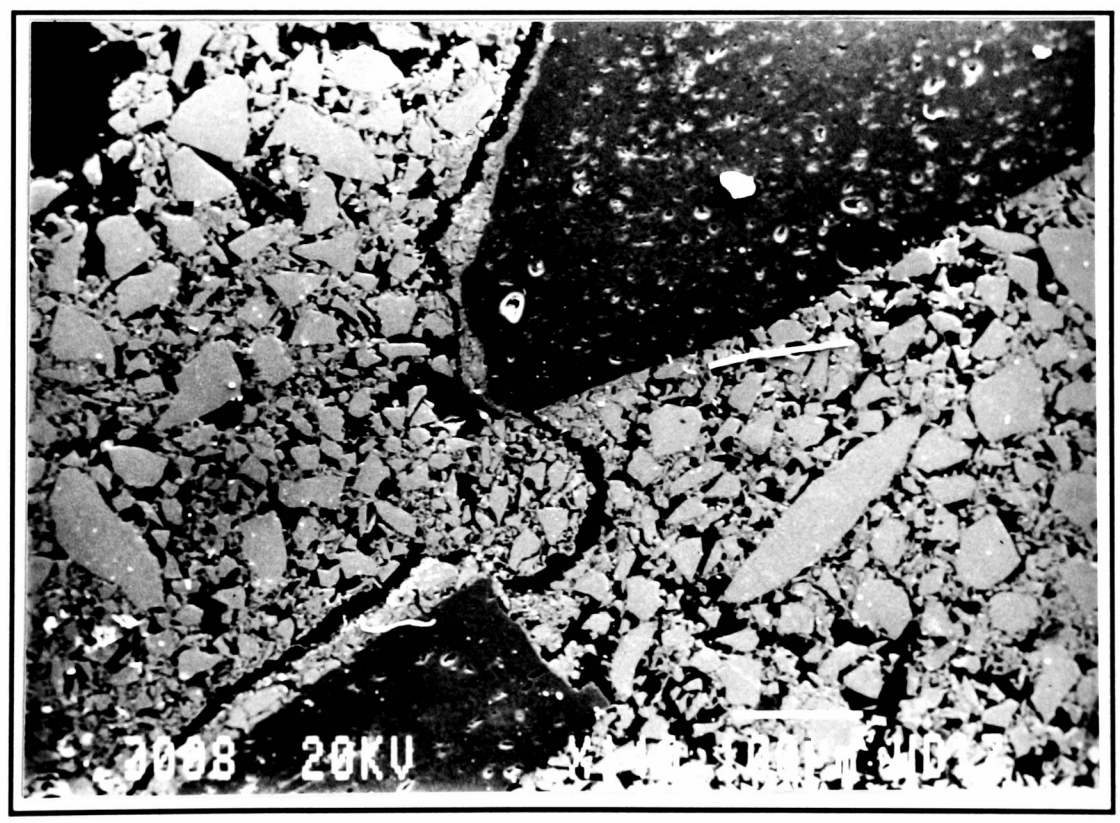


Figure 203: Micrograph of a crack found in the secondary coat section of a silica based mould sample after creep testing at 1,420°C mag = x 140

A direct analogy such as this should be considered with caution. Many other factors such as the role of the backing refractory and the structural stability of shell material experiencing lower casting temperatures cannot be directly determined and must be taken into account. The heating of the inner coats of the mould to 1,420°C takes place instantaneously and not over 1 hour which is a constraint placed upon the equipment used at NEL. This was compensated for by delaying the application of the load until maximum temperature had been reached, but may still cause an increase in the overall deflection of the sample. This indicates that the mean deflection should not be used as an absolute value for creep deflection but should be used as an indication of the extent of mould wall movement and as a means of comparison between different mould systems. The results do, however, provide evidence that the casting bulge experienced by larger moulds is a direct result of high temperature creep within the mould wall.

Evidence to support this hypothesis is also provided by the presence of typical cracks within the ceramic constituents[87] which occur when a ceramic has undergone high temperature creep. These cracks can be clearly seen in a micrographs prepared from a section through one of the samples after testing (Figures 203 and 204) and are a further indication that extensive creep is taking place in the silica based samples. It should be noted that similar cracks have been found in the mould wall of a 60 kg mould that has been cast and allowed to cool (Section 4.7.2.1). Cracks were not found in the mould section of a 5 kg mould after casting, which is not surprising as a mould this size is not usually susceptible to casting failure as the result of mould wall movement.

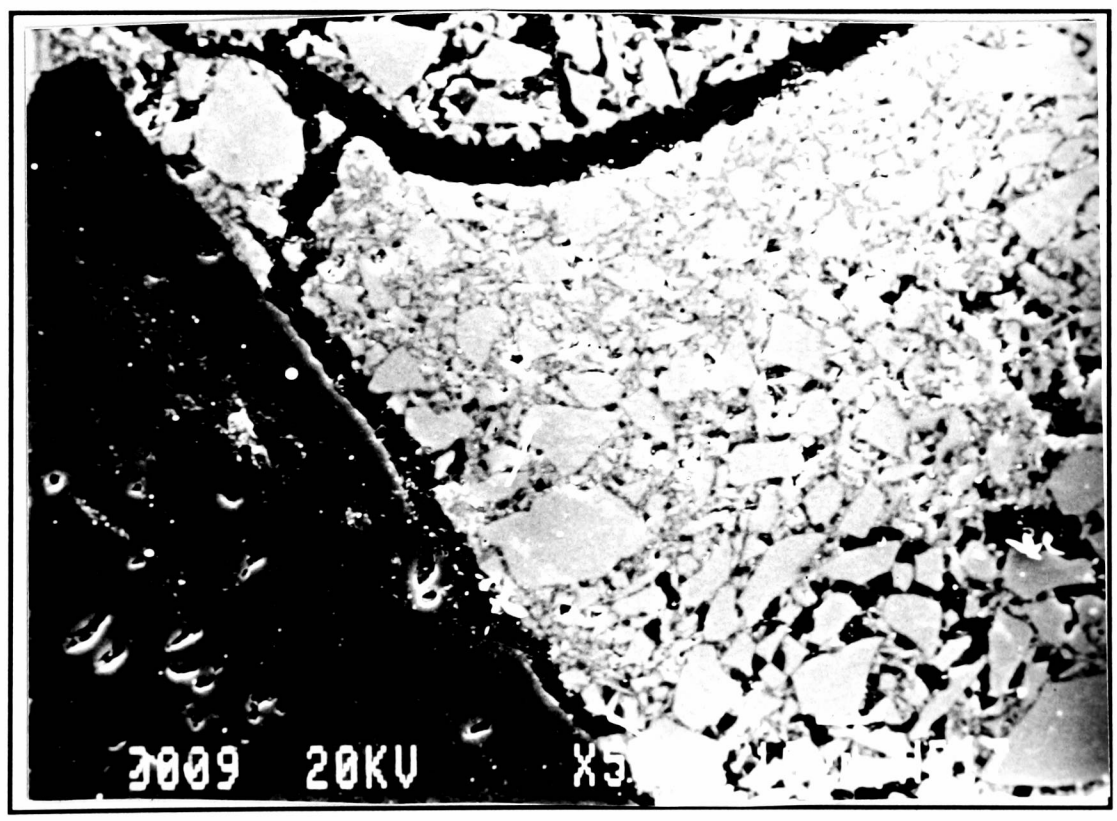


Figure 204: Micrograph of a crack found in the secondary coat section of a silica based mould sample after creep testing at 1,420°C mag = x 550

4.8.2: Mould System with Zirconia Binder

An equivalent mould system was prepared using the same refractories and mould dipping schedule, but with Remet zirconia sol as the binder instead of silica. The system was very weak at high temperatures and could not be tested using a 200g load as for the silica based system. As a result, the test was repeated at a variety of lower loads until one was found which the sample could accommodate (30g). Though many samples were tested, only one managed to complete the test, with the others breaking as soon as the load was applied or a few minutes after. The creep deformation measured for this sample is shown in Figure 205.

The deflection trace is similar to that of the silica based system in that deflection occurs during the isothermal section of the temperature regime and then remains steady during sample cooling. However the deflection rate in this sample is curvilinear in nature and decreases with time during the temperature hold. This does tend to suggest that the creep is due to a phase change or reaction which produces a product which is less prone to creep. In the case of the zirconia binder, this reaction could be due to densification which occurs during the transformation from monoclinic to tetragonal zirconia.

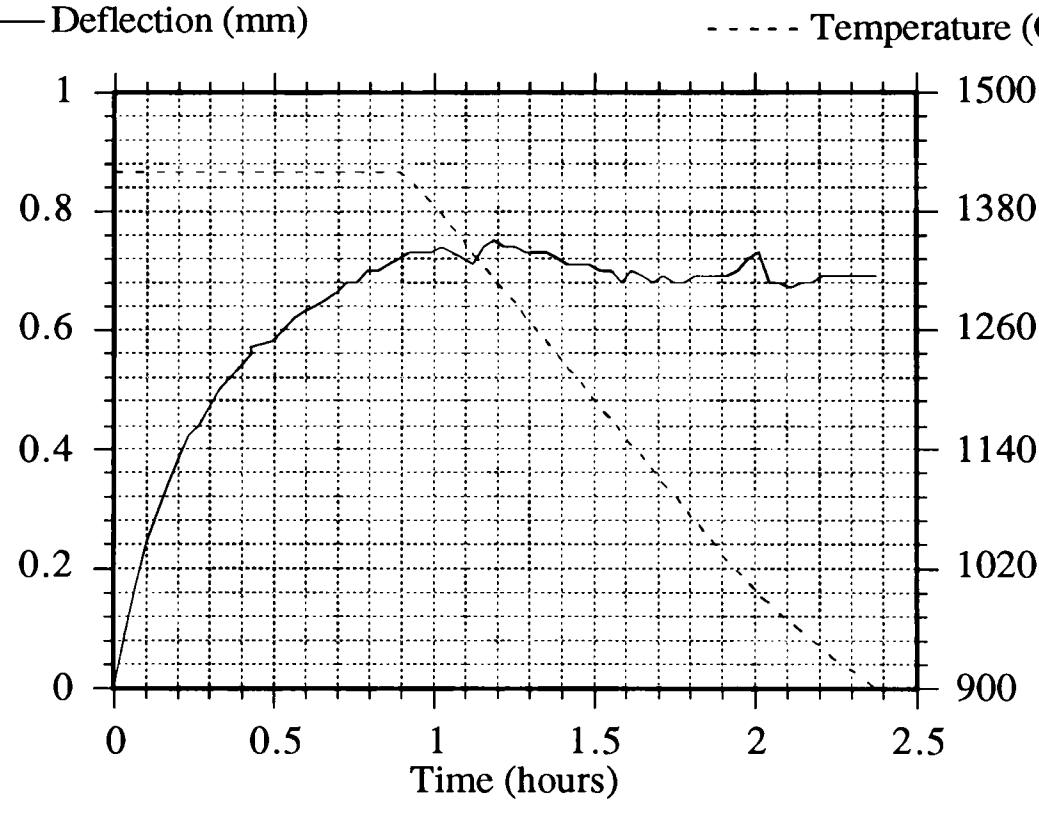


Figure 205: Creep result with a 30 g load for mould sample made using Remet zirconia binder

The overall deflection of 0.7 mm across a 100 mm span is still greater than the quoted tolerance levels but could be reduced by stabilisation of the fired phase structure and could be affected by increasing the physical strength of the mould section. The achievement of such a high relative displacement with a greatly reduced load does suggest that the tendency to creep is higher in zirconia binders than silica. If we assume that the total sample deflection is linearly proportional to the load, then the deflection in a zirconia based sample with a 200g load would be 4.67mm. This represents an average deflection which is at least 6 times that of a silicate based sample and more than 13 times that of the tolerance level. However, an equivalent increase in mechanical strength would probably affect the deflection and reduce the creep to a more acceptable level.

In its present state the zirconia binder would not make a good alternative to silica as the physical strength at 1,420°C is very low and the amount of mould wall deflection due to creep of the binder is higher than can be tolerated. As a binder system, the sol appears to be much more susceptible to creep than silica.

4.8.3: Mould System With Alumina Binder

An equivalent mould system was prepared using the same refractories and mould dipping schedule, but with Remal A20 alumina sol as the binder instead of silica. The system had a very low green strength and great care had to be taken when cutting the ceramic from the former. This low physical strength was also encountered at high temperatures and again the 200g load could not be used without sample failure. As a result, the test was repeated at a variety of lower loads until one was found which the sample could accommodate, in this case 50g. This is surprisingly higher than zirconia, which has a much greater green strength, and is obviously a reflection on the fact that any reactions or phase changes which take place in an alumina based system at high temperatures have a beneficial effect upon the overall strength. Out of eight samples that were tested, only five managed to complete the test, with the others breaking as soon as the load was applied or a few minutes after. Therefore the alumina based mould system is weaker than silica based systems at high temperatures and is more variable as 27.5% of the samples fail during testing.

The creep results for the five surviving samples are shown in Figure 206. The response is again similar to silica based systems, with linear deflection during the isothermal hold and steady state during the cooling section. The overall deflection is much lower, with four of the samples displaying deflections below 0.4 mm. The other sample is very different and has an creep deflection of approximately 0.75 mm which is similar in magnitude to silica. This difference is indicative of the variability of the mould system as a whole and gives a mean deflection of 0.328 mm ($\sigma(n-1) = 0.24$ mm).

Again, assuming a linear relationship between deflection and load, the deflection can be equated to 1.312 mm for a 200g load. This figure is only 1.75 times that of the silica system and 3.75 times the quoted tolerance. This suggests that a larger alumina bound mould would be much less prone to creep than zirconia and there is the possibility than an increase in the mechanical strength will produce a mould system which will undergo less deflection than silica. Attention must be paid to the variability of the samples as only 5 managed to survive to the end of the test using the 50g load. Much more research will be needed to overcome the low green and fired strengths and the problems encountered with the autoclaving of alumina binders if this material is to be used as a viable alternative to silica.

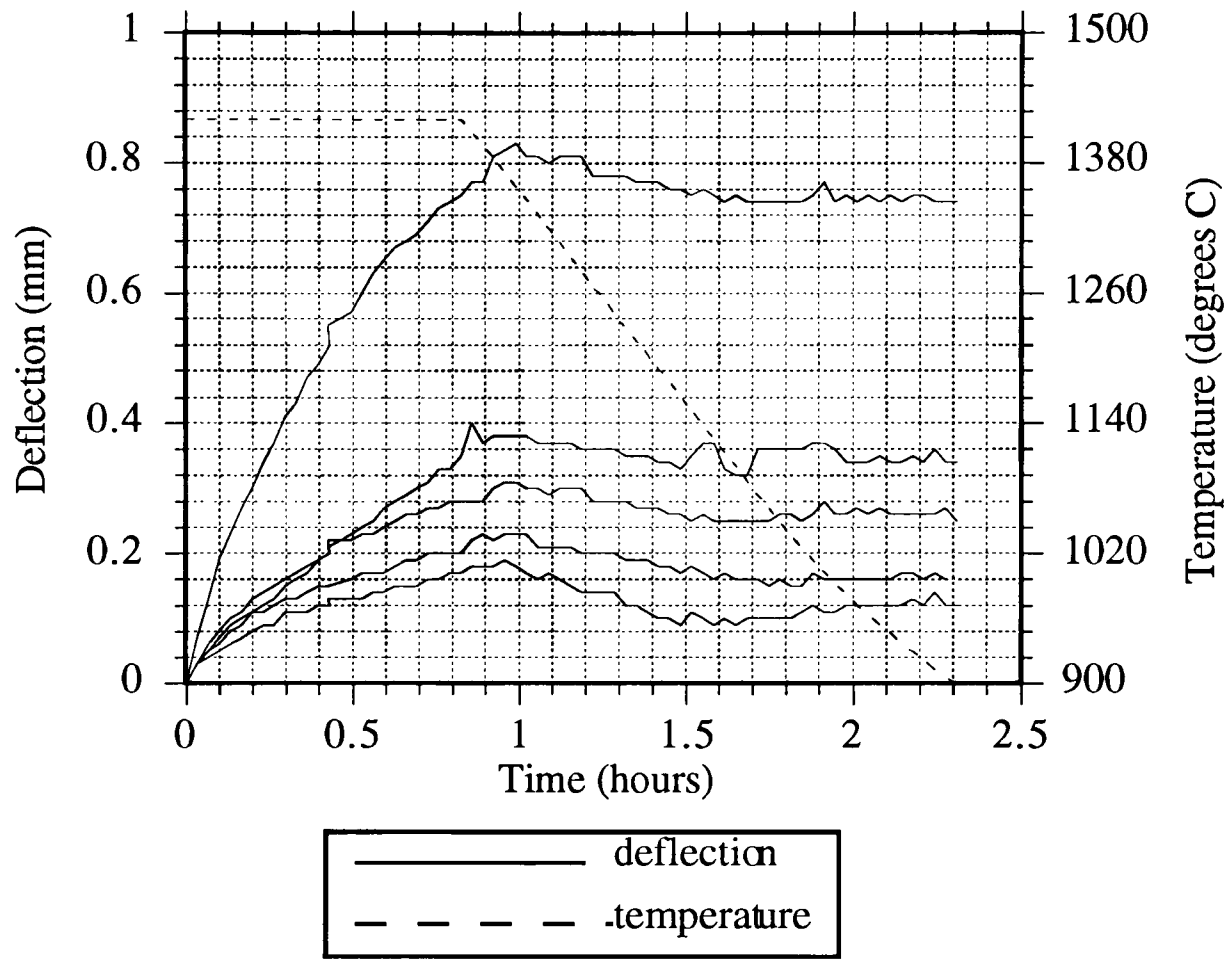


Figure 206: Creep result with a 50 g load for mould sample made using Remal A20 alumina binder

4.8.4: Mould System With Alumino-Silicate Binder

An equivalent mould system was prepared using the same refractories and mould dipping schedule, but with Magnabond B as the binder instead of silica. Low physical strength was encountered at high temperatures and again the 200g load could not be used without sample failure. As a result, the test was repeated at a variety of lower loads until one was found which the sample could accommodate, in this case 50g. All eight samples that were tested survived and the results are shown in Figure 207.

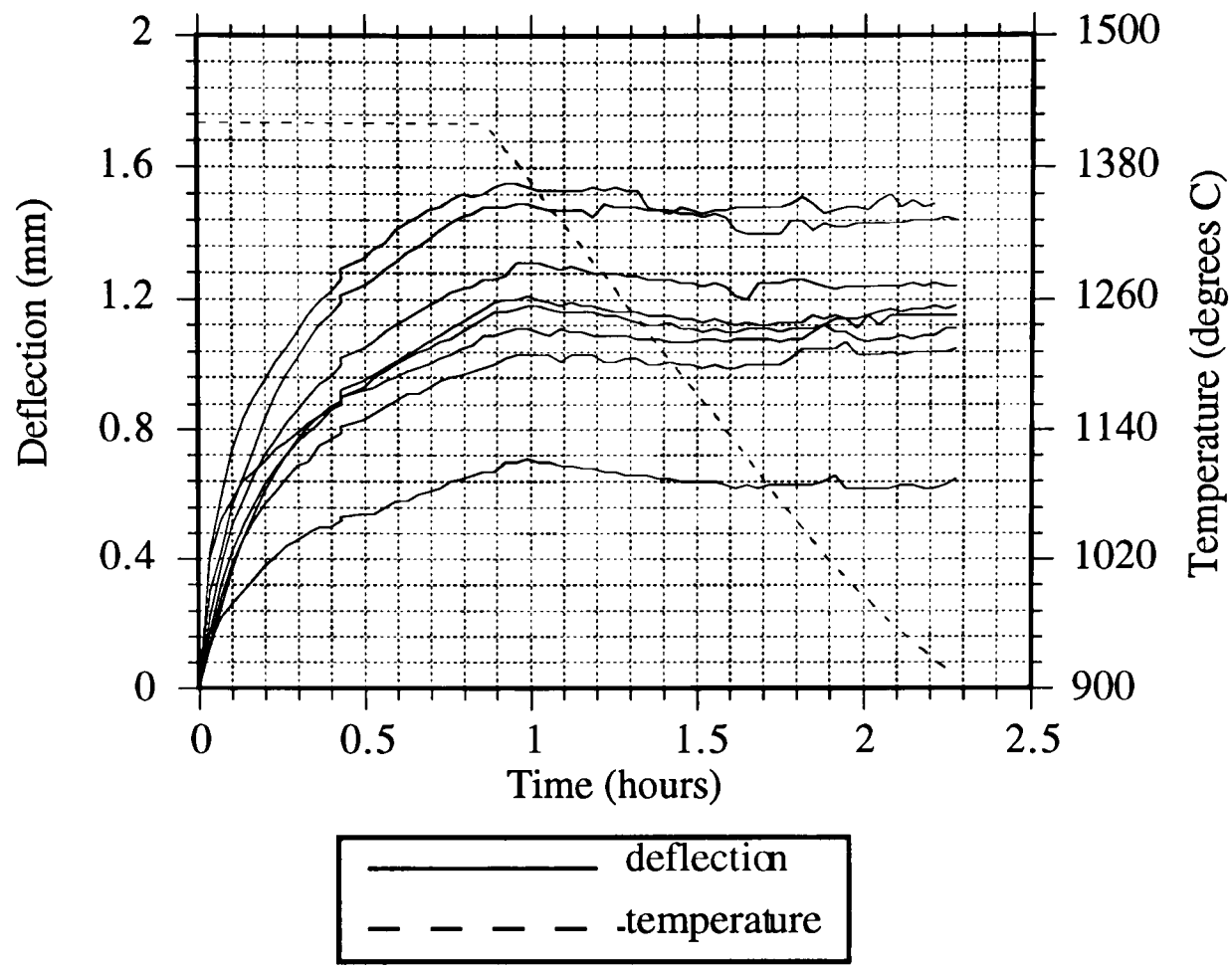


Figure 207: Creep result with a 50 g load for mould sample made using Magnabond B binder

The response is similar to that in the zirconia based system, with curvilinear deflection during the isothermal hold and steady deflection during cooling. This similarity may well be due to reactions between phase constituents which are also taking place within the alumino-silicate system at high temperatures. Since the system consists of a mixture of alumina and silica, it is possible that a glassy phase is being formed at high temperatures which is prone to creep due to the softening temperature being relatively low.

The mean deflection is 1.135 mm ($\sigma_{(n-1)}$ = 0.26 mm) which, when equilibrated to a 200g load, becomes 4.54 mm. This is very similar to the zirconia system, with the deflection being 6 times that of silica and 15 times the tolerance level. However, the variability is better than zirconia since all of the samples survive to complete the test. This suggests that a larger alumino-silicate based mould would be much more prone to creep than a standard silica based system and would not be a viable alternative binder system for large investment moulds.Again, there is the possibility that an increase in strength would reduce the deflection to acceptable levels and the reproducible behaviour under load should be considered an advatage.

4.8.5: Mould System With Mullite Based Binder

An equivalent mould system was prepared using the same refractories and mould dipping schedule, but with Magnabond A as the binder instead of silica. This binder consists of a mixture of alumina and silica sol particles which react together to form mullite at high temperatures. Low physical strength was encountered at high temperatures and again the 200g load could not be used without sample failure. As a result, the test was repeated at a variety of lower loads until one was found which the sample could accommodate, in this case 50g. All eight samples that were tested survived and the results are shown in Figure 208.

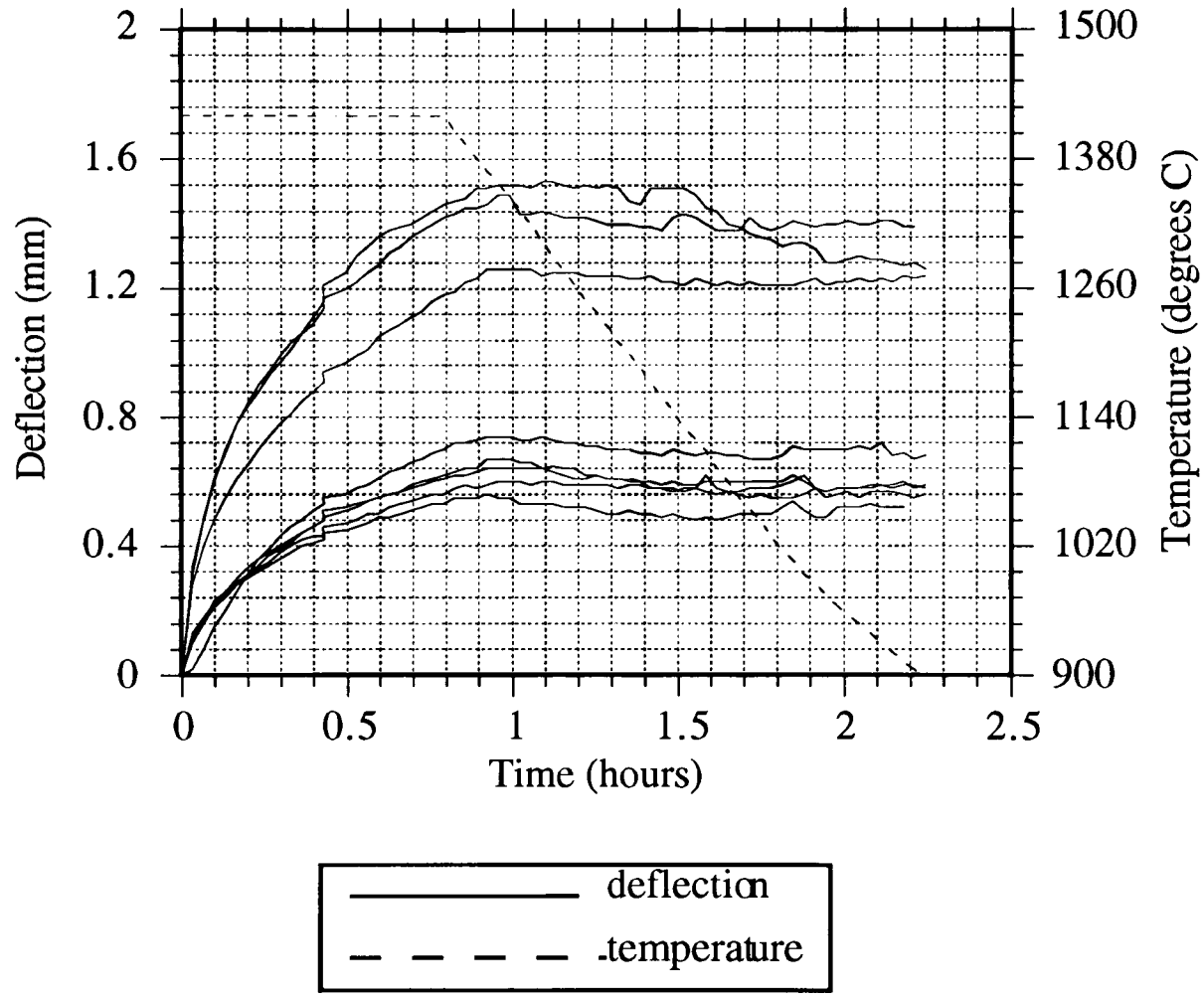


Figure 208: Creep result with a 50 g load for mould sample made using Magnabond A binder

The response is similar to that in the zirconia based system, with curvilinear deflection during the isothermal hold and steady deflection during cooling. Since complete mullitisation takes place at high temperatures it is possible that this reaction is taking place during this prolonged duration at a high temperature. Since the system consists of a mixture of alumina and silica, it is possible that incomplete reaction of all the silica is leading to the presence of free silica within the binder structure. This silica is prone to creep at high temperatures and will promote sample deformation.

The results indicate a variable structure and physical response, with 5 of the samples having deflections less than 0.70 mm and the other three having deflections above 1.20 mm. As such, the mean deflection is 0.87 mm ($\sigma(n-1)$ = 0.40 mm) which equates to 3.48 mm for a 200g load. This deflection is 4.6 times that in a silicate based system and 10 times the quoted tolerance. This is an improvement over the alumino-silicate and zirconia systems but is still higher than that found with the alumina system. This suggests that the presence of free silica is detrimental to the creep properties of the mullite binder and that a larger mullite based mould would be still be prone to mould wall deflection. However, research to promote complete mullitisation and the removal of free silica from the system may decrease this deflection and allow mullite binders to be used as alternative binder systems. Much more research will also be needed to overcome the low green and fired strengths.

4.8.6: Summary

A mould system which is based upon a silica binder is susceptible to deflection when subjected to a thermal profile which is based upon that experienced within the inner coats of a 60 kg investment casting mould. The mean deflection under a load of 200 kg, calculated from a batch of eight test pieces, is 0.75 mm. This value is much higher than the tolerance specification of 0.35 mm for a 100 mm cast metal section. According to this, the average creep within a silica based mould is twice as large as that which is tolerated and the castings would fail. A direct analogy such as this should be treated with caution because the mould wall movement during casting is influenced by many other factors such as the backing refractory and the lower temperatures experienced within the outer coats of the mould. However, these results do provide direct evidence to suggest that the casting bulge experienced with larger castings is a direct result of high temperature creep within the mould wall.

Equivalent mould systems, prepared using a range of non-silica based binders, were tested and compared with the silica based system. A zirconia based binder will produce mould samples which have variable properties and low strength at high temperatures. Comparisons can be made using multiplication factor to reflect the expected deflection at a 200g load. In this case the creep has been shown to be 6 times that of the silica system and 13 times the tolerance level. In its present state, the zirconia binder would not make a good alternative to silica but the properties could be improved by the addition of phase stabilising agents to improve the physical strength.

An alumina based binder produces a mould system with very low green strengths and a capacity to be tested with a maximum load of 50g. The results are less variable than zirconia, but the average deflection recorded is approximately 1.75 times that of the silica system and 3.75 times the tolerance level. This suggests that the alumina bond is more resistant to high temperature creep. However, much more research would be needed to overcome the low green and fired strengths if the binder is to be used as a viable alternative to silica.

An alumino-silicate bound mould system can only be tested with a load of 50 g, but all samples tested at this load survive to complete the test. The mean deflection is 6 times that of the silica system and 15 times the tolerance level. The deflection level is slightly higher than that measured in zirconia but the variability in samples is much lower. This suggests that the unpredictable nature of the reactions which take place between silica and alumina and the presence of free silica within the system produces a binder phase which is more prone to creep.

Using a stoichiometric mixture of alumina and silica to produce mullite when fired reduces the tendency of a mould sample to deflect at high temperatures. The system can still only be tested at 50g, but the average deflection is reduced to 4.6 times that of silica. Research to promote full mullitisation to remove free silica from the system may reduce the deflection even further and allow mullite binders to be used as alternative systems. More research will be necessary to overcome the low green and fired strengths.

In conclusion it can be stated that none of the alternative binders which were evaluated using the creep tests could be used in their present forms as alternatives to silica in the production of an investment casting mould. However, some of the non-silicate based binders such as alumina and mullite do show potential for this application. Further research into the possibility of carrying out minor modifications of the physical properties of non-silicate binders is advocated.

4.9: Physical Properties

Together with high temperature strength and creep resistance, an investment mould must also possess adequate green and fired strengths at room temperature in order to withstand the physical requirements of autoclaving and casting. Maximum strength is not required, since it must also be possible to remove the shell easily after the metal has cooled. Often a strong shell will lead to casting defects if the structure is not weak enough to deflect a little with the cooling mass of metal. The actual strength of a mould is engineered to be somewhere in between maximum and minimum, so that a compromise between several criteria is met. Thus, when evaluating a new mould system, it is necessary to investigate mould strength properties at lower temperatures as well as high. As such, samples of several mould systems, including those that underwent creep evaluation, were tested using standard procedures (see Section 2.6).

4.9.1: Thermal Expansion/Contraction Tests

In its green (unfired) state, an investment casting mould possesses very little mechanical strength. During firing, the fundamental structure of the binder is altered as the constituents sinter and fuse to

one another. A result of this sintering is the development of sufficient strength to withstand the rigours of metal casting. The amount of physical strength developed is dependent upon the firing parameters, which for a silica based system have been fully categorised. However, non-silica based binders may require different parameters and thermal expansion/contraction tests were carried out upon the mould systems that underwent creep evaluation.

The preparation of samples and testing procedures can be found in Section 3.13. Sample behaviour was monitored during both heating and cooling in order to examine the relative amounts of permanent deformation produced by the sintering process. The standard shell produced using an ethyl-silicate binder and zirconium silicate filler (Figure 209) does not appear to undergo significant contraction until 1,200°C. As this system is fired at 1,000°C the result is a little surprising, but may serve to indicate that the sintering and coalescence of silica particles is not accompanied by large material transport and the individual particles appear to remain static. Closer examination of the trace reveals that the line begins to depart from linearity and produce slight contraction at 1,000°C which suggests that the sintering process does take place at 1,000°C but the deformation does not become significant until the sample reaches much higher temperatures. The heating cycle produces a hysteresis effect, with a permanent deformation of 0.25%.

The trace obtained for the Zirconia bound shell sample (Figure 210) begins to deviate from linearity at 550°C but instead of contraction the sample expands by approximately 0.5% up until 1,250°C. After this contraction is fairly rapid and upon cooling the sample exhibits a 0.25% permanent deformation. It is recommended that mould samples are fired at 1,300°C in order to develop sufficient strength.

The shell system produced using Remal A20 alumina sol as the binder (Figure 211) does not deviate from linearity during heating and significant contraction is initiated at 1,150°C. After cooling there is a permanent deformation of 0.3% in the sample. It is recommended that mould sample made with this binder should be fired at 1,150-1,200°C in order to develop sintered bonds and physical strength within the system.

The Magnabond A, which is the mullite producing binder, also remains linear up to 1,250°C and when sintering does occur it produces very little contraction in the sample (Figure 212). As such, the permanent deformation in the system after cooling is limited to 0.1% and therefore the recommended sintering temperature is 1,300°C with firing time increased to develop mould strength. Magnabond B, however, undergoes a small expansion during heating, with contraction being initiated at approximately 1,150°C (Figure 213). The contraction at these temperatures is large and leads to a permanent deformation of 0.32% after cooling. It is recommended that a mould sample produced with this binder is fired at 1,150°C to develop the mould strength.

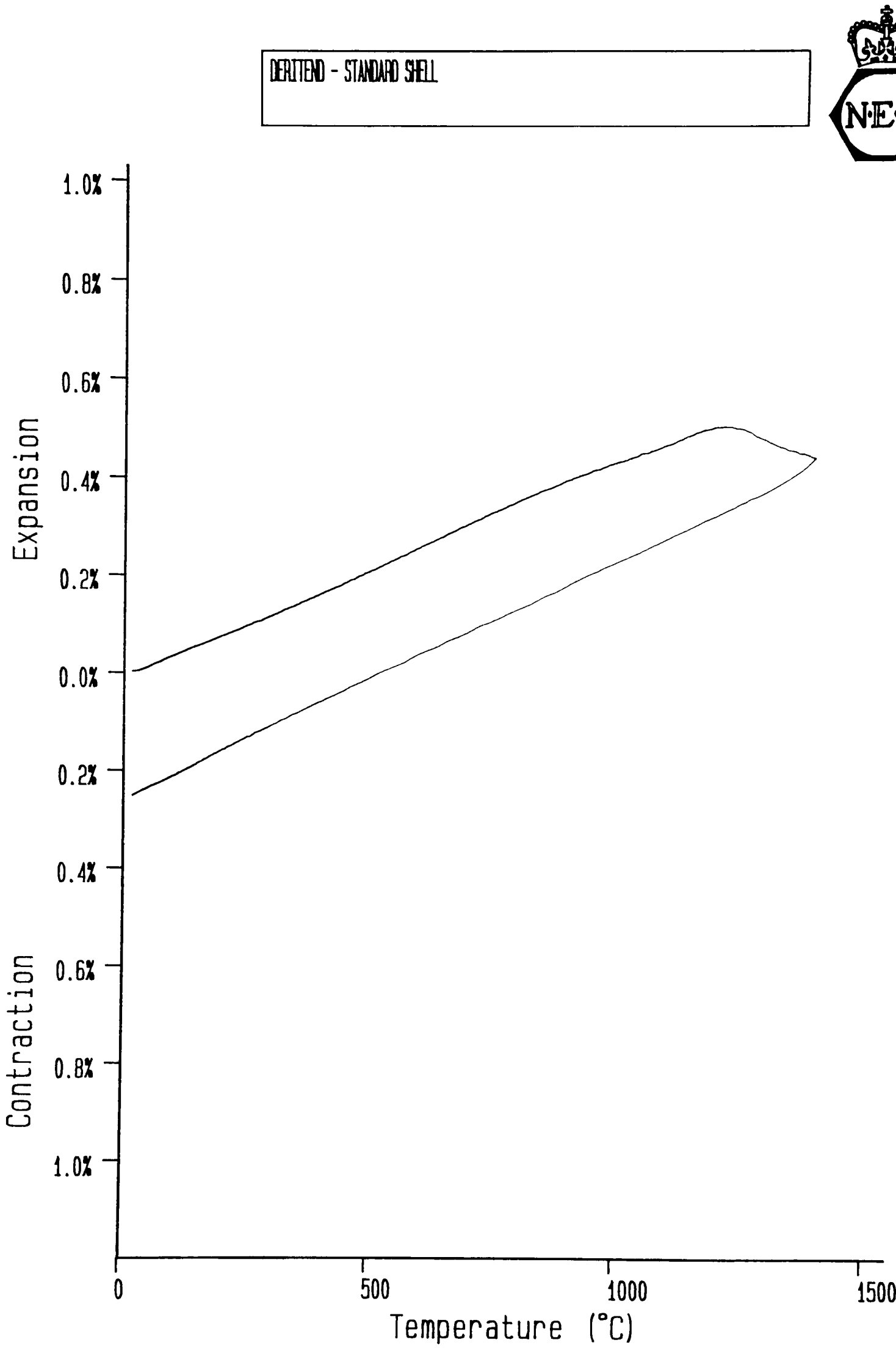


Figure 209: Expansion/contraction trace for standard ethyl-silicate shell produced at Deritend Precision Castings

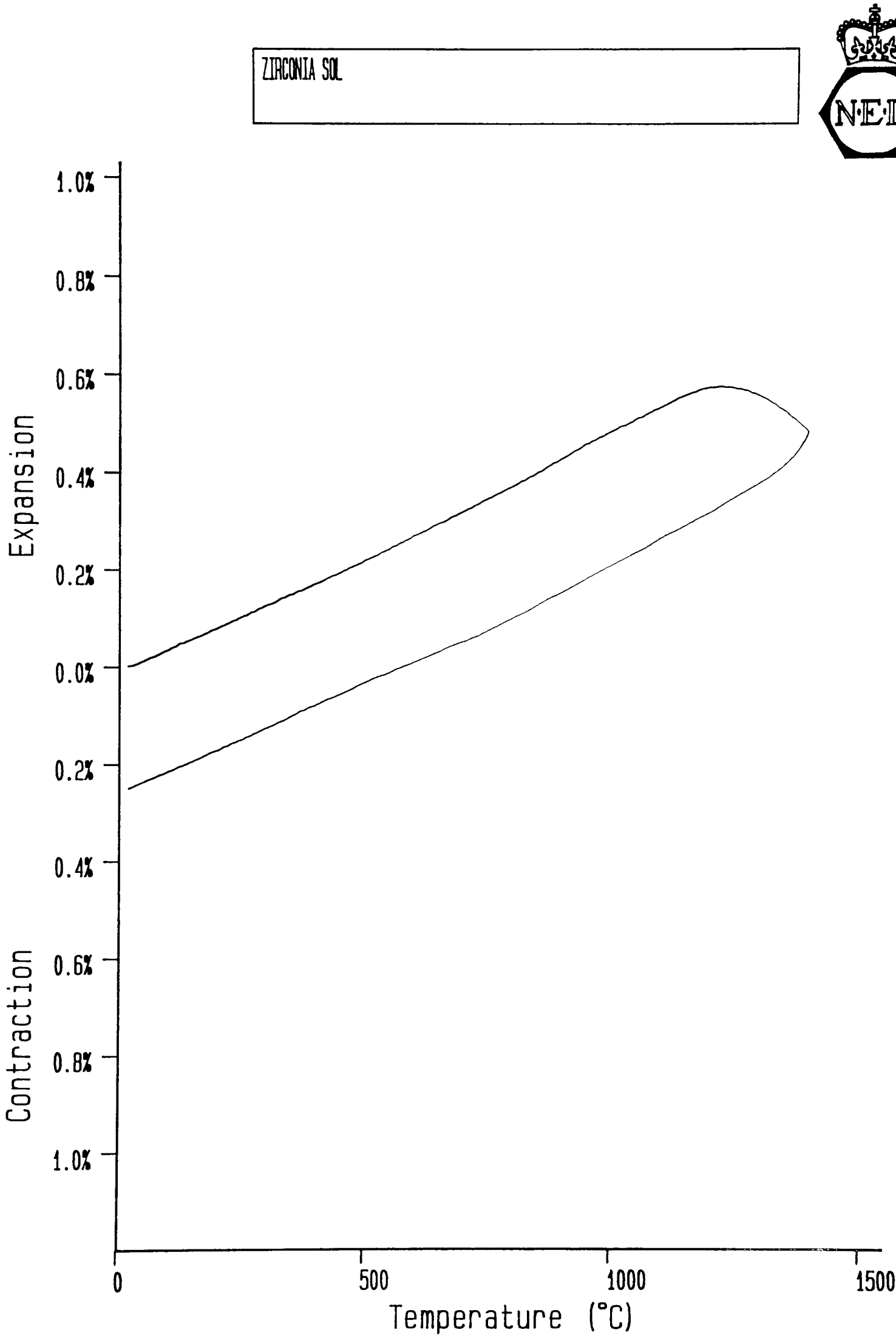


Figure 210: Expansion/contraction trace for shell sample produced with Remet zirconia sol binder system

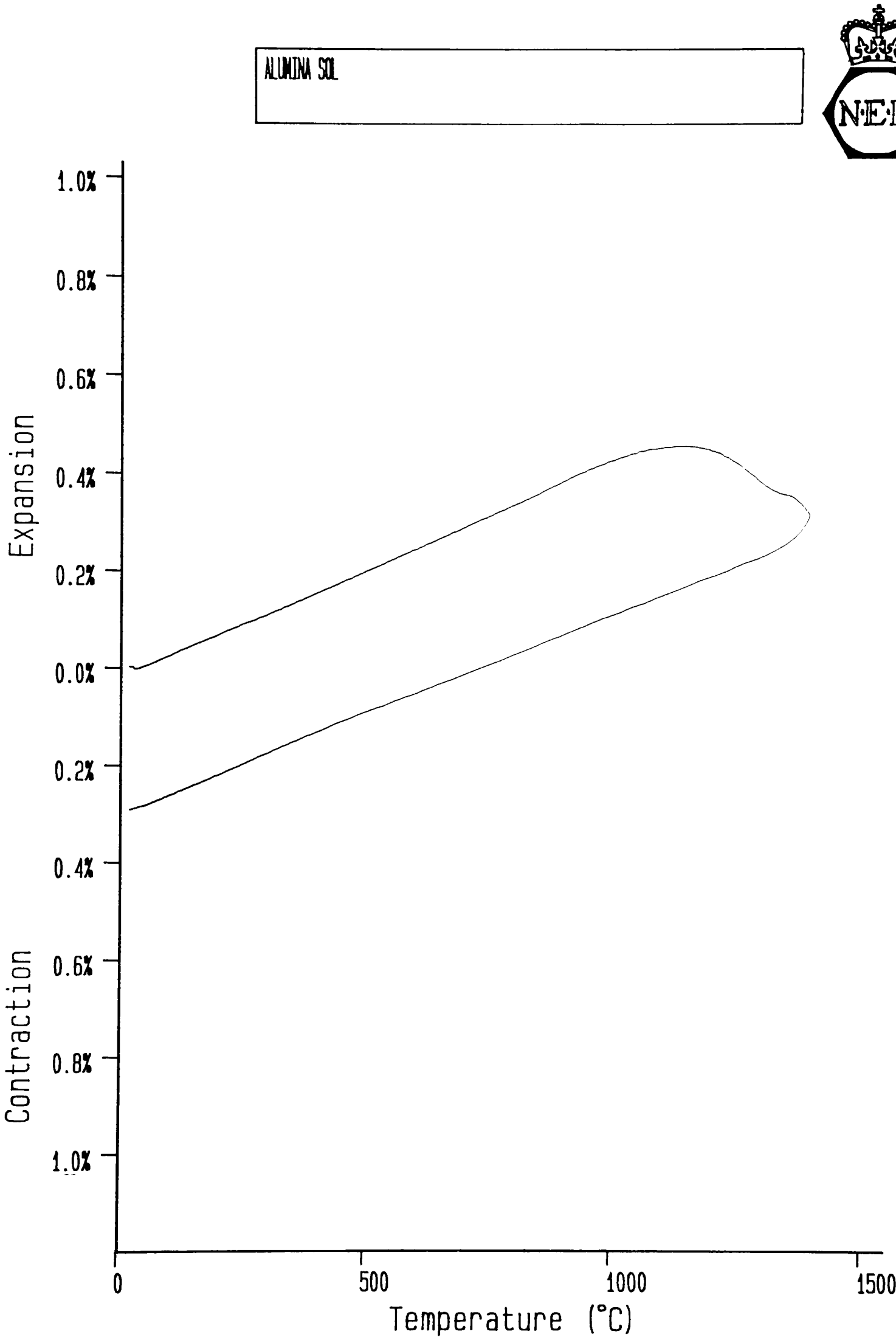


Figure 211: Expansion/contraction trace for shell sample produced with Remal A20 binder system

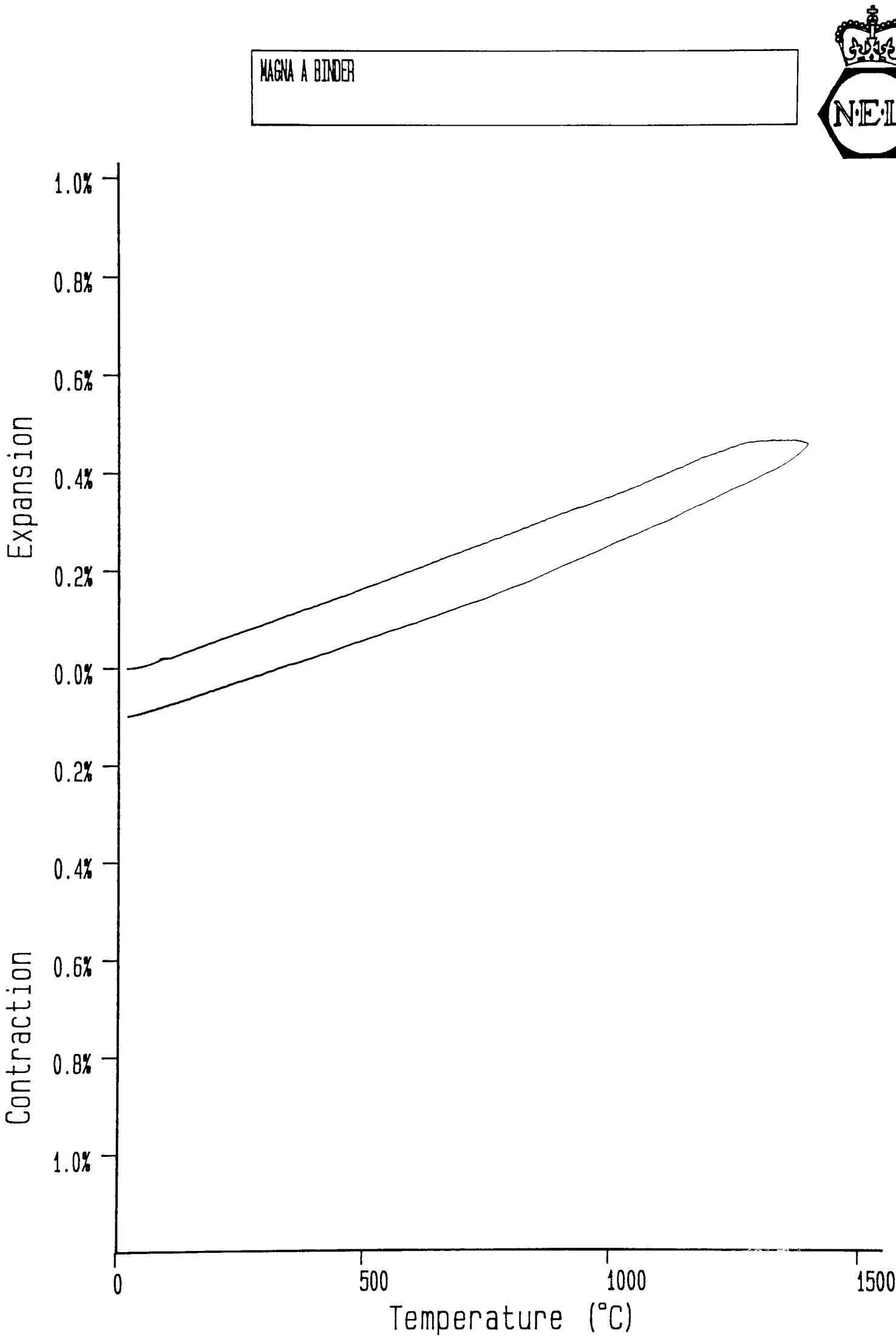


Figure 212: Expansion/contraction trace for shell sample produced with Magnabond A binder system

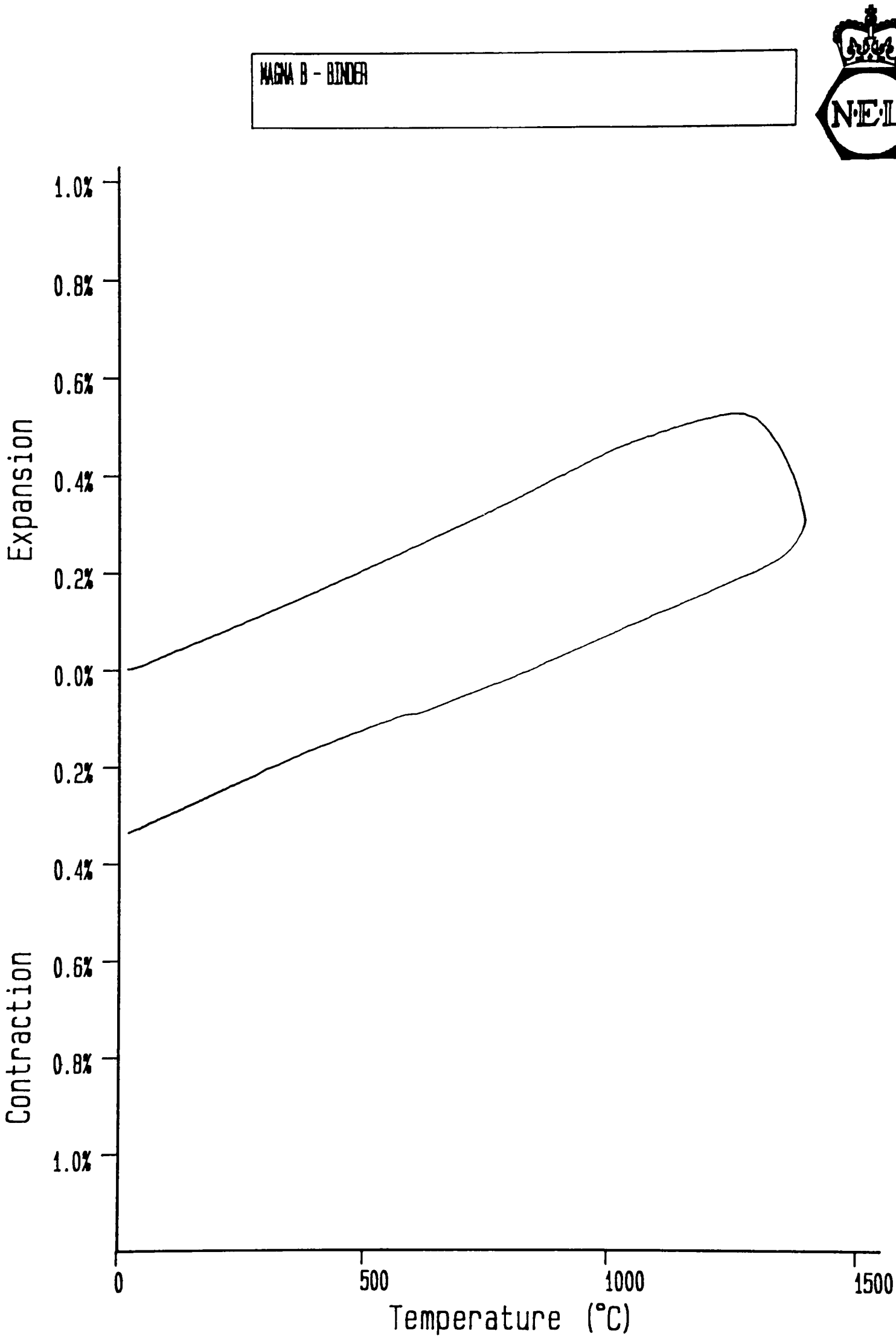


Figure 213: Expansion/contraction trace for shell sample produced with Magnabond B binder system

4.9.2: Bursting Disc Test

Samples were prepared and tested according to the schedule laid out in Section 3.11.1. Care was taken that the point at which failure was deemed to occur was consistent and this was chosen to be the moment that a crack began to appear in the surface of the sample. This was important as several samples failed instantly, but others would continue to withstand an applied load even with cracks running the entire diameter of the specimen. The results are shown in Table 26.

The results obtained for the standard slurries used at Deritend Precision Castings (S_2 and S_3) can be used as an indication of the green and fired strength required by mould system in order to produce successfully an investment cast component. A mould produced using Syton X30 with a silica content of 30 weight % has an adequate green strength, but the fired strength is very high and the shell may prove difficult to remove. This strength is due to the fact that the sol based binder will crystallise to form a rigid structure which may be prone to microcracking and thermal shock because of phase changes within the material. In the past, investment foundries have diluted the sol to around 20 weight % silica and this has reduced the fired strength to a level which is more suitable.

The results for the zirconia sol based system are useful because of the indication that firing temperatures and durations will have to be reassessed and altered for the non-silica based moulds. The green strength of the system is comparable with standard shells but when fired at 1,000°C the mould samples are very weak. Increasing the firing temperature to 1,300°C produces a much stronger shell system probably due to the completion of sintering and phase transformations within the binder. The economics of the 300°C temperature rise will have to be considered before recommending the use of zirconia binders in the investment industry.

The shell system produced using Remal A20 alumina sol binder was fired at 1,150°C for 60 minutes. As with other alumina based systems the green strength is very low and the mould would be too weak to withstand manual handling during removal of wax. It should be noted that alumina systems are susceptible to the presence of water vapour and cannot be autoclaved in the traditional manner. The fired strength is comparable with silica based systems and would be sufficient to produce a cast component.

The shell systems produced using Magnabond alumino-silicate binders were fired at 1,150°C because of evidence gathered during thermal expansion testing. The green strengths are slightly lower than those obtained with a standard silica binder but should be adequate for mould production. The fired strength of Magnabond A samples is very high and comparable silica bound moulds. The green strength would not be fully developed because the firing temperature used is lower than that indicated by thermal expansion tests. As such, Magnabond B has a much higher fired strength and both binders would undoubtably produce moulds that possess far too much physical strength to produce a

sound investment casting. If these systems are to be used then modifications will have to be made to reduce the solids content of the binder which will in turn reduce the fired strength.

Table 26: Bursting disc test results for shell samples
(for mould regimes see Appendix 9)

Shell System	Firing conditions	Green Strength (kPa)	Fired Strength (kPa)
Syton X30	1,000°C for 60 minutes	68.9, 75.8	127.5, unbroken
DPC Slurry S_2*	1,000°C for 60 minutes	55.2, 62.1	68.9
DPC Slurry S_3*	1,000°C for 60 minutes	68.9, 75.8	75.8, 96.5
Remet Zirconia Sol	1,150°C for 120 minutes	68.9, 68.9	20.68, 27.5
	1,300°C for 120 minutes	68.9, 68.9	82.7, 68.9
RemalA20	1,150°C for 60 minutes	13.79, 20.68	89.63, 82.73
Magnabond A	1,150°C for 60 minutes	62.05, 41.36	151.7, 172.4
Magnabond B	1,150°C for 60 minutes	62.05	241.3, unbroken

* S_2: alumino-silicate filler and Silester XAR binder
S_3: zirconium silicate filler and Silester XAR binder

4.9.3: Modulus of Rupture (Transverse) Tests

Samples were prepared and tested according to the schedule laid out in Section 3.11.2. Trends in behaviour are slightly different to those reported with the bursting disc test with measured strengths at least two orders of magnitude higher. This highlights the problems associated with using only one test method as a basis for assessing the strength of a shell sample. The results are tabulated in Table 27.

Table 27: Transverse Test (3 point bend mode) results for shell samples (for mould regimes see Appendix 9)

Shell System	Firing conditions	Green Strength (MPa)	Fired Strength (MPa)
Syton X30	1,000°C for 60 minutes	1.20	6.16, 5.94
DPC Slurry S_2*	1,000°C for 60 minutes	0.49, 0.55	0.66, 0.74
DPC Slurry S_3*	1,000°C for 60 minutes	0.67, 0.57	0.73, 0.69
Remet Zirconia Sol	1,150°C for 120 minutes	0.50	0.55
	1,300°C for 120 minutes	0.50	5.6
RemalA20	1,150°C for 60 minutes	1.39	1.72
Magnabond A	1,150°C for 60 minutes	3.56, 4.08	6.16, 6.21
Magnabond B	1,150°C for 60 minutes	1.21	5.47+ (unbroken)

* S_2: alumino-silicate filler and Silester XAR binder

S_3: zirconium silicate filler and Silester XAR binder

Again the results obtained for the standard slurries used at DPC were used as an example of the required strength. By comparison it can be seen that all of the alternative systems tested had green strengths greater than the required level. This is in direct contrast with the bursting disc results, which indicated that the mould sample based upon Remal A20 binder was much weaker than all the other systems. Experimental errors must be responsible for this anomaly since alumina based systems are well known to have very low green strengths and physical examination of the samples suggests that the green strengths were lower than the other systems.

An increase in firing temperature for the zirconia based samples produces a factor of 10 increase in the fired strength. The strength obtained at this temperature is much higher than that found in a silica based system and is comparable with undiluted Syton X30 samples which are usually unsuccessful as mould materials in this form. The same observation also applies to the alumino-silicate systems such as Magnabond A and Magnabond B which also display very high strengths when fired. Often a high strength material is less tolerant of thermal gradients and 'shock-loading' which is unavoidable when pouring a high metal weight into an investment mould.

Though systems S_2 and S_3 appear to have low strengths when compared to the other systems, these are the moulds that are currently successful in casting production. Obviously high strength is not the ultimate requirement in a mould material: other factors such as tolerance to loading parameters and thermal shock resistance must be important. Care must also be taken when using these results to determine a suitable system to be used as a mould material since the strength of a sample at room temperature may bear no resemblance to that at high temperatures. Earlier characterisation of the binders (Section 4.5) has shown that some of the non-silica based materials are prone to phase changes and reactions at high temperatures which will reduce the strength and also reduce the loading capacity of the systems (see Section 4.8).

4.9.4: Summary

Thermal expansion/contraction testing is useful when wishing to determine the best temperature at which a mould system should be fired in order that sintering should take place and adequate fired strength should be attained. Mould systems produced using a zirconia based binder appear to require firing temperatures of around 1,300°C for approximately 120 minutes. Alumina based moulds require a firing temperature of at least 1,150°C and the same applies for alumino-silicate binders. It is recommended that mullite forming binders should be fired at temperatures as high as 1,300°C in order that the mullitisation reaction can take place and be completed.

Bursting disc and modulus of rupture are strength tests that are carried out at room temperature on both fired and unfired mould samples. The results gained from these tests are a useful means of determining the green strength of a mould system, since if a mould is too weak it will not withstand the wax removal stage without failure. The results seem to indicate that, apart from the alumina sol based system, all the alternative binder systems will possess adequate green strength for use in an investment mould. However the tests carried out upon the fired samples indicate that all of the alternative mould systems may be difficult to remove from the casting once the material has returned to room temperature since the measured strengths are very high. Alterations to the binders, such as dilution, may be necessary in order to produce a mould system that can be used as an investment casting mould.

The physical property tests also serve to indicate that the strength of a mould sample, measured at room temperature, gives little insight into the strength of the same system when heated to high temperatures. Room temperature test results suggest that all of the alternative non-silica based systems should possess higher strengths than silica based systems and as such should be able to withstand greater loads. However, when tested at high temperatures during the creep investigations (Section 4.8), the only system which could accommodate a load of 200g was silica based. All the alternative systems were weak at high temperatures and could only be tested at loads of up to 50g. This is probably due to the presence of phase changes and incomplete reaction within the binder phases which have been highlighted earlier using other analysis techniques.

As such, when evaluating the properties of a mould system it is necessary to combine all information received from both high and low temperature testing before reaching a decision as regards suitability for use in an investment mould. All of the alternative binder systems tested will require further modifications to the basic structure and properties before they are suitable for use.

CHAPTER FIVE

5.1: Conclusions

The following conclusions can be drawn when reviewing the programme of research as a whole:

1. An investment casting mould consists of a series of refractory filler particles bound together by a binder phase. The structure contains a non-uniform filler and porosity distribution which may be responsible for uneven heat dissipation from the metal.

2. Moulds contain a large amount of open porosity within the primary coat which will provide a direct pathway for metal infiltration.

3. The main network contact between the refractory particles consists of very thin regions of binder. As such, the overall structural response of the mould will be governed by the response of the binder.

4. The phase structure of the silica binder is determined by silicate type, amount of stabilising agent and by the presence of impurity elements leached from the filler particles during slurry production and firing of the mould. These elements alter the thermal response of the silica during casting of the mould.

5. The primary coats of a mould are bound by a crystalline silica network and the secondary coats by a mainly amorphous silica network with small regions of crystallinity due to the effect of the impurity elements. This will lead to variable and unpredictable binder responses during reheating and casting of the metal.

6. The thermal responses of a silica sol binder can be modified by incorporation of alumina sol particle into the structure. The aluminium ions reduce the effect of the sodium stabiliser and increase the crystallisation temperature to above 1,200°C. This phenomena may have several potential applications, but as an investment casting binder the system would be more likely to produce mould wall movement and creep.

7. Zirconia binders have been found to be prone to extensive contraction during firing and several phase changes which are accompanied by large volume contractions/expansions. These uncontrolled phase changes will be detrimental to the stability of an investment casting mould made with a zirconia binder. The samples are susceptible to creep at high temperatures and have very low physical strength. In their present form, the binders would not make good alternatives to silica. However, the use of a stabilising agent may reduce the effect of the transformations and increase the physical strength to acceptable levels.

8. Alumina based binders have a complex series of reactions up to 1,150°C, ending with a phase transformation to form α alumina. This phase is fairly dense in structure, and the binder undergoes extensive contraction when approaching the transformation temperature. When incorporated as a binder system in a mould, the sample displays a slightly better creep response than silica but is considerably weaker. As such, an alumina based mould may be less prone to creep but much more research will be needed to increase the very low green and fired strengths achieved with the system.

9. Alumino-silicate binders undergo a series of reactions between the constituents which make mould samples very prone to creep at high temperatures. However, a binder which contains the correct proportions of silica and alumina to form mullite when fired is much more stable and has an encouraging creep response. Much more research will be required to produce a system in which complete mullitisation has occurred since the presence of free silica is very detrimental to mould properties.

10. The maximum temperature generated in the mould section during metal casting is directly related to the size of the component, such that a 5 kg mould reaches 980°C and a 60 kg mould reaches 1,420°C. The higher temperatures are responsible for the initiation of creep within silicate based binders, which begin to soften at 1,200°C. As such, high temperature creep of the silica binders has been identified as the main cause of casting bulge in larger cast components.

11. The extent of metal mould interaction is influenced by both the type of metal being cast and the size of the component since higher mould temperatures encourage softening of the silica binder which in turn encourages the influx of metal and deoxidant into the mould structure.

12. As a final conclusion, it can be stated, that research appears to have highlighted several performance weaknesses that are inherent when using a silicate based binder system for the production of larger cast components. As such it seems clear that extensive modifications or even complete replacement of silica within the system will be needed if the failure rates are to be reduced to levels that are acceptable within the casting industry.

5.2: Future Work

1. Modification of existing silica based binder systems to produce one which has greater dimensional stability at higher temperatures.This will allow the industry to alter the present system without undue difficulties or expense.

2. To continue evaluating the performance of non-silica based binders as viable alternatives to silica. The physical strengths and phase transformations within many of the systems will have to be monitored as none of the binders can be used as direct replacements in their present forms.

3. Further investigation into the interactions which take place between refractories and metals to suggest an alternative refractory which can be used within the inner coats of a mould to reduce the incidence of casting failure due to reaction defects.

4. Research should be carried out to further characterise the impurities found within the filler materials with a view to reducing the inconsistent and variable occurrence of the phase separation. Once the system has been standardised this should increase the reproducibility of the moulds themselves to prevent inconsistencies in mould performance.

APPENDIX 1 : Statistical Procedures

Statistics can be defined[141] as, a science concerned with the collection, classification and interpretation of quantitative data and with the application of probability theory to the analysis and estimation of population parameters. Definitions and descriptions[142] of all statistical parameters calculated and used to manipulate sample data within this thesis are contained in this appendix.

1. Arithmetic Mean

Definition

The arithmetic mean is an figure used as a *measure of central tendency* for a group of data. Most of the time when we refer to the 'average' of something we are talking about the arithmetic mean. This is true in such cases as the average winter temperature, average lifetime of a battery or the average yield of corn from an acre of land[142]. Two types of arithmetic mean are quoted depending upon the origins of the data:

Population mean: $\mu = \frac{\Sigma x}{N}$ **Equation 21**

x = individual observation
Σx = sum of values of all observations
N = number of elements in the population

Sample mean: $x = \frac{\Sigma x}{n}$ **Equation 22**

x = sample mean
n = number of elements in the sample

2: The Mode

Definition

The mode is the value that is repeated *most often* in the data set and as such is also a measure of central tendency. It is a value greatly affected by chance and is rarely used for ungrouped data in which unrepresentative values can easily be the most frequent.

3: The Median

Definition

The median is a single value from a data set that measures the central item in the data. This single item is the *middlemost* or *most central* item in the set of numbers. Half of the items lie above this point and the other half lie below it.

$$\text{Median} = \text{the } \frac{(n+1)}{2} \text{ th item in a data array} \qquad \textbf{Equation 23}$$

n = no. of items in the array

4: Average Deviation Measures

The most comprehensive descriptions of dispersions are those that deal with the average deviation from some measure of central tendency. Two of these measures are important tools in statistical analysis: the variance and the standard deviation. Both of these give an indication of the average distance of any observation in the data set from the mean of the distribution.

4:1: Variance

Definition

The variance is a measure of dispersion and is highly representative because it takes every individual value into account. Each population and sample has a variance and the formulas for calculation are shown below in Equations 24 and 25. Using the sum of the squared distances between the mean and each item automatically makes every number positive, eliminating the need for absolute values.

Population: $$\sigma^2 = \frac{\Sigma (x - \mu)^2}{N} \qquad \textbf{Equation 24}$$

Sample: $$s^2 = \frac{\Sigma (x - \bar{x})^2}{n - 1} \qquad \textbf{Equation 25}$$

σ^2 = the population variance
s^2 = the sample variance
x = the item or observation
n = no. of items in the sample
μ = population mean
$\bar{x}$ = sample mean
N = no. of items in the population
Σ = sum of all the values

4.2: Standard Deviation

Definition

The standard deviation is a value which represents the average deviation from some measure of central tendency. It represents the average distance of any observation in the data set from the mean of the distribution. The standard deviation is the square root of the variance (Equations 26 and 27). Since the variance is the average of the squared distances of the observations from the mean, the standard deviation is the square root of the average of the squared distances of the observations from the mean. It is expressed in the same units as the data.

Population: $$\sigma = \sqrt{\sigma^2} = \sqrt{\frac{\Sigma (x - \mu)^2}{N}}$$ **Equation 26**

Sample: $$s = \sqrt{s^2} = \sqrt{\frac{\Sigma (x - x)^2}{n - 1}}$$ **Equation 27**

5: Coefficient of Variation

Definition

The coefficient of variation (Equations 28 and 29) is a measure of the magnitude of deviation relative to the magnitude of the mean. It relates the standard deviation deviation and the mean by expressing the standard deviation as a percentage of the mean. The unit of measure is percent rather than the same units as the original data. This parameter is used as the basis for a comparison between two sets of data.

Population coefficient of variation = $$\frac{\sigma}{\mu} . (100)$$ **Equation 28**

Sample coefficient of variation = $$\frac{s}{x} . (100)$$ **Equation 29**

6: The F-Hypothesis Test

Definition

The F Hypothesis test is a statistical technique known as *analysis of variance*, which allows several samples to be compared together to test for the significance of the difference between the sample means. From this inferences can be made about whether the samples are drawn from populations which have the same mean i.e. 'is there any significant statistical difference between the populations from which the samples have been drawn'. The basic equation to represent this hypothesis is shown below:

$$F = \frac{\text{First estimate of the population variance based on the variance among the sample means}}{\text{Second estimate of the population variance based on the variances within the samples}} \qquad \textbf{Equation 30}$$

This can be rewritten as;

$$F = \frac{\text{Between column variance (a)}}{\text{Within column variance (b)}} \qquad \textbf{Equation 31}$$

To carry out a F hypothesis test, standard tables representing degrees of freedom in both numerator and denominator are used. Separate tables exist for the chosen level of significance.

Procedure

1. Calculate the between column variance for the samples.

Between column variance = $s^2 \times n$ **Equation 32**

= variance among the sample means x no. of items in each sample

Calculate s^2 using the standard formula applied to the sample means.

2. Calculate the within column variance for the samples.

Within column variance = the mean of the sample variances **Equation 33**

$$= \frac{s_1^2 + s_2^2 + s_3^2}{n}$$

Remember that the value used for n in this case is the number samples being compared.

3. Calculate the F statistic.

4. Calculate the degrees of freedom in the numerator of the F equation

No. of degrees of freedom in the numerator = (Number of samples - 1) **Equation 34**

Again number of samples refers to the number of results being compared together.

5. Calculate the degrees of freedom in the denominator of the F equation.

No. of degrees of freedom in the denominator = Number of items in a sample - 1 x Number of samples **Equation 35**

6. Refer to the appropriate F distribution table. Using the separate degrees of freedom calculated previously, read the value from the table. Compare this value with the value of F calculated earlier. If the calculated value is higher than the tabulated value then it can be assumed that the samples tested came from significantly different populations. If the calculated value is lower than the tabulated value then the samples can be assumed to have been taken from similar populations.

APPENDIX 2 : Image Analysis Results

Table 28: Zircon Sand A

Image analysis results for photographs 1 - 10

		$ZrSiO_4$ (cm^2)	Separation (cm^2)	Total $ZrSiO_4$ (cm^2)	Total Separation (cm^2)	Phase Separation (by area)
Photo 1	Area 1	18.89	0.09	49.96	0.14	0.28%
	Area 2	9.49	0			
	Area 3	10.65	0.03			
	Area 4	10.93	0.02			
Photo 2	Area 1	13.65	0	59.27	0.09	0.15%
	Area 2	15.29	0.04			
	Area 3	13.64	0			
	Area 4	16.69	0.05			
Photo 3	Area 1	18.36	0.09	64.77	0.15	0.23%
	Area 2	13.53	0			
	Area 3	17.66	0.06			
	Area 4	15.22	0			
Photo 4	Area 1	13.21	0.07	59.20	0.17	0.287%
	Area 2	15.33	0			
	Area 3	17.16	0			
	Area 4	13.50	0.10			
Photo 5	Area 1	16.06	0.31	58.23	0.76	1.305%
	Area 2	16.13	0			
	Area 3	17.41	0.15			
	Area 4	8.63	0.30			
Photo 6	Area 1	15.05	0	57.36	6.68	11.65%
	Area 2	19.93	0.05			
	Area 3	12.85	0.50			
	Area 4	9.53	6.13			
Photo 7	Area 1	11.64	2.59	57.38	2.93	5.11%
	Area 2	15.51	0.14			
	Area 3	19.18	0.14			
	Area 4	11.05	0.06			
Photo 8	Area 1	20.93	0.10	68.30	0.19	0.278%
	Area 2	13.97	0			
	Area 3	21.79	0.09			
	Area 4	11.61	0			
Photo 9	Area 1	14.55	0	55.67	0.46	0.826%
	Area 2	14.12	0.08			
	Area 3	13.09	0.29			
	Area 4	13.91	0.09			
Photo 10	Area 1	20.42	0	61.4	0.16	0.26%
	Area 2	14.01	0			
	Area 3	11.23	0			
	Area 4	15.74	0.16			

Table 29: Zircon Sand A

Image analysis results for photographs 11 - 20

		$ZrSiO_4$ (cm^2)	Separation (cm^2)	Total $ZrSiO_4$ (cm^2)	Total Separation (cm^2)	Phase Separation (by area)
Photo 11	Area 1	22.21	0.09	63.03	0.11	0.17%
	Area 2	8.45	0			
	Area 3	18.61	0			
	Area 4	13.76	0.02			
Photo 12	Area 1	13.36	4.85	39.31	8.68	22.08%
	Area 2	6.34	3.75			
	Area 3	13.02	0			
	Area 4	6.59	0.08			
Photo 13	Area 1	20.27	1.21	44.56	23.59	52.94%
	Area 2	7.01	4.81			
	Area 3	1.74	17.57			
	Area 4	15.54	0			
Photo 14	Area 1	11.81	0	56.09	0.03	0.05%
	Area 2	19.18	0.03			
	Area 3	14.42	0			
	Area 4	10.68	0			
Photo 15	Area 1	11.99	0.52	36.46	10.72	29.40%
	Area 2	7.59	0			
	Area 3	5.04	10.20			
	Area 4	11.84	0			
Photo 16	Area 1	13.92	0.08	53.55	0.17	0.317%
	Area 2	8.94	0			
	Area 3	19.78	0.03			
	Area 4	10.91	0.06			
Photo 17	Area 1	15.03	0.36	52.57	0.36	0.68%
	Area 2	9.54	0			
	Area 3	10.57	0			
	Area 4	17.16	0			
Photo 18	Area 1	25.54	0	66.35	0	0
	Area 2	17.32	0			
	Area 3	9.12	0			
	Area 4	14.37	0			
Photo 19	Area 1	17.07	0	60.30	0	0
	Area 2	14.32	0			
	Area 3	16.10	0			
	Area 4	12.81	0			
Photo 20	Area 1	18.72	0.07	59.86	0.19	0.317%
	Area 2	17.29	0.03			
	Area 3	12.42	0			
	Area 4	11.43	0.09			

Table 30: Zircon Sand B

Image analysis results for photographs 1 - 10

		$ZrSiO_4$ (cm^2)	Separation (cm^2)	Total $ZrSiO_4$ (cm^2)	Total Separation (cm^2)	% Phase Separation (by area)
Photo 1	Area 1	17.12	0.22	56.71	0.51	0.9%
	Area 2	13.08	0.05			
	Area 3	13.91	0.04			
	Area 4	12.6	0.2			
Photo 2	Area 1	19.61	0.78	53.52	1.03	1.925%
	Area 2	11.72	0.25			
	Area 3	13.57	0			
	Area 4	8.62	0			
Photo 3	Area 1	17.22	0.32	55.25	0.62	1.122%
	Area 2	10.10	0.23			
	Area 3	19.28	0			
	Area 4	8.65	0.07			
Photo 4	Area 1	17.14	0.44	54.97	0.91	1.655%
	Area 2	12.12	0.15			
	Area 3	9.46	0.14			
	Area 4	16.25	0.18			
Photo 5	Area 1	15.73	1.06	69.27	2.43	3.508%
	Area 2	13.85	0.25			
	Area 3	21.71	0.48			
	Area 4	17.98	0.64			
Photo 6	Area 1	18.2	0.55	53.71	1.15	2.141%
	Area 2	13.65	0.05			
	Area 3	18.45	0.43			
	Area 4	3.4	0.12			
Photo 7	Area 1	15.23	0	42.76	0.62	1.45%
	Area 2	6.72	0			
	Area 3	11.46	0			
	Area 4	9.35	0.62			
Photo 8	Area 1	15.3	0.93	55.81	2.23	3.995%
	Area 2	15.43	0.89			
	Area 3	14.1	0.15			
	Area 4	10.98	0.26			
Photo 9	Area 1	21.1	0.1	59.1	0.14	0.237%
	Area 2	10.69	0.04			
	Area 3	18.4	0			
	Area 4	8.91	0			
Photo 10	Area 1	22.18	0.45	61.75	0.77	1.247%
	Area 2	10.91	0			
	Area 3	15.3	0.26			
	Area 4	13.36	0.06			

Table 31: Zircon Sand B

Image analysis results for photographs 11 - 20

		$ZrSiO_4$ (cm^2)	Separation (cm^2)	Total $ZrSiO_4$ (cm^2)	Total Separation (cm^2)	% Phase Separation (by area)
Photo 11	Area 1	14.99	0.77	51.71	1.22	2.36%
	Area 2	14.82	0.09			
	Area 3	14.75	0.36			
	Area 4	7.15	0			
Photo 12	Area 1	24.77	0.34	73.89	0.87	1.177%
	Area 2	19.59	0.39			
	Area 3	19.03	0.11			
	Area 4	10.50	0.03			
Photo 13	Area 1	22.	0	62.94	0.24	0.381%
	Area 2	14.02	0			
	Area 3	14.84	0.24			
	Area 4	11.88	0			
Photo 14	Area 1	19.15	0.23	59.95	1.11	1.85%
	Area 2	11.61	0.27			
	Area 3	15.71	0.61			
	Area 4	13.48	0			
Photo 15	Area 1	13.25	3.17	42.78	18.39	42.99%
	Area 2	7.13	3.43			
	Area 3	10.15	9.78			
	Area 4	12.25	2.01			
Photo 16	Area 1	12.1	0	59.62	0.23	0.386%
	Area 2	18.31	0.09			
	Area 3	20.29	0.06			
	Area 4	8.92	0.08			
Photo 17	Area 1	4.2	10.69	32.9	22.11	67.20%
	Area 2	14.66	0			
	Area 3	5.48	11.39			
	Area 4	8.56	.03			
Photo 18	Area 1	12.71	0.39	65.92	2.5	3.79%
	Area 2	15.74	0.16			
	Area 3	20.18	1.92			
	Area 4	17.29	0.03			
Photo 19	Area 1	19.24	0	51.64	12.18	23.586%
	Area 2	3.63	12.04			
	Area 3	15.72	0.14			
	Area 4	13.05	0			
Photo 20	Area 1	18.75	0.50	66.39	0.65	0.979%
	Area 2	12.23	0.05			
	Area 3	20.82	0.10			
	Area 4	14.59	0			

Table 32: Zircon Sand C

Image analysis results for photographs 1 - 10

		$ZrSiO_4$ (cm^2)	Separation (cm^2)	Total $ZrSiO_4$ (cm^2)	Total Separation (cm^2)	% Phase Separation (by area)
Photo 1	Area 1	14.92	0.26	49.23	0.91	1.848%
	Area 2	10.31	0			
	Area 3	11.19	0.54			
	Area 4	12.81	0.11			
Photo 2	Area 1	9.36	0.07	40.53	0.64	1.579%
	Area 2	10.49	0.36			
	Area 3	10.5	0.18			
	Area 4	10.18	0.03			
Photo 3	Area 1	9.72	0.30	45.78	1.43	3.124%
	Area 2	12.11	0.58			
	Area 3	12.74	0.32			
	Area 4	11.21	0.23			
Photo 4	Area 1	11.10	0.40	37.43	1.36	3.633%
	Area 2	11.09	0.20			
	Area 3	7.90	0.69			
	Area 4	7.34	0.07			
Photo 5	Area 1	10.24	0.43	38.33	1.31	3.418%
	Area 2	7.11	0.43			
	Area 3	8.79	0.24			
	Area 4	12.19	0.21			
Photo 6	Area 1	16.57	0.76	58.19	1.83	3.145%
	Area 2	7.09	0			
	Area 3	16.21	0.46			
	Area 4	18.32	0.61			
Photo 7	Area 1	12.8	0.31	49.19	2.01	4.086%
	Area 2	14.2	0.74			
	Area 3	10.44	0.8			
	Area 4	11.75	0.16			
Photo 8	Area 1	14.31	0.99	40.01	2.42	6.048%
	Area 2	11.43	0.93			
	Area 3	7.51	0.34			
	Area 4	6.76	0.16			
Photo 9	Area 1	16.37	2.41	52.59	5.49	10.439%
	Area 2	14.27	0.88			
	Area 3	12.04	1.48			
	Area 4	9.91	0.72			
Photo 10	Area 1	13.14	0.63	51.07	4.26	8.341%
	Area 2	9.37	0.46			
	Area 3	18.55	1.23			
	Area 4	10.01	1.94			

Table 33: Zircon Sand C

Image analysis results for photographs 11 - 20

		$ZrSiO_4$ (cm^2)	Separation (cm^2)	Total $ZrSiO_4$ (cm^2)	Total Separation (cm^2)	% Phase Separation (by area)
Photo 11	Area 1	9.39	0.25	40.19	1.16	2.886%
	Area 2	11.25	0.87			
	Area 3	8.60	0			
	Area 4	10.95	0.04			
Photo 12	Area 1	13.02	0.34	45.7	1.7	3.720%
	Area 2	5.57	0.35			
	Area 3	10.85	0.38			
	Area 4	16.26	0.63			
Photo 13	Area 1	16.49	1.10	46.69	2.07	4.433%
	Area 2	10.06	0.36			
	Area 3	5.12	0			
	Area 4	15.02	0.61			
Photo 14	Area 1	5.58	0	45.46	1.38	3.036%
	Area 2	8.25	0.25			
	Area 3	13.94	0.47			
	Area 4	17.69	0.66			
Photo 15	Area 1	19.36	0.27	56.01	0.95	1.696%
	Area 2	10.94	0.24			
	Area 3	17.05	0.29			
	Area 4	8.66	0.15			
Photo 16	Area 1	14.71	1.77	61.04	4.38	7.176%
	Area 2	12.16	0.54			
	Area 3	18.90	0.50			
	Area 4	15.27	1.57			
Photo 17	Area 1	16.35	0.58	48.79	3.77	7.727%
	Area 2	5.79	0.97			
	Area 3	13.63	1.20			
	Area 4	13.02	1.02			
Photo 18	Area 1	13.5	0.80	42.37	3.26	7.694%
	Area 2	7.32	1.17			
	Area 3	11.68	0.93			
	Area 4	9.87	0.36			
Photo 19	Area 1	12.89	0.98	50.33	3.92	7.789%
	Area 2	11.91	1.52			
	Area 3	13.08	0.12			
	Area 4	12.45	1.30			
Photo 20	Area 1	18.39	1.45	52.81	5	9.468%
	Area 2	8.41	1.52			
	Area 3	15.32	1.02			
	Area 4	10.69	1.01			

Table 34: Zircon Sand N

Image analysis results for photographs 1 - 10

		$ZrSiO_4$ (cm^2)	Separation (cm^2)	Total $ZrSiO_4$ (cm^2)	Total Separation (cm^2)	% Phase Separation (by area)
Photo 1	Area 1	20.36	0.18	55.13	0.28	0.508%
	Area 2	10.44	0.10			
	Area 3	10.03	0			
	Area 4	14.30	0			
Photo 2	Area 1	6.23	0.12	32.77	0.71	2.17%
	Area 2	11.21	0.13			
	Area 3	6.00	0.30			
	Area 4	9.33	0.16			
Photo 3	Area 1	12.57	0.27	41.85	0.51	1.219%
	Area 2	11.35	0.03			
	Area 3	10.73	0.03			
	Area 4	7.20	0.18			
Photo 4	Area 1	12.38	0.21	33.33	0.31	0.93%
	Area 2	12.33	0.10			
	Area 3	7.86	0			
	Area 4	0.76	0			
Photo 5	Area 1	13.87	0.21	36.82	0.23	0.625%
	Area 2	4.42	0			
	Area 3	10.38	0			
	Area 4	8.15	0.02			
Photo 6	Area 1	11.98	0.44	34.29	0.69	2.01%
	Area 2	5.86	0.04			
	Area 3	11.44	0.11			
	Area 4	5.01	0.10			
Photo 7	Area 1	13.25	0.02	36.17	6.37	17.61%
	Area 2	2.92	6.24			
	Area 3	12.38	0.06			
	Area 4	7.62	0.05			
Photo 8	Area 1	9.16	0.03	25.17	0.51	2.026%
	Area 2	3.06	0.20			
	Area 3	5.88	0.20			
	Area 4	7.07	0.08			
Photo 9	Area 1	11.98	0.02	36.17	0.15	0.42%
	Area 2	7.80	0.11			
	Area 3	10.47	0.02			
	Area 4	5.92	0			
Photo 10	Area 1	7.89	0	31.77	0.04	0.126%
	Area 2	8.55	0			
	Area 3	8.37	0.04			
	Area 4	6.96	0			

Table 35: Zircon Sand N

Image analysis results for photographs 11 - 20

		$ZrSiO_4$ (cm^2)	Separation (cm^2)	Total $ZrSiO_4$ (cm^2)	Total Separation (cm^2)	% Phase Separation (by area)
Photo 11	Area 1	18.58	0.12	54.55	0.32	0.587%
	Area 2	7.48	0.15			
	Area 3	18.34	0.02			
	Area 4	10.15	0.03			
Photo 12	Area 1	16.81	0.22	36.39	0.59	1.62%
	Area 2	4.04	0			
	Area 3	9.20	0.18			
	Area 4	6.34	0.19			
Photo 13	Area 1	15.17	0.26	37.72	0.78	2.07%
	Area 2	12.33	0.32			
	Area 3	8.00	0.2			
	Area 4	2.22	00			
Photo 14	Area 1	7.91	0.49	39.67	0.60	1.513%
	Area 2	4.99	0			
	Area 3	9.34	0.11			
	Area 4	7.43	0			
Photo 15	Area 1	10.53	0	38.84	0.05	0.129%
	Area 2	12.51	0.05			
	Area 3	8.93	0			
	Area 4	6.87	0			
Photo 16	Area 1	15.3	0.20	47.0	0.24	0.511%
	Area 2	10.76	0			
	Area 3	12.57	0.04			
	Area 4	8.37	0			
Photo 17	Area 1	10.59	0	29.68	0.03	0.101%
	Area 2	9.96	0.02			
	Area 3	4.31	0.01			
	Area 4	4.82	0			
Photo 18	Area 1	16.5	0.26	45.32	0.62	0.62%
	Area 2	11.13	0.04			
	Area 3	9.81	0.07			
	Area 4	7.88	0.25			
Photo 19	Area 1	14.97	0.17	36.72	0.54	1.47%
	Area 2	11.47	0.13			
	Area 3	0	0.08			
	Area 4	10.28	0.16			
Photo 20	Area 1	16.01	0.05	40.32	0.26	0.645%
	Area 2	6.20	0.04			
	Area 3	12.11	0.17			
	Area 4	6.00	0			

APPENDIX 3: Silica Based Binders

1. Syton* Sols

Syton colloidal silica sols are are slightly opalescent or milky white dispersions of silica particles in an aqueous medium. The sols are available in a range of particle sizes and concentrations and also with different stabilising additives according to requirements. Full specifications of the binders are shown in Table 36. Syton sols are compatible over a range of concentrations with water-miscible organic solvents, such as ethyl-alcohol and acetone, and also with many aqueous emulsions of materials such as melamine-urea, phenolic resins, PVA adhesives, sttarch and styrene-acrylic copolymers. They are miscible with water soluble acids (except hydroflouric) and with ammonia.

Table 36: Typical physical and chemical properties of Syton colloidal silica sols

Property	Unit	Syton X30	Syton W30	Syton T40.AS
Approximate particle size (by light scattering	nm	15	125	40
Specific surface area	m^2/g	250	75	140-180
SiO_2 content	% w/w	30	30	40
Na_2O content	% w/w	0.34	0.13	0.08 max
SiO_2/Na_2O	-	88	230	-
Chlorine content (as NaCl)	% w/w	0.007	0.02	0.08 max
Sulphate content (as Na_2SO_4)	% w/w	-	-	0.1 max
pH at 20°C	-	9.9	10.2	9.4 max
Specific gravity at 15.5°C/15.5°C	-	1.20	1.20	1.28-1.30
Viscosity at 20°C	cps	5.5	2.5	20
Description	-	slightly opalescent mobile liquid	milky mobile liquid	turbid mobile liquid

* Syton is the trademark of Monsanto plc

2. Silester* OS

A condensed polymeric ethyl ortho-silicate of neutral character. Binders are prepared 'in house' by hydrolysis in a mutual solvent, such as ethyl alcohol or isopropyl alcohol, with a hydrochloric acid catalyst. The ratio of water to ethyl silicate in the hydrolysis reaction is carefully controlled to prepare a finished mixture of the required silica content.

Table 37: Typical physical and chemical properties of Silester OS

Property	Unit	Value
Description	-	Colourless transparent liquid
Colour	alpha	30 max
% Transmission (Haze)	%	93 min
Specific gravity 15.5°C/15.5°C	-	1.07
Silica content	% w/w	40 - 41
Acidity	% w/w HCl	0.002
Denatured alcohol	% w/w	1.0
Flash point (Pensky Marten Closed Cup)	°C	63
Freezing point	°C	- 50
Viscosity at 25°C	cps	5.0

3. Silester* XAR

Silester XAR is a prehydrolysed ethyl-silicate solution, consisting of ortho-silicate in an alcohol base. Full specifications are shown in Table 38. The binder can be gelled by the addition of a catalyst, such as ammonia.

* Silester is the trademark of Monsanto plc

Table 38: Typical physical properties of Silester XAR

Property	Unit	Value
Description	-	White cloudy liquid
Specific gravity 15.5°C/15.5°C	-	0.915
Silica content	% w/w	20
Acidity	% w/w H_2SO_4	0.06
Denatured alcohol	% w/w	27.5
Flash point (Abel Closed Cup)	°C	13
Freezing point	°C	<-70
Viscosity at 25°C	cps	4
Isopropanol	% w/w	52.5

4: Ethyl Silicate AAZ+

Ethyl silicate AAZ is a hybrid binder based upon a mixture of ortho-sillicates, colloidal silica sol particles and other proprietary constituents in the hydrolysis formula (Table 39). The binder is compatible with all filler materials including zircon, alumina, fused silica and sillimanite and has a well defined gel point brought about by both air drying or ammonia hardening.

5. Primcote[a]

Primcote is a colloidal silica based binder formulated to be used as a primary coat binder to eliminate casting surface defects. The base formulation contains proprietary additives such as wetting agent, antifoam and a colour indicator which changes from green to orange when the mould coating is sufficiently dried (Table 40). As with other colloidal silica binders, gellation is achieved by solvent evaporation.

[a] Trademark of Ransom and Randolph - a division of Dentsply International
+ Trademark of Wex (Chemicals) Ltd

6. Fascote[+]

Fascote is a water based colloidal silica binder formulated to be used in the backup coats of an investment mould. Typical formulation is shown in Table 40. It has a lower viscosity than conventional binder systems which allows stronger shells to be rapidly produced since the drying time between slurry coats is reduced. In addition the binder also contains a colour indicator which changes from green to orange when the slurry coat has dried sufficiently for the component to be dipped again.

Table 39: Typical physical and chemical properties for Ethyl Silicate AAZ

Property	Unit	Value
Base Material	-	Silica
Medium	-	Alcohol
Appearance	-	Pearly white opalescent liquid
SiO_2 content	% w/w	18.5
Specific gravity	-	0.910
pH at 25°C	-	approx 1.5
Flash point	°F	52

[a] Trademark of Ransom and Randolph - a division of Dentsply International

Table 40: Typical physical and chemical properties of Primcote and Fascote colloidal silica binders

Property	Unit	Primcote	Fascote
Base composition	-	colloidal silica	colloidal silica
Other composition	-	proprietary	proprietary
Total solids content (including SiO_2)	% w/w	30%	25%
Particle size	nm	10	10
pH at 25°C	-	10.6	10.6
Specific gravity	-	1.18	1.15
Weight/volume	kg/litre	1.18	1.15
Viscosity at 25°C	cps	< 10	< 10
Na_2O content	% w/w	0.48	0.41
Particle charge	-	negative	negative

APPENDIX 4: Non-Silica Based Binders

1. Zirconia Based Binders

Magnabond Z[a] is a water based zirconia binder developed for the binding of refractory constituents such as mullite, Molochite, tabular alumina, fused alumina or any alumino silicate. Specifications for the binder are given in Table 41. Gellation can be achieved by the use of an accelerator such as finely ground reactive calcium or magnesia. Alternatively more conventional gellation techniques such as solvent evaporation or ammonia vapour can be used with care. The binder gives high green strength and maximum bond strength is developed upon firing of the refractory body. Only ZrO_2 remains in the refractory following heating above 1,000°C.

Remet zirconia sol[b] is a water based zirconia binder which produces a ZrO_2 bond in investment casting, ceramic, electronic, refractory and other applications. Specifications for the binder is shown in Table 42. The sol is stabilised with acetate anions and gellation will occur by solvent evaporation, the presence of electrolytes which increase the pH or in the presence of multivalent anions such as sulphate or phosphate.

Table 41: Physical properties of Magnabond Z

Property	Unit	Value
Base Material		Amorphous zirconia
Medium	-	Water
Appearance	-	Clear translucent liquid
Viscosity	cps	1.30
Specific gravity		1.10
Zirconia content	% w/w	20
ZrO_2 content of fired refractory	% w/w	1.3%
pH at 25 °C	-	1.1
Shelf life	months	6
Cl content	ppm	6.5
Fe content	ppm	20

[a] Trademark of Magna Industrials Ltd [b] Manufactured by the Remet Corporation

Table 42: Physical and chemical properties of Remet zirconia sol

Property	Unit	Value
Base material	-	Amorphous zirconia
Medium	-	Water
Stabilising Agent	-	Acetate ions
ZrO_2 content	% w/w	20
Acetate content (per mole of ZrO_2)	mol	1.5
Colour	-	Nearly colourless slightly cloudy liquid
pH at 25°C	-	3.5
Specific gravity at 25°C	-	1.26
Particle size	nm	2

2. Alumina Based Binders

Remal A20[c] is a stable, aqueous, colloidal alumina dispersion. Full specifications are given in Table 43. The crystal structure of the sol particles is not amorphous and is actually in the form alpha aluminium oxide mono hydrate (commonly known as boehmite). The sol is used as a binder for many materials including refractories, ceramics, pigments and fibers and has a powerful film forming capacity. The sol can be gelled by solvent evaporation or by pH modification since the suspension is only stable in the pH range 3.7 to 4.3. Upon dehydration and firing the residue is almost pure Al_2O_3.

Bacosol[d] alumina sols are supplied as sol-like dispersions (AlO(OH)) in water or as very finely divided dry powders which can be reconstituted into a dispersion by the customer (Table 44). There are several dispersion forms including positive, negative and low sodium ammonia stabilised. High strength alumina bonds are formed upon firing.

[c] Trademark of Remet Corporation, USA.
[d] Trademark of BA Chemicals Ltd, U.K.

Table 43: Physical and chemical properties of Remal A20

Property	Units	Value
Al_2O_3 content	% w/w	20
pH at 20°C	-	4.0
Specific gravity at 20°C	-	1.19
Crystal structure	-	Boehmite
Particle charge	-	Positive
Crystallite size	Å	70
Carbon	% w/w	0.1
Cl	% w/w	<0.001
SiO_2	% w/w	<0.001
Fe_2O_3	% w/w	<0.001
Na_2O	% w/w	<0.001
TiO_2	% w/w	0.043
NO_3	% w/w	0.3
Viscosity at 25°C	cps	<50
Average particle size	nm	70
Surface area	m^2/g	180

Table 44: Physical and chemical properties of Bacosol grade alumina sols

Property	Unit	Bacosol 2A	Bacosol 2C	Bacosol 3A	Bacosol 3C
Solids content	% w/w	32.5	34.0	32.5	34.0
Alumina content	% w/w	27.5	29.0	27.5	29.0
Silica content	% w/w	0.007	0.007	0.007	0.007
Medium	-	water	water	water	water
pH at 20°C	-	10.0	5.5	10.0	3.5
Density	g/cm^3	1.25	1.32	1.25	1.32
Viscosity	cP*	400	350	400	350
Particle charge	-	anionic	cationic	anionic	cationic
Mineralogy	-	boehmite	boehmite	boehmite	boehmite
Particle size	µm	0.1-0.2	0.1-0.2	0.1-0.2	0.1-0.2
Surface area	m^2/g	150-200	150-200	150-200	150-200
Na_2O	%w/w	0.35	0.35	0.15	0.15

* Brookfield Viscometer Model RVT (Spindle 1, 100 rpm, 20°C)

3. Alumino-Silicate Based Binders

1. Magnabond Binders

Magnabond A[e] and Magnabond B[e] are two proprietary colloidal alumino-silicate based binders manufactured to be used in the high temperature bonding of refractory materials. Both systems can be gelled using reactive magnesia or solvent evaporation and when fired at 1,000°C the refractory consists of Al_2O_3 and SiO_2 in varying proportions. Magnabond A contains the correct proportions of silica and alumina such that mullite is formed upon firing. Magnabond B will form an alumino-silicate refractory with alumina and silica in the ration 5:17. Full specifications for both binders can be found in Table 45.

[e] Trademark of Magna Industrials Ltd

Table 45: Physical and chemical specifications for Magnabond binders

Property	Unit	Magnabond A	Magnabond B
Appearance	-	milky white liquid	milky white liquid
Viscosity	cps	2.55	2.55
Specific gravity	-	1.20	1.20
Al_2O_3/SiO_2 content	% w/w	20	22
Particle size	µm	10-15	10-15
Fired composition	-	mullite	alumino-silicate
Al_2O_3/SiO_2 ratio in fired structure	-	72/28	5/17
pH at 20°C	-	4 - 4 .4	4 - 4 .4

APPENDIX 5: Refractories

1. Zircon Sand*

High purity zircon (zirconium silicate - $ZrSiO_4$) sand mineral which has been seperated from other mineral sands by ore dressing techniques. The mineral has no definite melting point but decomposes to form zirconium oxide and silica between 1550°C and 1700°C. Available in a range of particle sizes and used as a primary coat stucco in investment casting moulds (Table 46). The refractory can also be obtained in the calcined form.

Table 46: Tyical chemical and physical properties of Zircon Sand

Property	Unit	Value
$ZrO_2 + HfO_2$	%	66.0
SiO_2	%	33.0
Al_2O_3	%	0.50
TiO_2	%	0.20
Fe_2O_3	%	0.10
Density	$x10^3$ kg/m^3	4.60
Bulk Density ASTM B212-76	$x10^3$ kg/m^3	2.80
A. F. SGrain Fineness Number	-	62

2. Zircosil 200/200M*

Zircosil refractory flours consist of high purity $ZrSiO_4$ mineral, prepered by the milling of Zircon Sand. They are used as filler materials due to low thermal expansions and other physical properties which combine to produce a refractory which has excellent high temperature properties. Zircosil is available in an uncalcined (200) and a calcined form (200M) depending upon the proposed application. Typical physical and chemical properties are shown in Table 47.

* Trade mark of Cookson Minerals Limited

Table 47: Typical physical and chemical properties of Zircosil refractories

Property	Unit	200	200M
$ZrO_2 + HfO_2$	%	66.0	66.0
SiO_2	%	33.0	33.0
Al_2O_3	%	0.50	0.50
TiO_2	%	0.20	0.10
Fe_2O_3	%	0.10	0.06
Density	$x10^3$ kg/m^3	4.60	4.60
Bulk Density ASTM B212-76	$x10^3$ kg/m^3	1.80	1.80
Material retained on a 150µm aperture sieve (100 mesh)	wt%	< 0.1	< 0.1
Material retained on a 75µm aperture sieve (200 mesh)	wt%	1.0	0.5
Material retained on a 53µm aperture sieve (300 mesh)	wt%	8.0	8.0
Average particle size (Coulter)	µm	15.8	15.8

3. Investagrog[1]

Investagrog is a high grade calcined alumino-silicate refractory aggregate, available in a range of particle sizes, and used as a filler material in ceramic slurries. Typical chemical and physical properties of the refractory are shown in Table 48.

[1] Trade mark of Hoben Davis

Table 48: Typical chemical properties of Investagrog refractory

Property	Unit	Value
SiO_2	%	54.8
Al_2O_3	%	41.2
Fe_2O_3	%	0.66
TiO_2	%	2.73
CaO	%	0.08
MgO	%	0.09
K_2O	%	0.27
Na_2O	%	0.02
Mullite	%	55
Cristobalite	%	17
Quartz	%	1
Amorphous silica	%	remainder

4. Molochite[2]

An alumino-silicate refractory aggregate consisting of mullite needles embedded in a amorphous silica glass. Available in a wide range of particle sizes and used extensively as a secondary coat stucco for investment casting moulds due to high angularity of the particles. This angularity provides a good keying surface for the successve slurry layers. The chemical and physical properties of the refractory are shown in Table 49.

[2] Trade mark of ECC International Limited

Table 49: Typical chemical and physical properties of Molochite refractory

Property	Unit	Value
SiO_2	%	52 - 53
Al_2O_3	%	42 - 44
Fe_2O_3	%	1.0
TiO_2	%	0.08
CaO	%	0.1
MgO	%	0.1
K_2O	%	1.5 - 2.0
Na_2O	%	0.1
Mullite	%	56
Amorphous silica glass	%	44
Refractoriness squatting test (over PCE 34)	°C	1770
Coefficient of linear thermal expansion (20 - 1,000°C)	-	4.4×10^{-6}
True specific gravity	-	2.70
True porosity	%	6 - 8
Hardness	Mohs	7 - 8

APPENDIX 6: Slurry Additives

1. Isopropoyl alcohol (Propan-2-ol)

Organic alcohol with the chemical formula: CH_3-CHOH-CH_3. Physical properties are specified in Table 50. The material is used as a dispersion medium for ethyl silicate binders.

Table 50: Physical and chemical properties of isopropyl alcohol

Property	Unit	Value
Colour	-	max 10
Relative density	15.5/15.5°C	0.789 - 0.791
Water content	% w/w	max 0.5
Initial boiling point	°C	min 81.5
Dry point	°C	max 83.0
Acidity (acetic acid)	% w/w	max 0.002
Residue on evaporation	% w/w	max 0.002
Miscibility with water	-	complies with B S Test
Aldehydes and ketone (as acetone)	% w/w	max 0.10

2. Synperonic NX

The Synperonic NX series of nobyl phenol ethoxylates is based on nonyl phenol produced by the alkylation of phenol trimer. The properties and application of the ethoxylates vary with ethyleneoxide content. NX is used as an additive to the basic ceramic slurry which increases the wettability of the primary slurry. This will allow the surface of the wax pattern to be wetted by the liquid slurry which forms the primary coat of the mould. Physical and chemical properties are shown in Table 51.

Table 51: Physical and chemical properties of Synperonic NX

Property	Unit	Value
Water Content	% w/w	0.3
Colour	Hazen Units	150
Hydroxyl	mgs KOH/g	95
Calculated HLB value	-	12.3
Cloud point	°C	32
Solubility in water	-	soluble
Pour Point	°C	<0
Viscosity at 20°C	cps	353
Specific gravity at 20°C	cps	1.053

3. Octan-1-ol

Octanol is an organic alcohol with the chemical formula: $CH_3(CH_2)_6CH_2OH$. It is used as an anti-foaming agent which is added to ceramic slurries to prevent the formation of bubbles. Specifications are shown in Table 52.

Table 52: Physical properties of Octan-1-ol

Property	Unit	Value
Molecular weight	g	130.23
Wt/mol at 25°C	g	0.822 - 0.825
Boiling range (95%)	°C	192 to 200
Refractive index	-	1.4285 - 1.4305

APPENDIX 7: Primary Coat Slurry Formulations and Control Limits

Primary coats are water based and contains an addition of a proprietary wetting agent to increase the wettability of the slurry. This allows even coating of the wax so that all features will be accurately replicated in the finished mould cavity. The anti-foaming agent prevents the formation of bubbles which, if transferred to the surface of the wax, can produce an uneven coating and spalling in the primary coat. Note that only the calcined version of the refractory filler is used in the primary slurry.

Table 53: Primary coat slurry formulation and control limits

COMPONENT /CONTROL LIMIT	UNIT	VALUE
Syton X30	litres	10
Zircosil 200	-	nil
Zircosil 200M	kg	46
Synperonic NX	ml	30
Octanol	ml	60
Distilled Water	-	accordingly
Isopropyl Alcohol	-	nil
Temperature (° C)	°C	22 ± 2
pH	-	8 - 9
Humidity(relative percentage)	%	55 max

APPENDIX 8: Secondary Coat Formulations and Control Limits

Secondary coats are alcohol based, the binder being a mixture of ortho-silicates in an isopropanol dispesion medium. Wetting and anti-foaming agents are not required as the slurry is not used in direct contact with the wax pattern. The back-up coats of a mould are there to provide strength only and do not come into contact with the metal. Experience has shown that a mixture of calcined and uncalcined refractory can be used as the filler which reduces material costs for the slurry itself. The slurry binder is gelled with an ammoniating atmosphere and not by evaporation, so the humidity can be held around the upper limit. This also reduces costs since the rainy weather found in Britain produces a natural atmospheric humidity of 55%.

Table 54: Secondary coat formulation and control limits

COMPONENT /CONTROL LIMIT	UNIT	VALUE
Silester XAR	litres	10
Zircosil 200	kg	17.5
Zircosil 200M	kg	17.5
Synperonic NX	ml	-
Octanol	ml	-
Distilled Water	-	nil
Isopropyl Alcohol	-	accordingly
Temperature (° C)	°C	20 ± 2
pH	-	2.3 - 2.8
Humidity(relative percentage)	%	55 max

APPENDIX 9: Mould Dipping Regime for Creep/Physical Properties Test Pieces

The test pieces were hand dipped and stuccoed at Deritend Precision Castings using a variety of silica and non-silica based binders. When using a non-silica based binder only one slurry was made up according to the schedule shown in Apppendix 7. However, the wetting and anti-foaming agents were omitted, as it was often difficult to predict their effect upon the binder sols. All coats were air dried for approximately 3 hours in a drying cabinet. The dipping regime used is contained in Table 55.

Table 55: Mould dipping regime for creep/physical properties samples

COAT	SLURRY	STUCCO	DRYTIME
1	primary	Zircon Sand	3 hours
2	secondary	30/80 Molochite	3 hours
3	secondary	30/80 Molochite	3 hours
4	secondary	18/36 Molochite	3 hours
5	secondary	18/36 Molochite	3 hours
6	secondary	18/36 Molochite	3 hours
7	secondary	18/36 Molochite	3 hours
8	secondary	18/36 Molochite	3 hours
9	secondary	18/36 Molochite	3 hours
10	secondary	-	3 hours

APPENDIX 10: Preparation of Binder Compositions

1: Liquid state

Sodium was added in the form of NaOH, as a calculated weight percentage of the binder system. Initially 10 ml of the binder was weighed and used to calculate appropriate NaOH additions. Compositions in the range 0 to 0.5 wt% NaOH were prepared. After mixing, the solutions were gelled and dried as normal. The following is a worked example of the calculation used to determine the NaOH additions needed to produce the required compositions.

weight of 10ml Syton T40 AS = 12.3089g
therefore 0.0250g NaOH is equivalent to:-

$$\frac{0.0250}{12.3089} \times 100 = 0.203 \text{ wt\%}$$

$$\frac{\text{wt of addition}}{\text{total weight of the liquid}} \times 100 = \text{wt\% of the addition}$$

2: Solid State

The following is a worked example of the preparation of a binder composition in the solid state. Constituents were added as carbonates, so that CO_2 gas would be liberated during firing to leave the required oxide composition.

composition:- silicon 97.109 atomic% (SiO_2)
calcium 2.485 atomic% (Ca^{2+})
sodium 0.406 atomic% (Na^{+})

source of elements:- SiO_2 atomic weight = 60.09g
Na_2CO_3 atomic weight =105.99g
$CaCO_3$ atomic weight = 100.09g

We need to produce 10g of sample that, when fired and the CO_3 is removed as CO_2, will leave a residue with the required atomic% composition. If we consider the composition as a substituted silica, the formula can be written:-

$$(Si_{97.109} Ca_{2.485} Na_{0.406}) O_{200}$$

In molar terms the formula can be rewritten:-

$$(97.109\ SiO_2 + 2.485\ CaCO_3 + 0.203\ Na_2CO_3)$$

$$(97.109 \mathbf{x} 60.09)+(2.485 \mathbf{x} 100.09)+(0.203 \mathbf{x} 105.99)= w$$

$$a \quad + \quad b \quad + \quad c \quad = w$$

a= no. of moles Si **x** atomic weight SiO_2
b= no. of moles Ca **x** atomic weight $CaCO_3$
c= no. of moles Na **x** atomic weight Na_2CO_3
w= weight factor = **6105.52**

$$\frac{\text{(total weight required)}}{\text{weight factor}} \mathbf{x}\ a = \frac{10}{w} \mathbf{x}\ a = \text{wt of silica required}$$

$$\frac{10}{w} \mathbf{x}\ a = \frac{10}{6105.5} \mathbf{x}\ 5835.28 = \mathbf{9.5574g}\ \mathbf{SiO_2}$$

$$\frac{10}{w} \mathbf{x}\ b = \frac{10}{6105.5} \mathbf{x}\ 248.72 = \mathbf{0.4074g}\ \mathbf{CaCO_3}$$

$$\frac{10}{w} \mathbf{x}\ c = \frac{10}{6105.5} \mathbf{x}\ 21.52 = \mathbf{0.0352g}\ \mathbf{Na_2CO_3}$$

REFERENCES

1. P. R. Taylor
'An Illustrated History of Lost Wax Casting'
17th Annual B. I. C. T. A. Conference, September, **1983**.

2. E. L. Kotzin
'Metalcasting and Molding Processes'
American Foundrymens Society Inc., Illinois, USA, **1981**.

3. B. I. C. T. A. Working Group
'Designers Handbook for Investment Casting'
B. I. C. T. A., **1990**.

4. H. T. Bidwell
'Investment Casting'
The Machinery Publishing Co., **1969**.

5. S. O. Barnett
'Investment Casting - The Multi-Process Technology'
Foundry Trade Journal International, **11** (3), 33-37, **1988**.

6. R. L. Wood
'Progress in Investment Casting'
Metallurgical Reviews, 5 (17), **1960**.

7. Anonymous
'The Investment Casting Market'
Foundry, article S25, **1990**.

8. R. F. Smart
'Developments in Investment Casting'
Foundry Trade Journal International, **11** (4), 234 - 236, **1988**.

9. R. L. Wood and D. VonLudwig
'Investment Casting for Engineers'
Reinhold Publishing Corporation, New York, **1952**.

10. P. R .Taylor
'Trends in Investment Casting'
Foundry, April **1970.**

11. L. S. Taylor
'Trends in Investment Casting'
20th B. I. C. T. A. Conference, Maxstoke,October **1989.**

12. R. C. Feagin
'Mould and Crucible Refractories for the Investment Casting Industry'
Foundry Trade Journal, July 2nd **1964.**

13. W. E. Worrall
'Ceramic Raw Materials - Second Revised Edition'
Pergamon Press, **1982.**

14. J. M. Libouton
'Precision Foundry - The Ceramic Shell Process'
Bulletin published by Monsanto Europe plc.

15. S. Barnett
'An Alternative Back-Up Filler to Zircon'
Foundry Trade Journal, 8th June, **1990.**

16. H. G. Emblem
'The Use of Ethyl Silicate as a Binder in Refractory Technology'
Proc.and Journal of the British Ceramis Society, **74**, 223-227, **1975.**

17. H. G. Emblem
'The Chemistry of Alkyl Silicate Binders In Refractory Technology'
Proc and Journal of the British Ceramic society.

18. D. Mills
'Understanding Silica Binders'
Foundry Trade Journak, April 21st, **1989.**

19. H. Schwartz
'Faster and Safer Shell Production'
36th Annual Meeting of the Investment Casting Institute, October, **1988.**

20. M.J.Hendricks
'The Impact of Ceramic Shell Materials on Shell Performance'
37th Annual Meeting of the Investment Casting Institute, October, **1989**.

21. Noboru Ichinose (Editor)
'Introduction to Fine Ceramics - applications in Engineering'
John Wiley and Sons, **1987**.

22. R.C.Feagin
'Alumina and Zirconia Binders'
29th Annual Meeting of the Investment Casting Institute, October, **1981**.

23. Magna Industrials Limited
Product Specification **MIL/21**
'Zirmast - zirconia binder of refractory grade'

24. R.C.Feagin
'Method of Making a Ceramic Shell Mould'
US Patent 4,216,815, August 12th, **1980**.

25. A.J.Skoog and R.E.Moore
'Refractory of the Past for the Future: Mullite and its use as a bonding phase'
Ceramic Bulletin, **67**(7), **1988**.

26. M.G.M.U. Ismail et al
'Microstructure and Mechanical Properties of Mullite prepared by the sol-gel Method'
J.Am.Ceram.Soc. **70**(1), C7-C8, **1987**.

27. Magna Industrials Ltd
Product Specification **MIL/16**
'Magna Bond B - Alumino silicate binder - refractory grade'

28. Magna Industrials Ltd
Product Specification **MIL/13**
'Magna Bond Z/M - Fused Zirconia /Mullite binder - refractory grade'

29. Magna Industrials Ltd
Producy Specification **MIL/14**
'Magna Bond Z/A - Fused Zirconia/Alumina binder - refractory grade'.

30. A. Dunlop
'Investment Precision Castings Without Expendable Patterns'
American Foundryman, June **1954**, 64 - 69.

31. N. J. Grant
'Recent Developments in the Art of Precision Casting'
Metal Progress, **70**, no.3, Sept **1956**.

32. I. R. Kramer
American Foundryman, **27**, (2), **1955**, p38.

33. J. S. Turnbull
Proc. Inst. Mech. Eng., 169, p319, **1955**.

34. R. L. Wood
'Progress in Investment Casting'
Metallurgical Reviews, 5 (17), **1960**.

35. Anonymous
'Making Precision Castings in Glass Moulds'
Foundry, **83**, no 8, 140-143, Aug **1955**.

36. J. R. Brown
'The Lost Foam Casting Process'
Metals and Materials, 8, no 10, 550-555, October **1992**.

37. T. R. Smith
US Patent 3,157,924, **1964**.

38. R. W. Grimshaw
'The Chemistry and Physics of Clays and Allied Materials - 4th Edition'
Ernest Benn Ltd., London, **1971**.

39. R. B. Sosman
Trans. Brit. ceram. Soc., 54, 663, **1955**.

40. McGraw-Hill Encyclopaedia of Science and Technology (2nd Edition)
Volume 16
McGraw-Hill Book Company, **1987**.

41. J. D. Dana and E. S. Dana
'Dana's System of Minerology'
Seventh Edition, Volume 3 - Silica Minerals
John Wiley and Sons, **1962**.

42. K. Warren
J. Appl. Phys. **8**, 645, **1937**.

43. T. Graham
'Liquid Diffusion Applied to Analysis'
Phil. Trans. Roy. Soc. (London), **151**, 183-224, **1861**.

44. D. H. Everett
'Basic Principles of Colloid Science'
Royal Society of Chemistry, Whitstable, England, **1988**.

45. D. J. Shaw
'Introduction to Colloid and Surface Chemistry - 3rd Edition'
Butterworth and Co. Ltd, Boston, **1980**.

46. H. van Olphen
'An introduction to Clay Colloid Chemistry - 2nd Edition'
John Wiley and Sons, New York, **1977**.

47. R. K. Iler
'The Colloid Chemistry of Silica and the Silicates'
Cornell University Press, **1955**.

48. T. Graham
Ann. Physik., **190**, 187, **1861**.

49. 'Gessellschaft fur Elektro-Osmose'
British Patent 9,237, **1914**.

50. B. Schwerin
U. S. Patent 1,557,491, **1925**.

51. W. D. Treadland and W. Wieland
'Zur Kenntnis der Kiesseldurehdrate'
Helv. Chim. Acta., 13, 842-864, **1930**.

52. R. K. Iler
'The Chemistry of Silica - 2nd Edition'
John Wiley and Sons, **1979**.

53. P. G. Bird
U. S. Patent 2,244,325 (National Aluminate Co.), **1941**.

54. M. F. Bechtold and O. E. Snyder
U. S. Patent 2.574,902 (Du-Pont), **1951**.

55. G. B. Alexander
U. S. Patent 2,570,345 (Du-Pont), **1956**.

56. G. B. Alexander and R. K. Iler
U. S. Patent 2,605,228 (Du-Pont), **1952**.

57. G. B. Alexander, R. K .Iler and F. J. Wolter
U.S.Patent 2,601,235 (Du-Pont), **1952**.

58. R. K. Iler
U.S.Patent 3,668,088 (Du-Pont), **1972.**

59. R. K. Iler and F. J. Wolter
U.S.Patent 2,631,134 (Du-Pont), **1953.**

60. J. E. Ahlberg and E. A. Simpson
U.S.Patent 2,900,348 (W.R.Grace and Co), **1959.**

61. W. Stober, A. Fink and E. Bohn
J. Colloid Interface Science, **26**, 62, **1968.**

62. R. Schnurch and A. Koster
U.S Patent 3,346,335 (Philadelphia Quartz Co), **1967.**

63. J. H. Balthius
U.S.Patent 2,614,994 (Du Pont), **1952.**

64. V. I. Montenyohl and C. M. Olson
U.S.Patent 2,614,993 (Du Pont), **1952.**

65. H. E. Bergna and F. Simko
U.S.Patent 3,284,369 (Du Pont), **1966.**

66. R. K .Iler and A. G. Jelinek
U.S.Patent 2,886,466 (Du Pont), **1959.**

67. E. P. Moore
U.S.Patent 3,752,673 - 3,752,681 (Du Pont), **1951.**

68. P. F. Collins
U.S.Patent 2,380,945 (Austenal Labs Inc), **1945.**

69. R. E. Albert
U.S.patent 3,615,778 (Du Pont), **1971.**

70. F. E. Edlin
U.S.Patent 3,311,585 (Du Pont), **1967.**

71. F.G.Fisher, R.K.Allen and G.W.Luvisi
Trans. A S M E, **80**, 1037, **1958**.

72. R. K. Iler
U.S.Patent 2,597,871 (Du Pont), **1952**.

73. D. H. Powers and D. H. Harrison
U.S.Patent 2,443,512 (Monsanto Chemical Co.Ltd), **1948**.

74. R. J. Walsh and A. H. Herzog
Chem. Abstr. **62**, 11293(a), **1965**.

75. J. A. Heaney
U.S.Patent 2,442,976, **1948**.

76. E. H. Land et al
U.S.Patent 2,698,236 (Polaroid Corp), **1954**.

77. J. Phalippou, M. Prassas and J. Zarzycki
'Crystallization of Gels and Glasses Made From Hot-Pressed Gels'
J. of Non-Cryst. Solids **48**, 17-30, **1982**.

78. W. O. Milligan and H. H. Hachford
J. Phys. Colloid. Chem. **51**, 333, **1957**.

79. H. W. Kohlschutter and G. Kampf
Z. Anorg. Chem. **292**, 298, **1957**.

80. J. F. Goodman and S. J. Gregg
J. Chem. Soc., 694, **1959**.

81. J. Fraissard and B. Imelik
J. Chim. Phys. **59**, 415, **1962**.

82. J. Phalippou et al
Ann. Chim. **3**, 99, **1978**.

83. R. Jabra et al
Rev. Chim. Min. **16**, 245, **1979**.

84. A. Dietzel
Zeit. Elektrochem. **48**, 1-9, **1942**.

85. Z. Congshan et al
'Influence of Trace Alkali Ions on The Crystallization Behaviour of Silica Gels'
J. of. Non-Cryst. Solids, **82**, 321-328, **1986**.

86. I. H. Hall
'Deformation of Solids'
Thomas Nelson and Sons Ltd., London, **1968**.

87. C. D. Pomeroy (Editor)
'Creep of Engineering Materials'
The Institute of Mechanical Engineers, Cambridge, **1978**.

88. I. Finnie and W. R. Heller
'Creep of Engineering Materials'
Mc-Graw Hill Book Company Inc., New York, **1959**.

89. R. W. Davidge and A. G. Evans
'The Strength of Ceramics'
Mater. Sci. and Eng., **6**, 281-289, **1970**.

90. G. R. Terwillinger and K. C. Radford
'High Temperature Deformation of Ceramics'
Ceram. Bull., **53**, 172-179 and 465-472, **1974**.

91. G. W. Groves and A. Kelly
'Independent Slip Systems in Ceramics'
Phil. Mag., **8**, 877-890, **1963**.

92. D. J. Godfrey
'Use of Ceramics in High Temperature Engineering'
Metals and Materials, 305-311, **1968**.

93. B. Burton and G. L. Reynolds
'Diffusional Creep of UO_2'
Acta Met.,1073-1078, **1973**.

94. J. M. Birch, B. Wilshire, D. J. R. Owen and D. Shantaram
'Influence of Stress Distribution on Deformation and Fracture Behaviour of Ceramics Under Compressive Creep Conditions'
J. Mater. Sci., **11**, 1817-1825, **1976**.

95. F. H. Norton
J. Amer. Ceram. Soc., 31, 236, **1948**.

96. P. R. Taylor and M. A. Roberts
'Ceramic Shell Mould High Temperature Distortion'
25th Annual Conf. of the American Investment Casting Institute, Oct **1977**.

97. M. Grech et al
'Bulging of Investment Castings'
19th B. I. C. T. A. Conf., Sept **1987**.

98. M. Grech and J. M. Young
'Correlation Between Sag in Strip Test-Pieces and Bulge in Investment Castings'
Cast Metals, **3**, no 1, 29 - 35, **1990**.

99. J. MacGibbon and S. C. Yates
'Some Observations on the Thermal Behaviour of Zircon-Molochite Shell Moulds'
19th, B. I. C. T. A. Conf., Sept **1987**.

100. D. R. Muzyka and G. A. Colligan
'Metal-Refractory Reaction Studies in the Iron-Chromium-Silica System'
The Metals Research Journal, June **1967**.

101. P. W. Wright
'Reactions of Zircon Refractories With Molten Steel'
J. Am. Ceram. Soc., 20, no 2, 47-50, **1985**.

102. S. M. Kim, W. K. Lu, P. S. Nicholson and A. E. Hamielec
'Corrosion of Aluminosilicate Refractories in Iron-Manganese Alloys'
Ceramic Bulletin, 53, no. 7, 543 - 547, **1974**.

103. A. Muan
'Reactions Between Iron Oxides and Alumina-Silica Refractories'
J. Am. Ceram. Soc., 41, no. 8, 275 - 286, August **1958**.

104. R. C. Feagin
'Casting of Reactive Metals Into Ceramic Moulds'
6th World Conf. on Investment Casting, paper 4, Washington D. C., **1984**.

105. Lirones
U. S. Patent 3,241,200.

106. Brown
U. S. Patent 3,994,346.

107. Brown
U. S. Patent 4,057,433.

108. Richerson et al
U. S. Patent 4,040,845.

109. Bureau of Mines Report of Investigations, RI 8624.

110. R. C. Feagin
'Alumina and Zirconia Binders'
29th Annual Meeting of the Investment Casting Institute, Arizona, Oct 14th, **1981**.

111. R. C. Feagin
U. S. Patent 4,415,673.

112. I. S. Taylor
'Prevention of Fusion ('Spotted-Dick') on High Chromium Steel'
7th Annual B. I. C. T. A. Conf., May 10-12th, **1965**.

113. G. Tschentke
'Annual Review of Alloy Steel Castings'
Giesserei, 53, (9), 293-297, **1966**.

114. E. M. Broad
'Carbon Restoration of Investment Castings'
Precision Metal Molding, 86-87, October **1961**.

115. W. Dittrich
'Higher Grade Inner Coats For Ceramic Moulds With Organic Zircon and Aluminium Componds'
3rd World Conf. on Investment Casting, Paris, **1972**, paper 24.

116. B. I. C. T. A Technical Commitee
'Investment Casting - Recognition and Definition of Flaws'

117. J. Campbell
'Castings'
Butterworth Heinemann, Oxford, 1991.

118. S. J. B Reed.
'Electron Microprobe Analysis'
Cambridge University Press, **1975**.

119. V.D. Scott, G. Love
'Quantitative Electron-probe Microanalysis"
John Wiley and Sons, **1983**.

120. G. Causey
'Electron Microscopy'
E and S Livingstone, **1962**.

121. M. I. Pope, M. D. Judd
'Differential Thermal Analysis'
Heyden and Son Ltd, **1980**.

122. H. J. Borchardt
'Differential Thermal Analysis'
Journal of Chemical Education, **33**(3), March **1956**.

123. Linseis DTA L62
Manufacturers Product Information

124. T. Daniels
'Thermal Analysis'
Kogan Page Ltd. **1973**.

125. J. Valentich
'Tube type Dilatometers'
Instrument Society of America, North Carolina, USA, **1981.**

126. M. McLean (editor)
'Characterisation of High Temperature Materials 4 : Physical and Elastic Characterisation'
The Institute of Metals, **1989.**

127. H. Fischmeister
'Digital Image Analysis in Quantitative Metallography'
Computers in Materials Technology
Pergamon Press, **1981.**

128. 'Image Analysis Principles and Practice'
Technical Handbook
Published by Joyce-Loebl, **1985.**

129. W. J. Price
'Analytical Atomic Absorption Spectrometry'
Heyden and Son Ltd, **1974.**

130. B. D. Cullity
'Elements of X-ray Diffraction - 2nd Edition'
Addison-Wesley Publishing Co., **1978.**

131. G. V. Samsonov and I. M. Vinitskii
'Handbook of Refractory Compounds'
IFI/Plenum Data Company, New York, **1980.**

132. J. T. Boyle and J. Spence
'Stress Analysis for Creep'
Butterworth and Co. Ltd, Southampton, **1983.**

133. M. Guerra and W. O. Roberts
'Factors Affecting Shell Strength and the Effect of Dry Time on Shell Strength'
22nd E. I. C. F. Conference, Paris, April **1992.**

134. S. Jones, X. Miao, C. B. Ponton, P. M. Marquis
'The Influence of Stabilising Agents and Alumina on the Crystallisation of Colloidal Silica'
European Ceramic Soc. 2nd Conf., Augsburg, Sept 11-14, **1991**.

135. R. Stevens
'Zirconia and Zirconia Ceramics-Second Edition'
Magnesium Elektron Ltd, U.K., **1986**.

136. W. C. Wei and J. W. Halloran
'Phase Transformations of Diphasic Aluminosilicate Gels'
J. Am. Ceram. Soc., 71 (3), 166-172, **1988**.

137. B. E. Waye
'Introduction to Technical Ceramics'
Maclaren and Sons Ltd., London, **1967**.

138. G. V. Samsonov and I. M. Vinitskii
'Handbook of Refractory Compounds'
IFI / Plenum Data Company, New York, **1980**.

139. Courtesy of Deritend Precision Castings

140. R. E. Reed-Hill
'Physical Metallurgy Principles - 2nd Edition'
D. Van Nostrand Company, U. S. A., 1973

141. Editor: W. T. Mcleod
'The New Collins Concise Dictionary of the English Language'
William Collins Sons and Co. Ltd., Glasgow, Scotland, **1986**.

142. R. I. Levin
'Statistics for Management'
Prentice-Hall Inc., New Jersey, USA, **1978**.